Can Otolith Microchemistry be used to Identify Spawning Stocks and Characterize the Life History of Hickory Shad (*Alosa mediocris*)?

By:

Christopher Ryan Hill

December 2020

Director of Thesis: Dr. R.A. Rulifson

Major Department: Biology

Abstract

The goal of this study was to determine if otolith microchemistry could be used to identify spawning stocks and learn about the life history characteristics of Hickory Shad (*Alosa mediocris* (Mitchell 1814), which are an anadromous clupeid found in Atlantic coastal systems that have been neglected in the scientific literature. Hickory Shad were captured in 26 locations within 18 major rivers along the known spawning range. LA-ICP-MS was used to quantify seven elements (Mg, Mn, Cu, Zn, Sr, Ba, and Pb) along a continuous transect that ran from the ventral to dorsal edge through the otolith core, resulting in a time resolved model of the environmental exposure history of each fish. Hickory Shad captured in the same locations had similar element profiles that were distinct from other capture locations, which immediately suggested natal homing. To test this hypothesis quantitatively, a combination of Bayesian inference and unsupervised learning techniques were used to estimate the natal river element signature of each

fish and determine if it was similar in Hickory Shad captured in the same location. Hidden Markov models were used to identify the natal river element signature of each fish, a Gaussian mixture model was used to cluster natal river signatures. In most cases, between 50% and 100% of Hickory Shad captured in the same location were assigned to the same cluster, indicating that they had similar natal watershed element signatures. A Chi-Square test confirmed that there was a significant relationship between capture location and cluster assignment ($p<0.01$). These results provide the first piece of evidence that Hickory Shad do exhibit natal homing, and provide an important inferential baseline for further characterization of the rate of natal homing. While these results provided strong evidence that Hickory Shad exhibit natal homing, quantifying the spatial extent of natal homing and straying would require knowledge of the spatiotemporal variability of elements in the spawning rivers. Water chemistry data were not available for the capture locations in this study, so elements deposited on the edge of Hickory Shad otoliths (~30 μm of absolute distance) were used as a proxy and compared across capture locations. Hickory Shad captured in five locations had distinct ratios of and one or two elements, and these differences were minute. Based on knowledge from previous literature and several empirical observations, I concluded that the edge of Hickory Shad otoliths did not reflect the ambient element ratios of the capture location, which was likely a function of a rapid spawning migration.

Overall, the results of this study suggest that otolith element signatures incorporated during the first year of life may be useful for further characterizing the rate of natal homing and straying, but element signatures produced later in life may not provide accurate descriptions of environmental exposure histories and may not be as useful for stock discrimination.

Can Otolith Microchemistry be used to Identify Spawning Stocks and Characterize the Life History of Hickory Shad (*Alosa mediocris*)?

A Thesis

Presented to the Faculty of the Department of Biology

East Carolina University

In Partial Fulfillment of the Requirements for the Degree

M.S. Biology

By

Christopher Ryan Hill

December 2020

Can Otolith Microchemistry be used to Identify Spawning Stocks and Characterize the Life History of Hickory Shad (*Alosa mediocris*)?

By

Christopher Ryan Hill

Approved by:

DIRECTOR OF THESIS: _____

(Roger A. Rulifson, PhD)

COMMITTEE MEMBER: _____

(Timothy Erickson, PhD)

COMMITTEE MEMBER: _____

(Michael McCoy, PhD)

COMMITTEE MEMBER: _____

(Norman Halden, PhD)

CHAIT OF THE DEPARTMENT OF (Biology): _____

(John Stiller, PhD)

DEAN OF THE GRADUATE SCHOOL: _____

(Paul J. Gemperline, PhD)

ACKNOWLEDGEMENTS

I thank my advisor, Dr. Roger Rulifson for giving me the opportunity to do this project, for providing me with guidance from his years of experience as I completed this project. I thank Dr. Normal Halden for contributing his knowledge of geochemistry and experience with otolith chemistry, and I thank Dr. Halden's lab at the University of Manitoba for conducting LA-ICP-MS on my samples. I also thank the other members of my committee including Dr. Timothy Erickson and Dr. Michael McCoy for their interest in this project, and for reviewing my work and providing me with valuable feedback and advise.

I thank the North Carolina Wildlife Resources Commission, Division of Inland Fisheries, and the Sport Fish Restoration Act for funding this project. I especially thank Jeremy McCargo, the N.C. Wildlife Resources Commission Anadromous Fish Coordinator, and monitor of this project. I thank all the state and federal employees that captured and donated the Hickory Shad that made this project possible: Chuck Stence, Johnny Moore, Alan Weaver, Eric Brittle, Michael Odom, Kyle Rachels, Holly White, Katy Potaka, Ben Ricks, Chris Steward, Daniel Zapf, Beth Egbert, Bill Post, Bryant Bowen, Joseph Swan, and Reid Heid.

I thank Samantha Dowiarz for her friendship during this journey and the numerous contributions she made to this project. I thank all of the undergraduates that assisted me including Mackenzie Fain, Lacey Hall, Hannah Vernon, Haley Fulghum, Luis Oliveria, Candice Killian, Brittany Wiley, Mattie High, and Reece McArthur.

I thank my parents, grandparents, and my God above all for loving and supporting me along this path. I especially thank Kim Staley for the endless love, support, encouragement, and patience that she has shown me as I completed my master's degree.

TABLE OF CONTENTS

LIST OF TABLES

LIST OF FIGURES

CHAPTER 1

GENERAL INTRODUCTION

The stock concept

The concept of a "stock" is a fundamental component of fisheries management (Begg and Waldman 1999). Despite the significance of the term, fisheries managers often struggle to reach consensus on the explicit definition of a stock. This issue stems from the fact that considerable amounts of ambivalence are associated with the term. The term "stock" is frequently used in both biological and management entities, which are two interconnected fields with much overlap. In a biological sense, the term "stock" refers to groups that are characterized by low to no levels of genetic exchange, which means that members of the group tend to breed with each other more often than with members of other groups (Wang 2018). When applied to fisheries management, the term "stock" refers to a management unit. In this sense, a "stock" (also called a "fish stock" or "management stock") is a conspecific group of interbreeding fish that occupy a particular geographic region who are managed subjectively by a single government agency (MacLean and Evans 1981). Management stocks are the fundamental biological unit of modern fisheries management. However, management stocks are not always equivalent to biological entities (Carvalho and Hauser 1994; Waples and Gaggiotti 2006; Reiss et al. 2009). Instead, delineation of management stocks are highly dependent on the goals of managers and are frequently defined by political boundaries (Wang 2018). Therefore, the "stock structure" of a species is determined by its geo-spatial distribution among management areas, which are defined at the discretion of entities who govern resource allocation in those areas.

One of the primary goals of fisheries management is to create management plans that promote the sustainable harvest of a species and prevent overexploitation of that species. In order for fisheries managers to do this, it is important for them to understand the population structure of the species and how the harvest of that species is distributed (Grimes et al. 1987). This is especially critical when managers are tasked with designing harvest regulations for fisheries where multiple fish stocks of the same species are exploited differently (Ricker 1981). It is particularly challenging for fisheries managers to devise effective management strategies for highly migratory fish stocks that move in between management borders.

Migratory fish

Diadromy is the term used to describe fish migrations between the ocean and freshwater. Diadromous migrations are physiologically regulated and occur during predictable life stages (McDowall 1997). Anadromy is one type of diadromy where fish spend the majority of their adult lives in the ocean and migrate into freshwater in order to reproduce (McDowall 1997). This unique method of reproduction is used by relatively few fish taxa, as it requires several physiological shifts in osmoregulation in order to maintain osmotic balance (Myers 1949; McDowall 1988). Yet, relative sparsity in the number of anadromous species does not undermine its importance as a life history strategy. In fact, anadromous fish play several key ecological roles. For instance, with biomass derived from marine resources, anadromous fish act as nutrient conveyors between marine and freshwater systems during their spawning migrations (Garman and Macko 1998). Several anadromous species are important prey items for resident fish species during the spawning migration (Pine et al. 2005). In addition, many anadromous species return to their natal spawning grounds to reproduce, a phenomenon called philopatry, natal fidelity, or

natal homing (Salles et al. 2016). High rates of genetic isolation associated with philopatry can result in the evolution of numerous locally adapted spawning populations within a single species (Taylor 1991; Hendry et al. 2000; McDowall 2001; Waples et al. 2004; Keefer and Caudill 2014). Individual spawning populations are exceptionally vulnerable to anthropogenic disturbance. Habitat alteration, such as dam construction, prevent spawning populations from reaching their historic spawning grounds (Humphries and Winemiller 2009; Hall et al. 2011). Such impacts prevent the exchange of nutrients between habitats and can lead to subsequent food web alteration, species extirpation, and biodiversity loss (Kline et al. 1990; Bilby et al. 1996; Pringle et al. 2000; Jackson et al. 2001; Pess et al. 2008; Morita et al. 2009; Walters et al. 2009; Hall et al. 2011).

The challenge lies not in understanding the significance of anadromous fish conservation, but in devising effective management strategies that promote their preservation and sustainability. This task is challenging for fisheries managers, as anadromous fish tend to move between management jurisdictions during their seasonal migrations and often have complex life histories that vary within species or by watershed (McDowall 2001). In order for anadromous species managers to employ effective management strategies, it is imperative that they gain a detailed understanding of the species life history, the factors that delineate members of that species, and how those factors relate to the interests of fisheries management. The goal of this project was to provide such information about an understudied member of the family Clupeidae.

Hickory Shad, *Alosa mediocris* (Mitchell 1814)

The Hickory Shad is an anadromous Clupeid first described in New York by Samuel Mitchell in 1814 (Mitchell 1814). Hickory Shad inhabit Atlantic coastal systems in continental shelf waters close to shore. The center of Hickory Shad abundance appears to be concentrated in North Carolina (Rulifson 1994). Historically, the reported northern spawning limit of Hickory Shad has been the Maryland portion of the Susquehanna River (Murdy et al. 1997). However, some evidence suggests Hickory Shad may be spawning in the Christina River (Desmond Kahn DE Fish and Game, personal communication) and the Schuylkill River, a tributary of the Delaware River (Perillo and Butler 2009). Whether this is a new phenomenon, which may indicate progressive northern migration associated with climate change, or simply an undocumented pre-existing occurrence is unclear. Hickory Shad commonly live up to 7 years (Harris et al. 2007), and the maximum documented age is 9 years (MDDNR 2016). Most males and females reach sexual maturity between years 3 and 4 (Murauskas and Rulifson 2011). Fecundity estimates suggest that female Hickory Shad produce between 43,000 and 500,000 eggs per spawning season (Street 1969; Pate 1972; Batsavage and Rulifson 1998; Watkinson 2004). Eggs are initially adhesive and buoyancy increases with water flow; eggs hatch in 2-3 days (Mansueti 1962). Freshly hatched larvae are carried downstream until they reach the estuarine nursery areas and leave the system within the first year of life (Mansueti 1962; Hardy 1978; Rulifson 1994).

In early spring, Hickory Shad begin the inshore migration to spawn in freshwater tributaries. In North Carolina, adults enter tributaries in February, but more recently, agency monitoring studies capture earliest arrivals in inshore waters in the late fall (Rulifson et al. 2020). This trend occurs progressively later in the year in correlation with higher latitudes (Murauskas

and Rulifson 2011). During the annual spawning migration, Hickory Shad are a popular target species supporting multimillion-dollar sport fishery. While Hickory Shad represent a significant economic asset, little information exists concerning the life history (Waldman and Limburg 2003). The current management strategy for Hickory Shad groups them with three related Clupeids: Alewife (*Alosa pseudoharengus*), Blueback Herring (*Alosa aestivalis*), and American Shad (*Alosa sapidissima*). Management decisions rely on the common assumption that behavior and life history are similar for Hickory Shad and American Shad (Harris et al. 2007). However, the accuracy of using the life history for one species as a surrogate for another related species is unknown. For instance, it is assumed that like American Shad, Hickory Shad exhibit fidelity to their natal rivers and return there to spawn (Melvin et al. 1986). Yet expression of natal homing by Hickory Shad has never been confirmed in the literature. Hickory Shad do show evidence of iteroparity (Murauskas and Rulifson 2011) meaning they have more than one reproductive season over the course of life. Yet whether there is a shift to semelparity (spawn once and die) at the lowest latitudes of the range, like that observed in American Shad (Legett and Carscadden 1978), remains undocumented as well. While the full extent of life history similarities between the two species remains a mystery, there is more evidence to refute assumptions of homology than to support them. Recent genetic analyses demonstrate that Hickory Shad are more closely related to Alewife and Blueback Herring than to American Shad (Bloom and Lovejoy 2014).

Several other factors indicate clear discrepancies between the Hickory Shad and its relatives. As adults, Hickory Shad are larger than Alewife and Blueback Herring, and American Shad are larger than Hickory Shad. Hickory Shad have a lower jaw that extends beyond the upper jaw, while the lower jaw of American Shad fits into a groove within the upper jaw (Mitchell 1814; Uhler and Lugger 1876; Smith 1907; Hildebrand and Schroeder 1928).

American Shad, Alewife, and Blueback Herring populations have suffered drastic declines throughout their ranges (Dadswell and Rulifson 1994; Limburg and Waldman 2009; ASMFC 2017). Alewife and Blueback Herring are listed as "Species of Concern" by the National Marine Fisheries Service (NMFS 2006). Their statuses were recently reviewed under the Endangered Species Act (ESA). Using the best scientific information available, a status of threatened or endangered was not warranted under this review. Yet due to "significant data deficiencies", the status will be reviewed again in three to five years (NMFS 2019). It is clear that insufficient data regimes are a limiting factor in the ability to effectively manage all four of these species. Though the Hickory Shad seems to be increasing in abundance in some locations (Rulifson 1994; Waldman and Limburg 2003; Watkinson 2004; Murauskas and Rulifson 2011; Rulifson and Batsavage 2014), little is known regarding its life history characteristics or stock status. Considering the apparent vulnerability of the four anadromous alosines, it is critical that we gain a better understanding of the members and the stock status of each. If Hickory Shad are increasing in abundance, understanding the factors allowing them to do so may help support the recovery of their relatives. In contrast if Hickory Shad populations are imperiled, this would warrant management action in order to endorse their sustainability. The first step toward an effective management plan for Hickory Shad is to better understand the life history characteristics and spawning population structures. Much of this information can be interpreted from the chemical elements deposited within the calcified structures of the fish inner ear, also known as otoliths.

Otoliths

The functional morphology of the teleostean inner ear is homologous to that observed in other vertebrates. The inner ear is innervated by the eighth (auditory) cranial nerve and is comprised of three semicircular canals and three paired otolithic organs: the utricle, lagena, and saccule. Each otolithic organ contains a single otolith. Otoliths are linked mechanically to a polarized arrangement of cilia, which are embedded in a sensory epithelium (macula). Most somatic tissues in fish have a similar density to that of water, making them transparent to hydroacoustic vibrations. Being primarily composed of calcium carbonate (Campana 1999), otoliths are comparatively denser than most somatic tissues. The increased density of otoliths causes them to vibrate at a lagged rate with respect to the rest of the body. This provides a mechanism for auditory and vestibular perception, as differential movement between the otolith and macula cause lateral displacement of cilia. This in turn triggers action potentials in the sensory neurons of the innervating auditory nerve (Schellart and Wubbels 1998; Popper and Lu 2000; Helfman et al. 2009;).

Structures isolated within the lumen of each otolithic organ are suspended in a viscous, acellular medium called endolymph, which is secreted by the semipermeable inner ear epithelium. Otolith growth is characterized by the precipitation of dissolved ions from the endolymphatic fluid onto an organic protein matrix (Panella 1971; Payan et al. 1999). This precipitation occurs daily as organic material is deposited in layers that follow an endogenous rhythm (Panella 1971; Campana and Neilson 1985). High levels of aspartic and glutamic amino acids present in the protein matrix provide nucleation sites for the proceeding layer of calcium carbonate crystals (Degens et al. 1969; Wright 1991). Otoliths are metabolically inert structures, so features that become incorporated into the growing matrix cannot be resorbed and are

permanently retained in the otolith crystalline structure (Campana 1999; Friedrich and Halden 2008; Doubleday et al. 2014; Izzo et al. 2016; Thomas et al 2017). This unique form of biomineralization produces time-correlated concentric bands in the form of alternating optically translucent L-Zones and optically opaque D-zones (Campana and Neilson 1985; Mugiya et al. 1981; Secor et al. 1995; Borelli et al. 2003; Reis-Santos et al. 2013). Early literature on daily growth increments refers to L- and D-zones as incremental and discontinuous zones, respectively. In general, L-zones are the organically rich zones and their structure is dominated by protein fibers, while D-zones the highly calciferous layers most often present the polymorph of aragonite (Irie 1955; Carlstrom 1963; Degens et al. 1969; Mann et al. 1983; Morales-Nin 1986; Maisey 1988; Lecompte-Finger 1992; Oliveira et al. 1996; Campana 1999; Hussey and Mosegaard 2004). The accretion rate of L- and D- zones, and therefore otolith growth, is influenced simultaneously by a variety of endogenous and exogenous factors including temperature, metabolic activity, food availability, somatic growth, and circadian rhythm (Pannella 1971; Neilson and Geen 1982; Casselman 1990; Coghlan et al. 2007). Over time these patterns form concentric layers in the form of optically opaque and translucent zones that can be used to estimate the age of fish (Kalish et al. 1996).

Beyond the ability to display temporal patterns, otoliths also record spatial and metabolic information. The chemical composition of otolith increments are dependent on the chemical composition of the endolymph at the time of deposition. The chemical composition of the endolymph is influenced by the ambient environment because ions are transported from the gill epithelium into the endolymph through osmoregulatory, metabolic, and circulatory functions (Campana 1999; Allemand et al. 2008). Divalent cations (e.g., Sr^{2+}, Ba^{2+}) with ionic radii like that of calcium (Ca^{2+}) can substitute for calcium in the crystalline lattice of the otolith or can

coprecipitate as carbonates (Campana 1999). Incorporation of elements that are not under strict physiological regulation (e.g., Sr^{2+}, Ba^{2+}) reflect the abundance of those elements in the ambient environment (Bath et al. 2000; Kafemann et al. 2000; Elsdon and Gillanders 2003; Lill et al. 2019). Incorporation of physiologically regulated elements (e.g., Mg^{2+}) reflect the metabolic activity of the fish near the time of deposition (Campana 1999). Hence, unique chemical properties of the ambient environment are constantly recorded and permanently retained in the otolith.

The same biogeochemical properties allowing otoliths to serve their respective physiological functions make them convenient research tools. The acellular nature, continuous accretion patterns, and ability to record environmental histories make otoliths useful structures in a range of scientific disciplines. Widespread interest in the potential research application of otoliths was established when Reibisch (1899) discovered that rings were formed annually in otoliths and could be used to age fish (Reibisch 1899, cited by Campana 1999). Since that time, use of otoliths has become common in many branches of fisheries science. Modern advancements in chemical analysis of otoliths using probe-based analytical technologies such as LA-ICP-MS allow elemental and isotopic assays of samples to be analyzed with precision (Limburg and Elfman 2017). In the case of otoliths, these techniques can be used to make quantitative inferences concerning the life histories and environmental exposures of fishes. A plethora of examples exist that demonstrate the use of otolith chemistry to rendering valuable information, including the reconstruction migration routes (Tsukamonto and Arai 2001; Jessop et al. 2002; Gillanders 2005; Elsdon and Gillanders 2006; Daverat et al. 2011), determination of natal and nursery areas (Rooker et al. 2001; Brown 2006; Vasconcelos et al. 2007; Bradbury et al. 2011), detection of diadromy (McCulloch et al. 2005), identification of stock structure (Kalish

et al. 1996; Campana et al. 2000; Bergenius et al. 2005), and many more. Otolith chemistry is a particularly convenient tool for studying diadromous fishes because the movement between salinity gradients create distinct chemical signatures in otoliths that reflect the various ambient conditions through which they travel. For instance, strontium and barium have been used extensively in to reconstruct environmental histories (Halden et al. 1995; Elfman et al. 2000; Milton and Chenery 2001; Arai and Mortia 2005; McCulloch et al. 2005; Walther and Limburg 2012) because they have an inverse relationship across salinity gradients; strontium is high in saltwater and low in freshwater, while barium is high in freshwater and low in saltwater (Brown and Severin 2009; Miller 2011). Other elements such as zinc (Limburg and Elfman 2017) and magnesium (Elsdon and Gillanders 2002; Miller 2007) may also be correlated with salinity and growth. To date, thirty-one different elements have been observed in fish otoliths (Campana 1999). While the exact mechanisms and rates at which many of these elements assimilate in otoliths remains poorly understood, a number of these have been used to track environment exposure histories (Elsdon et al. 2008). Seven such elements (Mg^{2+}, Mn^{2+}, Cu^{2+}, Zn^{2+}, Sr^{2+}, Ba^{2+}, and Pb^{2+}), were used in this project to characterize the life history of Hickory Shad.

Goals and objectives

The overall goal of this project was to determine if element signatures in otoliths can be used to separate spawning populations of Hickory Shad throughout the species range. Hickory Shad were captured in 26 locations along the known spawning range (Figure 1-1; Table 1-1), and LA-ICP-MS analysis was conducted on the left sagittal otolith. LA-ICP-MS was used to quantify the relative abundance of elements along a continuous transect that ran from the ventral edge of the otolith through the core to the dorsal edge (Figures 1-2, 1-3). For each Hickory Shad, this

resulted in seven “element profiles” (one for each element) representing a record of the ambient conditions experienced during the life of each fish (Figures 1-3, 1-4). The goal of Chapter 2 was to look for evidence that Hickory Shad exhibit natal homing. Evidence of natal homing was based on 1) overall similarities between the element profiles of Hickory Shad that were captured in the same locations, and 2) quantitative estimates of natal watershed element signatures referred to as the “otolith core data”, which were obtained from otolith regions accreted in the first year of life. I used a Gaussian mixture model to identify clusters in the otolith core data, and compared the number of Hickory Shad from each capture location that were assigned to the same clusters or clusters with similar characteristics. The following hypothesis was tested in Chapter 2:

H_0 Hickory Shad that were captured in the same location will be assigned to the same cluster.

H_A Hickory Shad that were captured in the same location will not be assigned to the same cluster.

Accepting the null hypothesis suggested natal homing, and rejecting the null hypothesis indicated no natal homing. A major caveat of Chapter 2’s approach to inference is that if Hickory Shad do exhibit natal homing, then otolith chemistry would only to be able to separate spawning populations if there are actually differences in element signatures in the watersheds to which they home. In other words, even if there is a very high rate of natal homing, Hickory Shad that are born in and return to watersheds with similar element signatures would be indistinguishable. The objective of Chapter 2 was to see if Hickory Shad that were captured in the same location were also born in the same location (i.e., if they were assigned to the same cluster based on the element signature of their otolith cores). Therefore, if Hickory Shad captured in several different

locations are assigned to the same cluster (because they all have similar elemental characteristics), does that indicate mixing between these capture locations, or does it simply mean there is no difference between the element signatures of these capture locations? In order to answer this question with confidence, information about the element signatures of the capture watersheds are required.

In Chapter 3, element ratios on the ventral edges of the otoliths were used to estimate the element signatures of capture locations, which in turn were used to estimate which watersheds have different element signatures. A generalized additive model was fit to each element profile between the otolith core and the last data point on the ventral edge. The single last data point on the ventral edge (which represents approximately 30 μm) was assumed to be a prediction of the element signature of the capture watershed. In Chapter 3, the following hypothesis was tested:

H_0 Elements will not be different between capture locations.

H_A Elements will be different between capture locations.

Finally, Chapter 4 provides a brief conclusion that relates the results of Chapters 2 and 3 and addresses our recommendations based on these findings.

Literature Cited

Allemand, D., N, Mayer-Gostan, H. De Pontual, G. Boeuf, and P. Payan. 2008. Fish otolith calcification in relation to endolymph chemistry. Pages 291-308 *in* E. Bäuerlein, editor. Handbook of Biomineralization. Wiley-VCH Verlag GmbH and Company, Weinheim, Germany. doi:10.1002/9783527619443.ch17.

Arai, T., and K. Morita. 2005. Evidence of multiple migrations between freshwater and marine habitats of *Salvelinus leucomaenis*. Journal of Fish Biology 66: 888–895.

ASMFC (Atlantic States Marine Fisheries Commission). 2017. Interstate fisheries management program overview: Shad and River Herring. ASMFC, Washington, DC.

Bath, G., S. Thorrold, C. Jones, S. Campana, J. MacLaren, and J. Lam. 2000. Strontium and barium uptake in aragonitic otoliths of marine fish. Geochimica et Cosmochimica Acta: 64:1705-1714.

Batsavage, C. F., and R. A. Rulifson. 1998. Life history aspects of the Hickory Shad (Alosa mediocris*)* in the Albemarle Sound/Roanoke River watershed, North Carolina. Completion Report. East Carolina University, ICMR Contribution Series No. ICMR-98-02.

Begg, G. A., and J. Waldman. 1999. An holistic approach to fish stock identification. Fisheries Research 43(1):35-44. DOI: 10.1016/S0165-7836(99)00065-X

Bergenius, M. A. J., B. D. Mapstone, G. A. Begg, and C. D. Murchie. 2005. The use of otolith chemistry to determine stock structure of three epinepheline serranid coral reef fishes on the Great Barrier Reef, Australia. Fisheries Research 72: 253-270.

Bilby, R. E., B. R. Fransen, and P. A. Bisson. 1996. Incorporation of nitrogen and carbon from spawning coho salmon into the trophic system of small streams: evidence from stable isotopes. Canadian Journal of Fisheries and Aquatic Sciences 53:164–173.

Bloom, D. D., and N. R. Lovejoy. 2014. The evolutionary origins of diadromy inferred from a time-calibrated phylogeny for Clupeiformes (Herring and allies). Proceedings of the Royal Society B: Biological Sciences 281:20132081.

Borelli, G., M. E. Guibbolini, N. Mayer-Gostan, F. Priouzeau, H. De Pontual, D. Allemans, S. Puverel, E. Tambutte, and P. Payan. 2003. Daily variations of endolymph composition: relationship with the otolith calcification process in trout. The Journal of Experimental Biology 206: 2685-2692.

Bradbury, I. R., S. Hubert, B. Higgins, S. Bowman, I. G. Paterson, P. V. R. Snelgrove, C. J. Morris, R. S. Gregory, D. C. Hardie, T. Borza, and P. Bentzen. 2011. Evaluating SNP ascertainment bias and its impact on population assignment in Atlantic cod, *Gadus morhua*. Molecular Ecology Resources 11: 218–225. doi:10.1111/j.1755-0998.2010. 02949.x.

Brown, J. A. 2006. Classification of juvenile flatfishes to estuarine and coastal habitats based on the elemental composition of otoliths. Estuarine Coastal and Shelf Science 66:594–611.

Brown R. J., and K. P. Severin. 2009. Otolith chemistry analyses indicate that water Sr:Ca is the primary factor influencing otolith Sr:Ca for freshwater and diadromous fish but not for marine fish. Canadian Journal of Fisheries and Aquatic Sciences 66:1790–1808.

Campana, S. E. 1999. Chemistry and composition of fish otoliths: pathways, mechanisms, and applications. Marine Ecology Progress Series 188:263–297.

Campana, S. E. and J. D. Neilson. 1985. Microstructure of fish otoliths. Canadian Journal of Fisheries and Aquatic Science 42:1014-1032.

Campana, S. E., G. A. Chouinard, J. M. Hanson, A. Frechet, and J. Brattey. 2000. Otolith elemental fingerprints as biological tracers of fish stocks. Fisheries Research 46:343–357.

Carlstrom D. 1963. A crystallographic study of vertebrate otoliths. Biology Bulletin (Woods Hole) 125:441–463.

Carvalho, C. R., and L. Hauser. 1994. Molecular genetics and the stock concept in fisheries. Reviews in Fish Biology and Fisheries 4: 326:350.

Casselman, J. M. 1990. Growth and relative size of calcified structures of fish. Transactions of the American Fisheries Society 119:673–688.

Coghlan Jr., S. M., M. S. Lyerly, T. R. Bly, J. W. Williams, D. Bowman, and R. Hannigan. 2007. Otolith chemistry discriminates among hatchery-reared and tributary-spawned Salmonines in a tailwater system. North American Journal of Fisheries Management 27:531-541.

Dadswell, M. J., and R. A. Rulifson. 1994. Macrotidal estuaries: A region of collision between migratory marine animals and tidal power development. Biological Journal of the Linnean Society 51:93-113.

Daverat, F., N. Tapie, L. Quiniou, R. Maury-Brachet, R. D. Riso, M. Eon, J. Laroche, and H. Budzinski. 2011. Otolith microchemistry interrogation of comparative contamination by Cd, Cu and PCBs of eel and flounder, in a large SW France catchment. Estuarine Coastal and Shelf Science 92(3):332-338. DOI: 10.1016/j.ecss.2011.01.011.

Degens E. T., W. G. Deuser, and R. L. Haedrich. 1969. Molecular structure and composition of fish otoliths. Marine Biology 2(2): 105–113. doi:10.1007/BF00347005.

Doubleday Z. A., H. H. Harris, C. Izzo, B. M. Gillanders. 2014. Strontium randomly substituting for calcium in fish otolith aragonite. Analytical Chemistry. 86(1):865–869. doi:10.1021/ac4034278.

Elfman, M., K. E. Limburg, P. Kristiansson, H. Svedäng, L. Westin, H. Wickström, K. Malmqvist, and J. Pallon. 2000. Complex life histories of fishes revealed through natural information storage devices: case studies of diadromous events as recorded by otoliths. Nuclear Instruments and Methods in Physics Research B: 161–163, 877–881.

Elsdon, T. S., and B. M. Gillanders. 2002. Interactive effects of temperature and salinity on otolith chemistry: challenges for determining environmental histories of fish. Canadian Journal of Fisheries and Aquatic Sciences 59(11) https://doi.org/10.1139/f02-154.

Elsdon, T. S., and B. M. Gillanders. 2003. Reconstructing migratory patterns of fish based on environmental influences on otolith chemistry. Fish Biology and Fisheries 13: 219-235.

Elsdon, T. S., and B. M. Gillanders. 2006. Identifying migratory contingents of fish by combining otolith Sr:Ca with temporal collections of ambient Sr:Ca concentrations. Journal of Fish Biology 69:643-657.

Elsdon, T. S., B. K. Wells, S. E. Campana, B. M. Gillanders, C. M. Jones, K. E. Limburg, D. H. Secor, S. R. Thorrold, and B. D. Walther. 2008. Otolith chemistry to describe movement and life-history parameters of fishes: hypotheses, assumptions, limitations and inferences. Oceanography and Marine Biology: an Annual Review 46: 297-330.

Friedrich, L. A., and N. M. Halden. 2008. Alkali element uptake in otoliths: a link between the environment and otolith microchemistry. Environmental Science and Technology 42: 3514-3518.

Garman, G. C., and S. A. Macko. 1998. Contribution of marine-derived organic matter to an Atlantic coast, freshwater, tidal stream by anadromous clupeid fishes. Journal of the North American Benthological Society 17: 277–285.

Gillanders, B. M. 2005. Otolith chemistry to determine movements of diadromous and freshwater fish. Aquatic Living Resources 18(3):291–300.

Grimes, C. B., A. G. Johnson, and W. A. Fable, Jr. 1987. Delineation of king mackerel (*Scoberomorus vacalla*) stocks along the US east coast and in the Gulf of Mexico. In: Kumpf, H. E., R. N. Vaught, C. B. Grimes, A. J. Johnson, and E. L. Nakamura (Editors), Proceedings of the stock identification workshop, 5-7 November 1885, Panama City Beach, FL. NOAA Technical Memorandum NMFS- SEFC-199. US Government Printing Office pp. 186-187.

Halden, N. M., J. A. Babaluk, J. L. Campbell, and W. J. Teesdale. 1995. Scanning proton micropobe analysis of strontium in an Arctic charr, *Salvanius alpinus*, otolith: implication for the interpretation of anadromy. Environmental Biology of Fishes 43:333-339.

Hall, C. J., A. Jordaan, and M. G. Frisk. 2011. The historic influence of dams on diadromous fish habitat with a focus on herring and hydrologic longitudinal connectivity. Landscape Ecology 26:95-107.

Hardy, J. D. 1978. Development of fishes of the Mid-Atlantic bight: An atlas of egg, larval and juvenile stages; Acipenseridae through Ictaluridae. U.S. Fish and Wildlife Service. Volume 1:75-88.

Harris, J. E., R. S. McBride, and R. O. Williams. 2007. Life history of Hickory Shad in the St. Johns River, Florida. Transactions of the American Fisheries Society 136(6): 1463-1471. doi:10.1577/T06-187.1.

Helfman, G. S., B. B. Collette, D. E. Facey, and B. W. Bowen. 2009. The diversity of fishes: biology, evolution, and ecology. Chichester, UK. Wiley-Blackwell.

Hendry, A. P., J. K. Wenburg, P. Bentzen, E. C. Volk, and T. P. Quinn. 2000. Rapid evolution of reproductive isolation in the wild: evidence from introduced salmon. Science 290:516–518.

Hildebrand, S. F., and W. C. Schroeder. 1928. Fishes of Chesapeake Bay. Bulletin of the United States Bureau of Fisheries 43(1):1-366.

Humphries, P., and P. O. Winemiller. 2009. Historical impacts on river fauna, shifting baselines, and challenges for restoration. Bioscience 59(8): 673-684.

Hüssy, K., and H. Mosegaard. 2004. Growth and otolith accretion characteristics modelled in a bioenergetics context. Canadian Journal of Fisheries and Aquatic Sciences 61(6):1021–1031. doi:10.1139/f04-038.

Irie, T. 1955. The crystal texture of the otolith of a marine teleost, *Pseudosciaena*. Journal of the Faculty of Fisheries and Animal Husbandry Hiroshima University 1:1-13.

Izzo, C., Z.A. Doubleday, and B. M. Gillanders. 2016. Where do elements bind within the otoliths of fish? Marine and Freshwater Research 67(7): 1072-1076. doi: https://doi.org/10.1071/MF15064.

Jackson, J. B. C., M. Kirby, W. Berger, K. A. Bjorndal, L. Botsford, B. J. Bourque, R. H. Bradbury, R. G. Cooke, J. Erlandson, J. A. Estes, T. P. Hughes, S. Kidwell, C. Lange, H. Lenihan, J. M. Pandolfi, C. Peterson, R. Steneck, M. J. Tegner, and R. R. Warner. 2001. Historical overfishing and the collapse of coastal ecosystems. Science 293:629–638.

Jenkins, R. E., and N. M. Burkhead. 1993. Freshwater Fishes of Virginia. American Fisheries Society, Bethesda, Maryland. pp. 223-224.

Jessop, B., J. Shiao, Y. Iizuka, and W. Tzeng. 2002. Migratory behavior and habitat use by American eels *Anguilla rostrata* as revealed by otolith microchemistry. Marine Ecology Progress Series 233:217–229. doi:10.3354/meps233217.

Kafemann, R., S. M. Adlerstein, and R. Neukamm. 2000. Variation in otolith strontium and calcium ratios as an indicator of life histories strategies of freshwater species within a brackish water system. Fisheries Research 46: 313-325.

Kalish, J. M., J. M. Johnston, J. S. Gunn, and N. P. Clear. 1996. Use of the bomb radiocarbon chronometer to determine age of southern bluefin tuna *Thunnus maccoyii*. Marine Ecology Progress Series 143(1/3):1-8.

Keefer, M. L., and C. C. Caudill. 2014. Homing and straying by anadromous salmonids: a review of mechanisms and rates. Reviews in Fish Biology and Fisheries 24:333-368.

Kline T. C., J. J. Goering, O. A. Mathisen, P. H. Poe, and P. L. Parker. 1990. Recycling of elements transported upstream by runs of Pacific salmon I ∂^{15}N and ∂^{13}C evidence in Sashin Creek, southeastern Alaska. Canadian Journal of Fisheries and Aquatic Sciences 47:136–144.

Lecomte-Finiger, R. 1992. Growth history and age at recruitment of European glass eels (*Anguilla anguilla*) as revealed by otolith microstructure. Marine Biology 114: 205-210.

Leggett, W. C., and J. E. Carscadden. 1978. Latitudinal variation in reproductive characteristics of American shad (*Alosa sapidissima*): evidence for population specific life history strategies in fish. Journal of the Fisheries Research Board of Canada 35:1469–1478.

Lill, J. O., V. Finnas, Y. Heimbrand, M. Blass, S. Frojdo, Y. Lahaye, J. M. K. Slotte, J. Nyman, E. Jokikokko, M. von Numbers, and H. Hagerstrand. 2019. Information depths of analytical techniques assessing whitefish otolith chemistry. Nuclear Institute and Methods in Physics Research B 77:104:108.

Limburg, K. E., and M. Elfman. 2017. Insights from two-dimensional mapping of otolith chemistry. Journal of Fish Biology 90(2): 480-491.

Limburg, K. E., and J. R. Waldman. 2009. Dramatic declines in North American diadromous fishes. BioScience 59:955-965.

MacLean, J. A., and D. O. Evans. 1981. The stock concept, discreteness of fish stocks, and fisheries management. Canadian Journal of Fisheries and Aquatic Sciences 38: 1889-1898.

Maisey, J. 1988. Notes on the structure and phylogeny of vertebrate otoliths. Copeia 1998(1):257-259.

Mann, S., S. B. Parker, M. D. Ross, A. J. Skarnucis, and W. J. P. Williams. 1983. The ultrastructure of the calcium carbonate balance organs of the inner ear: an ultra-high resolution electron microscopy study. Proceedings of the Royal Society B Biological Science 218: 415-424.

Mansueti, R. J. 1962. Eggs, larvae, and young of the Hickory Shad, *Alosa mediocris*, with comments on its ecology in the estuary. Chesapeake Science 3:173-205.

McCulloch, M., M. Cappo, J. Aumend, and W. Muller. 2005. Tracing the life history of individual barramundi using laser ablation MC-ICP-MS Sr-isotopic and Sr/Ba ratios in otoliths. Marine and Freshwater Research 56:637–644.

McDowall, R. M. 1988. Diadromy in Fishes: migrations between freshwater and marine environments. Portland: Timber Press.

McDowall, R. M. 1997. The evolution of diadromy in fishes (revisited) and its place in phylogenetic analysis. Reviews in Fish Biology and Fisheries 7(4): 443-462.

McDowall R. M. 2001. Anadromy and homing: two life-history traits with adaptive synergies in salmonid fishes? Fish and Fisheries 2:78–85.

MDDNR (Maryland Department of Natural Resources). 2016. Hickory Shad. www.Dnr2.Maryland.gov/Fisheries.

Melvin, G. D., M. J. Dadswell, and J. D. Martin. 1986. Fidelity of American shad, *Alosa sapidissima* (Clupeidae), to its river of previous spawning. Canadian Journal of Fisheries and Aquatic Sciences 43:640-646.

Miller, J. A. 2007. Scales of variation in otolith elemental chemistry of juvenile staghorn sculpin (*Leptocottus armatus*) in three Pacific Northwest estuaries. Marine Biology 151(2): 483–494.

Miller, J. A. 2011. Effects of water temperature and barium concentration on otolith composition along a salinity gradient: implications for migratory reconstructions. Journal of Experimental Marine Biology and Ecology 405:42–52.

Milton, D. A., and S. R. Chenery. 2001. Sources and uptakes of trace metals in otoliths of juvenile barramundi (*Lates calcarifer).* Journal of Experimental Marine Biology and Ecology 264: 47-65.

Mitchill, S. L. 1814. Report, in part, on the fishes of New-York. Transactions of the Literary and Philosophical Society. New York. p. 450.

Morales-Nin, B. 1986. Chemical composition of the otoliths of the sea bass (*Dicentrarchus labrax* Linnaeus, 1758) (Pisces, Serranidae). Cybium 10(2):115–120.

Morita K., S. H. Morita, and S. Yamamoto. 2009. Effects of habitat fragmentation by damming on salmonid fishes: lessons from white-spotted charr in Japan. Ecological Research 24(4):711–722.

Mugiya, Y., N. Watabe, J. Yamada, J. M. Dean, D. G. Dunkelberger, and M. Shimuzu. 1981. Diurnal rhythm in otolith formation in the goldfish, *Carassius auratus*. Comparative Biochemistry and Physiology 68A: 659-662.

Murdy, E. O., R. S. Birdsong., and J. A. Musick. 1997. Fishes of Chesapeake Bay. Smithsonian Institution Press, Washington and London. pp. 75-76.

Murauskas, J. G., and R. A. Rulifson. 2011. Reproductive development and related observations during the spawning migration of Hickory Shad. Transactions of the American Fisheries Society 140:1035-1048.

Myers, G. S. 1949. Usage of anadromous, catadromous and allied terms for migratory fishes. Copeia 2:89-97.

NMFS. 2006. Endangered and Threatened Species; Revision of Species of Concern List, Candidate Species Definition, and Candidate Species List. 71 FR 61022-61025. https://federalregister.gov/a/E6-17249

NMFS. 2019. Endangered and Threatened Wildlife and Plants; Endangered Species Act Listing Determination for Alewife and Blueback Herring. 84 FR 28630. 28630-28666. 2019-12908. https://www.federalregister.gov/d/2019-12908

Neilson, J. D., and G. H. Geen. 1982. Otoliths of Chinook salmon (*Oncorhynchus tshawytscha*): daily growth increments and factors influencing their production. Canadian Journal of Fisheries and Aquatic Sciences 39:1340–1347.

Oliveira, A. M., M. Farina, I. P. Ludka, and B. Kachar. 1996. Vaterite, calcite and aragonite in the otoliths of three species of piranha. Naturwissenschaften 83: 133–135.

Palace, V. P., N. M. Halden, P. Yang, R. E. Evans, and G. Sterling. 2007. Determining residence patterns of rainbow trout using laser ablation inductively coupled plasma mass spectrometry (LA-ICP-MS) analysis of selenium in otoliths. Environmental Science and Technology 41:3679-3683.

Pannella, G. 1971. Fish otoliths: daily growth layers and periodical patterns. Science 173:1124:1127.

Pate, P. P. 1972. Life history aspects of the hickory shad, *Alosa mediocris* (Mitchell), in the Neuse River, North Carolina. Master's thesis. North Carolina State University, Raleigh.

Payan, P., A. Edeyer, H. De Pontual, et al. 1999. Chemical composition of saccular endolymph and otolith in fish inner ear: lack of spatial uniformity. American Journal of Physiology 277: 123–131.

Perillo, J. A., and L. H. Butler. 2009. Evaluating the use of Fairmont Dam fish passage facility with application to anadromous fish restoration in the Schuylkill River, Pennsylvania. Journal of the Pennsylvania Academy of Science 83(1): 24-33.

Pess, G. R., M. L. McHenry, T. J. Beechie, and J. Davies. 2008. Biological impacts of the Elwha River dams and potential salmonid reasons to dam removal. Northwest Science 82:72–90.

Pine, W. P., T. J. Kwak, D. S. Waters, and J. A. Rice. 2005. Diet selectivity of introduced flathead catfish in coastal rivers. Transactions of the American Fisheries Society 134:901-909. DOI: 10.1577/T04-166.1.

Popper, A. N., and Z. Lu. 2000. Structure-function relationships in fish otolith organs. Fisheries Research 46:15-25.

Pringle C. M., M. C. Freeman, and B. J. Freeman. 2000. Regional effects of hydrologic alterations on riverine macrobiota in the New World: tropical-temperate comparisons. Bioscience 50:807–823.Reibisch, J. 1899. Ueber die Eizahl bei Pleuronectes platessa und die Altersbestimmung dieser Form aus den Otolithen. Wissenschaftliche Meeresuntersuchungen, K. Kommission Kiel, Band 4:231–248.

Reis-Santos, P., S. E. Tanner, R. P. Vasconcelos, T. S. Elsdon, H. N. Cabral, and B. M. Gillanders. 2013. Connectivity between estuarine and coastal fish populations: contributions of estuaries are not consistent over time. Marine Ecology Progress Series 491:177-186.

Reiss, H., H. Galice, M. Dickey-Collas, and W. J. Wolff. 2009. Genetic population structure of marine fish: mismatch between biological and fisheries management units. Fish and Fisheries 10: 361-395.

Ricker, W. E. 1981. Changes in the average size and average age of Pacific salmon. Canadian Journal of Fisheries and Aquatic Sciences 38: 1636-1656.

Rooker J. R., D. H. Secor, V. S. Zdanowicz, and T. Itoh. 2001. Discrimination of northern bluefin tuna from nursery areas in the Pacific Ocean using otolith chemistry. Marine Ecology Progress Series 218:275–282.

Rulifson, R. A. 1994. Status of anadromous Alosa along the east coast of North America. Pages 134–158 in J. E. Cooper, R. T. Eades, R. J. Klauda, and J. G. Loesch, editors.

Anadromous Alosa Symposium. American Fisheries Society, Tidewater Chapter, Bethesda, Maryland.

Rulifson, R. A., and C. F. Batsavage. 2014. Population demographics of hickory shad (*Alosa mediocris*) during a period of population growth. Fisheries Bulletin 112(2-3): 221-236. Doi:10.7755/FB.112.2-3.8.

Rulifson, R. A., J. P. Smith, S. A. Dowiarz, S. Meyers, C. R. Hill, and M. Brewer. 2020. Population Status and Stock Identification of NC Hickory Shad Using Multiple Techniques. Sport Fish Restoration Act, Final Report to North Carolina Wildlife Resources Commission, Contract DIF-0029, Raleigh.

Salles, O. C., B. Pujol, J. A. Maynard, G. R. Almany, M. L. Berumen, G. P. Jones, P. Saenz-Agudelo, M. Srinivasa, S. R. Thorrold, and S. Planes. 2016. First genealogy for a wild marine fish population reveals multigenerational philopatry. Proceedings of the National Academy of Sciences of the United States of America 113(46): 13245-13250.

Schellart, N. A. M, and R. J. Wubbels. 1998. The auditory and mechanosensory lateral line system. The Physiology of Fishes, 2nd ed. New York: CRC Press, pp. 283–312.

Secor, D. H., A. Henderson-Arzapalo, and P. M. Piccoli. 1995. Can otolith microchemistry chart patterns of migration and habitat utilization in anadromous fishes? Journal of Experimental Marine Biology and Ecology 192(1):15–33. doi:10.1016/0022-0981(95)00054-U

Smith, H. M. 1907. The fishes of North Carolina. Systematic Catalogue of Fishes. p119-122. E.M. Uzzell & Co. Raleigh, NC.

Street, M. W. 1969. Fecundity of the hickory shad in the Altamaha River, Georgia. Georgia Game and Fish Commission, Marine Fisheries Division Contribution Series 14, Brunswick.

Taylor E. B. 1991. A review of local adaptation in Salmonidae, with particular reference to Pacific and Atlantic salmon. Aquaculture 98:185–207.

Thomas. O. R. B., K. Ganio, B. R. Roberts, and S. E. Swearer. 2017. Trace element–protein interactions in endolymph from the inner ear of fish: implications for environmental reconstructions using fish otolith chemistry. Metallomics. 9(3):239–249. doi:10.1039/C6MT00189K.

Tsukamoto, K., and T. Arai. 2001. Facultative catadromy of the eel *Anguilla japonica* between freshwater and seawater habitats. Marine Ecology Progress Series 220: 265-276.

Uhler, P. R., and O. Lugger. 1876. Report of the Commissioners of Fisheries of Maryland. Annapolis, Maryland. pp. 159-160.

Vasconcelos R. P., P. Reis-Santos, S. E. Tanner, V. Fonseca C. Latkoczy, D. Günther, M. J. Costa, and H. Cabral. 2007. Discriminating estuarine nurseries for five fish species through otolith elemental fingerprints. Marine Ecology Progress Series 350: 117−126. doi: 10.3354/meps07109.

Waldman, J. R., and K. E. Limburg. 2003. The world's Shads: summary of their status, conservation, and research needs. American Fisheries Society Symposium 35:363-368.

Walters A. W., R. T. Barnes, and D. M. Post. 2009. Anadromous alewives (*Alosa pseudoharengus*) contribute marine-derived nutrients to coastal stream food webs. Canadian Journal of Fisheries and Aquatic Sciences 66:439–448.

Walther, B. D., and K. E. Limburg. 2012. The use of otolith chemistry to characterize diadromous migrations. Journal of Fish Biology 81:796-825.

Wang, J. Y. 2018. Encyclopedia of Marine Mammals. Academic Press 941:945. https://doi.org/10.1016/B978-0-12-804327-1.00248-X.

Waples R. S., and O. Gaggiotti. 2006. What is a population? An empirical evaluation of some genetic methods for identifying the number of gene pools and their degree of connectivity. Molecular Ecology 15: 1419–1439.

Waples, R. S., D. J. Teel, K. W. Myers, and A. R. Marshall. 2004. Life-history divergence in Chinook salmon: historic contingency and parallel evolution. Evolution 58:386– 403.

Watkinson, E. R. 2004. Age, growth, and fecundity of hickory shad (*Alosa mediocris*) in a Virginia coastal river. Master's thesis. Virginia Commonwealth University, Richmond.

Wright P. J. 1991. The influence of metabolic rate on otolith increment width in Atlantic salmon parr, *Salmo salar*. Journal of Fisheries Biology 38(6):929–933. doi:10.1111/j.1095-8649.1991. tb03632.x.

Tables and figures

Table 1-1. Description of capture locations and associated sample sizes used for otolith microchemistry.

River	Males	Females	N	Parent River	Estuary	State
Susquehanna	5	5	10	Susquehanna	Chesapeake Bay	MD
Patapsco	6	5	11	Patapsco	Chesapeake Bay	MD
Potomac	4	7	11	Potomac	Chesapeake Bay	DC
Patuxent	4	6	10	Patuxent	Chesapeake Bay	MD
Choptank	5	5	10	Choptank	Chesapeake Bay	MD
Nanticoke	3	7	10	Nanticoke	Chesapeake Bay	DE
Rappahannock	7	5	12	Rappahannock	Chesapeake Bay	VA
Appomattox	7	5	12	James	Chesapeake Bay	VA
James	9	7	16	James	Chesapeake Bay	VA
Blackwater	6	5	11	Chowan	Albemarle Sound	VA
Nottoway	9	5	14	Chowan	Albemarle Sound	VA
Roanoke	9	7	16	Roanoke	Albemarle Sound	NC
Cashie	6	6	12	Roanoke	Albemarle Sound	NC
Tar	9	4	13	Pamlico	Pamlico Sound	NC
Tar- Swift Creek	4	5	9	Pamlico	Pamlico Sound	NC
Contentnea	5	6	11	Neuse	Pamlico Sound	NC
Swift	4	5	9	Neuse	Pamlico Sound	NC
Neuse-Upper	6	4	10	Neuse	Pamlico Sound	NC
Pitchkettle	10	9	19	Neuse	Pamlico Sound	NC
Cape Fear-Town Creek	7	3	10	Cape Fear	Cape Fear	NC
Cape Fear- Upper	6	3	9	Cape Fear	Cape Fear	NC
Waccamaw	0	7	7	Waccamaw	Winyah Bay	SC
Santee	4	2	6	South Santee	South Santee	SC
Ogeechee	6	6	12	Ogeechee	Ossabaw Sound	GA
Altamaha	3	7	10	Altamaha	Altamaha Sound	GA
St. Johns	5	5	10	St Johns	St Johns	FL

Table 1-2. List of alpha codes used to refer to each river for aesthetic simplicity.

River	Code
Susquehanna	Sus
Patapsco	Pata
Potomac	Poto
Patuxent	Patux
Choptank	Chop
Nanticoke	Nant
Rappahannock	Rapp
Appomattox	App
James	James
Blackwater	Blk
Nottoway	Notto
Roanoke	Roan
Cashie	Cash
Tar	Tar
TarSwift	TarSwift
Contentnea	Cont
Swift	Swift
Neuse-Upper	NU
Pitchkettle	Pitch
Cape Fear -Town Creek	CFTC
Cape Fear-Upper	CFU
Waccamaw	Wacca
Santee	Sant
Ogeechee	Ogee
Altamaha	Alt
St Johns	StJo

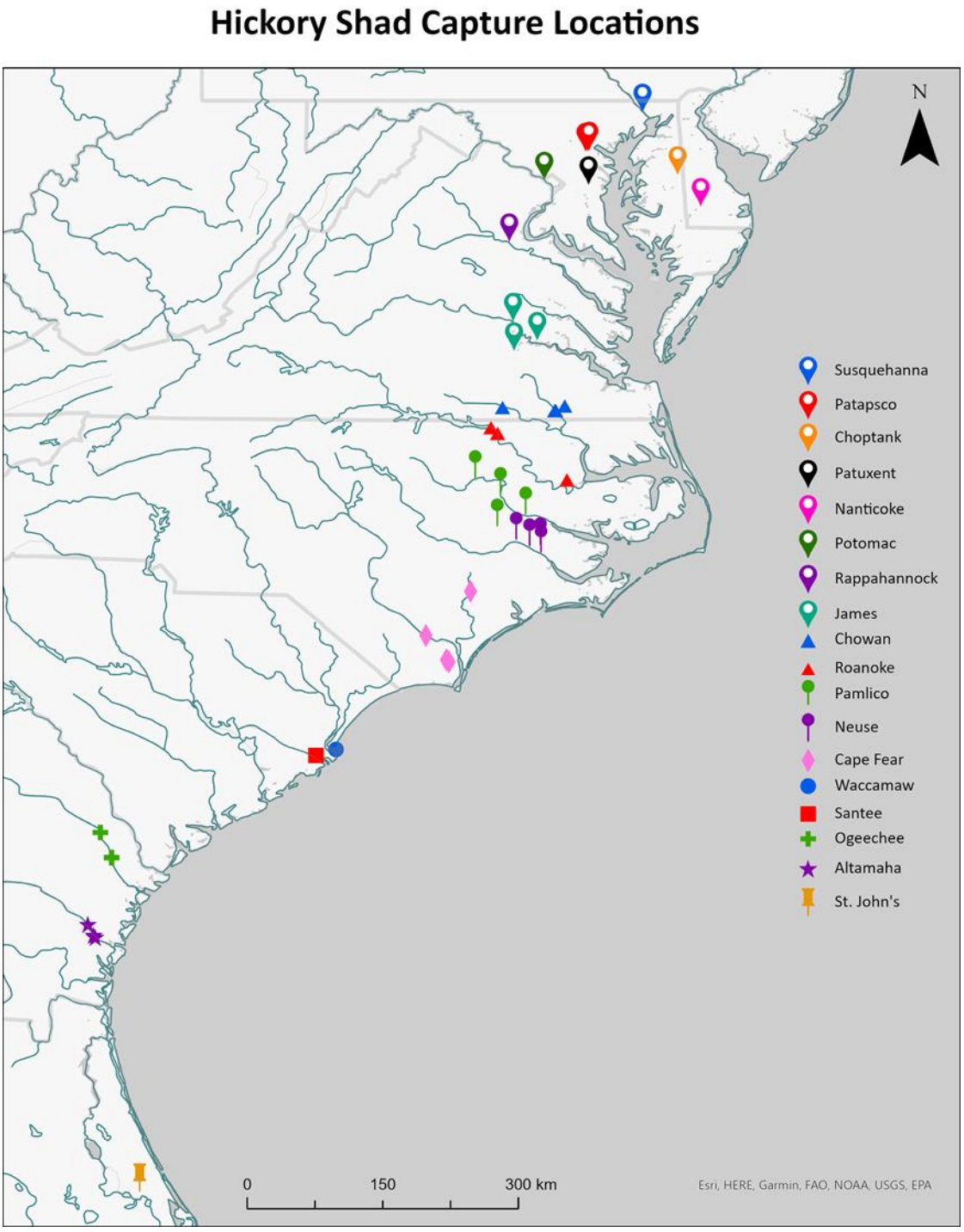

Figure 1-1. Map of Hickory Shad capture locations.

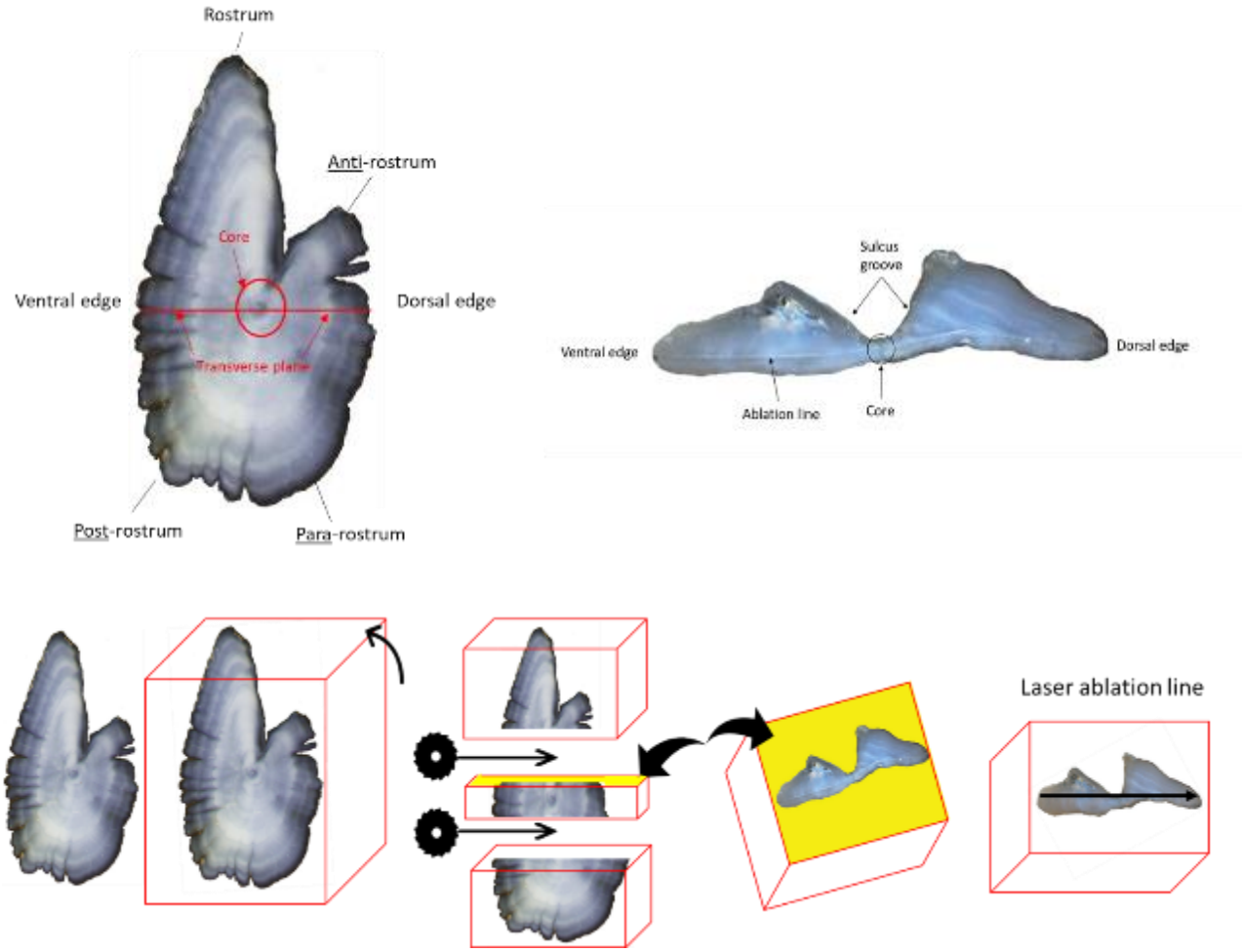

Figure 1-2. Visual description of the preparation process of LA-ICP-MS. The top left the left image is a whole sagittal otolith from the right side of a Hickory Shad. The transverse plane describes the approximate axis in which each otolith was cut, starting from the ventral edge, and going through the core to the dorsal edge. The top right image is a sectioned otolith after LA-ICP-MS has been completed. The bottom image attempts to illustrate the preparation process for LA-ICP-MS. Whole otoliths, such as the one in the top left image, are mounted in epoxy and sectioned along the transverse plane. These sections are rotated (the view seen in the top right image) and polished on each face of the transverse plane (illustrated by the yellow shading), until the core of the otolith is exposed, and laser ablation is conducted.

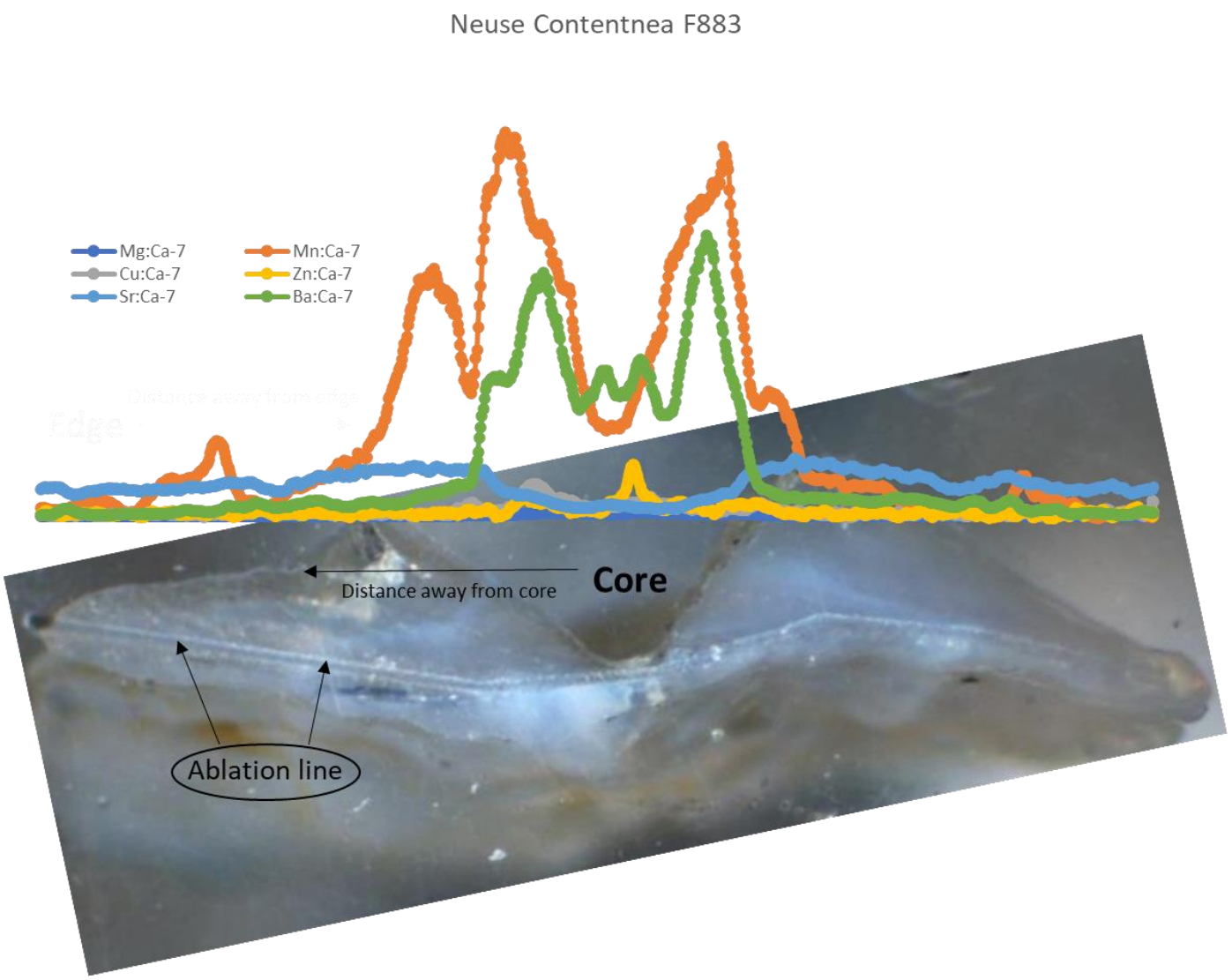

Figure 1-3. Example of sectioned otolith showing the ablation line and the values returned by LA-ICP-MS for each element. Notice the distinct peak in Zn (yellow) present at the core. LA-ICP-MS returned a new data point for each of the 7 elements approximately every 2.5 µm along the ablation line. These lines will collectively be referred to as “element profiles”.

CHAPTER 2

OTOLITH MICROCHEMISTRY PROVIDES EVIDENCE OF NATAL HOMING IN HICKORY SHAD (*ALOSA MEDIOCRIS*)

Abstract

The goal of this study was to look for evidence that adult Hickory Shad exhibit natal homing. Hickory Shad were captured in eighteen major rivers along the known spawning range. LA-ICP-MS was used to quantify seven elements (Mg, Mn, Cu, Zn, Sr, Ba, and Pb), along a continuous transect that ran from the ventral edge of the otolith through the core to the dorsal edge of each otolith, resulting in a time resolved model of the environmental exposure history of each fish. Hickory Shad captured in the same location frequently had similar element profiles distinct from other capture locations, which suggested natal homing. To test this hypothesis quantitatively, a combination of Bayesian inference and unsupervised learning techniques were used to estimate the natal river element signature of each fish and determine if it was similar in Hickory Shad captured at the same location. A distinct peak in zinc was used to identify the central node of each otolith core in the LA-ICP-MS data. To identify the initial transition between the natal freshwater river and euryhaline environments, a hidden Markov model was fit to the strontium profile of each otolith, and average element ratios within the first regime were assumed to be the element signature of the natal river. Since the true number of natal rivers included in the data set were unknown, a Gaussian mixture model was used to estimate the number of mixture distributions present in the data and assign each Hickory Shad to a cluster based on its natal signature. In most cases, between 50% and 100% of Hickory Shad captured in

the same location were assigned to the same cluster, indicating that they had similar natal watershed element signatures. A Chi-Square test confirmed that there was a significant relationship ($p<0.01$) between capture location and cluster assignment. These results provide the first piece of evidence that Hickory Shad exhibit natal homing, and provide an important inferential baseline for further characterization of their life history characteristics.

Introduction

Natal homing is a life history characteristic with important management ramifications, and it appears to be a common trait among anadromous species (Quinn 1984; Quinn and Dittman 1990; Quinn 1993; Neville et al. 2006; Walther et al. 2008; Randon et al. 2018) including alosines (Jessop 1990; Jessop 1994; Bentzen and Paterson 2005; Walther and Thorrold 2008; Walther et al. 2008; Gahagan et al. 2012). One benefit of natal philopatry (i.e., natal homing) is thought to be an increased probability of finding suitable mates and habitat for spawning and juvenile survival (Hendry et al. 2004; Quinn 2005; Keefer and Caudill 2014). Natal homing can lead to highly localized spawning populations that are genetically isolated and adapted to local conditions (Taylor 1991; Hendry et al. 2000; McDowall 2001; Hendry et al. 2004; Waples et al. 2004; Keefer and Caudill 2014). These localized spawning populations are inherently vulnerable to obstructions such as dams and other forms of habitat disturbance (Humphries and Winemiller 2009; Hall et al. 2011). Several species that practice natal homing play keystone ecological roles such as nutrient conveyance (Garman and Macko 1998; Pine et al. 2005), so understanding the population structures of these species is not only imperative for their own sustainability, but for the health of the ecosystems they utilize.

The Hickory Shad is an anadromous clupeid that inhabits Atlantic coastal systems of the US eastern seaboard. Little is known about the life history characteristics of Hickory Shad; they are more closely related to Alewife (*Alosa pseudoharengus*) and Blueback Herring (*Alosa aestivalis;* Bloom and Lovejoy 2014) but published literature typically associates them with the life history characteristics of American Shad (*Alosa sapidissima*). In accordance, it is assumed that natal homing is exhibited by Hickory Shad, although it has not been formally documented. Hickory Shad, American Shad, Alewife, and Blueback Herring all are currently managed under the Atlantic States Marine Fisheries Commission (ASMFC) Interstate Fishery Management Plan IFMP) for Shad and River Herring, which was approved in 1985 (ASMFC 1985). Two amendments have been approved since the original Fisheries Management Plan was enacted, but neither of them address Hickory Shad because of insufficient data. Accordingly, no stock assessment has ever been conducted for Hickory Shad. American Shad, Alewife, and Blueback Herring populations have suffered major declines throughout their ranges (Dadswell and Rulifson 1994; Limburg and Waldman 2009; ASMFC 2017), and Alewife and Blueback Herring are currently listed as "Species of Concern" by the National Marine Fisheries Service (NMFS 2006). Given the lack of information about the status of Hickory Shad, research aimed at understanding its population structure should be considered a high priority so that appropriate management strategies can be devised to ensure its sustainability in commercial and recreational fisheries. Knowing whether or not Hickory Shad exhibit natal homing will have influence in developing, or adding to, any management plan.

Historically, information about anadromous migrations and metapopulation dynamics have been derived from mark-recapture, meristic, morphometric, and genetic studies (Dadswell et al. 1987; Hendry et al. 2004; Walther and Thorrold 2008). However, in recent decades, there

has been a growing interest in the application of otolith microchemistry to estimate natal homing rates and delineate spawning populations (Thresher and Proctor 2007; Arkhipkin et al. 2009; Tanner et al. 2012). Otoliths are calcified structures that grow from a central accretion point comprised of the maternal input at birth, and within hours or days incorporates elements from the ambient aqueous environment as the larva develops full function of skin and gill filaments (Kalish 1990). These two regions of the otolith centroid are referred to here as the "core". The exact timing of the initial deposition and appearance of the core varies as a function of species, as well as several endogenous (i.e., individual physiology) and exogenous (i.e., environmental) factors. Within the inner ear, otoliths are submerged in an acellular endolymphatic fluid that is secreted by the inner ear epithelium. Dissolved ions are secreted to the endolymph as a result of several osmoregulatory, metabolic, and circulatory functions. Therefore, the chemistry of the endolymph at any given time is influenced by the abundance of ions in the ambient water, as well as how those ions are regulated physiologically (Campana 1999; Bath et al. 2000; Kafemann et al. 2000; Elsdon and Gillanders 2003; Lill et al. 2019). Otolith growth occurs as dissolved ions precipitate from the endolymphatic fluid of the inner ear onto an organic protein matrix, which is deposited in layers following an endogenous rhythm (Panella 1971; Campana and Neilson 1985; Payan et al. 1999). High levels of aspartic and glutamic amino acids present in the protein matrix provide nucleation sites for the proceeding layer of ions, which are generally calcium carbonate or similarly sized divalent cations (Degens et al. 1969; Wright 1991). Otoliths are metabolically inert structures, so features that become incorporated into the growing matrix cannot be resorbed and are permanently retained in the otolith crystalline structure (Campana 1999; Friedrich and Halden 2008; Doubleday et al. 2014; Izzo et al. 2016; Thomas et al 2017). This unique form of biomineralization produces time-correlated concentric bands in the form of

alternating optically translucent L-Zones and optically opaque D-zones (Mugiya et al. 1981; Campana and Neilson 1985; Secor et al. 1995; Borelli et al. 2003; Reis-Santos 2013). Early literature on daily growth increments refers to L- and D-zones as incremental and discontinuous zones, respectively. In general, L-zones are the organically rich zones, and the structure is dominated by protein fibers, while D-zones are the highly calciferous layers, most often present the polymorph of aragonite (Irie 1955; Carlstrom 1963; Degens et al. 1969; Mann et al. 1983; Morales-Nin 1986; Maisey 1988; Lecomte-Finiger 1992; Kalish et al. 1995; Oliveira et al. 1996; Campana 1999; Hussey and Mosegaard 2004). The accretion rate of L- and D- zones, and therefore otolith growth, is influenced simultaneously by a variety of endogenous and exogenous factors including temperature, metabolic activity, food availability, somatic growth, and circadian rhythm (Pannella 1971; Neilson and Geen 1985; Casselman 1990; Coghlan et al. 2007).

Physical locations on an otolith that correspond with specific life stages (e.g., the core, annuli, hatch checks, elver marks, etc.), are collectively referred to as “microstructures”. If microstructures are known to represent specific life stages, then LA-ICP-MS can be used to quantify the composition of elements at or between them. In turn, element assays along microstructures can provide insight about where the fish was during those periods, where it moved, or its metabolic activity (Campana 1999). Otolith chemistry has been used to identify natal origins and nursery areas of several species (Thorrold and Shuttleworth 2000; Milton and Chenery 2003; Vasconcelos et al. 2007; Clarke et al. 2009; Reis-Santos et al. 2012), and to estimate rates of natal homing and straying (Thorrold et al. 2001; Reis-Santos et al. 2013; Tanner et al. 2013). Broadly, common approaches for studies investigating natal homing and population structures using otolith microchemistry involve collecting juvenile otoliths and/or water samples

to characterize the chemical signature of spawning habitats (Thorrold et al. 1998a; Walther et al. 2008; Walther and Thorrold 2008), which in turn can be used to link chemical signatures in juvenile portions of adult otoliths to those spawning habitats (Limburg 1998; Wells et al. 2012; Reis-Santos et al. 2013). Depending on the study design and specific objectives, these approaches often rely on assumptions about the spatiotemporal stability of water chemistry (Elsdon et al. 2008), as well as the effects of various endogenous and exogenous factors that influence element incorporation into otoliths (Effects of diet: Hoff and Fuiman 1995; Limburg 1995; Farrell and Campana 1996; Thorrold and Swearer 2009; Doubleday et al. 2013; Woodcock et al. 2013; Woodcock and Walther 2014; Ontogeny, age, and growth: Sadovy and Severin 1994; Fowler et al. 1995a, 1995b; Thorrold et al. 1998a, 1998b; Farrell and Campana 1996; Morales-Nin et al. 2005; Morales-Nin et al. 2012, Sturrock et al. 2014; Genetics: Clark et al. 2011; Barnes et al. 2013; Salinity: Campana 1999; Kraus and Secor 2004; Brown and Severin 2009; Walther and Limburg 2012; Temperature: Thorrold et al. 1997). Nevertheless, otoliths have proven to be useful biogenic tracers of environmental histories, and have provided valuable insight for stock discrimination studies (Thresher and Procter 2007; Arkhipkin et al. 2009; Tanner et al. 2016).

One of the first steps toward effective Hickory Shad management is developing an understanding of the population structure. In the interest of doing so, the goal of this study was to look for evidence that Hickory Shad exhibit natal homing. Several unique challenges were associated with addressing this question. Virtually nothing is known about the life history characteristics of Hickory Shad, particularly concerning the population structure, ocean migration pattern, and use of multiple watersheds for spawning. One critical assumption when using otoliths as natural tags to study population structure is that all possible subgroups contributing to a mixed population have been characterized (addressed in detail by Elsdon et al.

2008). Hence, the most obvious way to approach this was to collect a balanced sample from as many locations as possible during spawning runs, which served to maximize the probability that potential subgroups would be distinct. The known spawning range of Hickory Shad extends from the St. Johns River, FL to the Susquehanna River, MD, with suspected (small) spawning runs in the Christina River, DE (a tributary of the Delaware River), and a tributary of the Schuylkill River, PA, also a tributary of the Delaware River. The most efficient way to achieve sampling at this geographic scale was to have staff from state and federal agencies keep (by freezing) and send Hickory Shad captured during their routine monitoring efforts. The major caveats of this approach were that we were not able to collect water samples or juvenile Hickory Shad from each capture location. Therefore, we were unable to directly quantify the relationship between Hickory Shad otolith chemistry and the ambient water chemistry of each capture location. In order to alleviate these issues, a combination of Bayesian inference and unsupervised learning techniques under a probabilistic paradigm were adopted, which are described in more detail in the methods section.

Identifying the boundaries of natal regions in the element chemistry profiles of adult otoliths presents a significant challenge in otolith chemistry studies that deal with diadromous species. Several previous studies have approached this by manually selecting data points in strontium and barium profiles by hand (e.g., Brennan et al. 2015; Turner and Limburg 2014), which leads to a lack of transparency and reproducibility. Other studies have identified shifts between freshwater and saltwater by establishing thresholds using element levels on the edge of adult otoliths (e.g., Lochet et al. 2008; Lin et al. 2012; Mohan et al. 2014; Lin et al. 2015), or in juvenile otoliths that were known to be captured in the location of interest (e.g., Gahagan et al. 2012). These approaches assume that fish otoliths incorporate elements consistently in different

life stages, but age and growth are known to be among the strongest drivers of otolith protein content (Hüssy et al. 2020), which ultimately controls element deposition (Campana 1999). Using the otolith edge also relies on the assumption that it reflects the ambient environment, which may be influenced by the analytical resolution of microprobe techniques and the temporal extent of environmental exposure prior to capture (see Chapter 3). Previous studies have also constrained microprobe analyses to specific regions of interest within the otolith (e.g., Secor and Piccoli 1996), but the validity of this technique relies on evidence that microstructures that are related to specific life history events develop consistently for the species of interest.

Clearly there is a need for a standardized way to identify natal regions in otolith chemistry data. Otolith chemistry studies would benefit from a quantitative approach applied consistently across samples, which would remove a potentially large source of bias. In addition to combating the assumptions outlined above, my study faced several unique challenges: no studies have validated microstructure development in Hickory Shad otoliths, nothing is known about their migration patterns or the duration of their spawning migrations, and we were unable to quantify the relationship between otolith chemistry and water chemistry at different life stages because water chemistry and juvenile Hickory Shad were not available. Therefore, given the data at hand, a Bayesian approach was adopted to identify the natal river boundaries in Hickory Shad otoliths; strontium incorporation into Hickory Shad otoliths was assumed to reflect two underlying states (fresh and saltwater), so Hidden Markov Models were used to predict the point at which each Hickory Shad initially transitioned into euryhaline water.

Methods

LA-ICP-MS

Hickory Shad were captured during spawning runs in 26 locations of 18 major watersheds between the months of January and April in the years 2016 through 2018. Due to the large number of watersheds, the expense, and the preparation time required for LA-ICP-MS, 5 males and 5 females from each capture location were selected for otolith chemistry analysis, but this balanced design was not possible in each circumstance. Left sagittal otoliths were shipped to the University of Manitoba where sectioning and LA-ICP-MS was conducted by the Department of Geological Sciences. Whole otoliths were embedded in transparent epoxy resin using BUEHLER Epoxicure Epoxy (20-8130-032) and hardener (20-8132-032). Embedded otoliths were then cut across the transverse plane, from the dorsal edge through the core ("the area or areas surrounding one or more primordia and bounded by the first prominent D-zone" (Kalish et al. 1995)), to the opposing ventral edge. Sectioning was completed with a BUEHLER Isomet 1000 precision saw using a BUEHLER diamond wafering blade (11-4276). Cut sections (along with the primary coating of epoxy in which they were embedded) were placed into 1-inch diameter acrylic tubing in groups of 3 to 7 otoliths (depending on the size of the otoliths). Here a second layer of epoxy was added to the group of embedded otolith sections in order to secure them in place. Otoliths were then ground with 320, 600, and 1200 grit sandpaper (BUEHLER Carbimet) until the core was exposed. Otoliths were then polished with 3-µm diamond paste (Buehler Mfg.) and 0.3-µm aluminum oxide paste. LA-ICP-MS was then conducted using a NewWave UP-213 ablation system (New Wave Research) attached to a ThermoFinnigan Element 2 High Resolution ICP-MS (Thermo Electron Corporation). All ablation was preceded with pre-ablation to remove surface contaminants. Pre-ablation used a 55-µm laser beam

diameter at a pulse repetition rate of 5 Hz and scan speed of 120 µm/s. Laser ablation settings were reconfigured to a 30-µm laser beam diameter at a pulse repetition rate of 20 Hz and scan speed of 2-5 µm/s (depending on the size of the otoliths). A helium carrier gas blank was collected for 50 seconds prior to each ablation to correct for background. Ablation transects ran from the outer edge of the otolith through the core to the opposite edge following the maximum axis of otolith growth. However, many ablation lines were not straight due to the shape of the otolith, as the goal was to follow the maximum growth axis. The isotopes quantified in this analysis were ^{55}Mn, ^{25}Mg, ^{63}Cu, ^{66}Zn, ^{86}Sr, ^{137}Ba, ^{208}Pb and ^{43}Ca, which was used as an internal standard. All isotopic counts were converted to ratios with ^{43}Ca. A reference standard by the National Institute of Standards and Technology (NIST SRM 610) was analyzed at one-hour intervals to correct for machine drift. Data were reduced using the program Iolite (Version 2.21). The output data from LA-ICP-MS were returned in Microsoft Excel spreadsheets. Each record in the spreadsheet contained the time and distance from the first observation on the dorsal side of the otolith along with the ratio of each element at each corresponding observation. Observations occurred approximately every 2.5 µm over the entire length of the dorso-ventral surface of each cross section. All statistical analyses were performed in R Studio (R Development Core Team 2019, Version 3.6.3).

Identifying the otolith core in the element transects

The otolith core contains the initial nucleation sites that are developed shortly after birth. In order to isolate natal river element signatures, the first objective was to identify a point to represent the centroid of the otolith core within the element transect so that distances could be measured in relation to birth. Plots were placed over photographs of the corresponding sectioned otolith and manually aligned with the ablation line as seen in Figure 1-3. A distinct peak in zinc

was used to identify the otolith core in the LA-ICP-MS data with the highest zinc value selected to represent the central node, known hereon as the "core point" (Figure 2-1). A subset of data was created for each element from the central point to the last data point on the ventral edge; these comprised the data sets used for analyses. In this context, the data point representing the nucleus of the otolith core was the birth "node" (data point 0) containing the maternal contribution to the embryonic otolith, and the last data point on the ventral edge of the otolith (point n) was the most recently deposited material (Figure 2-2). For a given element, the data between and including these points was the elemental profile for that individual.

Using Bayesian inference to estimate natal river element signatures

From a visual perspective, interannual patterns (i.e., those presumed to hold a close association with the ambient environment in both time and space), were most evident in strontium profiles (Figure 2-3). Assuming that anadromous migrations between marine and freshwater respectively correspond to high and low strontium ratios, or more specifically, if strontium incorporation into an otolith is a stochastic process in nature, and its distribution is reflective of two underlying "states" or "regimes", then this relationship can be modeled as a Markovian process. To estimate the point of transition between freshwater egression and marine ingression, a hidden Markov model (HMM) was fit to each strontium profile using the Gaussian distribution. The first regime identified by the Markov model was assumed to represent the natal watershed. For each Hickory Shad, the average element:calcium ratio within the first regime was used for further analyses (Figure 2-3).

Exploratory data analysis and correlation structure

The average element:calcium ratios within the first regime identified by the HMM were square root transformed. Several data exploration techniques were applied. There was a high level of correlation between zinc and copper, so a principle components analysis (PCA) was used to investigate the relative importance of each element and determine if one or more could be removed. All elements were centered and scaled prior to conducting the PCA. The squared cosine (cos^2) of each element was calculated within each principle component by squaring the product of the principle component loading scores and standard deviations. The cos^2 values were used to evaluate the quality of an element's representation within principle component space. Principle components having eigenvalues ≥ 1, and/or having contributed to explaining at least 70% of the cumulative variance, were considered important.

Results of the PCA suggested that lead contributed minimally to the explanatory power of the data, so it was removed from further analyses. The PCA also suggested that zinc and copper contributed approximately equal amounts of explanatory weights, so each of the steps described hereafter were conducted once using the elements strontium, barium, magnesium, manganese, and copper, and a second time by replacing copper with zinc. These data sets are referred to as the "copper subset" and the "zinc subset", respectively. To avoid subjectively assuming that clusters did exist in the data, the Hopkins test statistic was used to evaluate the clustering tendency of each data set prior to further analyses. The geometric structure of the core data was explored through several unsupervised clustering solutions and ordination techniques. Quantitative inference was achieved through Gaussian mixture models (one for each subset) as outlined in the following sections.

Model selection, parameterization, and fitting of the Gaussian mixture models

Robust covariance estimation via the nearest neighbor variance estimation (NNVE) was used to down-weight potential outliers during the process of model selection and parameter estimation (Wang et al. 2017). The optimal covariance structure for each dataset was selected using Bayesian Information Criterium (BIC) and Integrated Complete Data-Likelihood criterion (ICL), both of which subtract penalty terms from the log-likelihood as the number of parameters increase. Specifically, in this context (adopting a similar notation to that of Scrucca et al. 2016), BIC took the form

$$BIC_{M,K} = 2\ell_{M,K}(x|\psi) - v\ log(n),$$

where for model M with K components, $2\ell_{M,C}(x|\psi)$ is the log-likelihood at the maximum likelihood estimate (ψ), n is the number of mixture components, and v is the number of estimated parameters. When BIC is applied to multivariate Gaussian mixture models, it tends to select the number of mixture components that provides a reasonable approximation of the density, as opposed to the number of clusters (Scrucca et al. 2016). ICL attempts to account for this by penalizing BIC with an entropy term that measures cluster overlap (Biernacki et al.2000). ICL took the form

$$ICL_{M,G} = BIC_{M,G} + 2\sum_{i=1}^{n}\sum_{k=1}^{G} c_{ik}\log(z_{ik}),$$

where z_{ik} is the conditional probability that an individual data point comes from the kth mixture component. Here, c_{ik} = 1 if the *i*th point is assigned to cluster k, and in any other case c_{ik} = 0 (Scrucca et al. 2016). To determine the optimal number of mixture components for each model, a parametric bootstrap likelihood ratio test was applied using an alpha level of 0.05. Models were fit accordingly. Standard errors and confidence intervals were calculated with both a

nonparametric bootstrap and a weighted likelihood bootstrap, each using 999 iterations. A Chi-Square test of independence was calculated to determine if capture location and cluster assignment were independent. Since the sample size from some capture locations was small compared to the number of capture locations, Monte Carlo simulation was used to generate a distribution of 2000 Chi-Square test statistics (Hope 1968) to compare the observed value. Evidence of natal homing was based on similarities in the overall patterns observed in the element profiles and by comparing the number of Hickory Shad that were captured in the same location and assigned to the same cluster based on their otolith core signatures.

Results

Important notes for the reader

Hickory Shad were captured during spawning runs in 26 locations. Several pairs of these capture locations close in geographic proximity and tributaries of the same larger "parent river". Several observations in this chapter, and in the results of Chapter 3, suggested that element signatures varying at small scales were not likely to be detected in Hickory Shad otoliths, and geographically similar pairs in this study were better represented as homogenous groups. Therefore, when referring to capture locations, all results presented here refer to the 18 parent rivers.

Empirical observations in element profiles

Anadromy was evident in the strontium profile of all fish. For the majority of Hickory Shad, strontium was low in the juvenile region of the otoliths, which corresponded to freshwater habitation, and at a given distance away from the otolith core there was an abrupt inversion that

clearly indicated the initial transition into euryhaline water (Figure 2-4). Accordingly, this region of the otolith was typically characterized by high barium ratios surrounding the otolith core, with a sharp decline in the same location as the strontium inversion (Figure 2-5). Anadromous migrations later in life were frequently apparent in strontium profiles, indicated by rapid shifts between high and low strontium (e.g., Figure 2-3). These shifts to low strontium were typically very rapid and narrow, suggesting the fish were not in freshwater for long periods of time. On the other hand, anadromous migrations later in life were not apparent in barium profiles, as barium was generally stable (around a value of zero) after the initial transition in the first year of life (Figure 2-5). Therefore, we concluded that the stability of barium and the short shifts to low strontium were likely caused by very rapid spawning migrations.

The pattern of high strontium and low barium in the juvenile region of the otolith was not the case for all fish. Interestingly, Hickory Shad that were captured in the Choptank, Nanticoke, Patapsco, and St. Johns rivers had very high strontium in the juvenile region (Figure 2-4). Further, with the exception of the St. Johns samples, these Hickory Shad also had the typical high barium in this region. This strange pattern, along with the location and magnitude of the strontium and barium inversions, were generally very similar within Hickory Shad that were captured in the same locations (Figures 2-4, 2-5). The high level of similarities within capture locations was likely caused by natal homing.

Magnesium, manganese, zinc, and copper were typically the highest within the otolith core (Figures 2-6 through 2-9). High Mn:Ca values at the otolith core generally extended a considerable distance with a gradual decline in values, typically reaching steady values around 250 μm away from the central point but still within the otolith core (Figure 2-7). Magnesium ratios also extended away from the central point and displayed a gradual decline in Mg:Ca but

values flattened around 100 µm away from the central point, still within the otolith core (Figure 2-6). The peaks in zinc and copper within the otolith core were much steeper, with the peak in zinc much more distinct and consistent across samples compared to copper (Figures 2-8, 2-9). Lead fluctuated randomly and showed no identifiable pattern (Figure 2-10). After initial declines from high otolith core values, magnesium, manganese, zinc, and copper profiles did exhibit cyclical patterns, but these patterns were not immediately similar within capture location as were observed in the strontium and barium profiles.

Statistical analyses

Once the central point of the otolith core (Figure 2-1) was identified in the element transects, hidden Markov models (HMM) were fit to the strontium profile of each otolith between the core point and the ventral edge (Figure 2-2). The first regime identified by the HMM represented the initial transition into euryhaline water (Figure 2-3). For each otolith, the average ratio of all seven elements was calculated independently. Assuming these average values were estimates of the element signature of each natal river, these data (hereon, the "natal watershed data"), were used for the remaining analyses. There was a high level of positive correlation ($r = 0.7$, $p < 0.05$) between zinc and copper in the natal watershed data (Figure 2-11), and the correlation structure between the remaining elements was negligible. When PCA was used to investigate the importance of elements, the first three principle components had eigenvalues greater than one (PC1 = 2.63; PC2 = 1.35, PC3 = 1.1), while the remaining principle components had eigenvalues less than 1 (Figure 2-12). Seventy-two percent of the total variance was explained in the first three principle components: PC1 = 37.55%, PC2 = 19.33%, and PC3 explained 15.68% (Figure 2-12). All elements were well represented ($cos^2 > 0.3$) in at least 1 of the first 3 principle components (Figure 2-13). Zinc and copper were the most important

elements on the PC1 axis, with loading scores (LS) of 27.73 and 25.74, respectively **(**Figure 2-14**)**. In order of importance to the first principle component, zinc and copper were followed by magnesium and lead (Figure 2-13). The least important PC1 elements were strontium, manganese, and barium (Figure 2-13). For PC2, manganese and strontium were the most important elements and the remaining elements had loading scores of less than 10 (Figure 2-6). Barium was the most important element on the PC3 axis while the remaining elements had loading scores less than 13 (Figure 2-13). Since PCA indicated that lead ratios contributed minimally to the explanatory power of the data, it was removed from further analyses. Alternatively, PCA suggested that copper and zinc had very similar properties regarding their contributions to structure of the data. Considering these elements were both important for separating different combinations of capture locations based on the core data, two data subsets were created: one that included zinc, and one that included copper.

To validate the presence of clusters, Hopkin's test was used to evaluate the clustering tendency of both subsets (Figure 2-16). The Hopkin's test statistic for the copper subset was 0.76, and the Hopkin's test statistics for the zinc subset was 0.75, indicating a high clustering tendency in each subset (Figure 2-16).

BIC and ICL were used to select the optimal covariance structure for both subsets of the natal watershed data, while outliers were controlled for using robust covariance estimation via the nearest neighbor variance estimation. Figure 2-17 shows that model VVE (ellipsoidal, equal orientation) was the optimal model (Cu subset: BIC = -3488.013, ICL = -3525.125; Zn subset: BIC = -3471.559, ICL = -3526.534) for both subsets. Using this covariance structure, a bootstrapped likelihood ratio test with 999 iterations was performed to determine the optimal number of mixture components (i.e., clusters) for the copper subset and for the zinc subset of the

natal watershed data. Table 2-1 shows that five mixture components were selected as the optimal number for both subsets (Cu subset: LRTS = 37.99, $p < 0.05$; Zn subset: LRTS = 46.31, $p < 0.01$). Gaussian mixture models were fit to the natal watershed data in accordance with the properties outlined above. Standard errors were calculated using a non-parametric bootstrap and a weighted likelihood bootstrap, each using 999 iterations. Differences between these approaches were found to be negligible (Figure 2-19), so estimates from the classic non-parametric bootstrap are reported (Tables 2-2, 2-3).

Gaussian mixture models assigned each Hickory Shad into one of five clusters using the ratios of element:calcium in the natal watershed data. For both natal watershed subsets a Chi-Square test of independence was used to determine if capture location and cluster assignment were independent, and Monte Carlo simulation was used to generate a distribution of 2000 Chi-Square test statistics to compare the observed value. The p-values of the observed Chi-Square tests for both subsets were significant (Cu subset: $X^2 = 429$, $p < 0.01$; Zn subset: $X^2 = 348.8$, $p < 0.01$), suggesting that cluster assignment was dependent on capture location (Table 2-7). Results were also significant ($p < 0.01$) under both null distributions (Table 2-7), confirming that there was a significant relationship between capture location and cluster assignment.

Description of clusters

The intraspecific clusters identified in both natal watershed subsets had elemental characteristics that were highly distinguishable, and several geographic patterns were evident (Figures 2-21, 2-22, 2-23). Each one of the copper subset clusters had an analogous cluster in the zinc subset with similar elemental characteristics (Figure 2-21). Most Hickory Shad assigned to a given cluster in the copper subset were also assigned to the complimentary cluster in the zinc

subset. For descriptive clarification, these complimentary pairs of clusters were given dichotomous cluster labels A through E.

Individual Hickory Shad were denoted by the element signatures in the natal watershed region of the otolith. Of the 289 Hickory Shad that were input to the models, 28 fish were assigned to cluster A in the copper subset ($\pi = 0.09$, SE = 0.03) and 36 were assigned to cluster A in the zinc subset ($\pi = 0.12$, SE = 0.03). For Cluster B, 28 fish were assigned to the copper subset ($\pi = 0.12$, SE = 0.03), and 44 were assigned to the zinc subset ($\pi = 0.17$, SE = 0.04) For Cluster C, 124 fish were assigned to the copper subset ($\pi = 0.43$, SE = 0.04), and 83 were assigned to the zinc subset ($\pi = 0.28$, SE = 0.06). For Cluster D, 79 were assigned to the copper data ($\pi = 0.26$, SE = 0.04) and 97 were assigned to the cluster D zinc subset ($\pi = 0.26$, SE = 0.25). Cluster E had 30 fish assigned to the copper subset ($\pi = 0.1$, SE = 0.02) and 29 assigned to the cluster E zinc subset ($\pi = 0.1$, SE = 0.02; Table 2-6).

Figure 2-21 shows the element characteristics that make each cluster unique. Figures 2-22 and 2-23 show the percent of Hickory Shad from each capture location that were assigned to each cluster. Cluster A was characterized by low strontium and barium ratios, and high manganese ratios. Between 60% and 80% of Hickory Shad captured in the Susquehanna and Patuxent rivers were assigned to cluster A in both subsets. Cluster B had the highest ratios of strontium, barium, magnesium, and zinc. Seventy-three percent and 90% of Hickory Shad captured in the Patapsco and Nanticoke rivers, respectively, were assigned to cluster B. Clusters C and D had similar ratios of strontium, barium, and manganese, but cluster C had higher ratios of magnesium, copper, and zinc than cluster D. In both subsets, the majority of Hickory Shad that were captured in North Carolina watersheds along with fish from the Potomac,

Rappahannock, James, Waccamaw, Santee, Ogeechee, and Altamaha rivers were assigned to cluster C or cluster D. Cluster E was characterized by the highest strontium ratios, and the lowest ratios of each of the remaining elements.

Discussion

Natal homing is a life history trait with important management ramifications, and it appears to be common among alosines (Jessop 1990; Jessop 1994; Bentzen and Paterson 2005; Walther and Thorrold 2008; Walther et al. 2008). Prior to my study there was no evidence of natal homing by Hickory Shad, but the quantitative examination of natal river signatures in the central core strongly indicates that homing is exhibited.

A distinct peak in the zinc:calcium ratio, followed by a sharp decline was observed at the core of Hickory Shad otoliths. Elevated levels of zinc have been observed in the early life otolith region of several species (Papadopoulou et al. 1978; Friedrich and Haldon 2010), including anadromous species (Limburg and Elfman 2010. However, in contrast to the pattern observed in Hickory Shad otoliths, zinc ratios in other species typically peak for a short distance after the otolith core and then gradually decrease with age (Hüssy et al. 2020). The peak in zinc observed at the core of Hickory Shad otoliths likely indicates that zinc plays an important role in early ontogeny. After the first year of life, zinc:calcium ratios exhibited cyclical patterns in Hickory Shad otoliths, which has also been observed in other species (Halden and Friedrich 2008; Friedrich and Halden 2010; Limburg and Elfman 2010). Previous studies investigating zinc incorporation into otoliths have found that otolith zinc levels are not related to ambient water concentrations (Thorrold et al. 1997; Ranaldi and Gagnon 2008), but have been related to metabolic processes (Ranaldi and Gagnon 2008). Zinc incorporation has been shown to be

related to the soluble part of the otolith protein matrix (Miller et al. 2006). Otolith protein deposition is highly correlated with growth and protein acquisition (Hüssy,and Mosegaard 2004), which vary by season and may provide an explanation for the cyclical patterns observed in otolith zinc profiles (Hüssy et al. 2016).

In addition to zinc, element:calcium ratios of manganese, magnesium, and copper were also elevated in the core of Hickory Shad otoliths. Copper ratios decreased rapidly, while magnesium and manganese ratios decreased gradually. Previous studies have observed similar patterns in other species (Morales-Nin et al. 2005; Miller 2009; Friedrich and Halden 2010; Clarke et al. 2011; Limburg and Casni 2018), including other clupeids (Ruttenberg et al. 2005). While the underlying mechanisms that influence incorporation of these elements into otoliths are not well understood (Campana 1999; Elsdon et al. 2008; Hüssy et al. 2020), they are known to play important biological roles, and incorporation into the otolith protein matrix is thought to be more closely related to diet and metabolism than ambient water (Martin and Thorrold 2005; Ranaldi and Gagnon 2008; Turner and Limburg 2014; Limburg et al. 2018; Thomas and Swearer 2019; Macdonald et al. 2019). Nevertheless, these elements can still serve as useful markers if they are concentrated in specific areas, or if they are associated with specific events or life stages (Halden et al. 2000; Saquet et al. 2002; Friedrich and Halden 2008; Ranaldi and Gagnon 2008; Friedrich and Halden 2010; Limburg et al. 2015).

In order to isolate a natal river signature, two points had to be identified in the LA-ICP-MS data that represented the boundaries of the natal river: one point to denote birth, and one point to denote the initial point at which fish were exposed to euryhaline water. Previous studies have identified these boundaries by manually selecting data points in strontium and barium profiles by hand (e.g., Brennan et al. 2015; Turner and Limburg 2014), establishing thresholds to

identify shifts between salt and freshwater using strontium and barium levels on the edge of adult otoliths (e.g., Lochet et al. 2008; Lin et al. 2012; Mohan et al. 2014; Lin et al. 2015) and in juvenile otoliths (e.g., Gahagan et al. 2012), and conducting microprobe analyses only along specific regions of interest within the otolith (e.g., Secor and Piccoli 1996; Limburg 2001). There is clearly a need for a standardized quantitative approach to identify underlying regimes that reflect habitation in different salinities and identify the transition between them without succumbing to assumptions that are not likely met.

Hidden Markov models applied in this study were able to identify the initial transition between natal freshwater rivers and exposure to euryhaline water without the presence of covariates such as water chemistry and juveniles without making assumptions about otolith growth or element incorporation during different life stages; they were completely reproduceable and applied homogenously across all samples, and the regimes they identified were comparable to the conclusions that would have come from manual interpretation (e.g., Figure 2-3). Further, this technique can be applied consistently to new data sets, and to other species, which would remove what is potentially a large source of bias in the field of otolith chemistry. While this study focused on early life regions, specifically the initial transition between freshwater and euryhaline water, hidden Markov models have the potential to be useful for identifying life history events later in life, such as repeat spawning events. Additionally, they have the potential to elucidate the amount of time fish spend in fresh, brackish, and seawater during different life stages, especially if regime shifts can be related to microstructures that have been validated in a species.

All elements except for lead were useful for clustering Hickory Shad based on natal river element signatures. In most cases, at least 50% of Hickory Shad captured in the same locations

were assigned to the same clusters, meaning they had similar natal river element signatures and were likely returning to natal rivers to spawn. Between 70% and 100% of Hickory Shad from some capture locations were assigned to the same cluster. For example, 89% of Hickory Shad that were captured in the St. Johns River were assigned to cluster E, which was characterized by having the highest strontium ratios, and the lowest ratios of the remaining elements. This makes intuitive sense, as Florida's limestone bedrock is known to cause high strontium concentrations, particularly in the St. Johns River (Odum 1951; Skougstad and Horr 1963). Additionally, Walther and Thorrold (2008) found that strontium in otoliths from American Shad captured in the St. Johns River were significantly higher than those captured in the Potomac, Rappahannock, Roanoke, and Altamaha rivers.

Several other patterns involving strontium and barium ratios provided evidence of natal homing. Strontium and barium are commonly included in otolith chemistry studies because they are known to have predictable relationships with salinity in most systems (Elsdon and Gillanders 2002; Miller 2007; Brown and Severin 2009; Limburg and Elfman 2010; Miller 2011), and this relationship persists in otoliths because fish are not known to regulate these elements physiologically (Farrell and Campana 1996; Campana 1999; Walther and Thorrold 2006). Inherently, the inverse relationship between strontium, barium, and salinity is remarkably convenient for studying anadromous species, and the classic inverse relationship associated with anadromy was evident during the first year of life in most Hickory Shad otoliths. When the inversion was present, it generally occurred at a similar distance away from the otolith core point for Hickory Shad captured in the same locations, which may reflect the distance between the spawning grounds and euryhaline water in those rivers. On the other hand, Hickory Shad captured in the Choptank, Nanticoke, Patapsco, and St. Johns rivers had high strontium and

barium ratios at the otolith core, and through the first year of life. Hickory Shad captured in each of these locations had strikingly similar strontium and barium profiles that were unique to each location, enough so that natal homing was strongly supported for these specific rivers.

Strontium was comparatively low in the natal region of Hickory Shad otoliths (i.e., between the core and the initial transition into euryhaline water) which was indicative of freshwater birth. However, in many cases we observed a brief spike in strontium at the otolith core (Figure 2-27). The primordium (original nucleation sites) of an otolith is known to retain information about the mother (Thorrold et al. 1998a; Walther and Thorrold 2010; Hamann and Kennedy 2012; Hegg et al. 2013; Schaffler et al. 2014; Shrimpton et al. 2014; Turner and Limburg 2014; Hegg et al. 2019; Lill et al. 2019). A "mothers signature" is present because otolith primordia development occurs while the developing embryo is provisioned by maternally derived nutrients before it begins making significant ionic exchanges with the ambient water (Hegg et al. 2019). Therefore, the initial "ambient environment" reflects the recent environmental history and nutrient acquisition of the mother prior to spawning, which likely differs from the ambient environment of post-hatch larvae (Kalish 1990; Volk et al. 2000; Thorrold et al. 2006; Hegg et al. 2019). Therefore, we presumed that when present in Hickory Shad otoliths, this peak was caused by the maternal signature to the developing embryo, indicating the mother had been in freshwater for only a short period of time. The presence of a "maternal signature" was another trait consistent within capture locations, providing yet another indication of natal homing.

While natal homing seems apparent from these results, straying is more difficult to characterize. Most Hickory Shad from each capture location had similar element:calcium profiles and were assigned to the same clusters, which we interpret as evidence of natal homing.

Alternatively, when Hickory Shad from the same capture location were assigned to other clusters, meaning their natal river element signatures were more similar to those from other captured in other locations, we cannot estimate where they may have been born without understanding more about the distribution of elements in the ambient water of these capture locations, and how well they are reflected in the otoliths of Hickory Shad at the earliest life stages. It is also important to acknowledge that water chemistry varies over both space and time, as it is affected by several factors including ion exchange, mixing of water masses, microbial activity, and substrate composition (Wilson 1975; Aston 1978; Rohling and Bigg 1998; Elsdon et al. 2008). My study would have greatly benefited from a greater understanding of the spatial and temporal variability of element concentrations in the systems under consideration, and this should be prioritized in future studies.

Conclusion

Otolith chemistry has the potential to provide important information about Hickory Shad life history characteristics. Hickory Shad that were captured in the same locations typically had very similar element profiles and natal river signatures. Additionally, there was a statistically significant relationship between capture location and cluster assignment based on the natal river signatures. Given these results, my study provides strong evidence that Hickory Shad do exhibit natal homing. However, more information about the spatiotemporal variation of elements and the mechanisms that influence their incorporation into Hickory Shad otoliths is needed to better understand the specific rate and extent of natal homing and straying. Nevertheless, the results of this study will provide an important inferential baseline for future studies to investigate these questions.

Literature Cited

Arkhipkin, A. I., P. C. Schuchert, and L. Danyushevsky. 2009. Otolith chemistry reveals fine population structure and close affinity to the Pacific and Atlantic oceanic spawning grounds in the migratory southern blue whiting (*Micromesistius australis australis*). Fisheries Research 96: 188–194.

ASMFC. 1985. Fishery management plan for the anadromous alosid stocks of the eastern United States: American Shad, Hickory Shad, Alewife, and Blueback Herring. Phase II in interstate management planning for migratory alosids of the Atlantic coast. Fisheries Management Report No. 6, 374p. ASMFC, Washington, D.C.

ASMFC. 2017. Interstate fisheries management program overview: Shad and River Herring. ASMFC, Washington, D.C.

Aston, S. R. 1978. Estuarine chemistry. Pages 361-440 *In* J.P. Riley & R. Chester, editors. Chemical Oceanography. London Academic Press.

Barnes, T. C., B. M. Gillanders, and K. Rose. 2013. Combined effects of extrinsic and intrinsic factors on otolith chemistry: implications for environmental reconstructions. Canadian Journal of Fisheries and Aquatic Sciences 70:1159–1166.

Bath, G., S. Thorrold, C. Jones, S. Campana, J. McLaren, and J. Lam. 2000. Strontium and barium uptake in aragonitic otoliths of marine fish. Geochimica et Cosmochimica Acta: 64:1705-1714.

Bentzen, P., and I. G. Paterson. 2005. Genetic analyses of freshwater and anadromous alewife (*Alosa pseudoharengus*) populations from the St. Croix River, Maine/New Brunswick. Maine Rivers, Hallowell.

Bezdek, J., and R. Hathaway. 2002. VAT: a tool for visual assessment of cluster tendency. Proceedings of the 2002 International Joint Confrence on Neural Networks. IJCNN`02 (Cat. No.02CH37290) 3:2225-2230. doi:10.1109/IJCNN.2002.1007487

Biernacki, C., G. Celeux, and G. Govaert. 2000. Assessing a mixture model for clustering with the integrated completed likelihood. IEEE Transactions on Pattern Analysis and Machine Intelligence 22(7):719–725.

Bloom, D. D., and N. R. Lovejoy. 2014. The evolutionary origins of diadromy inferred from a time-calibrated phylogeny for Clupeiformes (herring and allies). Proceedings of the Royal Society B: Biological Sciences 281:20132081.

Borelli, G., M. E. Guibbolini, N. Mayer-Gostan, F. Priouzeau, H. De Pontual, D. Allemans, S. Puverel, E. Tambutte, and P. Payan. 2003. Daily variations of endolymph composition: relationship with the otolith calcification process in trout. The Journal of Experimental Biology 206: 2685-2692.

Brennan, S. R. C. E. Zimmerman, D. P. Fernandez, T. E. Cerling, M. V. McPhee, and M. J. Wooller. 2015. Strontium isotopes delineate fine-scale natal origins and migration histories of Pacific salmon. Science Advances 1(4): e1400124. 10.1126/sciadv.1400124

Brown R. J., and K. P. Severin. 2009. Otolith chemistry analyses indicate that water Sr:Ca is the primary factor influencing otolith Sr:Ca for freshwater and diadromous fish but not for marine fish. Canadian Journal of Fisheries and Aquatic Sciences 66:1790–1808.

Campana, S. E. 1999. Chemistry and composition of fish otoliths: pathways, mechanisms, and applications. Marine Ecology Progress Series 188:263–297.

Campana, S. E. and J. D. Neilson. 1985. Microstructure of fish otoliths. Canadian Journal of Fisheries and Aquatic Science: 42:1014-1032.

Campana, S. E. 1999. Chemistry and composition of fish otoliths: pathways, mechanisms, and applications. Marine Ecology Progress Series 188:263–297.

Carlstrom D. 1963. A crystallographic study of vertebrate otoliths. Biology Bulletin (Woods Hole) 125:441–463.

Casselman, J. M. 1990. Growth and relative size of calcified structures of fish. Transactions of the American Fisheries Society 119:673–688.

Clarke, L. M., B. D. Walther, S. B. Munch, S. R. Thorrold, and D. O. Conover. 2009. Chemical signatures in the otoliths of a coastal marine fish, *Menidia menidia*, from the northeastern United States: spatial and temporal differences. Marine Ecology Progress Series 384:261–271.

Clarke, L. M., S. R. Thorrold, and D.O. Conover. 2011. Population differences in otolith chemistry have a genetic basis in *Menidia menidia*. Canadian Journal of Fisheries and Aquatic Sciences 68: 105–114. doi: 10.1139/F10-147.

Coghlan Jr., S. M., M. S. Lyerly, T. R. Bly, J. W. Williams, D. Bowman, and R. Hannigan. 2007. Otolith chemistry discriminates among hatchery-reared and tributary-spawned Salmonines in a tailwater system. North American Journal of Fisheries Management 27:531-541.

Dadswell, M. and R. A. Rulifson. 1994. Macrotidal estuaries: A region of collision between migratory marine animals and tidal power development. Biological Journal of the Linnean Society 51:93-113.

Dadswell, M. J., R. J. Klauda, C. M. Moffitt, R. L. Saunders, R. A. Rulifson, and J. E. Cooper 1987. Common strategies of anadromous and catadromous fishes. American Fisheries Society Symposium 1, Bethesda, Maryland.

Degens E. T., W. G. Deuser, and R. L. Haedrich. 1969 Molecular structure and composition of fish otoliths. Marine Biology 2:105–113.

Doubleday Z. A., C. Izzo, S. Woodcock, and B. M. Gillanders. 2013. Relative contribution of water and diet to otolith chemistry in freshwater fish. Aquatic Biology 18(3):271–280. doi:10. 3354/ab00511.

Doubleday Z. A., H. H. Harris, C. Izzo, and B. M. Gillanders. 2014. Strontium randomly substituting for calcium in fish otolith aragonite. Analytical Chemistry 86(1):865–869. doi:10.1021/ ac4034278

Elsdon, T. S., and B. M. Gillanders. 2002. Interactive effects of temperature and salinity on otolith chemistry: challenges for determining environmental histories of fish. Canadian Journal of Fisheries and Aquatic Sciences 59(11):1796-1808.

Elsdon, T. S., and B. M. Gillanders. 2003. Reconstructing migratory patterns of fish based on environmental influences on otolith chemistry. Fish Biology and Fisheries 13: 219-235.

Elsdon, T. S., B. K. Wells, S. E. Campana, B. M. Gillanders, C. M. Jones, K. E. Limburg, D. H. Secor, S. R. Thorrold, and B. D. Walther. 2008. Otolith chemistry to describe movements

and life-history parameters of fishes: hypotheses, assumptions, limitations and inferences. Oceanography and Marine Biology: An Annual Review 46: 297–330.

Farrell, J., and S. E. Campana. 1996. Regulation of calcium and strontium deposition on the otoliths of juvenile tilapia, *Oreochromis niloticus*. Comparative Biochemistry and Physiology 115A: 103–109.

Fowler A. J., S. E. Campana, C. M. Jones, and S. R. Thorrold. 1995a. Experimental assessment of the effect of temperature and salinity on elemental composition of otoliths using solution based ICPMS. Canadian Journal of Fisheries and Aquatic Sciences 52:1421-1430.

Fowler A. J., S. E. Campana, C. M. Jones, and S. R. Thorrold. 1995b. Experimental assessment of the effect of temperature and salinity on elemental composition of otoliths using laser ablation ICPMS. Canadian Journal of Fisheries and Aquatic Sciences 52:1431-1441.

Friedrich, L. A., and N. M. Halden. 2008. Alkali element uptake in otoliths: a link between the environment and otolith microchemistry. Environmental Science and Technology 42:3514-3518.

Friedrich, L. A., and N. M. Halden. 2010. Determining exposure history of Northern Pike and Walleye to tailings effluence using trace metal uptake in otoliths. Environmental Science and Technology 44(5):1551-1558.

Gahagan, B. I., J. C. Vokoun, G. W. Whiteledge, and E. T. Schultz. 2012. Evaluation of otolith microchemistry for identifying natal origin of anadromous River Herring in Connecticut. Marine and Coastal Fisheries: Dynamics, Management, and Ecosystem Science 4:358-372. doi: 10.1080/19425120.2012.675967.

Garman, G. C., and S. A. Macko. 1998. Contribution of marine-derived organic matter to an Atlantic coast, freshwater, tidal stream by anadromous clupeid fishes. Journal of the North American Benthological Society 17: 277–285.

Halden, N. M., and L. A. Friedrich. 2008. Trace-element distributions in fish otoliths: natural markers of life histories, environmental conditions and exposure to tailings effluence. Mineral Magazine 72(2):593–605. doi:10.1180/minmag. 2008.072.2.593.

Halden, N. M., S. R. Mejia, J. A. Babaluk, J. D. Reist, A. H. Kristofferson, J. L. Campbell, and W. J. Teesdale. 2000. Oscillatory zinc distribution in Arctic char (*Salvelinus alpinus*) otoliths: the result of biology or environment? Fisheries Research 46(1–3): 289–298. doi:10.1016/S0165-7836(00)00154-5.

Halden, N. M., S. R. Mejia, J. A. Babaluk, J. D. Reist, A. H. Kristofferson, J. L. Campbell, and W. J. Teesdale. 2000. Oscillatory zinc distribution in Arctic char (*Salvelinus alpinus*) otoliths: the result of biology or environment? Fisheries Research 46(1–3): 289–298. doi:10.1016/S0165-7836(00)00154-5.

Hall, C. J., A. Jordaan, and M. G. Frisk. 2011. The historic influence of dams on diadromous fish habitat with a focus on herring and hydrologic longitudinal connectivity. Landscape Ecology 26:95-107.

Hamann, E. J., and B. P. Kennedy. 2012. Juvenile dispersal affects straying behaviors of adults in a migratory population. Ecology 93: 733–740.

Hegg, J. C., B. P. Kennedy, P. M. Chittaro, and R. W. Zabel. 2013. Spatial structuring of an evolving life-history strategy under altered environmental conditions. Oecologia 172:1017–1029.

Hegg, J. C., B. P. Kennedy, and P. Chittaro. 2019. What did you say about my mother? The complexities of maternally derived chemical signatures in otoliths. Canadian Journal of Fisheries and Aquatic Sciences 76: 81–94.

Hendry, A. P., J. K. Wenburg, P. Bentzen P, E. C. Volk, and T. P. Quinn. 2000. Rapid evolution of reproductive isolation in the wild: evidence from introduced salmon. Science 290:516–518.

Hendry A. P., V. Castric, M. T. Kinnison, and T. P. Quinn. 2004. The evolution of philopatry and dispersal: homing versus straying in salmonids. In: Hendry AP, Stearns SC (eds) Evolution illuminated: salmon and their relatives. Oxford University Press, New York, pp. 52–91.

Hoff, G. R., and L. A. Fuiman. 1995. Environmentally induced variation in elemental composition of red drum (*Sciaenops ocellatus*) otoliths. Bulletin of Marine Science 56: 578–591.

Hope, A. C. A. 1968. A simplified Monte Carlo significance test procedure. Journal of the Royal Statistical Society Series B 30: 582–598.

Hughes, C. S. 2015. Using water chemistry and otolith chemistry to determine strategic habitat areas for Striped Bass (*Morone saxatilis*) in the Albemarle Estuarine system of North Carolina. Dissertation. East Carolina University.

Humphries, P., and P. O. Winemiller. 2009. Historical impacts on river fauna, shifting baselines, and challenges for restoration. Bioscience 59(8): 673-684.

Hüssy K., and H. Mosegaard. 2004. Growth and otolith accretion characteristics modelled in a bioenergetics context. Canadian Journal of Fisheries and Aquatic Sciences 61(6):1021–1031. doi:10.1139/f04-038.

Hüssy, K., K. E. Limburg, H. De Pontual, O. R. B. Thomas, P. K. Cook, Y. Heimbrand, M. Blass, and A. M. Sturrock. 2020. Trace element patterns in otoliths: the role of biomineralization. Reviews in Fisheries Science and Aquaculture, https://doi.org/10.1080/23308249.2020.1760204.

Hüssy K, J. Gröger, F. Heidemann, H.-H. Hinrichsen, and L. Marohn. 2016. Slave to the rhythm: seasonal signals in otolith microchemistry reveal age of eastern Baltic cod (*Gadus morhua*). ICES Journal of Marine Science 73(4):1019–1032. doi:10.1093/icesjms/fsv247

Irie, T. 1955. The crystal texture of the otolith of a marine teleost, *Pseudosciaena*. Journal of the Faculty of Fisheries and Animal Husbandry Hiroshima University 1:1-13.

Izzo, C., Z. A. Doubleday, and B. M. Gillanders. 2016. Where do elements bind within the otoliths of fish? Marine and Freshwater Research 67(7): 1072-1076. doi: https://doi.org/10.1071/MF15064.

Jessop, B. M. 1990. Stock-recruitment relationships of alewives and blueback herring returning to the Mactaquac Dam, Saint John River, New Brunswick. North American Journal of Fisheries Management 10:19–32.

Jessop, B. M. 1994. Homing of Alewives (*Alosa pseudoharengus*) and Blueback Herring (*A. aestivalis*) to and within the Saint John River, New Brunswick, as indicated by tagging data. Canadian Technical Report of Fisheries and Aquatic Sciences 2015.

Kafemann, R., S. M. Adlerstein, and R. Neukamm. 2000. Variation in otolith strontium and calcium ratios as an indicator of life histories strategies of freshwater species within a brackish water system. Fisheries Research 46: 313-325.

Kalish, J.M. 1990. Use of Otolith Microchemistry to distinguish the progeny of sympatric anadromous and non-anadromous salmonids. Fisheries Bulletin 88(4): 657–666.

Kalish, J.M., R.J. Beamish, E.B. Brothers, J.M. Casselman, R.I.C.C. Francis, H. Mosegaard, J. Panfili, E.D. Prince, R.E. Thresher, C.A. Wilson, and P.J. Wright. 1995. Glossary for otolith studies. Pages 723-729 *in* Secor, D.H., Dean, J.M., and Campana, S.E., editors. Recent Developments in Fish Otolith Research. South Carolina University Press, Columbia, SC.

Keefer, M. L., and C. C. Caudill. 2014. Homing and straying by anadromous salmonids: a review of mechanisms and rates. Reviews in Fish Biology and Fisheries 24:333-368.

Kraus R. T., and D. H. Secor. 2004. Incorporation of strontium into otoliths of an estuarine fish. Journal of Experimental Marine Biology and Ecology 302(1): 85–106. doi:10.1016/j.jembe.2003.10.004.

Lecomte-Finiger, R. 1992. Growth history and age at recruitment of European glass eels (*Anguilla anguilla*) as revealed by otolith microstructure. Marine Biology 114: 205-210.

Lill, J. O., V. Finnas, Y. Heimbrand, M. Blass, S. Frojdo, Y. Lahaye, J. M. K. Slotte, J. Nyman, E. Jokikokko, M. von Numbers, and H. Hagerstrand. 2019. Information depths of analytical techniques assessing whitefish otolith chemistry. Nuclear Institute and Methods in Physics Research B 477:104-108. doi: https://doi.org/10.1016/j.nimb.2019.07.033.

Limburg, K. E. 1995. Otolith strontium traces environmental history of sub-yearling American shad *Alosa sapidissima*. Marine Ecology Progress Series 119:25–35.

Limburg, K. E. 1998. Anomalous migration of anadromous herrings revealed with natural chemical tracers. Canadian Journal of Fisheries and Aquatic Sciences 55:431–437.

Limburg, K. E., and M. Casini. 2018. Effect of marine hypoxia on Baltic Sea Cod *Gadus morhua*: Evidence from otolith chemical proxies. Frontiers in Marine Science 5(482). https://doi.org/10.3389/fmars.2018.00482.

Limburg, K. E., and M. Elfman. 2010. Patterns and magnitude of Zn:Ca in otoliths support the recent phylogenetic typology of Salmoniformes and their sister groups. Canadian Journal of Fisheries and Aquatic Sciences 67(4):597–604. doi:10.1139/F10-014.

Limburg, K. E., and J. R. Waldman. 2009. Dramatic declines in North American diadromous fishes. BioScience 59:955-965.

Limburg K. E., B. D. Walther, Z. Lu, G. Jackman, J. Mohan, Y. Walther, A. Nissling, P. K. Weber, and A. K. Schmitt. 2015. In search of the dead zone: use of otoliths for tracking fish exposure to hypoxia. Journal of Marine Systems. 141:167–178. doi:10. 1016/j.jmarsys.2014.02.014.

Limburg, K. E., M. J. Wuenschel, K. Hussy, Y. Heimbrand, and M. Samson. 2018. Making the otolith magnesium chemical calendar-clock tick: plausible mechanism and empirical evidence. Reviews in Fisheries Science and Aquaculture 26(4):479–493. doi:10.1080/23308249.2018.1458817.

Lochet, A., P. Jatteau, J. Tomax, and E. Rochard. 2008. Retrospective approach to investigating the early life history of diadromous fish: Allis Shad *Alosa alosa* (L.) in the Gironde-Garonne-Dordogne watershed. Journal of Fish Biology 72: 946-960. doi: 10.1111/j.1095-8649.2007.01776.x.

Lin, Y.-J., B. M. Jessop, O. L. F. Weyl, Y. Iizuka, S.-H. Lin, W.-N. Tzeng, and C.-L. Sun. 2012. Regional variation in otolith Sr:Ca ratios of African Longfinned Eel *Anguilla mossambica* and Mottled Eel *Anguilla marmorata*: a challenge to the classic tool for reconstructing migratory histories of fishes. Journal of Fish Biology 81:427-441. doi: 10.111/j.1095-8649.2012.03357.x.

Lin, Y.-J., B. M. Jessop, O. L. F. Weyl, Y. Iizuka, S.-H. Lin, and W.-N. Tzeng. 2015. Migratory history of African Longfinned Eel *Anguilla mossambica* from Maningory River, Madagascar: discovery of a unique pattern in otolith Sr:Ca ratios. Environmental Biology of Fishes. 98:457-468. doi: 10.1007/s106410014-0275-2.

Macdonald, J. I., R. N. Drysdale, R. Witt., Z. Cságoly, and G. Marteinsdóttir. 2019. Isolating the influence of ontogeny helps predict island wide variability in fish otolith chemistry. Reviews in Fish Biology and Fisheries 30:173-202. doi: https://doi.org/10.1007/s11160-019-09591-x.

Maisey, J. 1987. Notes on the structure and phylogeny of vertebrate otoliths. Copeia 1:257-259.

Mann, S., S. B. Parker, M. D. Ross, A. J. Skarnucis, and W. J. P. Williams. 1983. The ultrastructure of the calcium carbonate balance organs of the inner ear: an ultra-high resolution electron microscopy study. Proceedings of the Royal Society of London Series B Biological Science 218: 415-424.

Martin, G. B. and S. R. Thorrold. 2005. Temperature and salinity effects on magnesium, manganese, and barium incorporation in otoliths of larval and early juvenile spot *Leiostomus xanthurus*. Marine Ecology Progress Series 293: 223–232.

McDowall R. M. 2001. Anadromy and homing: two life-history traits with adaptive synergies in salmonid fishes? Fish and Fisheries 2:78–85.

Miller, J. A. 2007. Scales of variation in otolith elemental chemistry of juvenile staghorn sculpin (*Leptocottus armatus*) in three Pacific Northwest estuaries. Marine Biology 151(2): 483–494.

Miller, J. A. 2009. The effects of temperature and water concentration on the otolith incorporation of barium and manganese in black rockfish *Sebastes melanops*. Journal of Fisheries Biology 75(1):39–60. doi:10.1111/j.1095-8649.2009.02262.x.

Miller, J. A. 2011. Effects of water temperature and barium concentration on otolith composition along a salinity gradient: implications for migratory reconstructions. Journal of Experimental Marine Biology and Ecology 405:42–52.

Miller M.B., A. M. Clough, J. N. Batson, and R.W. Vachet. 2006. Transition metal binding to cod otolith proteins. Journal of Experimental Marine Biology and Ecology 329(1):135–143. doi:10.1016/j.jembe.2005.08.016

Milton, D. A., S. R. Chenery, M. J. Farmer, and S. J. M. Blaber. 1997. Identifying the spawning estuaries of the tropical shad *Tenualosa toli*, using otolith microchemistry. Marine Ecology Progress Series 153:283–291.

Milton, D. A., and S. R. Chenery. 2003. Movement patterns of the tropical shad hilsa (*Tenualosa ilisha*) inferred from transects of 87Sr/86Sr isotope ratios in their otoliths. Canadian Journal of Fisheries and Aquatic Sciences 60:1376-1385.

Mohan, J. A., N. H. Halden, and R. A. Rulifson. 2014. Habitat use of juvenile striped bass Morone saxatilis (Actinopterygii: Moronidae) in rivers spanning a salinity gradient across a shallow wind-driven estuary. Environmental Biology of Fishes 98(4): 1105:1116. DOI 10.1007/s10641-014-0344-6.

Morales-Nin, B. 1986. Chemical composition of the otoliths of the sea bass (*Dicentrarchus labrax* Linnaeus, 1758) (Pisces, Serranidae). Cybium 10(2):115–120.

Morales-Nin, B., S. C. Swan, J. D. M. Gordon, M. Palmer, A. J. Geffen, T. Shimmield, and T. Sawyer. 2005. Age-related trends in otolith chemistry of *Merluccius merluccius* from the north-eastern Atlantic Ocean and the western Mediterranean Sea. Marine and Freshwater Research 56(5):599–607. doi:10.1071/MF04151.

Morales-Nin, B., A. J. Geffen, S. Pérez-Mayol, M. Palmer, R. González-Quirós, and A. Grau. 2012. Seasonal and ontogenetic migrations of meagre (*Argyrosomus regius*) determined by otolith geochemical signatures. Fisheries Research 127-128:154-165.

Mugiya, Y., N. Watabe, J. Yamada, J. M. Dean, D. G. Dunkelberger, and M. Shimuzu. 1981. Diurnal rhythm in otolith formation in the goldfish. *Carassius auratus.* Comparative Biochemistry and Physiology 68A: 659-662.

Neilson, J. D., and G. H. Geen. 1985. Effects of feeding regimes and diel temperature cycles on otolith increment formation in juvenile chinook salmon, *Oncorhynchus tshawytscha*. Fisheries Bulletin 83(1):91–101.

Neville, H. M., D. J. Isaak, J. B. Dunham, R. F. Thurow, and B. E. Rieman. 2006. Fine-scale natal homing and localized movement as shaped by sex and spawning habitat in Chinook salmon: insights from spatial autocorrelation analysis of individual genotypes. Molecular Ecology 15: 1589-4602. doi: 10.1111/j.1365-294X.2006.03082.x.

NMFS (National Marine Fisheries Service). 2006. Endangered and Threatened Species; Revision of Species of Concern List, Candidate Species Definition, and Candidate Species List. 71 FR 61022-61025. https://federalregister.gov/a/E6-17249

Odum, H.T. 1951. Strontium in Florida waters. Pages 20-21 *in* A.P. Black and E. Brown, editors Chemical Character of Florida Waters. Florida State Board of Conservation, Division of Water Survey and Research Papers 6.

Oliveira, A. M., M. Farina, I. P. Ludka, and B. Kachar. 1996. Vaterite, calcite and aragonite in the otoliths of three species of piranha. Naturwissen schaften 83:133-135.

Palace, V. P., N. M. Halden, P. Yang, R. E. Evans, and G. Sterling. 2007. Determining residence patterns of rainbow trout using laser ablation inductively coupled plasma mass spectrometry (LA-ICP-MS) analysis of selenium in otoliths. Environmental Science and Technology 41:3679-3683.

Pannella, G. 1971. Fish otoliths: daily growth layers and periodical patterns. Science 173:1124-1127.

Papadopoulou C., G.D. Kanias, and E. Moraitopoulou-Kassimati. 1978. Zinc content in otoliths of Mackerel from the Aegean. Marine Pollution Bulletin 9:106:108.

Payan P., A. Edeyer, H. De Pontual, et al. 1999. Chemical composition of saccular endolymph and otolith in fish inner ear: lack of spatial uniformity. American Journal of Physiology 277: 123–131.

Pine, W. P., T. J. Kwak, D. S. Waters, and J. A. Rice. 2005. Diet selectivity of introduced flathead catfish in coastal rivers. Transactions of the American Fisheries Society 134:901-909. doi: 10.1577/T04-166.1.

Quinn, T. P. 1984. Homing and straying in Pacific salmon. Pages 357-361 *In* J.D. McCleave, G.P Arnold, J.M. Dodson and W.H. Neill, editors. Mechanisms of migration in fisheries. Plenum, New York.

Quinn, T. P. 1993. A review of homing and straying of wild and hatchery produced salmon. Fisheries Research 18:29:44.

Quinn T. P. 2005 The behavior and ecology of Pacific salmon and trout. American Fisheries Society, Bethesda, Maryland.

Quinn, T. P., and A. H. Dittman. 1990. Pacific salmon migrations and homing: mechanisms and adaptive significance. Trends in Ecology and Evolution 5:174-177.

R Development Core Team. 2019. R: A language and environment for statistical computing. Vienna, Austria: R Foundation for Statistical Computing.

Ranaldi, M. M., and M. M. Gagnon. 2008. Zinc incorporation in the otoliths of juvenile pink snapper (*Pagrus auratus* Forster): the influence of dietary versus waterborne sources. Journal of Experimental Marine Biology and Ecology 360:56-62.

Randon, M., F. Daverat, G. Bareille, P. Jatteau, J. Martin, C. Pecheyran, and H. Drouineau. 2018. Quantifying exchanges of *Allis* shads between river catchments by combining otolith microchemistry and abundance indices in a Bayesian model. ICES Journal of Marine Science 75: 9–21.

Reis-Santos, P., B. M. Gillanders, S. E. Tanner, R. P. Vasconcelos, T. S. Elsdon, and H. N. Cabral. 2012. Temporal variability in estuarine fish otolith elemental fingerprints: implications for connectivity assessments. Estuarine, Coastal and Shelf Science 112: 216–224. doi: 10.1016/j.ecss.2012.07.027.

Reis-Santos, P., S. E. Tanner, R. P. Vasconcelos, T. S. Elsdon, H. N. Cabral, and B. M. Gillanders. 2013. Connectivity between estuarine and coastal fish populations: contributions of estuaries are not consistent over time. Marine Ecology Progress Series 491: 177-186.

Rohling, E. J., and G. R. Bigg. 1998. Paleosalinity and δ^{18}O: A critical assessment. Journal of Geophysical Research 103:1307–1318.

Ruttenberg, B.I., S.L. Hamilton, M.J.H. Hamilton, G.L. Paradis, M.S. Sheehy, J.D. Standish, O. Ben-Tzvi, and R.R. Warner. 2005. Elevated levels of trace elements in cores of otoliths and their potential for use as natural tags. Marine Ecology Progress Series 297:273-281. doi:10.3354/meps297273

Sadovy, Y., and K. Severin. 1994. Elemental patterns in red hind (*Epinephelus guftatus*) otoliths from Bermuda and Puerto Rico reflect growth rate, not temperature. Canadian Journal of Fisheries and Aquatic Sciences 51:133-141.

Saquet, M., N. M. Halden, J. A. Babaluk, J. L. Campbell, and Z. Nejedly. 2002. Micro-PIXE analysis of trace element variation in otoliths from fish collected near acid mine tailings: potential for monitoring contaminant dispersal. Nuclear Instrument Methods in Physical Research, Section B Beam Interactions with Materials and Atoms 189: 196-201.

Schaffler, J. J., T. J. Miller, and C. M. Jones. 2014. Spatial and temporal variation in otolith chemistry of juvenile Atlantic Menhaden in the Chesapeake Bay. Transactions of the American Fisheries Society 243(4): 1061-1071. doi: https://doi.org/10.1080/00028487.2014.889748.

Scrucca, L., M. Fop, T. B. Murphy, and A. E. Raftery. 2016. Mclust5: Clustering, classification and density estimating using Gaussian finite mixture models. The R Journal 8(1): 289-317. ISBN 2073-4859.

Secor, D. S. and P. M. Piccoli. 1996. Age and sex dependent migrations of Striped Bass in the Hudson River as determined by chemical microanalysis of otoliths. Estuaries 19(4): 778-793.

Secor, D. H., A. Henderson-Arzapalo, and P. M. Piccoli. 1995. Can otolith microchemistry chart patterns of migration and habitat utilization in anadromous fishes? Journal of Experimental Marine Biology and Ecology 192(1):15–33. doi:10.1016/0022-0981(95)00054-U.

Shrimpton, J. M., K. D. Warren, N. L. Todd, C. J. McRae, G. J. Glova, K. H. Telmer, and A. D. Clarke. 2014. Freshwater movement patterns by juvenile Pacific salmon *Oncorhynchus* spp. before they migrate to the ocean: Oh the places you'll go! Journal of Fish Biology 85:987-1004.

Skougstad, M. W. and C. A. Horr. 1963. Occurrence and distribution of strontium in natural water. U.S. Geological Survey Water-Supply Paper 1496-0: 55-97.

Sturrock, A. M., C. N. Trueman, J. A. Milton, C. P. Waring, M. J. Cooper, and E. Hunter. 2014. Physiological influences can outweigh environmental signals in otolith microchemistry research. Marine Ecology Progress Series 500: 245–264. doi: 10.3354/meps10699.

Tanner, S. E., R. P. Vasconcelos, H. N. Cabral, and S. R. Thorrold. 2012. Testing an otolith geochemistry approach to determine population structure and movements of European hake in the northeast Atlantic Ocean and Mediterranean Sea. Fisheries Research 12:198–205. doi: 10.1016/j.fishres.2012.02.013.

Tanner, S. E., P. Reis-Santos, R. P. Vasconcelos, V. F. Fonseca, S. Franca, H. N. Cabral, and S. R. Thorrold. 2013. Does otolith geochemistry record ambient environmental conditions in a temperate tidal estuary? Journal of Experimental Marine Biology and Ecology 441: 7–15. doi: 10.1016/j.jembe.2013.01.009.

Tanner, S. E., P. Reis-Santos, and H. N. Cabral. 2016. Otolith chemistry in stock delineation: A brief overview, current challenges and future prospects. Fisheries Research 173: 206-213.

Taylor, E. B. 1991. A review of local adaptation in Salmonidae, with particular reference to Pacific and Atlantic salmon. Aquaculture 98:185–207.

Thomas, O. R. B., and S. E. Swearer. 2019. Otolith biochemistry—a review. Reviews in Fisheries Science and Aquaculture 27(4):458–489. doi:10.1080/23308249.2019.1627285.

Thomas, O. R. B., K. Ganio, B. R. Roberts, and S. E. Swearer. 2017. Trace element–protein interactions in endolymph from the inner ear of fish: implications for environmental reconstructions using fish otolith chemistry. Metallomics 9(3):239–249. doi:10.1039/C6MT00189K.

Thorrold, S. R., and S. Shuttleworth. 2000. In situ analysis of trace elements and isotope ratios in fish otoliths using laser ablation sector field inductively coupled plasma mass spectrometry. Canadian Journal of Fisheries and Aquatic Sciences 57(6):1232–1242. doi: 10.1139/f00-054.

Thorrold, S. R., and S. E. Swearer. 2009. Otolith chemistry. *In* B. S. Green, B. D. Mapstone, G. Carlos, and G. A. Begg, editors. Tropical fish otoliths: information for assessment, management and ecology. Springer, Netherlands.

Thorrold, S.R., G.P. Jones, S. Planes, and J.A. Hare. 2006. Transgenerational marking of embryonic otoliths in marine fishes using barium stable isotopes. Canadian Journal of Fisheries and Aquatic Sciences 63(6): 1193–1197. doi:10.1139/f06-048.

Thorrold, S. R., C. M. Jones, and S. E. Campana. 1997. Response of otolith microchemistry to environmental variations experienced by larval and juvenile Atlantic Croaker (*Micropogonias undulatus*). Limnology and Oceanography 42:102–111.

Thorrold, S. R., C. M. Jones, S. E. Campana, J. W. McLaren, and J. W. H. Lam. 1998a. Trace element signatures in otoliths record natal river of juvenile American Shad (*Alosa sapidissima*). Limnology and Oceanography 43:1826– 1835.

Thorrold, S. R., C. M. Jones, P. K. Swart, and T. E. Targett. 1998b. Accurate classification of juvenile Weakfish *Cynoscion regalis* to estuarine nursery areas based on chemical signatures in otoliths. Marine Ecology Progress Series 173:253–265.

Thorrold S. R., C. Latkoczy, P. K. Swart, and C. M. Jones. 2001. Natal homing in a marine fish metapopulation. Science 291:297–299.

Thresher, R. E., and C. H. Procter. 2007. Population structure and life history of orange roughy (*Hoplostethus atlanticus*) in the SW Pacific: inferences from otolith chemistry. Marine Biology 152: 461–473.

Turner, S. M., and K. E. Limburg. 2014. Determination of River Herring Natal Origin using Otolith Chemical Markers: Accuracy as a Function of Spatial Scale and Choice of Markers. Transactions of the American Fisheries Society 143(6):1530-1543. DOI: 10.1080/00028487.2014.949012

Turner, D., M. Whitfield, and A. Dickson. 1981. The equilibrium speciation of dissolved components in freshwater and sea water at 25 C and 1 atm pressure. Geochimica et Cosmochimica Acta 45(6):855–881. doi:10.1016/0016-7037(81)90115-0.

Vasconcelos R. P., P. Reis-Santos, S. E. Tanner, V. Fonseca C. Latkoczy, D. Günther, M. J. Costa, and H. Cabral. 2007. Discriminating estuarine nurseries for five fish species through otolith elemental fingerprints. Marine Ecology Progress Series 350: 117−126. doi: 10.3354/meps07109.

Volk, E.C., A. Blakley, S.L. Schroder, and S.M. Kuehner. 2000. Otolith chemistry reflects migratory characteristics of Pacific salmonids: using otolith core chemistry to distinguish maternal associations with sea and freshwaters. Fisheries research 46(1–3): 251–266.

Walther, B. D., and K. E. Limburg. 2012. The use of otolith chemistry to characterize diadromous migrations. Journal of Fish Biology: 81:796-825.

Walther, B. D., and S. R. Thorrold. 2006. Water, not food, contributes the majority of strontium and barium deposited in the otoliths of marine fish. Marine Ecology Progress Series 311:125-130. DOI: 10.3354/meps311125.

Walther, B. D., and S. R. Thorrold. 2008. Continental-scale variation in otolith geochemistry of juvenile American Shad. Canadian Journal of Fisheries and Aquatic Sciences 65:2623–2635.

Walther, B. D., and S. R. Thorrold. 2010. Limited diversity in natal origins of immature anadromous fish during ocean residency. Canadian Journal of Fisheries and Aquatic Sciences 67: 1699–1707.

Walther, B. D., S. R. Thorrold, and J. E. Olney. 2008. Geochemical signatures in otoliths record natal origins of American Shad. Transactions of the American Fisheries Society 137:57–69.

Naisyin Wang and Adrian Raftery with contributions from Chris Fraley fraley@uw.edu (2017). covRobust: Robust Covariance Estimation via Nearest Neighbor Cleaning. R package version 1.1-3.

Waples R. S., D. J. Teel, J. M. Meyer, A. R. Marshall. 2004. Life-history divergence in Chinook salmon: historic contingency and parallel evolution. Evolution 58:386–403.

Wells, R. J. B., J. R. Rooker, and D. G. Itano. 2012. Nursery origin of yellowfin tuna in the Hawaiian Islands. Marine Ecology Progress Series 461: 187-189.

Wilson, T. R. S. 1975. Salinity and the major elements of sea water. In Chemical Oceanography, J. P. Riley and G. Skirrow (eds). London: Academic Press, pp. 365–413.

Woodcock S. H. and B. D. Walther. 2014. Concentration-dependent mixing models predict values of diet-derived stable isotope ratios in fish otoliths. Journal of Experimental Marine Biology and Ecology 454: 63–69.

Woodcock S. H., C. A. Grieshaber., and B. D. Walther. 2013. Dietary transfer of enriched stable isotopes to mark otoliths, fin rays, and scales. Canadian Journal of Fisheries and Aquatic Sciences. 70(1): 1–4.

Wright P. J. 1991. The influence of metabolic rate on otolith increment width in Atlantic salmon parr, *Salmo salar*. Journal of Fisheries Biology 38(6):929–933. doi:10.1111/j.1095-8649.1991. tb03632.x.

Tables and figures

Table 2-1. Results of bootstrapped likelihood ratio test for selecting the number of mixture components (clusters) for the Cu subset (superscript a) and the Zn subset (superscript b) of otolith core elemental chemistry. The LRT suggested the optimal number of clusters were 5 in both data sets ($p < 0.05$)

PC	LRTS[a]	p-value[a]	LRTS[b]	p-value[b]
1 vs 2	254.79	0.001	255.23	0.001
2 vs 3	290.54	0.001	260.23	0.001
3 vs 4	166.76	0.001	84.51	0.001
4 vs 5	37.99	0.015	46.31	0.002
5 vs 6	30.24	0.079	0.78	0.993

Table 2-2. Average ratio of each element +/- the bootstrap standard error for each cluster in the Cu subset of otolith core chemistry.

Element	A	B	C	D	E
Mg	0.17 +/- 0.01	0.90 +/- 0.13	0.19 +/- 0.01	0.35 +/- 0.00	1.08 +/- 0.00
Mn	0.02 +/- 0.05	0.72 +/- 0.06	0.08 +/- 0.00	0.14 +/- 0.02	1.56 +/- 0.01
Sr	0.85 +/- 0.01	0.64 +/- 0.08	0.18 +/- 0.00	0.03 +/- 0.01	4.62 +/- 0.01
Ba	0.83 +/- 0.01	1.25 +/- 0.12	0.00 +/- 0.01	0.06 +/- 0.01	1.82 +/- 0.01
Cu	0.49 +/- 0.01	0.12 +/- 0.01	0.59 +/- 0.02	0.38 +/- 0.00	0.34 +/- 0.00

Table 2-3. Average ratio of each element +/- the bootstrap standard error for each cluster in the Zn subset of otolith core chemistry.

Element	A	B	C	D	E
Mg	0.19 +/- 0.01	0.62 +/- 0.08	0.37 +/- 0.03	0.21 +/- 0.00	1.06 +/- 0.00
Mn	0.00 +/- 0.05	0.15 +/- 0.08	0.03 +/- 0.01	0.19 +/- 0.02	1.59 +/- 0.01
Sr	0.74 +/- 0.01	0.36 +/- 0.05	0.27 +/- 0.01	0.04 +/- 0.00	4.62 +/- 0.01
Ba	0.76 +/- 0.01	0.58 +/- 0.07	0.00 +/- 0.01	0.13 +/- 0.01	1.88 +/- 0.01
Zn	0.49 +/- 0.01	1.19 +/- 0.05	0.42 +/- 0.02	0.40 +/- 0.01	0.62 +/- 0.01

Table 2-4. Combination of the clustering tables for all 5 clusters in the otolith core Cu subset and the Zn subset, along with the associated mixing probabilities and mixing proportion standard errors.

	Cluster:	A	B	C	D	E
Clustering table:	**Cu Subset**	28	28	124	79	30
	Zn Subset	36	44	83	97	29
Mixing probabilities:	**Cu Subset**	0.09	0.12	0.43	0.26	0.1
	Zn Subset	0.12	0.17	0.28	0.33	0.1
Mixing Proportions SE	**Cu Subset**	0.03	0.03	0.04	0.04	0.02
	Zn Subset	0.03	0.04	0.06	0.05	0.02

Table 2-5. Counts of Hickory Shad in each parent river that were assigned to each cluster in the Cu subset (left) and the Zn subset (right) of the otolith core data.

Cluster	A	B	C	D	E
Susquehanna	7		3		
Patapsco		8	1	2	
Potomac	3	1	7		
Patuxent	7	1		2	
Choptank				2	8
Nanticoke		9		1	
Rappahannock	2	1	7	1	1
James	7	1	16	4	
Chowan			14	6	4
Roanoke		1	15	9	1
Pamlico			13	8	2
Neuse		4	30	14	3
Cape Fear	2	1	7	8	1
Waccamaw			2	5	
South Santee			1	5	
Ogeechee			8	2	2
Altamaha				10	
St Johns		1			8
Total:	28	28	124	79	30

Cluster	A	B	C	D	E
Susquehanna	6		4		
Patapsco	1	8	1	1	
Potomac	4	1	6		
Patuxent	8	1	1		
Choptank		1		2	7
Nanticoke		9		1	
Rappahannock	3	3	5		1
James	7	3	13	5	
Chowan		3	7	10	4
Roanoke		4	10	11	1
Pamlico		1	5	15	2
Neuse		8	18	22	3
Cape Fear	6		5	7	1
Waccamaw			2	5	
South Santee			1	5	
Ogeechee	1	1	5	3	2
Altamaha				10	
St Johns		1			8
Total:	36	44	83	97	29

Table 2-6. Percent of Hickory Shad captured in each parent river that were assigned to each cluster in the copper subset (left) and the zinc subset (right) of the otolith core data.

Cluster	A	B	C	D	E
Susquehanna	70	0	30	0	0
Patapsco	0	73	9	18	0
Potomac	27	9	64	0	0
Patuxent	70	10	0	20	0
Choptank	0	0	0	20	80
Nanticoke	0	90	0	10	0
Rappahannock	17	8	58	8	8
James	25	4	57	14	0
Chowan	0	0	58	25	17
Roanoke	0	4	58	35	4
Pamlico	0	0	57	35	9
Neuse	0	8	59	27	6
Cape Fear	11	5	37	42	5
Waccamaw	0	0	29	71	0
South Santee	0	0	17	83	0
Ogeechee	0	0	67	17	17
Altamaha	0	0	0	100	0
St Johns	0	11	0	0	89
Total:	28	28	124	79	30

Cluster	A	B	C	D	E
Susquehanna	60	0	40	0	0
Patapsco	9	73	9	9	0
Potomac	36	9	55	0	0
Patuxent	80	10	10	0	0
Choptank	0	10	0	20	70
Nanticoke	0	90	0	10	0
Rappahannock	25	25	42	0	8
James	25	11	46	18	0
Chowan	0	13	29	42	17
Roanoke	0	15	38	42	4
Pamlico	0	4	22	65	9
Neuse	0	16	35	43	6
Cape Fear	32	0	26	37	5
Waccamaw	0	0	29	71	0
South Santee	0	0	17	83	0
Ogeechee	8	8	42	25	17
Altamaha	0	0	0	100	0
St Johns	0	11	0	0	89
Total:	36	83	97	44	29

Table 2-7. Results of Chi-Square test of independence for each subset of the otolith core data showing values calculated from the observed Chi-Square test and the simulated distribution of Chi-Square test statistics.

		Cu Subset	Zn Subset
observed	X^2	429	348.8
	df	68	68
	p-value	<0.01	<0.01
simulated	p-value	<0.01	<0.01

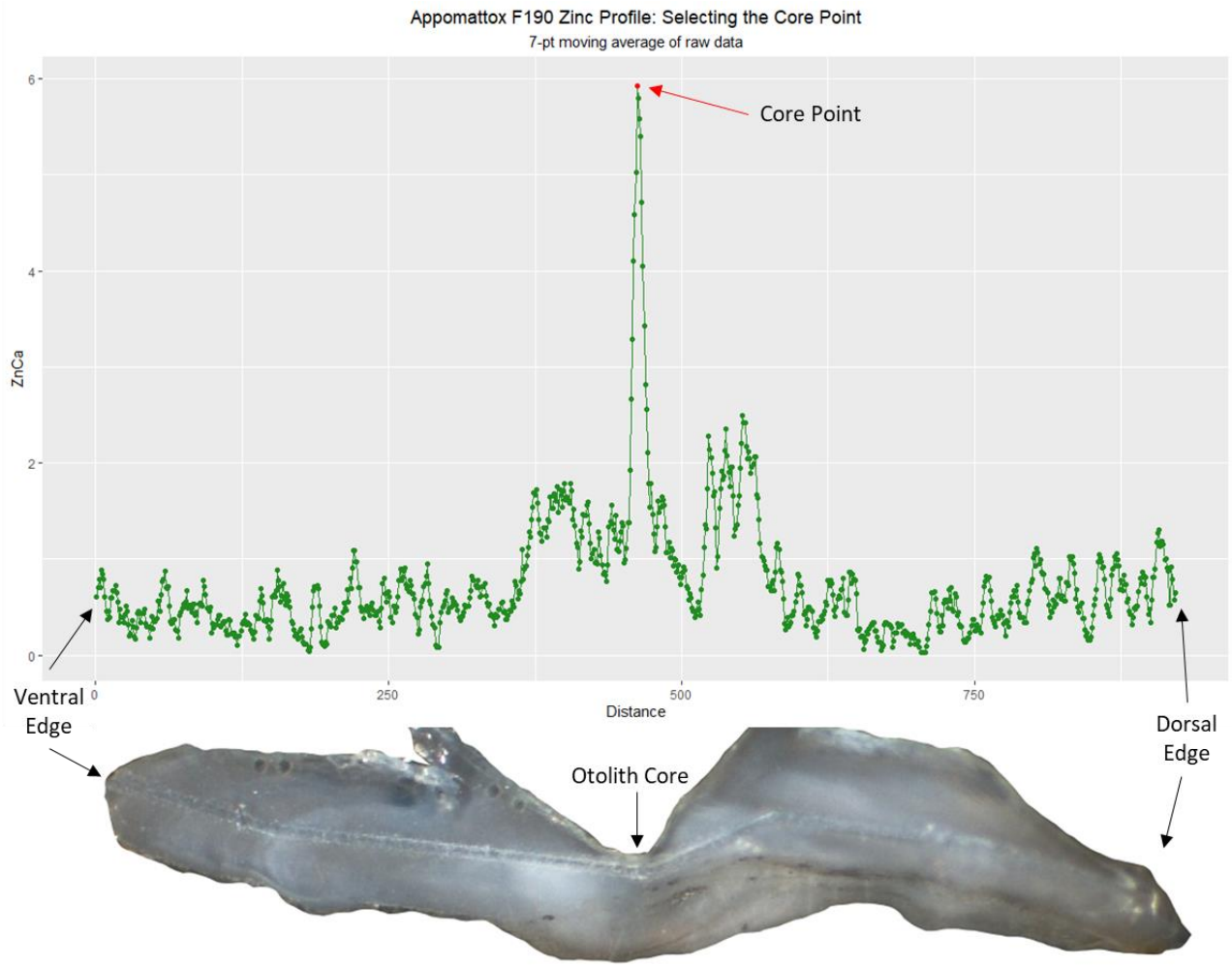

Figure 2-1. Sectioned otolith and zinc profile from a Hickory Shad captured in the Appomattox River showing the highest value of zinc near the central node of the otolith core (red dot) that was selected as the core point to represent birth. Distance (x-axis) represents data points, where each consecutive data point is approximately 2.5 micrometers away from the previous data point.

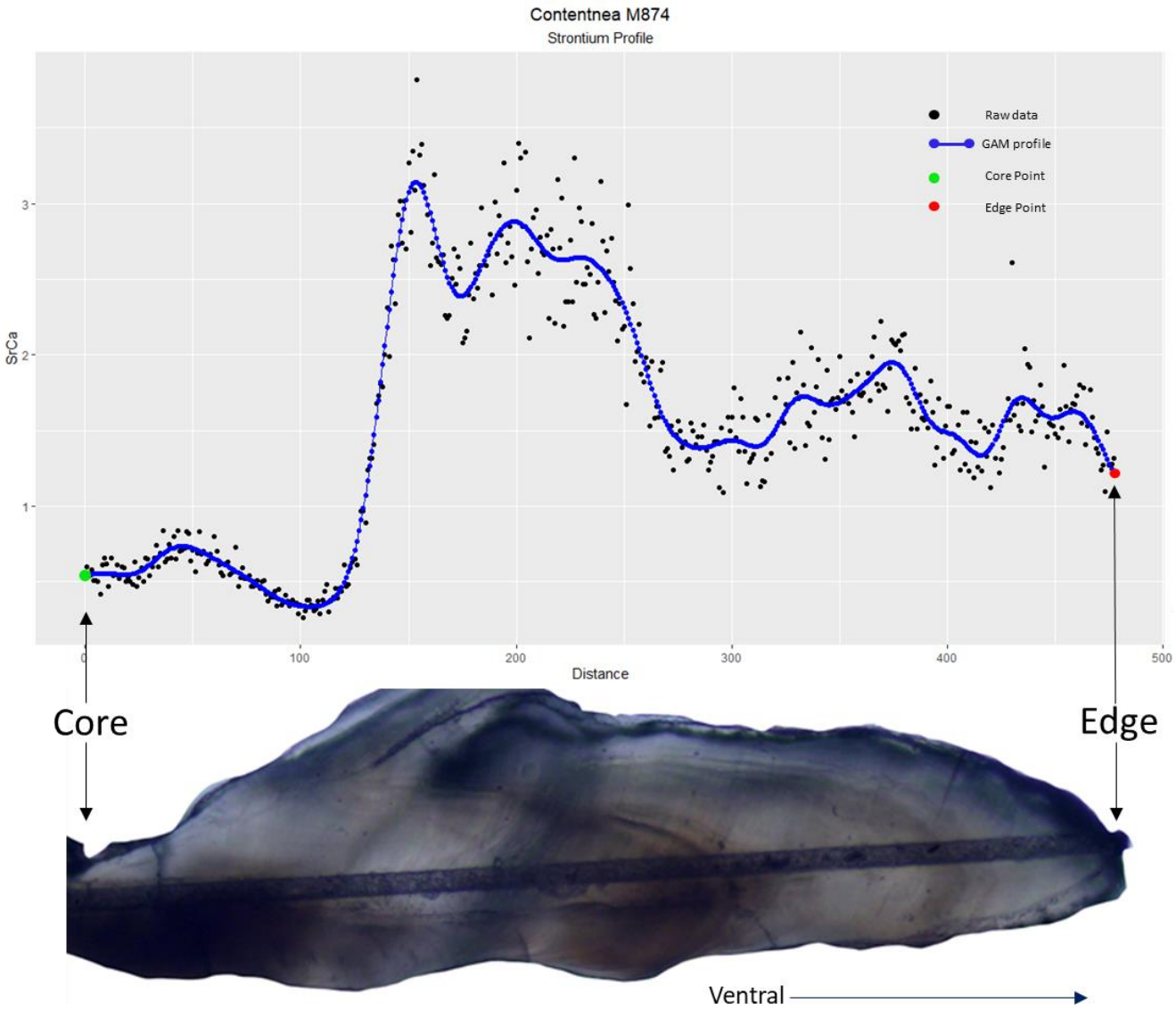

Figure 2-2. Sectioned otolith and strontium profile of a Hickory Shad captured in Contentnea Creek, NC showing distance away from the central node of the otolith core (green dot) on the x-axis, black dots denote the raw data, and the blue line denotes the data when smoothed with a generalized additive model. Distance (x-axis) represents data points, where each consecutive data point is approximately 2.5 micrometers away from the previous data point.

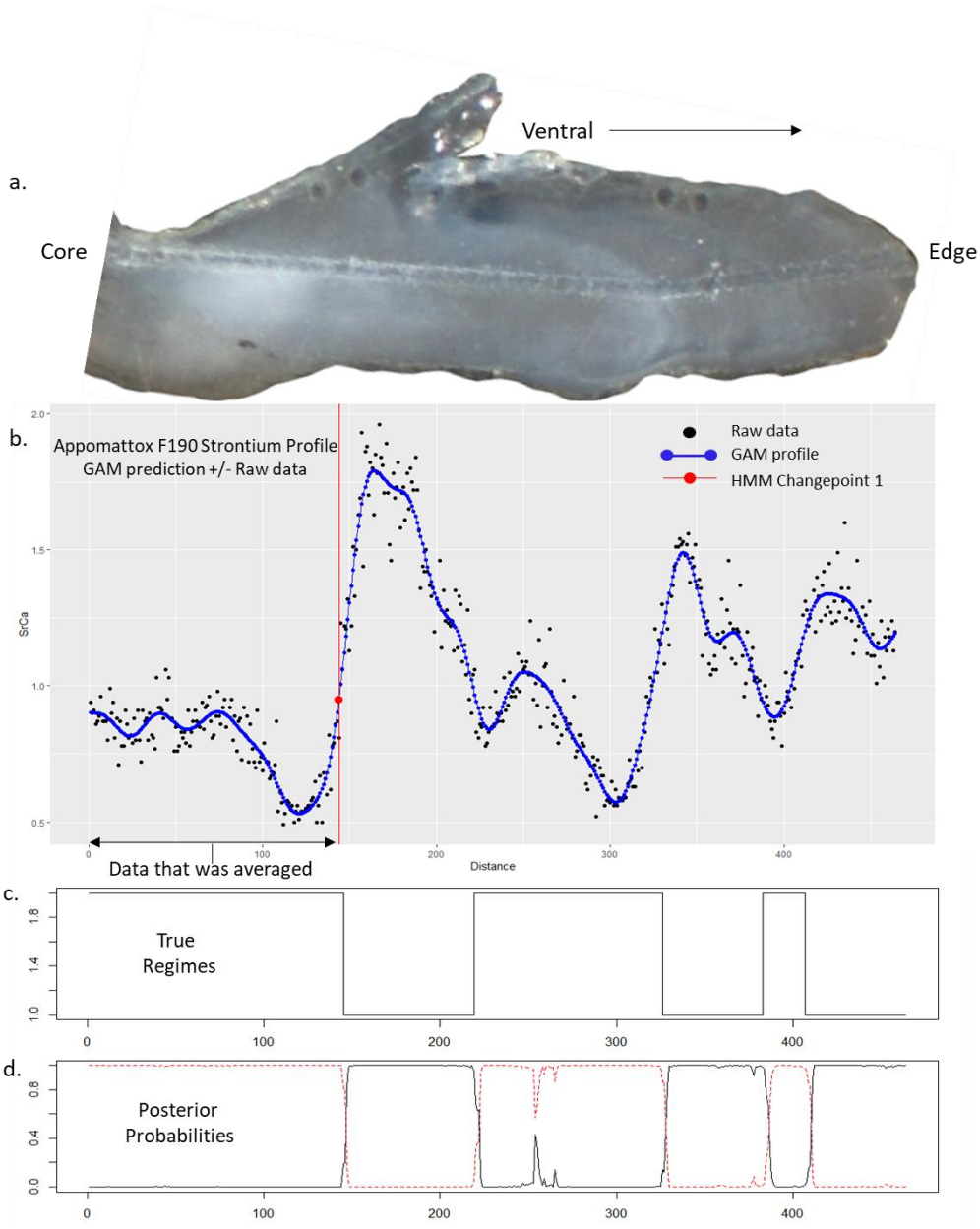

Figure 2-3. Sectioned otolith (a.), strontium profile (b.) of a Hickory Shad captured in the Appomattox River, VA showing the true regimes (c.) and posterior probabilities (d.) that were identified by the hidden Markov model, and the data that were averaged within the first regime to represent the element signature of the natal watershed. Distance (x-axis) represents data points, where each consecutive data point is approximately 2.5 micrometers away from the previous data point.

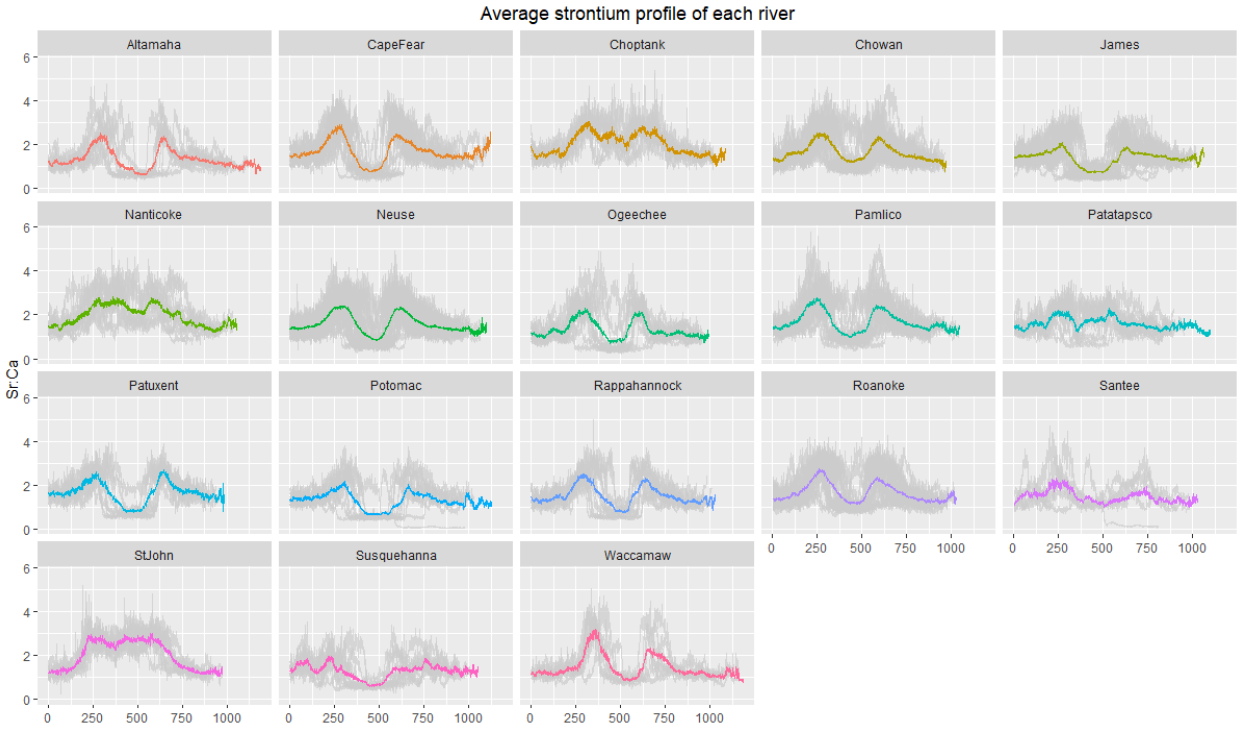

Figure 2-4. Plots showing the average strontium profile of each capture location as colored lines laid over the strontium profiles of all Hickory Shad from each respective capture location, which are shown behind the colored lines to illustrate the error associated with each average profile. Distance (x-axis) represents data points, where each consecutive data point is approximately 2.5 micrometers away from the previous data point.

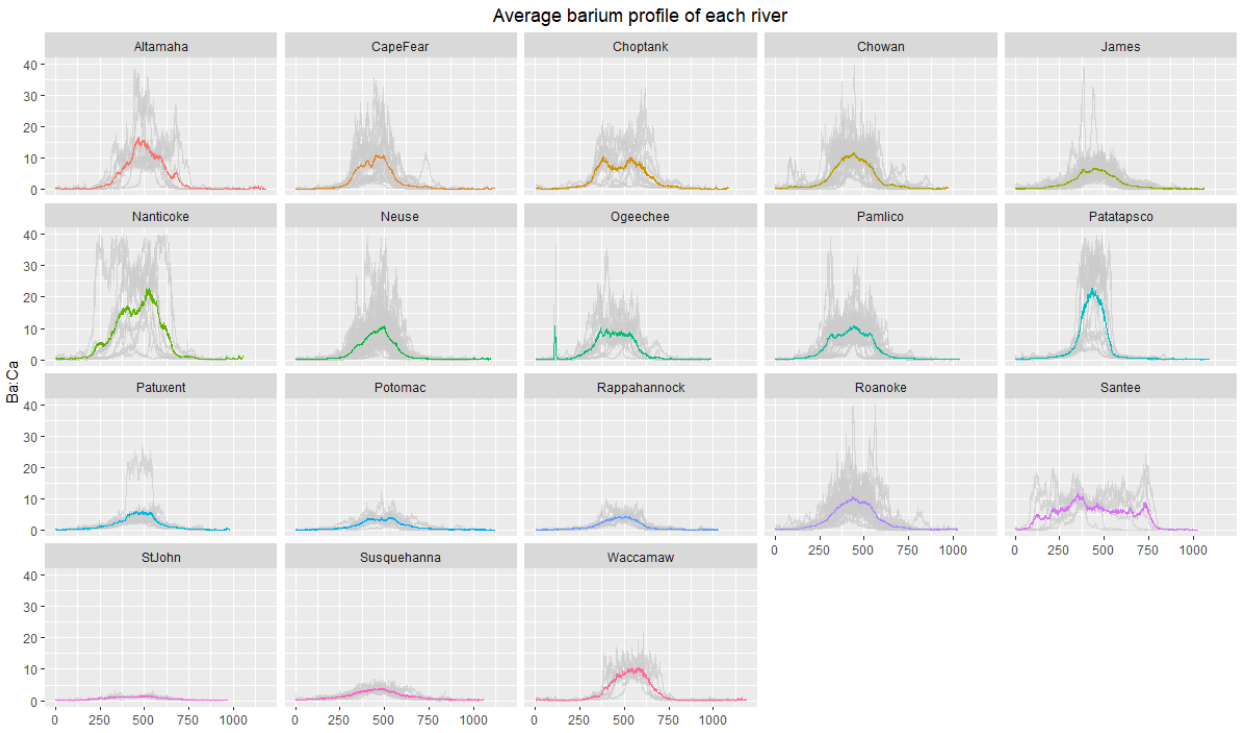

Figure 2-5. Plots showing the average barium profile of each capture location as colored lines laid over the barium profiles of all Hickory Shad from each respective capture location, which are shown behind the colored lines to illustrate the error associated with each average profile. Distance (x-axis) represents data points, where each consecutive data point is approximately 2.5 micrometers away from the previous data point.

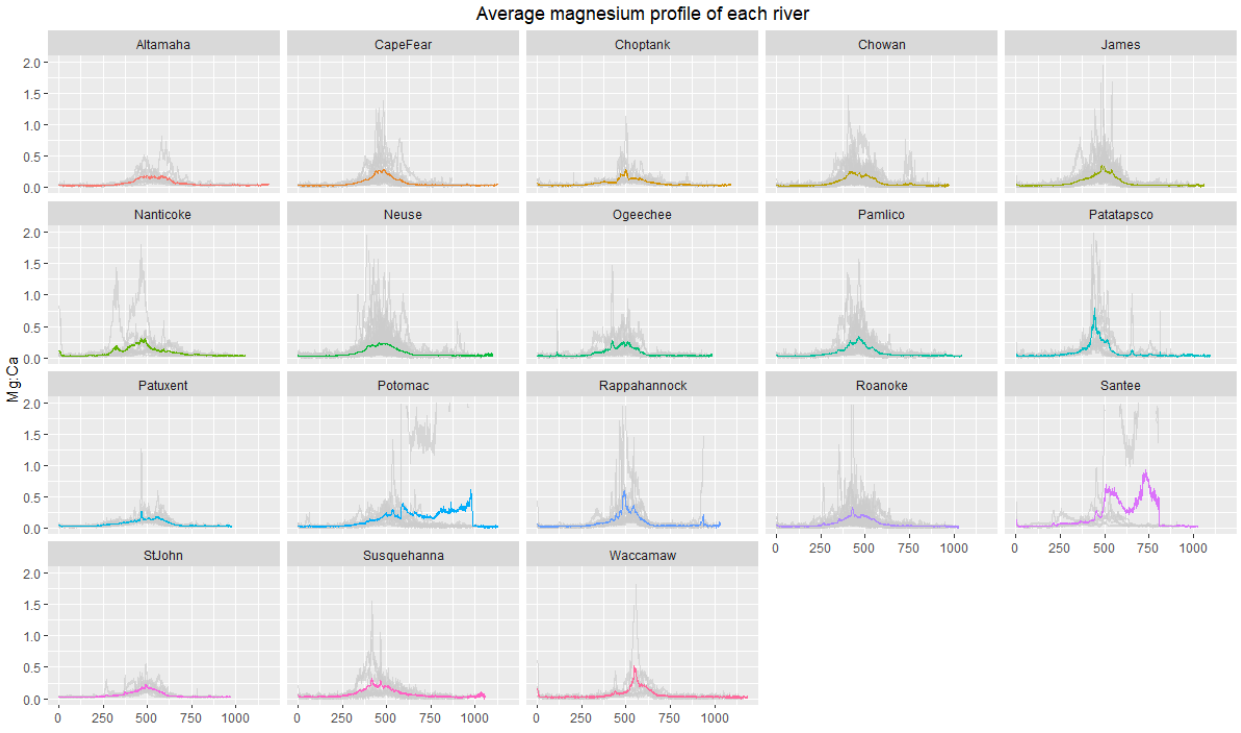

Figure 2-6. Plots showing the average magnesium profile of each capture location as colored lines laid over the magnesium profiles of all Hickory Shad from each respective capture location, which are shown behind the colored lines to illustrate the error associated with each average profile. Distance (x-axis) represents data points, where each consecutive data point is approximately 2.5 micrometers away from the previous data point.

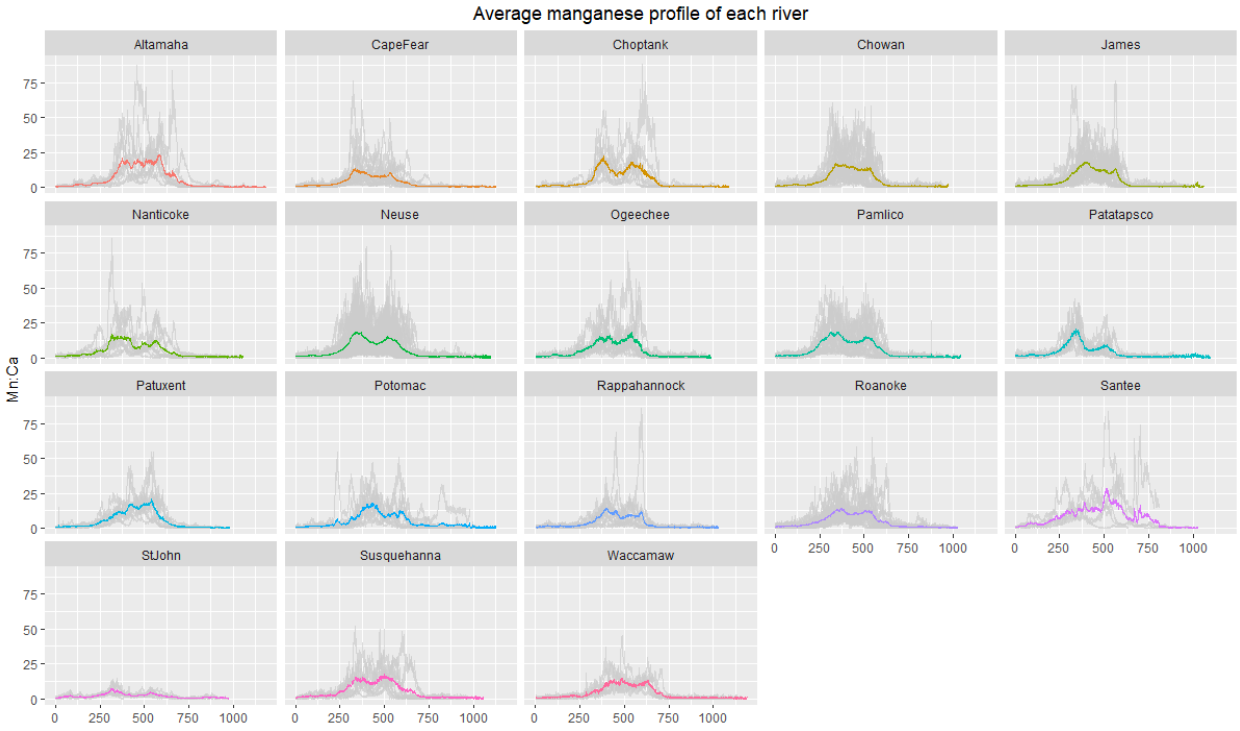

Figure 2-7. Plots showing the average manganese profile of each capture location as colored lines laid over the manganese profiles of all Hickory Shad from each respective capture location, which are shown behind the colored lines to illustrate the error associated with each average profile. Distance (x-axis) represents data points, where each consecutive data point is approximately 2.5 micrometers away from the previous data point.

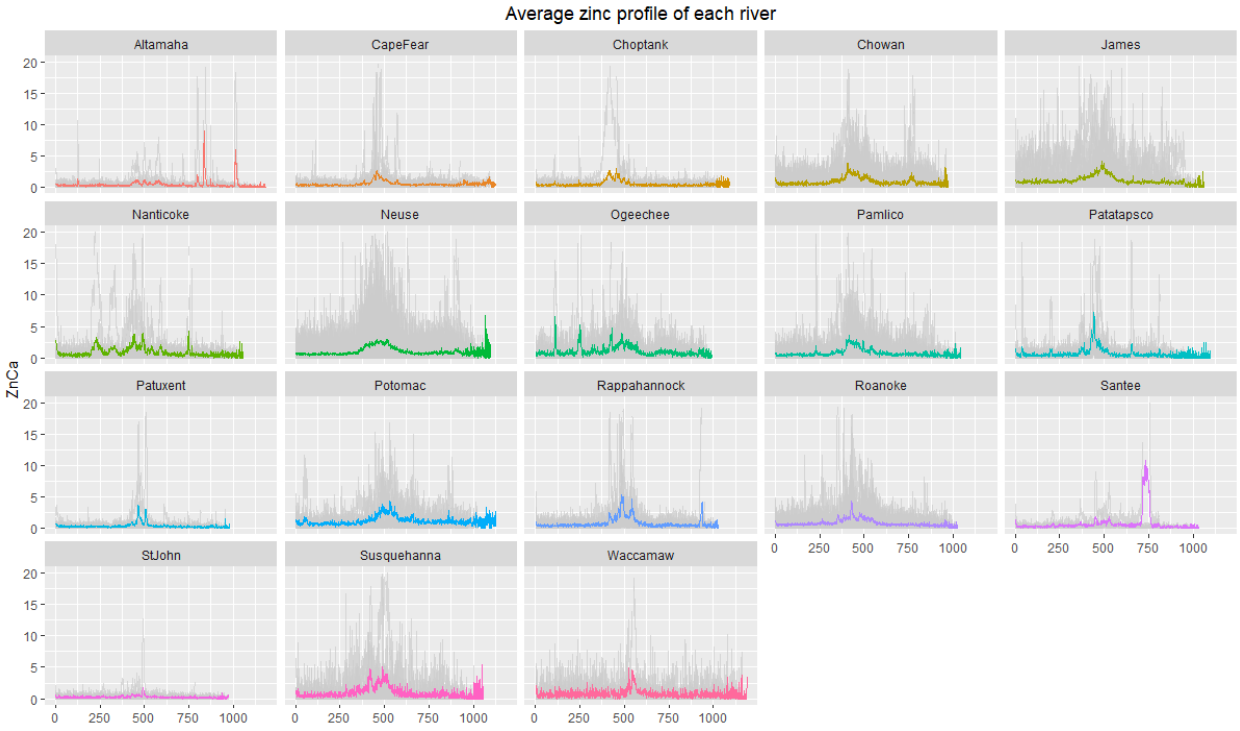

Figure 2-8. Plots showing the average zinc profile of each capture location as colored lines laid over the zinc profiles of all Hickory Shad from each respective capture location, which are shown behind the colored lines to illustrate the error associated with each average profile. Distance (x-axis) represents data points, where each consecutive data point is approximately 2.5 micrometers away from the previous data point.

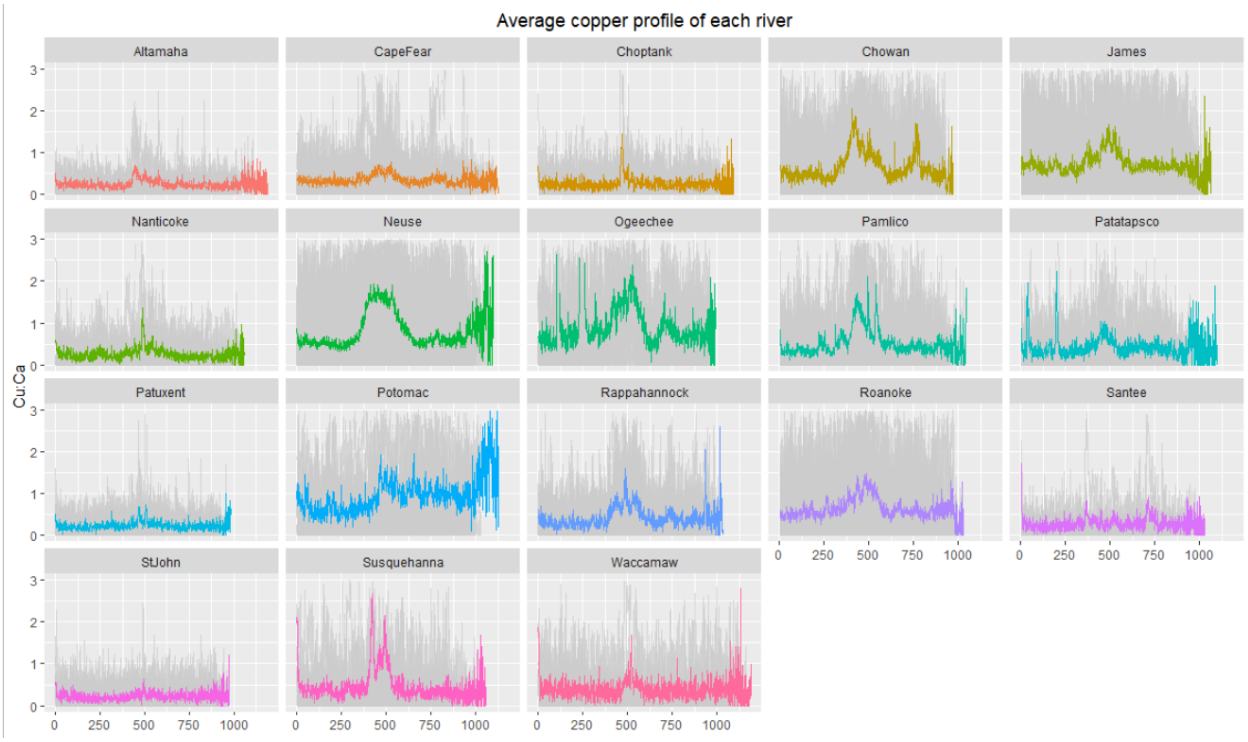

Figure 2-9. Plots showing the average copper profile of each capture location as colored lines laid over the copper profiles of all Hickory Shad from each respective capture location, which are shown behind the colored lines to illustrate the error associated with each average profile. Distance (x-axis) represents data points, where each consecutive data point is approximately 2.5 micrometers away from the previous data point.

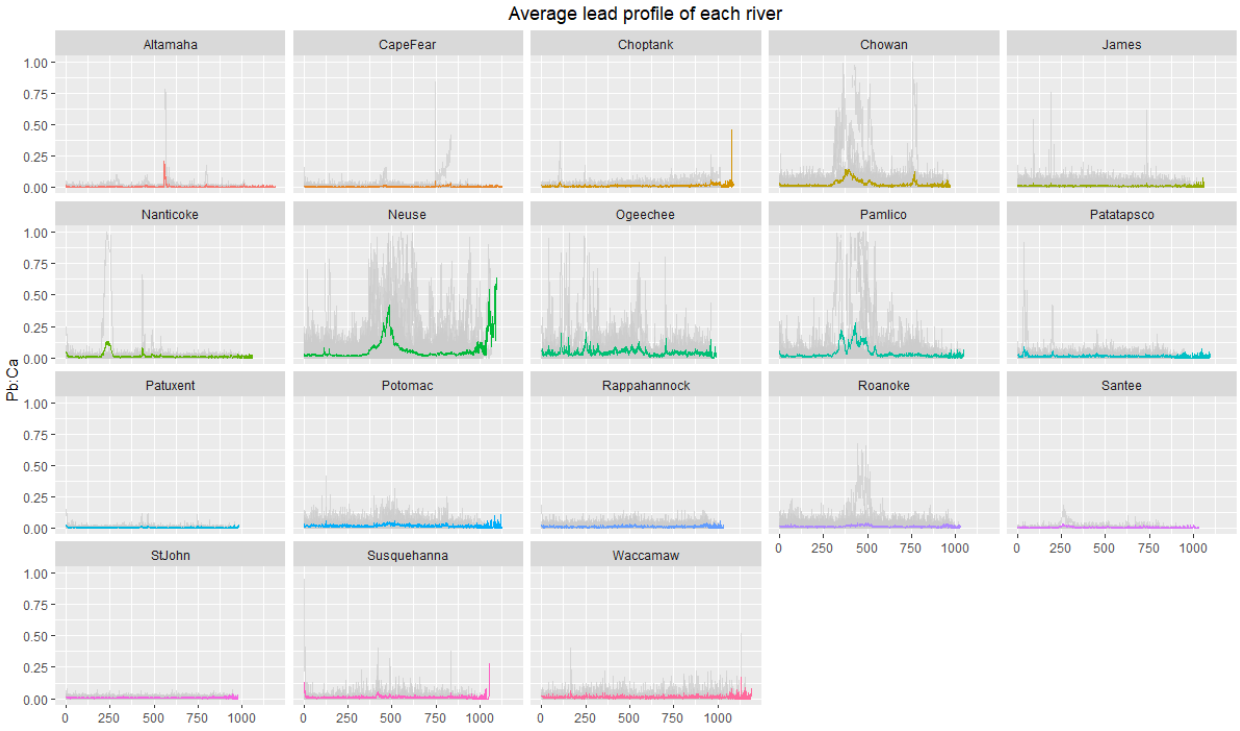

Figure 2-10. Plots showing the average lead profile of each capture location as colored lines laid over the lead profiles of all Hickory Shad from each respective capture location, which are shown behind the colored lines to illustrate the error associated with each average profile. Distance (x-axis) represents data points, where each consecutive data point is approximately 2.5 micrometers away from the previous data point.

	Sr	Mg	Ba	Mn	Pb	Zn	Cu
Sr	1						
Mg	-0.22*	1					
Ba	0.01	0.29*	1				
Mn	-0.44*	0.01	0.23*	1			
Pb	-0.07	0.25*	0.03	0.09	1		
Zn	-0.12*	0.6*	0.17*	0.08	0.4*	1	
Cu	-0.21*	0.35*	0.056	0.2*	0.5*	0.7*	1

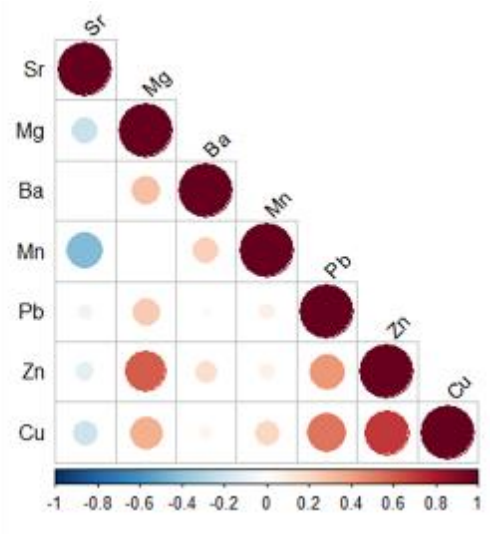

Figure 2-11. Results of correlation tests on the otolith core data showing Pearson's correlation coefficient (r) between each element, with significant r values ($p < 0.05$) denoted by stars* (table), high r values represented by large and dark red circles (factor plot), and low r values represented by large blue circles (factor plot).

	Eigenvalue	Variance%	Cumulative Variance %
comp 1	2.63	37.55	37.55
comp 2	1.35	19.33	56.87
comp 3	1.1	15.68	72.55
comp 4	0.81	11.56	84.11
comp 5	0.53	7.58	91.69
comp 6	0.37	5.31	97.01
comp 7	0.21	2.99	100

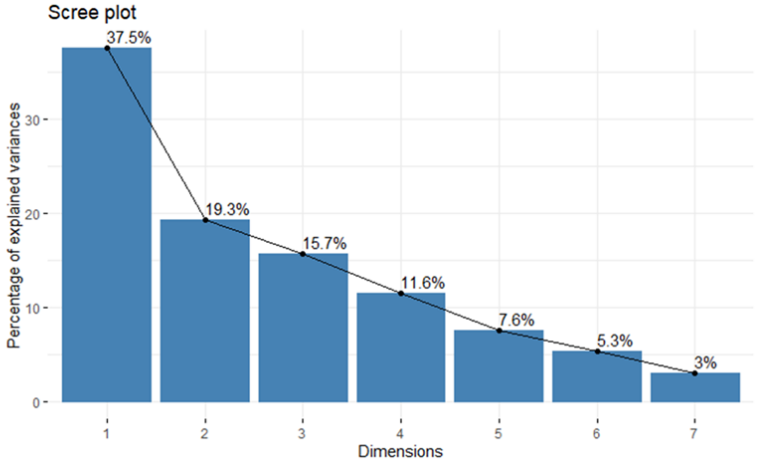

Figure 2-12. Results of principle component analysis on the otolith core data showing eigenvalues, cumulative variance (table), and individual variance (table and scree plot) explained by each principle component.

	Dim1	Dim2	Dim3	Dim4	Dim5	Dim6	Dim7
Mg	0.484	0.015	0.138	0.226	0.034	0.076	0.028
Mn	0.103	0.650	0.005	0.108	0.022	0.112	0.000
Sr	0.142	0.474	0.088	0.179	0.040	0.074	0.005
Ba	0.089	0.057	0.698	0.088	0.006	0.062	0.000
Zn	0.729	0.069	0.003	0.011	0.083	0.001	0.104
Pb	0.404	0.069	0.094	0.176	0.252	0.001	0.003
Cu	0.676	0.019	0.073	0.021	0.094	0.046	0.070

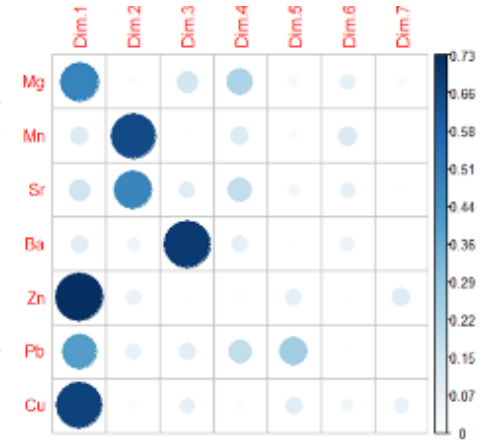

Figure 2-13. Results of principle component analysis on the otolith core data showing the squared cosine (cos^2) values on each principle component axis numerically (table), and graphically (factor map) where larger and darker circles represent higher cos^2 values, indicating better representation on a given axis.

	Dim.1	Dim.2	Dim.3	Dim.4	Dim.5	Dim.6	Dim.7
Mg	18.43	1.11	12.55	27.92	6.32	20.3	13.37
Mn	3.94	48.07	0.41	13.32	4.15	30.07	0.04
Sr	5.39	35.02	7.98	22.15	7.47	19.8	2.2
Ba	3.4	4.2	63.55	10.82	1.21	16.77	0.07
Zn	27.73	5.14	0.23	1.4	15.58	0.36	49.56
Pb	15.39	5.09	8.61	21.75	47.52	0.35	1.3
Cu	25.74	1.38	6.66	2.64	17.75	12.35	33.46

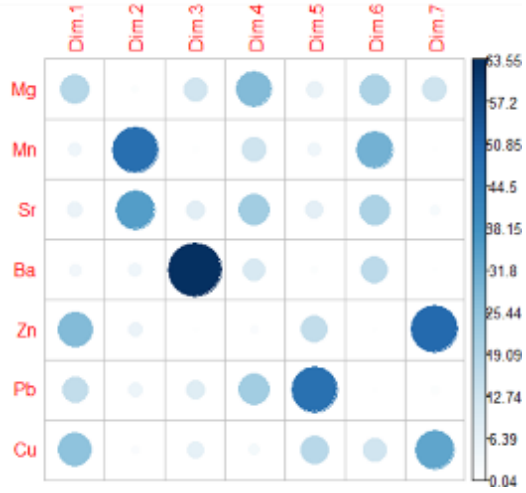

Figure 2-14. Results of principle components analysis on the otolith core data showing the loading scores of elements on each principle component axis displayed numerically (table), and graphically (factor plot), where increasing loading scores are represented by larger and darker circles.

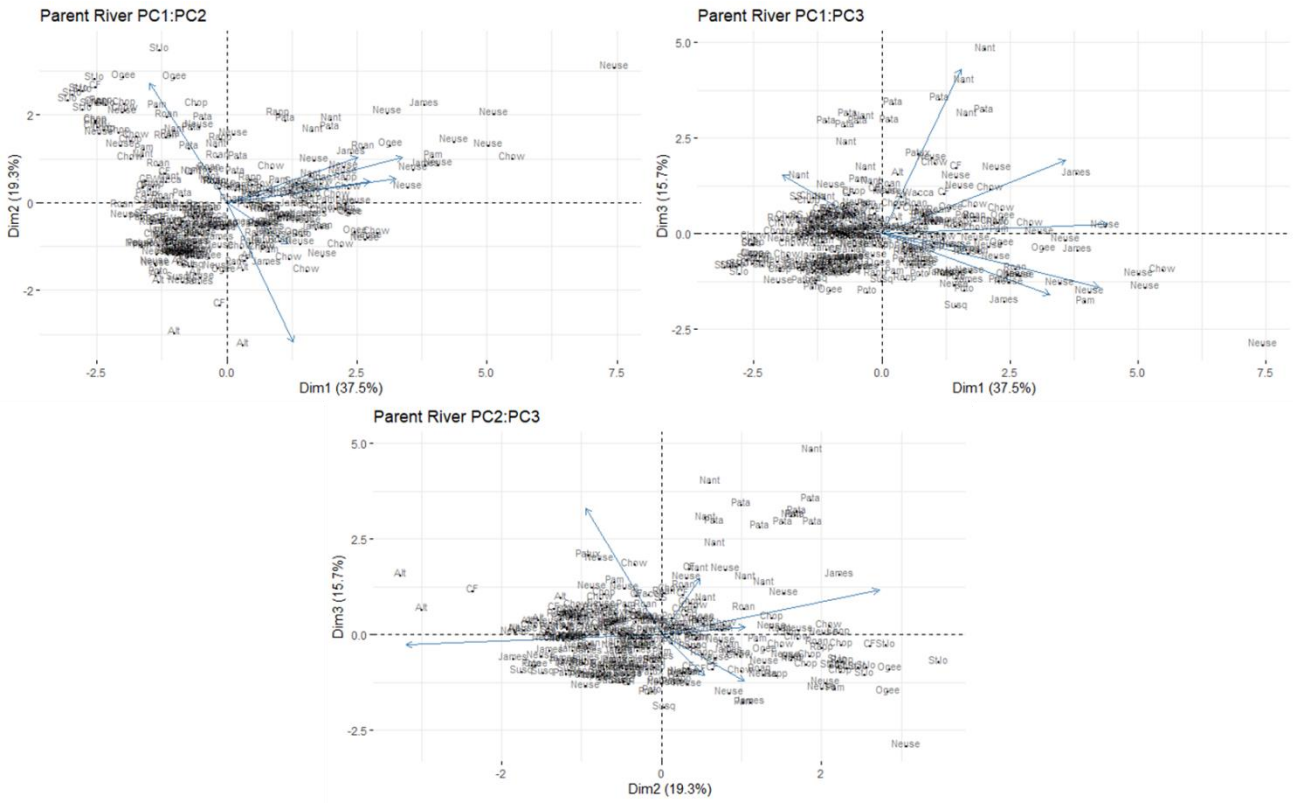

Figure 2-15. Biplots produced during principle components analysis on the otolith edge data comparing the first three principle components in 2-dimentional space with individual data points labeled by the parent river in which the Hickory Shad were captured.

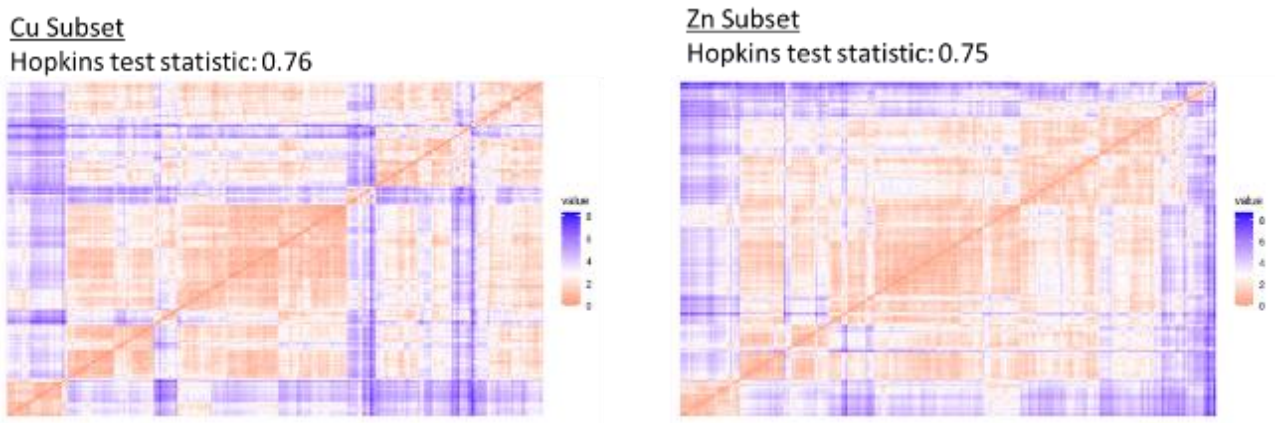

Figure 2-16. Results of Hopkin's test used to evaluate the clustering tendency of the Cu subset (left) and the Zn subset (right) of otolith core elemental chemistry. Graphics are visual representations of ordered dissimilarity matrices following the procedure of Bezdek and Hathaway (2002), where dissimilarity matrices between observations are calculated using Euclidean distance and objects are reordered so that similar objects are displayed near one another. Red colors represent high similarities and blue colors represent low similarities.

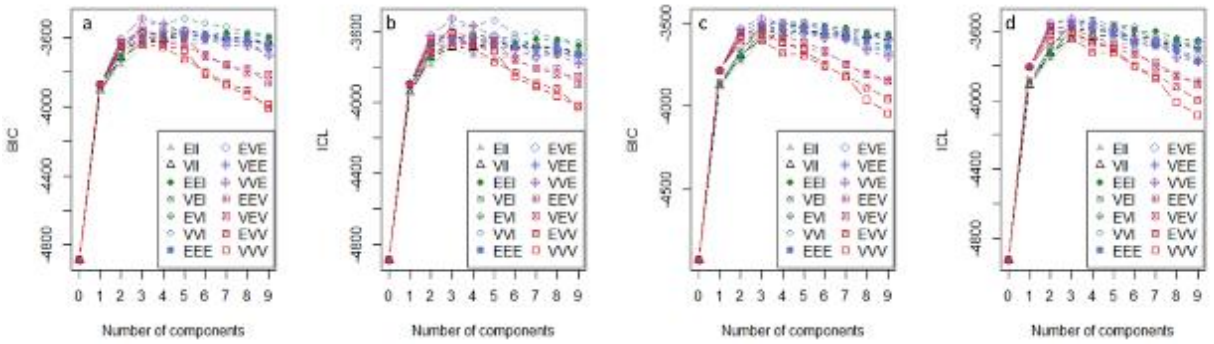

Figure 2-17. Plots showing BIC scores and ICL scores vs the number of components for the Cu subset (a:b), and the Zn subset (c:d) of otolith core elemental chemistry. Model VVE (ellipsoidal, equal orientation) was the optimal model in each case (Cu subset: BIC = -3488.013, ICL = -3525.125; Zn subset: BIC = -3471.559, ICL = -3526.534).

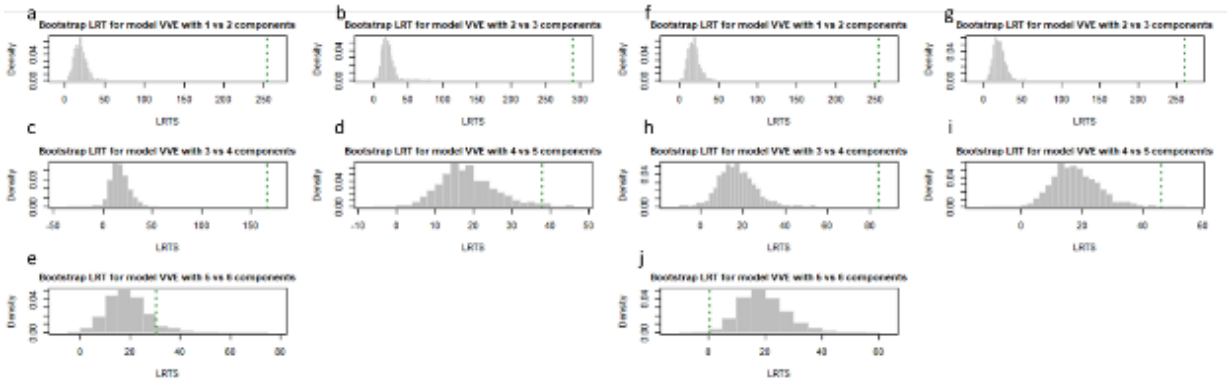

Figure 2-18. Histograms showing the bootstrapped likelihood ratio test distributions used to compare the number of mixture components for the Cu subset (a-e) and the Zn subset (f-j) of otolith core elemental chemistry, with dotted green lines that represent LRTS sample values.

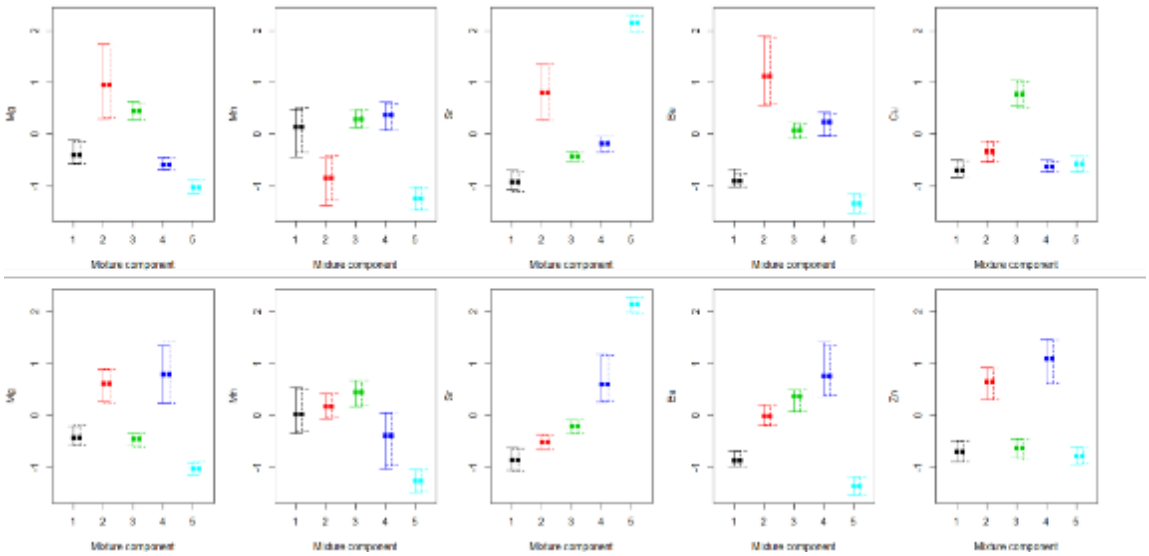

Figure 2-19. Comparison of bootstrap percentile intervals for the means of the Gaussian mixture model fit to the Cu subset (top row) and the Zn subset (bottom row) where solid lines denote the nonparametric bootstrap, and dashed lines denote the weighted likelihood bootstrap. Differences between the two methods were negligible.

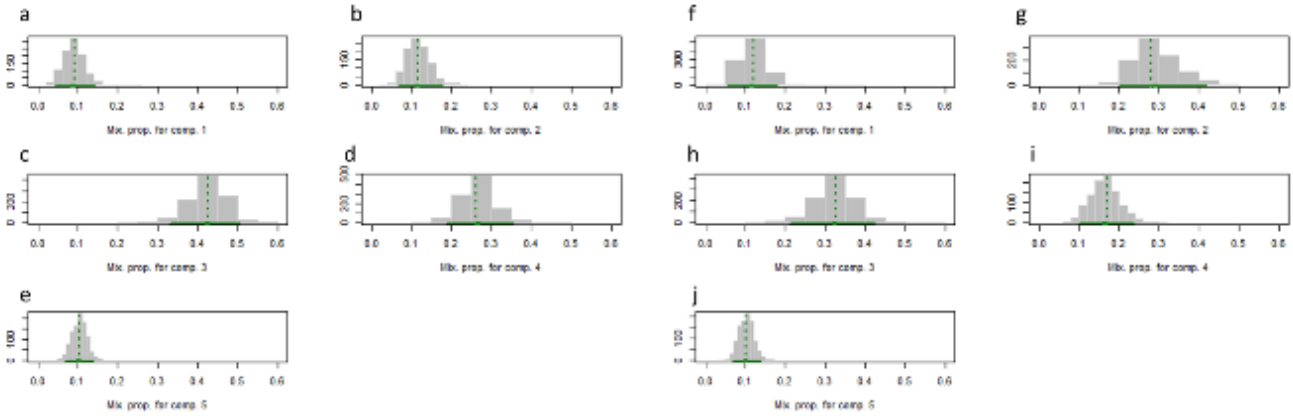

Figure 2-20. Histograms showing bootstrapped distributions of mixture proportions for the Cu subset (a-e) and the Zn subset (f-j) where dotted lines denote the maximum likelihood estimates for the fitted mixture model.

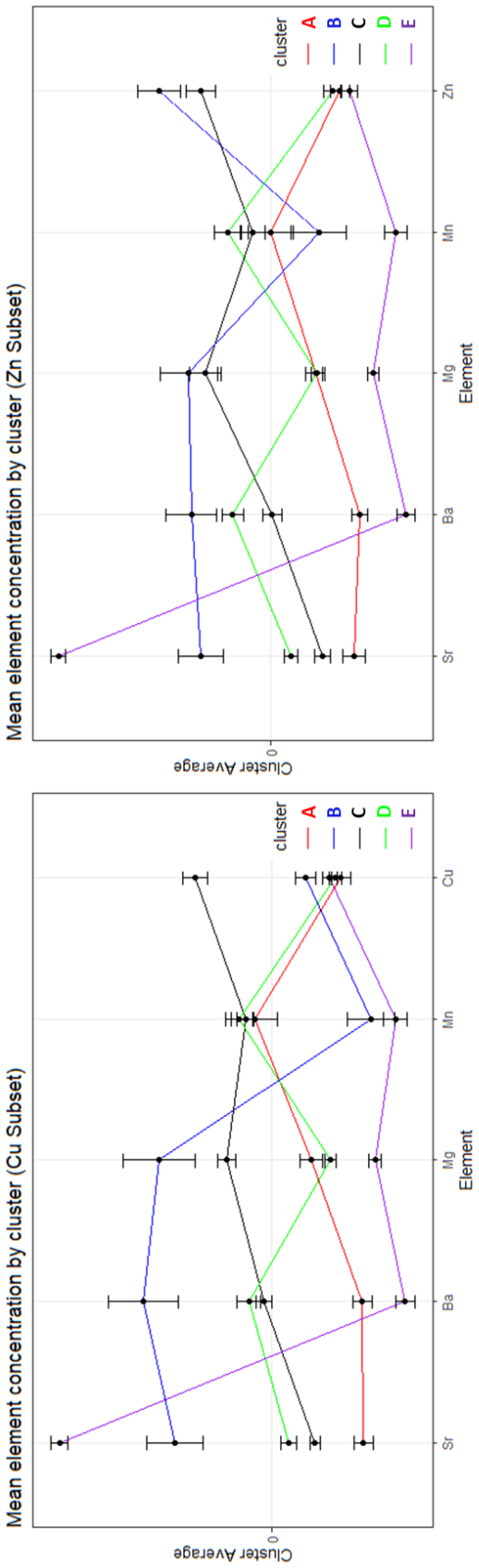

Figure 2-21. Average element concentrations of each cluster for the copper subset (left) and the zinc subset (right) of the natal watershed data. Vertical bars represent standard errors.

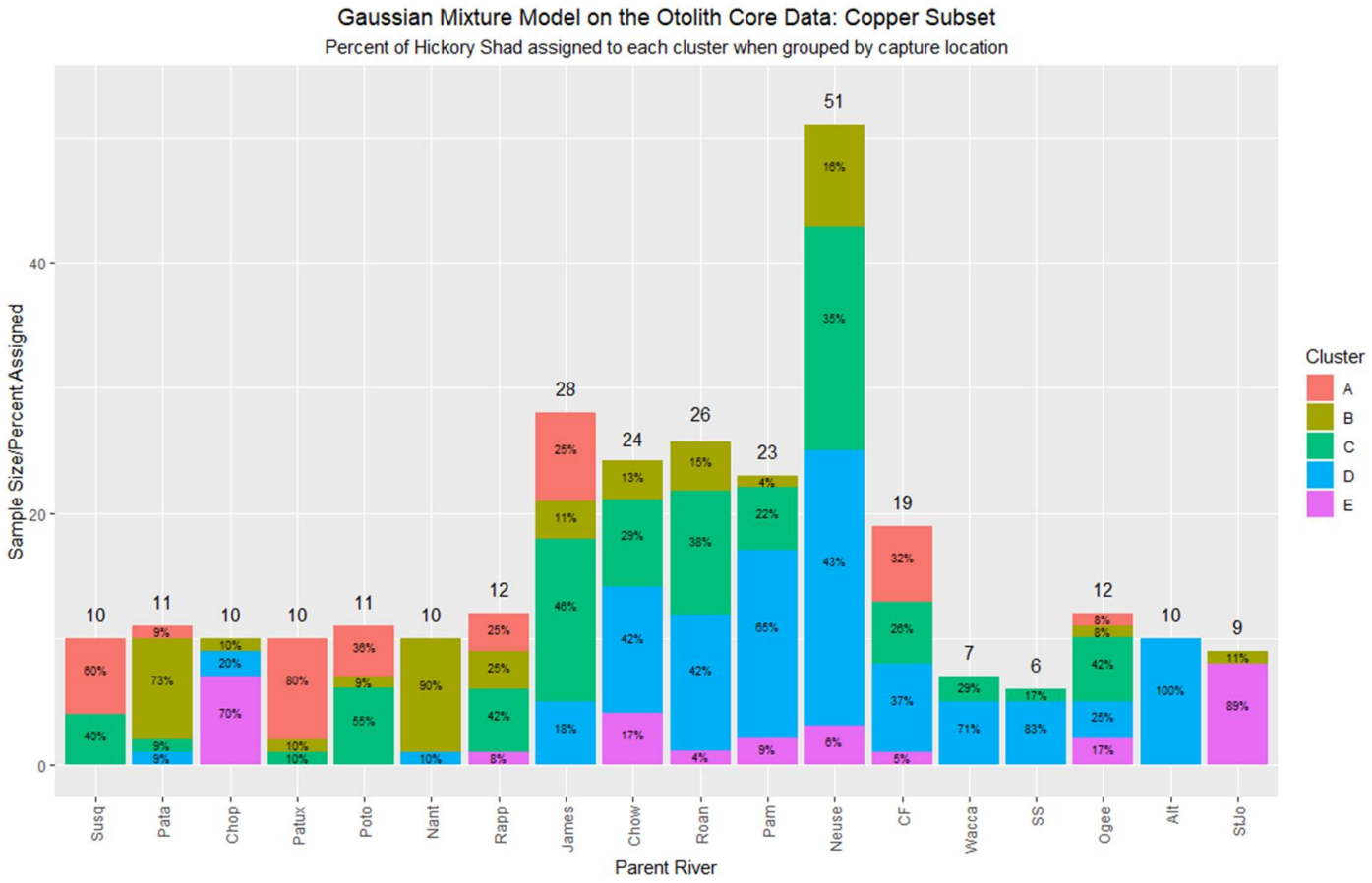

Figure 2-22. The percent of Hickory Shad from each capture location that were assigned to each cluster by the Gaussian mixture model fit to the copper subset of the natal watershed data. Numbers above each bar denote the sample size from each capture location which was used to calculate the percentage of assignment into each cluster. Colors comprising the bar for a given capture location are proportional to the percentage of Hickory Shad from that capture location that were assigned to each cluster, and each color is labeled with the corresponding percentage value

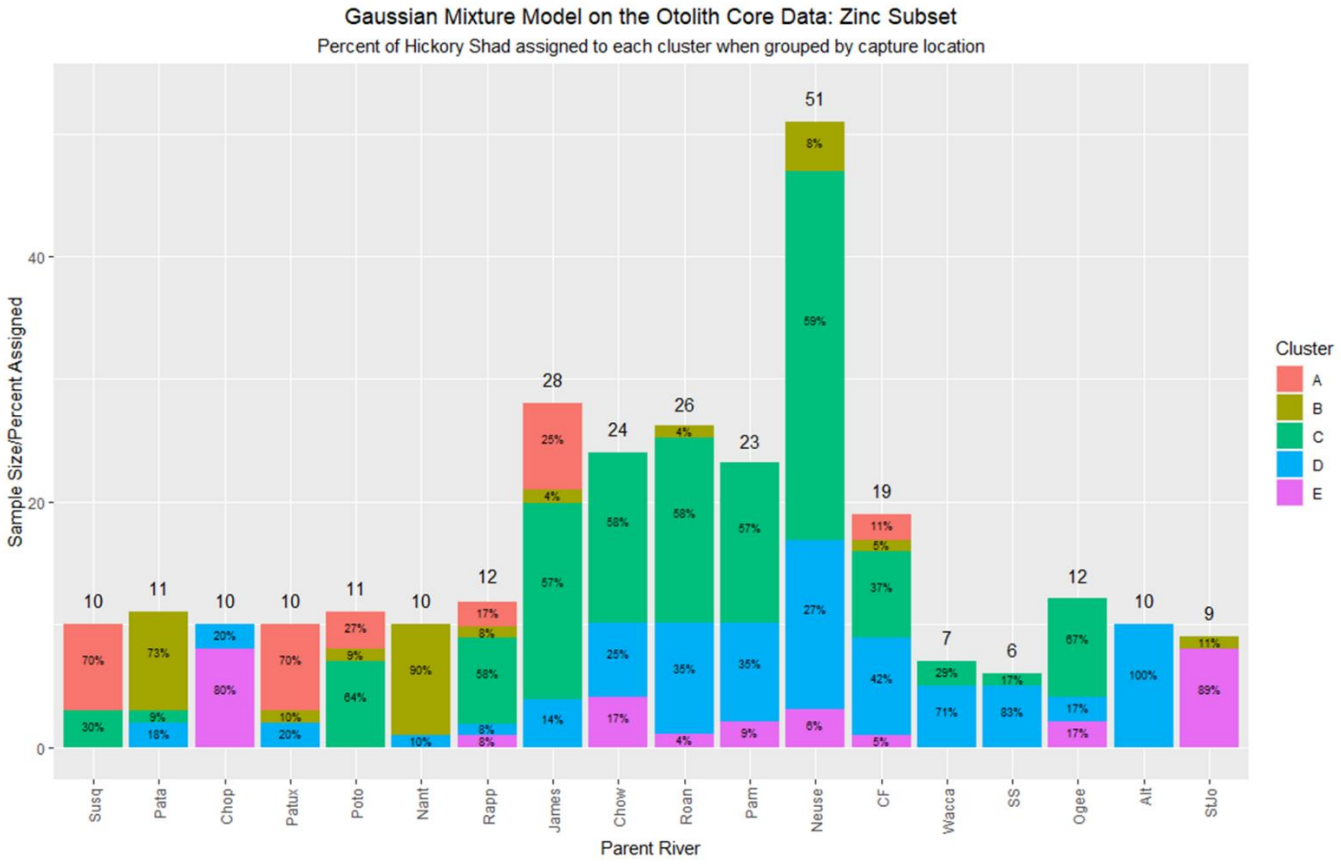

Figure 2-23. The percent of Hickory Shad from each capture location that were assigned to each cluster by the Gaussian mixture model fit to the zinc subset of the natal watershed data. Numbers above each bar denote the sample size from each capture location which was used to calculate the percentage of assignment into each cluster. Colors comprising the bar for a given capture location are proportional to the percentage of Hickory Shad from that capture location that were assigned to each cluster, and each color is labeled with the corresponding percentage value.

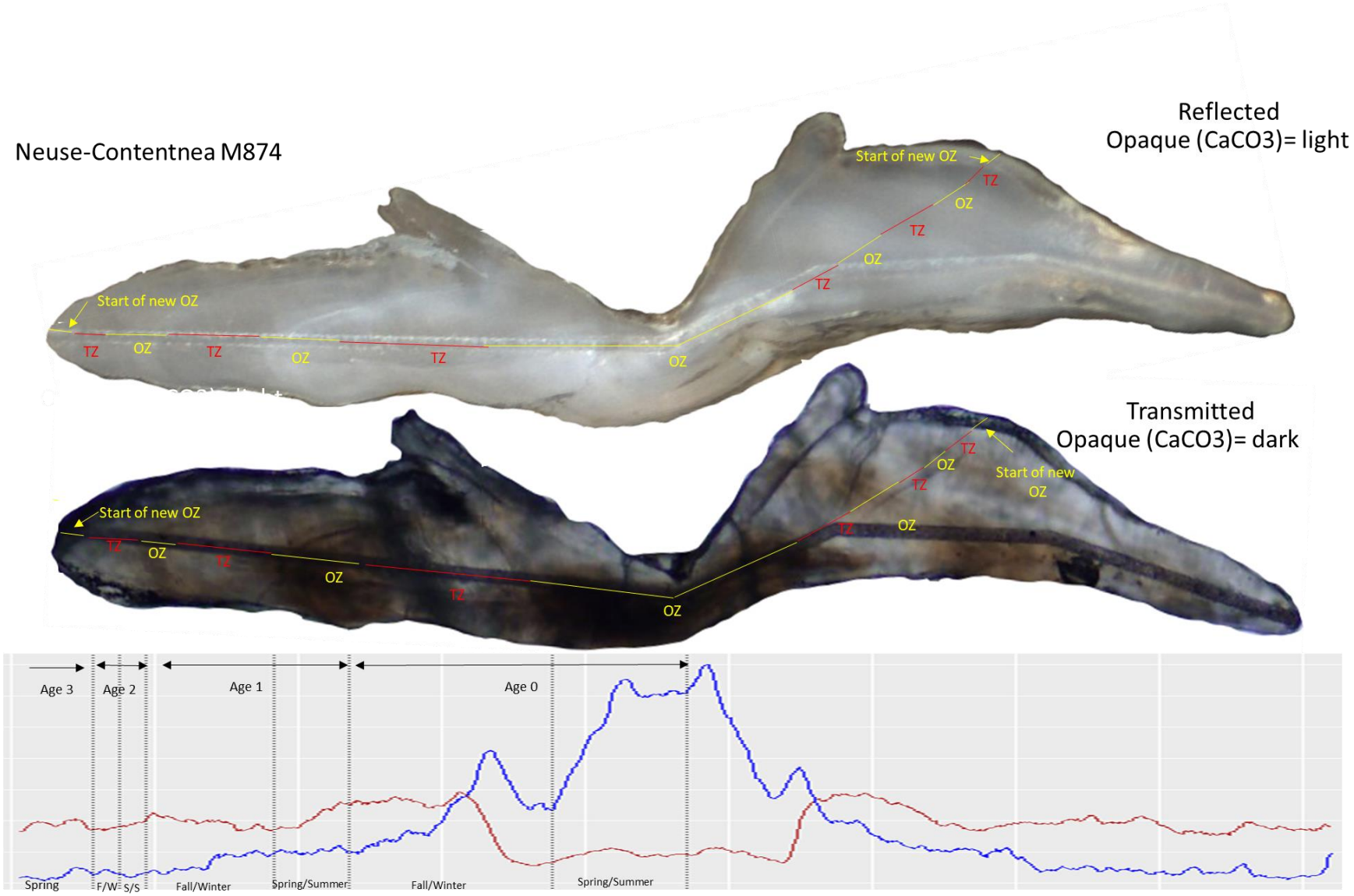
Neuse-Contentnea M874
Reflected
Opaque (CaCO3)= light
Start of new OZ
TZ
OZ
Transmitted
Opaque (CaCO3)= dark
Age 3
Age 2
Age 1
Age 0
Spring
F/W
S/S
Fall/Winter
Spring/Summer
Fall/Winter
Spring/Summer

Figure 2-24. Opaque and translucent zones are shown on a sectioned otolith that was viewed under reflected and transmitted light, and in the strontium and barium profiles of the same otolith; the readers interpretation of age and seasonal patterns, and how they relate to each opaque and translucent zone are included. Distance (x-axis) represents data points, where each consecutive data point is approximately 2.5 micrometers away from the previous data point. Note the inverse patterns of opacity between opaque and translucent zones that are shown under reflected and transmitted light (top). This otolith was taken from a Hickory Shad that was captured in Contentnea Creek (Neuse River, NC).

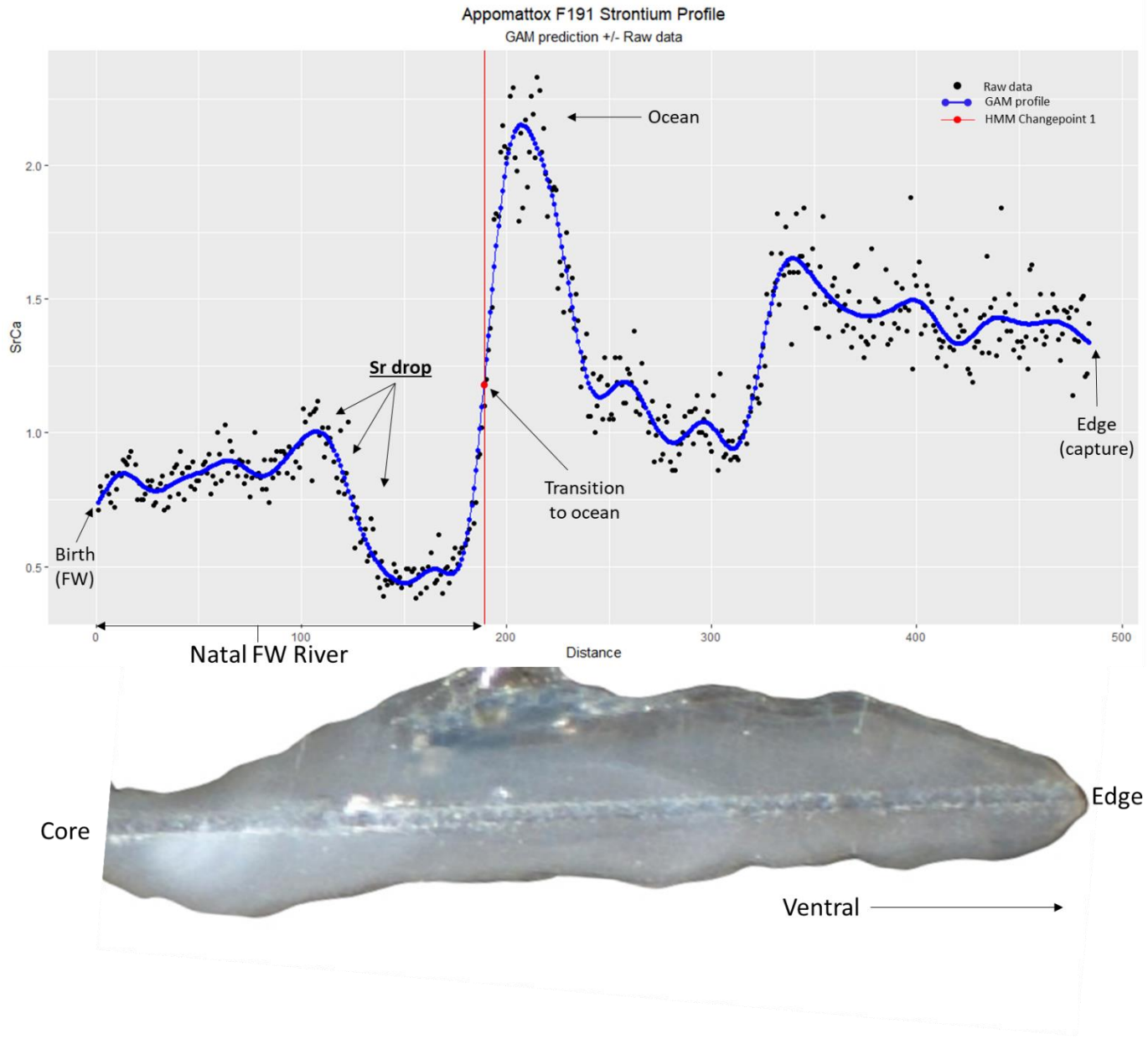

Figure 2-25. Sectioned otolith and strontium profile from a Hickory Shad that was captured in the Appomattox River, VA showing low strontium ratios near birth (core, distance == 0), and a drop in strontium before the initial emigration period suggesting the juvenile may have gone back upstream. Distance (x-axis) represents data points, where each consecutive data point is approximately 2.5 micrometers away from the previous data point.

Figure 2-26. Example of a scale showing resorption marks from a Hickory Shad that was captured in the Cashie River.

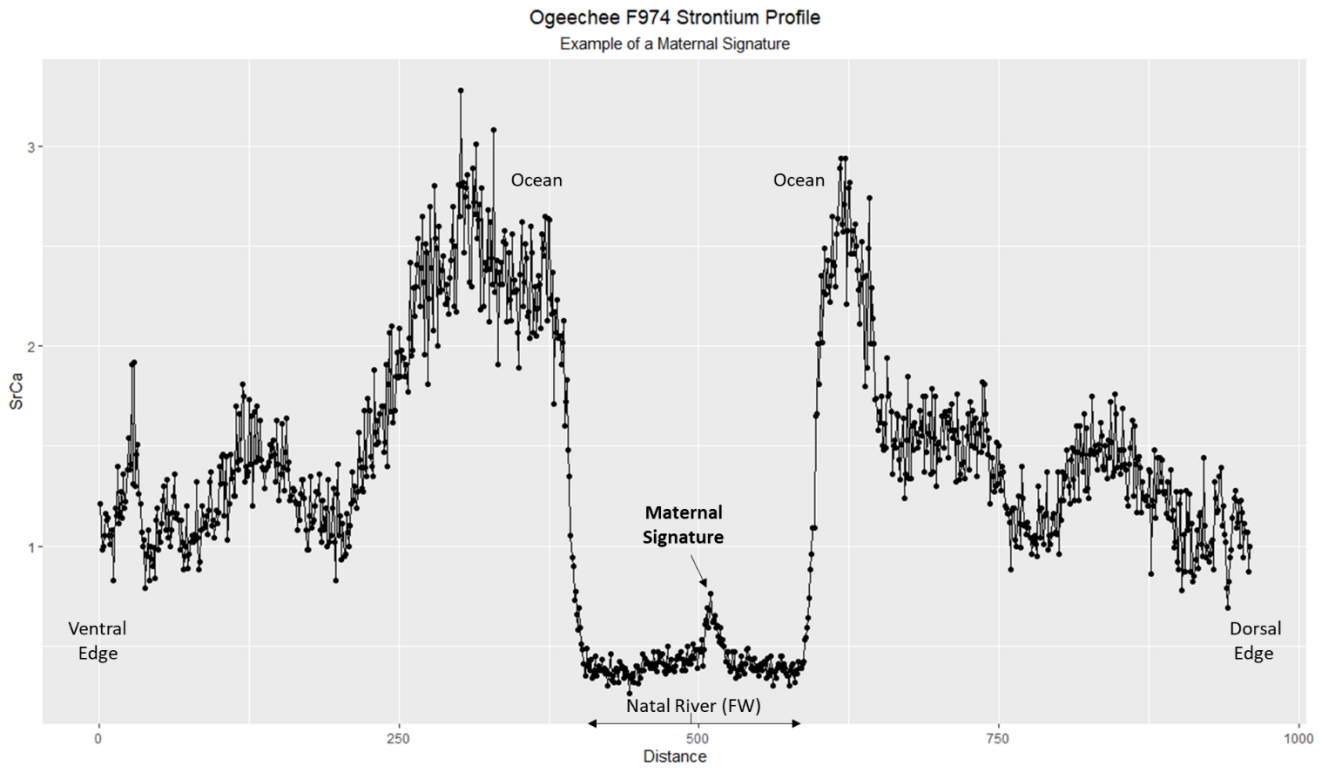

Figure 2-27. Strontium profile of Hickory Shad otolith that was captured in the Ogeechee River showing an example of a maternal contribution near the center of the transect. Distance (x-axis) represents data points, where each consecutive data point is approximately 2.5 micrometers away from the previous data point.

CHAPTER 3

A COMPARISON OF ELEMENT SIGNATURES ON THE EDGE OF OTOLITHS FROM SPAWNING HICKORY SHAD ALONG THE ATLANTIC COAST OF NORTH AMERICA

Abstract

An increasingly popular approach of discriminating spawning stocks of diadromous fish is the use of otolith microchemistry, which relies on the assumption that different habitats will produce unique element signatures in the otoliths of fish. To identify and interpret meaningful differences between groups in otolith chemistry data, one must understand what elemental characteristics make each habitat unique. The most recently deposited material is found on the edge of an otolith, so this area is frequently used to make inferences about where fish are captured. The Hickory Shad (*Alosa mediocris*) is an anadromous clupeid that is significantly understudied. Little information about the life history characteristics or stock status of Hickory Shad exists. The goal of this study was to determine if element concentrations would differ on the edge of otoliths from Hickory Shad that were captured at 26 locations within 18 major river systems during spawning runs. Several pairs of capture locations were in close geographic proximity, and part of the same larger parent river. Since the sample sizes were small compared to the number of capture locations, estimates of element concentrations from these geographically similar locations were compared separately to determine if observations should have been treated as independent or homogenous groups. There was no difference between element signatures from these locations, so observations from each capture location pair were combined and represented as homogenous groups, resulting in 18 “parent rivers” that were

compared to look for differences between capture locations. There were very few differences between element concentration on the edge of Hickory Shad otoliths; only five of the 18 capture locations had statistically different concentrations of one or two elements. Based on several empirical observations and evidence from previous literature, the results of this study suggest that the edge of Hickory Shad otoliths did not represent the element concentrations in the ambient water of each capture location, which supports the hypothesis that Hickory Shad move in and out of freshwater very rapidly during the spawning migration.

Introduction

Otoliths are paired calcified structures found within the inner ear of teleost fishes that aid in hearing, balance, and environmental orientation (Campana 1999). Otoliths are submerged in an acellular endolymphatic fluid that is secreted by the inner ear epithelium. Otolith growth occurs as the dissolved ions present in the endolymph precipitate onto an organic protein matrix, which is deposited following an endogenous rhythm (Panella 1971; Campana and Neilson 1985; Payan et al. 1999). Otoliths are composed primarily of calcium carbonate, usually in the form of aragonite, but divalent cations of ionic radii similar to that of calcium can substitute for calcium in the crystalline lattice of the otolith or can coprecipitate as carbonates (Campana 1999). Dissolved ions are transported into the endolymph through several membranes, so the chemical composition of the endolymph at any given time is influenced by metabolic processes and the availability of dissolved ions in the ambient water (Payan et al. 2004). Otolith growth is a metabolically inert process, so features that become incorporated into the growing matrix cannot be resorbed and are permanently retained in the otolith crystalline structure (Campana 1999; Friedrich and Halden 2008; Doubleday et al. 2014; Izzo et al. 2016; Thomas et al. 2017). The

composition of non-metabolically regulated elements (e.g., Sr^{2+}, Ba^{2+}), within otoliths have been shown to reflect the ambient water at the time of deposition (Campana 1999; Bath et al. 2000; Kafemann et al. 2000; Campana and Thorrold 2001; Elsdon and Gillanders 2003; Elsdon and Gillanders 2004; Lill et al. 2019).

Due to their intrinsic properties, otoliths have been of primary interest in the field of fisheries science for several decades (Panella 1971; Campana 1999; Berkeley et al. 2004; Tanner et al. 2016). Otolith chemistry has been used to detect diadromy (Elsdon and Gillanders 2005b; McCulloch et al. 2005), identify natal origins and nursery grounds (Rooker et al. 2001; Brown 2006; Clark et al. 2009; Bradbury et al. 2011; Reis-Santos et al. 2012; Reis-Santos et al 2013; Tanner et al. 2013), reconstruct migration patterns (Hamer et al. 2003; Gillanders 2005; Elsdon and Gillanders 2006; Reis-Santos et al 2013; Tanner et al. 2013), and discriminate stocks (Kalish 1996; Campana et al. 2000; Bergenius et al. 2005; Thresher and Procter 2007; Tanner et al. 2012; Tanner et al. 2015).

Otolith chemistry has proven to be a particularly useful application for the study of diadromous species (Secor 1992; Secor et al. 1995; Halden et al. 1995; Elfman et al. 2000; Secor and Rooker 2000; Gillanders 2005; Walther and Limburg 2012). This is because some elements are known to have distinct environmental gradients, and diadromous movements between salinity gradients create distinct chemical signatures in otoliths. In particular, strontium and barium are known to have an inverse relationship that is correlated with salinity in most systems; strontium is high in saline water and low in freshwater, while barium is high in freshwater and low in saline water (Secor et al. 2001; Zimmerman 2005; Brown and Severin 2009; Miller 2011). While strontium and barium have been the most commonly used elements to reconstruct environmental histories (Halden et al. 1995; Elfman et al. 2000; Milton and Chenery 2001; Arai

and Mortia 2005; Elsdon and Gillanders 2005b; McCulloch et al. 2005; Walther and Limburg 2012), growing evidence suggests that other elements such as zinc (Limburg and Elfman 2017) and magnesium (Elsdon and Gillanders 2002; Miller 2007) may also be correlated with salinity and growth, and may be useful for environmental history reconstruction. Otolith chemistry studies that focus on stock discrimination are heavily dependent on several assumptions, including that all subgroups within a mixed stock have been included in the sampling regimes, that variation in the chemical composition of watersheds under consideration is negligible over time, and that different physico-chemical properties of ambient water will produce distinct "signatures" in an otolith (Campana 1999; Tanner et al. 2016). Further, studies that relate the composition of otolith regions produced as juveniles (e.g., the core, hatch check, elver marks) and adults (e.g., annuli, otolith edge) are often constrained by the assumption that physiological processes such as ontogeny, diet, and genetics have a negligible effect on element uptake and deposition. Considering these assumptions, otolith chemistry is still a valuable and widely accepted approach to stock discrimination.

The Hickory Shad (*Alosa mediocris*) is an anadromous clupeid that inhabits Atlantic coastal systems in continental shelf waters close to shore. Spawning runs have been recorded from the St. Johns River, Florida, to the Maryland portion of the Susquehanna River (Murdy et al. 1997), and possibly in tributaries of the Delaware River (Perillo and Butler 2009; Desmond Kahn, Delaware Fish and Game, personal communication). Despite the ecological and economic significance of Hickory Shad, as well as the diminishing statuses of their close relatives (Alewife *Alosa pseudoharengus,* Blueback Herring *Alosa aestivalis*, and American Shad *Alosa sapidissima*), little is known about the life history of Hickory Shad. Although they are more closely related to the Alewife and Blueback Herring (Bloom and Lovejoy 2014), it is commonly

assumed that Hickory Shad and American Shad have similar life history characteristics (Melvin et al. 1986). Historically, this assumption has even formed the basis of management decisions (Harris et al. 2007), despite the lack of evidence supporting any similarities (other than appearance) between the two species. Information about the life history of Hickory Shad should be prioritized so that more appropriate management strategies can be devised.

In the study described herein, seven elements incorporated within the otolith matrix were used to ascertain whether spawning populations could be separated and, if so, whether this method could identify natal fidelity and wandering. If so, then results of this analysis could be used to identify unique spawning populations, estimate the amount of wandering, and provide additional information about life history events.

Methods

LA-ICP-MS

Hickory Shad were captured in 26 locations within 18 major river systems along the known spawning range between the St. Johns River, Florida, and the Maryland portion of the Susquehanna River. Collections were conducted by state and federal agency staff, and ECU students, during the 2016-2018 spawning seasons downstream of or on the identified spawning grounds. Left sagittal otoliths were removed, cut along the transverse plane, and LA-ICP-MS was conducted on the resultant cross section containing the otolith core. Seven elements commonly used in otolith chemistry studies (Mg, Mn, Cu, Zn, Sr, Ba, and Pb) were quantified using LA-ICP-MS, and element-to-calcium ratios of the otolith edge (last 30 microns) were compared across capture locations. In order to isolate natal river element signatures, the first

objective was to identify a point to represent the center of the otolith core within the element transect so that distances could be measured in relation to birth. Element;calcium ratio plots were placed over photographs of the corresponding sectioned otolith and manually aligned with the ablation track (Figure 1-3). Results of Chapter 1 identified that a distinct zinc peak in in the LA-ICP-MS data could be used to identify the central node or point within the otolith core. The highest zinc value was selected to represent the central point of the otolith core, referred to as the "core point". For each element, a subset of data was created between the core point and the last data point on the ventral otolith edge, which comprised the data used here. In this context, the core point (data point zero) contained the maternal contribution to the embryonic otolith, and the last data point on the ventral edge of the otolith (point n) was the most recently deposited material (Figure 3-2). For a given element, the data between and including these points was the elemental profile for that individual. All negative values in each element profile were replaced with zero. To avoid potential bias associated with selecting an optimal window size for a moving average, data were smoothed by fitting a separate generalized additive model (GAM) to each element:calcium ratio profile (Figure 3-2). GAMs were fit using the Gaussian distribution with the identity link and thin-plate regression spline smoothing functions. The basis dimension for the smooth term (k) in the models were determined by the formula

$$k = 10N^{2/9}$$

where N is the number of data points in each profile (Kim and Gu 2004; Brennan et al. 2015; Soeth et al. 2020). Hereon, the predicted values of the GAMs for each element are referred to as "GAM profiles". To clarify, at this point the reader should understand that each Hickory Shad has a unique GAM profile for each of the 7 elements. For a given Hickory Shad i, let sequence G contain the GAM profile element j,

$$GAM_{i,j} = (g_1, g_2, \ldots, g_n)\,.$$

The GAM profile can be described as starting at the core point (g_1) and extending to the ventral edge of the otolith (g_n). Therefore, for a given Hickory Shad, the length (number of data points; $\sum(g_{1,\ldots,}g_n)$) of its GAM profile ($|\vec{G}|$) was a function of two variables: the distance between the core point and the ventral edge (D), and the path of the laser ablation track (A),

$$Length\ (GAM_{i,j}) = |\vec{G}| = f(D, A).$$

Hence, the length of the GAM profiles ($|\vec{G}|$) were equivalent across element ratios for a given Hickory Shad but varied between individuals.

The last data point on the ventral edge of the GAM profiles (g_n) was used as a proxy to represent the chemistry of the capture watershed, and these data were used for the proceeding analyses. Several factors were considered in selecting the optimal number of data points to represent the chemistry of capture locations. General trends in the presence and absence of Hickory Shad in freshwater systems suggest that the freshwater ingression and egression occur in a relatively short amount of time. Additionally, little is known about the amount of time it takes for otoliths to incorporate detectable signatures of the ambient environment; however, Mohan et al. (2012) determined that caged Age 0 Striped Bass (*Morone saxatilis*) otoliths require about two weeks to acquire an ambient watershed signal large enough to be detected by LA-ICP-MS when using a beam width of 15 µm. The beam width of the ICP-MS laser used in this study was approximately 30 µm; assuming that otolith increments are formed on a daily basis, the element concentrations of increments smaller than 30 µm in width will be averaged in with adjacent daily increments.

Investigation of similar geographic locations: a means to validate statistical treatment

Several of the capture watersheds were close in geographic proximity, and some were tributaries of the same larger "parent rivers". We had no prior knowledge concerning the relative chemistry of these capture locations, so we did not know if capture locations geographically close to one another and part of the same larger parent river were better represented as independent groups, or as collective groups (i.e., we did not know the scale at which to expect differences in element signatures). The sample size was small when compared to the number of capture locations; to minimize loss of statistical power when comparing all capture locations, the first objective was to determine if geographically similar pairs of locations should be treated as one or two samples. Therefore, element concentrations from these geographically similar pairs were compared first. The geographically similar pairs included the following locations: Appomattox (tributary) and James (parent) rivers, Blackwater and Nottoway rivers (tributaries of Chowan River), Roanoke (parent) and Cashie (tributary) rivers, Tar (parent) and Tar-Swift (tributary) rivers, and Cape Fear-Town Creek (tributary) and Cape Fear-Upper (parent). The remaining paired comparisons were from the Neuse River watershed in North Carolina. This watershed contains the principle spawning run of Hickory Shad in the state, and fisheries management agency staff suspected that tributaries may provide spawning grounds for unique spawning groups within the watershed. Therefore, the following tributaries were compared for significant differences in elemental signatures: Contentnea Creek and Swift Creek, Contentnea and Neuse-Upper, Contentnea and Pitchkettle Creek, Neuse-Swift Creek and Neuse-Upper, Neuse-Swift Creek and Pitchkettle, and Neuse-Upper and Pitchkettle.

An F-test was used to check for homogenous variance in each element between each respective pair of locations. Since the assumption of homoscedasticity was not met in every case,

and the sample size between the groups was not balanced, two different resampling approaches were adopted to determine if each pair should be treated as independent samples or a homogenous group. For each pair, before implementing the appropriate resampling approach, a normal students t-test with the assumption of homoscedasticity was used to view the baseline parameter estimates for comparison with the appropriate null distribution.

Resampling approach 1: the bootstrap procedure for homogenous variance

To accommodate pairs in which the assumption of homoscedasticity was met (F-test: $p > 0.05$), the goal of the first approach was to estimate if the observed element ratios in each group were generated from the same underlying distribution. The following approach to resampling was used to ensure that samples would being generated under the correct null hypothesis (i.e., equal mean and variance). If the two capture locations that were compared make up a pair $\{(x_{1,i}, y_{1,i})\}$ where $i = 1, \dots, n$, and n represents the number of individuals from each location, the samples from both locations were combined into a single "pooled" group Z so that

$$Z = \sum_i^n \{x_1, y_1\}.$$

A bootstrapped sample of the pooled group was generated with replacement 999 times. Upon each iteration, two new "bootstrap" samples $\{(x_2, y_2)\}$ were generated from the pooled sample. Observations were assigned to the bootstrap samples $\{(x_2, y_2)\}$ so that the first n observations were assigned to x_2, making the length (i.e., number of data points) of x_2 equivalent to the length of x_1:

$$Length\ x_2 = \sum(x_{1,1}, x_{1,2}, \dots, x_n),$$

and the remaining n observations were assigned to y_2 making the length of y_2 equivalent to the length of y_1:

$$Length\ y_2 = \sum(y_{1,1}, y_{1,2}, \dots, y_n).$$

A studentized t-test was then used to compare the two new samples $\{(x_2, y_2)\}$, and the test statistic was stored in an external vector V. After the completion of 999 iterations, a p-value was calculated by dividing the number of times the bootstrapped test statistic was more extreme than the observed test statistic by 999 (the number of iterations). In other words, let vector V contain the bootstrapped test statistics for a given element:

$$V = (v_1, v_2, \dots, v_{999}) : v_i \in V\ .$$

The p-value ($p.value$) for that element was calculated as:

$$p.value = \frac{|\{i \in \{v_1, v_2, \dots, v_{999}\}: v_i > a\}|}{999}\ ,$$

where a represents the observed test statistic.

Resampling approach 2: the bootstrap procedure for heterogenous variance

To accommodate heteroscedastic pairs, the goal of the second approach was to determine if pairs could be represented as homogenous groups by comparing estimates of their population means without making any assumptions about their variances. To generate samples under the null hypothesis for this approach, for a given element, the average observed element ratio $\{(\bar{x}, \bar{y})\}$ was calculated for each group:

$$\bar{x} = \sum_{1}^{n} x_i \frac{(x_{1,\ldots,}x_n)}{n}$$

$$\bar{y} = \sum_{1}^{n} y_i \frac{(y_{1,\ldots,}y_n)}{n}$$

and the average element ratio of the pooled group ($\bar{z}$) was calculated:

$$z_i \in Z$$

$$\bar{z} = \sum_{1}^{n} z_i \frac{(z_1, \ldots, z_n)}{n}$$

The observed group mean was subtracted from each observation of the respective group, and the pooled mean ($\overline{z}$) was added:

$$\tilde{x}_i = x_i - \overline{x} + \overline{z}$$

$$\tilde{y}_i = x_i - \overline{y} + \overline{z}$$

Subtracting the respective group mean served to center both groups around zero. Adding the pooled mean to these observations resulted in two new sets of observations $\{(\tilde{x}, \tilde{y})\}$ that were the same size as the original groups $\{(x_2, y_2)\}$ but were centered around the pooled mean ($\overline{z}$), which corresponds to the null hypothesis. These will be referred to as the "null group":

$$null\ group = \{(\tilde{x}, \tilde{y})\}$$

Random samples of each null group were taken with replacement 999 times. Upon each iteration, a studentized t-test was used to compare the null groups. Test statistics were stored in an external vector, and p-values were calculated using the same procedure as the first resampling approach. Ultimately, there were no differences in the element concentrations between any of these pairs of

capture locations, so the samples from each pair were pooled into homogenous groups for the remaining analyses, resulting in a dataset of 18 “parent rivers” instead of the original 26 “capture locations”.

Establishing an approach to model the chemistry of capture watersheds: exploratory analysis of the otolith edge data

Data were visualized graphically using a variety of methods. Informative approaches for these data included boxplots, density plots, histograms, and residual plots from linear models. Multivariate normality was assessed by calculating Mardia’s multivariate skewness and kurtosis coefficients using the MVN package in R Studio (Korkmaz 2014). Variation in univariate element concentrations between capture locations were evaluated with Levene’s test. A correlation matrix between elements of the edge data was created using Pearson’s correlation coefficient. The correlation matrix was visualized with a factor map that was built through the corrplot package in R (Wei and Simko 2017).

Principle components analysis (PCA) and random forests were used to explore the potential importance of each element in describing capture locations. Values for each element were centered and scaled (giving each element the same mean and variance) prior to conducting principle components analysis. The Boruta algorithm, implemented with the Boruta package in R Studio (Kursa and Rudnicki, 2010), was used to explore the importance of each element in describing capture locations. 500 Random subsets (called shadow features) of the data were created iteratively. Upon each iteration, a random forest model was trained on the shadow features and the calculated z-scores were compared with the original elements. Element

importance was determined by comparing the number of times it outperformed the shadow features using a binomial distribution.

Omnibus tests

Exploratory data analysis revealed that the edge data violated several parametric assumptions, so a square root transformation was applied to the data. Most of the data converged to normality after the transformation, but not all, so non-parametric tests were used for comparative analyses on the square root transformed data. A dissimilarity matrix was calculated using Euclidean distance as the distance metric, and a PERMANOVA was used to test the null hypothesis that no difference existed between dispersion and/or location of the multivariate spatial median (centroid), between capture locations. The vegan package in R Studio (Oksanen et al, 2019), was used to conduct PERMANOVAs using 999 permutations. When significant differences were detected by PERMANOVA, multivariate dispersion was evaluated by calculating the average distance of group members to the group centroid and comparing the average distances across groups with both an analysis of variance (ANOVA) and permutation tests via 999 permutations (Anderson, 2006; Anderson et al., 2006). Further, a global multivariate analysis of similarities (ANOSIM: Clarke 1993) was also conducted with the vegan package using ranked Euclidean distance matrices.

Univariate (within-element) comparisons of capture locations were accomplished with a Kruskal-Wallis test and a permutational ANOVA via 999 permutations. In the permutational ANOVAs, the false discovery rate was controlled for using the approach of Benjamini and Hochberg (1995). Non-parametric estimates of effect size (η^2) for each element in the series of Kruskal-Wallis tests were calculated using the formula

$$\eta_H^2 = \frac{H-k+1}{n-k},$$

where H is the Kruskal-Wallis test statistic, k is the number of levels in each grouping variable, and n is the global number of observations (Tomczak and Tomczak, 2014). η^2 values between 0.01 and 0.06 were considered to be small effects, values between 0.06 and 0.14 were considered a moderate effect, and values greater than 0.14 were considered large effects (Leech and Onwuegbuzie 2002; Kassambara 2016). η^2 values were multiplied by 100 to be expressed as the percentage of variance in each element that is explained by the corresponding grouping variable.

Approaches to pairwise comparisons

Pairwise comparisons of capture locations were conducted using ratios of strontium, barium, manganese, zinc, lead, and copper on the ventral edge of each otolith. Magnesium was excluded because the prior omnibus tests provided no evidence supporting the presence of meaningful differences in manganese ratios between capture locations. A pairwise analysis of similarities (ANOSIM) was conducted to compare multivariate element dissimilarities between each pair of capture locations. ANOSIM was conducted on multivariate ranked dissimilarity matrices between capture locations that were calculated using Euclidean distance. When ANOSIM indicated the presence of potentially meaningful dissimilarities between the multivariate element ratios on the edge of otoliths from Hickory Shad captured in two different locations, similarity percentage (SIMPER) analysis was used to investigate which elements were driving the dissimilarities. To remain consistent with other approaches used in this study, 999 random permutations were used to generate the null distribution for each comparison in ANOSIM and SIMPER. ANOSIM p-values were calculated as the percentage of times that the

observed value of the ANOSIM statistic (R) was estimated to occur under the empirical distribution of R when the null model was generated through 999 permutations of the capture location membership. Therefore, at an alpha level of 0.05, a significant result (i.e., $p < 0.05$) for a given value of R was interpreted as an R value estimated to occur less than 95% of the time when the null distribution was generated through permuting capture location membership (i.e., when H_0 was assumed). P-values for SIMPER were calculated for observed dissimilarity contribution values in the same way that p-values were calculated for R in ANOSIM. An alpha level of 0.05 was used as a significance threshold across all analyses. Finally, univariate pairwise comparisons were conducted using Welch's t-test for unequal variance while controlling the false discovery rate using the approach of Benjamini and Hochberg (1995).

Results

Comparing similar geographic locations within watershed

Element:calcium ratios in the following pairs of capture locations were compared directly to determine if they were better represented as independent or homogenous groups: Appomattox and James, Blackwater and Nottoway, Roanoke and Cashie, Tar and Tar-Swift, Cape Fear-Town Creek and Cape Fear-Upper. Each Neuse River pair between Contentnea, Swift Creek, Neuse-Upper, and Pitchkettle (all branches of the Neuse River), were also compared in the same manner (Appendix A-1 through A-11).

Homoscedasticity could not be assumed for the following comparisons: barium, zinc, and lead in the comparison between Appomattox and James; strontium, manganese, zinc, and copper in the comparison between Tar and Tar-Swift; and strontium, manganese, zinc, and lead in the

comparison between Cape Fear-Town Creek and Cape Fear-Upper ($p < 0.05$). Therefore, the null hypothesis for each of these comparisons was that the observed element ratios for each pair were generated from distributions with equivalent means, and in each case, the bootstrap procedure for heterogenous variance failed to reject the null hypothesis ($p > 0.05$). The assumption of homoscedasticity could be assumed for each of the remaining elements in the previously mentioned comparisons, and for all elements in each of the remaining comparisons ($p > 0.05$). Therefore, the null hypothesis for each of the remaining comparisons was that the observed element ratios were generated from equivalent distributions. In each case, the bootstrap procedure for homogenous variance failed to reject the null hypothesis suggesting that these elements were generated from the same underlying distribution ($p > 0.05$). Since no differences were supported between capture locations in any of these comparisons, each respective pair was represented as a single group of independent observations in further analyses.

Exploratory data analysis of the otolith edge data

Table 3-1 shows that the element:calcium ratios in otoliths from six of the eighteen capture locations did not meet the assumption of multivariate normality including Chowan (skew = 131.44, $p < 0.01$), James (skew = 128.84, $p < 0.01$), Neuse (skew = 130.65, $p < 0.01$), Pamlico (skew = 121.79, $p < 0.01$), South Santee (kurtosis = -5.90, $p < 0.01$), and Waccamaw rivers (kurtosis = -2.00, $p = 0.05$). Table 3-2 shows that univariate homoscedasticity could be assumed for the elements strontium, manganese, and zinc ($p > 0.05$), but not the elements barium, magnesium, lead, and copper ($p < 0.05$).

There were moderate to high levels of positive correlation between the elements copper, zinc, and lead in the otolith edge data (Figure 3-10). The Pearson correlation coefficients (r) between copper and lead, and between copper and zinc were both 0.56 (both: $p < 0.05$). The Pearson's correlation between zinc and lead was 0.48 ($p < 0.05$). Magnesium had moderate positive correlation with manganese ($r = 0.44$, $p < 0.05$) and zinc ($r = 0.46$, $p < 0.05$). Strontium and barium were not significantly correlated with any of the other elements ($r < |0.3|$)

Principle components one and two had eigenvalues greater than one (PC1 = 2.48; PC2 = 1.45), while the remaining principle components had eigenvalues less than one (Figure 3-11). Seventy percent of the total variance was explained in the first three principle components: PC1 = 35.42% of the variance, PC2 = 20.76%, and PC3 = 13.7% (Figure 3-13). All elements were well represented ($cos^2 > 0.3$) in at least one of the first three principle components (Figure 3-13). Zinc, copper, lead, and magnesium were the most important elements in PC1 while barium, manganese, and strontium were less important. Manganese was the most important element for PC2, followed by barium and strontium. Barium and strontium were the most important elements in PC3 and PC4 (Figure 3-12). Exploratory results were only pertinent for the parent river grouping variable, so only those results were presented here. When parent river was used as the grouping variable, the Boruta algorithm performed 37 iterations, and suggested that magnesium was the only unimportant element (Figure 3-18). The most important element was lead (mean importance = 7.34), followed by zinc, strontium, manganese, barium, and copper, respectively (Figure 3-18).

Omnibus tests on the otolith edge data: validating the presence of differences between capture watersheds, and the need for further investigation

When PERMANOVA was conducted on the otolith edge data, the observed F-value ($F = 2.24$) was estimated to occur less than 99% of the time ($p < 0.01$) under null distribution generated through 999 permutations (Figure 3-19). Therefore, the null hypothesis was rejected, and it was assumed that that significant differences in multivariate dispersion and/or centroid location existed between the levels of both grouping variables (Figure 3-19). Both ANOVA and permutation tests indicated that there was no significant difference ($F = 1.28$, $p > 0.05$) in multivariate dispersion between capture locations (Figure 3-20), so the results of PERMANOVA were assumed to reflect differences in centroid locations. Table 3-11 shows that omnibus ANOSIM indicated that element ratios were more dissimilar between capture locations than within capture locations ($R = 0.10$, $p < 0.01$).

The Kruskal Wallis test indicated that significant differences between capture locations were found in all element ratios except for magnesium (Table 3-11). The effect size (η^2) was used to estimate how much variation in element ratios was explained by capture location. Capture location explained the most variation in strontium ($\eta^2 = 0.10$), which was followed by manganese ($\eta^2 = 0.09$), lead ($\eta^2 = 0.9$), copper ($\eta^2 = 0.9$), and barium ($\eta^2 = 0.6$), all of which were considered moderate effect sizes (Table 3-11). Capture location explained less variation in magnesium ($\eta^2 = 0.03$) and zinc ($\eta^2 = 0.05$), which were considered small effect sizes (Table 3-11). The effect size was moderate for all elements except for zinc and magnesium, which had small effect sizes. The univariate permutation ANOVA indicated significant differences between

capture locations in all elements except for magnesium and zinc (Table 3-12). The p-value for zinc was 0.05, so it was still considered in further analyses.

Results of pairwise analyses

The results of pairwise ANOSIM indicated that multivariate element dissimilarity was greater between capture locations than within capture locations when comparisons included Hickory Shad captured in the Susquehanna, Potomac, Choptank, Patuxent, and Ogeechee rivers (Table 3-13). None of these locations were distinguishable from all of the remining capture locations. Pertinent results for each location are outlined below.

Susquehanna and Potomac

Hickory Shad captured in the Susquehanna and Potomac rivers had similar multivariate element signatures of the otolith edge and were distinguishable from those of Hickory Shad captured in the Choptank, Patuxent, Pamlico, and Cape Fear rivers (Table 3-13). SIMPER indicated that copper, manganese, and zinc were the highest contributors to observed dissimilarity in these comparisons. Copper was the highest contributor for comparisons with Susquehanna, while manganese and zinc were higher contributors in comparisons with Potomac. When the null distributions were generated for comparisons with Susquehanna, the observed dissimilarity contribution values were significant ($p < 0.05$) under several null models for manganese and lead, and under every null distribution for copper (Table 3-16), which suggested that copper was highly important for separating the Susquehanna from other locations. When the null distributions were generated for comparisons with Potomac, the observed dissimilarity contribution values of manganese and zinc were significant ($p < 0.05$) under several null

distributions, and for copper under every null distribution (Table 3-17). Pairwise comparisons using Welch's t-test supported the results of ANOSIM and SIMPER; Hickory Shad that were captured in Susquehanna and Potomac had significantly higher copper than most of the remaining capture locations, and significantly higher manganese and lead than several other capture locations (Figures 3-24, 3-25, 3-26).

Choptank and Patuxent

Hickory Shad captured in Choptank and Patuxent rivers had similar multivariate element signatures of the otolith edge; both were distinguishable from Hickory Shad captured in Susquehanna, Potomac, South Santee, Ogeechee, and St. Johns rivers, and otoliths from Choptank River fish were distinguishable from several additional locations (Table 3-13). Aside from the Susquehanna and Patuxent fish, multivariate element signatures of otolith edges from Hickory Shad captured in the Choptank and Patuxent rivers were not distinguishable from other Chesapeake Bay tributaries, but they were distinguishable from several locations south of Chesapeake Bay (Table 3-13). SIMPER indicated that strontium was a high contributor to observed dissimilarity in comparisons that involved both of these locations, and barium was usually the highest contributor in comparisons with Choptank data (Tables 3-18). Both strontium and barium were significant under each null model in comparisons with Choptank, and strontium was significant under several null models with Patuxent (Table 3-17). Welch's t-test indicated that there were no significant differences ($p > 0.05$) in barium otolith edge ratios between any capture locations (Table 3-14). Notably, barium concentrations on the ventral edge of Hickory Shad captured in the Choptank were considerably more variable (SD = 0.46, SE = 0.15) than any of the remaining capture locations (Figure 3-4), which would have made barium appear influential in the results of SIMPER. Alternatively, Welch's t-test indicated that strontium ratios

on the ventral edge of otoliths from Hickory Shad captured in the Choptank and Patuxent rivers were significantly higher than those captured in the Potomac, South Santee, Ogeechee, Altamaha, and St. Johns rivers. In addition, the average strontium ratio on the ventral edge of otoliths from Hickory Shad captured in the Choptank was significantly higher ($p < 0.05$) than those ratios for fish captured in the Susquehanna, Rappahannock, James, Waccamaw, and all capture locations in North Carolina aside from Cape Fear (Figure 3-23).

Ogeechee

Pairwise ANOSIM indicated that the multivariate element signature on the ventral edge of otoliths was more dissimilar between capture locations than within capture locations ($p < 0.05$) when Hickory Shad captured in the Ogeechee River were compared to those captured in the Patapsco, Choptank, Patuxent, Nanticoke, Rappahannock, Cape Fear, South Santee, and Altamaha rivers (Table 3-13). SIMPER indicated that zinc, manganese, copper, and barium were usually the highest contributors to observed dissimilarity between the Ogeechee and those captured in other locations (Table 3-20). In this case, it was especially noteworthy that when comparisons were made with Hickory Shad captured in the Ogeechee, lead was frequently a higher contributor to dissimilarity compared to the other elements (Table 3-20), a result opposite that for comparisons between other capture locations where lead was the lowest contributor to observed dissimilarity. It was acknowledged that ANOSIM and SIMPER would be considerably less powerful techniques for making inferences concerning lead concentrations because a) lead values were less variable than the other elements, and b) even after the square root transformation, lead values were considerably smaller in absolute value than the other elements. For these reasons, it was no surprise that lead contributed the least to dissimilarity according to estimates from SIMPER. Therefore, the fact that lead contributed more to dissimilarity than even

a single element was indicative that lead was important for separating the Ogeechee from other locations. When the null distributions were generated for these comparisons, the observed dissimilarity contribution values for lead and barium were significant ($p < 0.05$) under the empirical null distribution for several comparisons. Welch's t-test supported the importance of lead on the edge of otoliths from Hickory Shad that were captured in Ogeechee, which were significantly higher ($p < 0.05$) than for those captured in the Cape Fear, South Santee, and Altamaha (Figure 3-25).

Discussion

Several studies have observed spatial variation of elements within watersheds (Mohan 2009; Mohan et al. 2012; Zapf 2012; Hughes 2015). However, when comparing closely associated capture location pairs, we found that none of these capture location pairs had different element signatures at the otolith ventral edge. Therefore, the Hickory Shad from each of these pairs were combined and treated as samples from single locations, which ultimately resulted in 18 "parent rivers" that were compared to the remaining locations. If the elements under consideration do vary spatially between these specific pairs of capture locations, it was not reflected on the edge of Hickory Shad otoliths. These results suggest that otolith edge signatures of this species would likely not separate spawning stocks of Hickory Shad if distinct spawning populations exist at very fine spatial scales.

The sampling approach used in this study was to collect a balanced sample from as many locations as possible during Hickory Shad spawning runs. The known spawning range of Hickory Shad extends from the St. Johns River, FL to the Susquehanna River, MD. The most

efficient way to achieve a sample size this large was to have staff from state and federal agencies keep and send Hickory Shad captured during their routine monitoring efforts. The major caveat of this approach was that we were not able to collect water samples from each capture location. Therefore, we were unable to make quantitative inferences about the relationship between Hickory Shad otolith chemistry and the ambient water chemistry of each capture location; the interpretation of our results was limited to what could be derived from the published literature. Although we were not able to quantify the chemical composition of the specific capture locations at the time of capture, there was no shortage of evidence suggesting that the elements under consideration vary both spatially and temporally in most of these systems. For instance, relatively fine scale variation in the abundance of strontium, barium, magnesium, and manganese has been reported within the Albemarle and Pamlico Sounds and their tributaries (Mohan 2009; Mohan et al. 2012; Zapf 2012; Hughes 2015), as well as Chesapeake Bay and its tributaries (Dorval et al. 2005a; Dorval et al. 2007; Schaffler et al. 2014). Further, reflection of this intraspecific variation has been observed in the otoliths of both resident (Thorrold et al. 1998b; Thorrold et al. 1997; Thorrold and Shuttleworth 2000; Thorrold et al. 2001; Shaffler et al. 2009; Mateo et al. 2012), and migratory fish (Thorrold et al. 1998a, 1998b; Walther and Thorrold 2008; Mohan 2009; Mohan et al. 2012; Zapf 2012; Hughes 2015). Fewer studies have focused on examining differences in element signatures between these major watersheds at large scales on the Atlantic Coast, but differences in streambed geology, anthropogenic influence, and topography are known to influence water chemistry (Hynes 1975), and the few studies comparing elements in fish otoliths from different Atlantic Coast watersheds have found that element signatures are highly specific to localized areas (e.g., Thorrold et al. 1998a, 1998b; Walther and Thorrold 2008; Walther et al. 2008; Payne Wynne et al. 2015). Very few differences

were found in element ratios on the edge of Hickory Shad otoliths in this study; fish from only five capture locations had discernable element signatures along the otolith ventral edge. Further, the differences were very subtle, and was restricted to a single element in the majority of cases. Ultimately, this evidence suggests that the edge of Hickory Shad otoliths did not accurately reflect the ambient water of the capture location.

The fact that the otolith edge did not reflect the element signature of each capture location is an intuitive hypothesis for several reasons. While not much is known about the spawning migration of Hickory Shad, it does seem to occur over a relatively narrow time frame. In this analysis, the beam diameter used for LA-ICP-MS was 30 µm meaning that each individual data point in the element assay corresponded to a 30-µm wide ablation on the otolith. In a hypothetical scenario, if we assume that daily increments were 1 µm wide and produced consistently, this means that a single data point equates to the average of a 30-day period. Therefore, if a given Hickory Shad spent less than a month in freshwater, it would be unreasonable to assume that the river's element signature would actually be reflected on the otolith edge. This is supported by previous research; using a caging study in Albemarle Sound and an ICP-MS beam width of 15 µm, Mohan et al. (2012) found that it took two weeks for young of year Striped Bass otoliths to incorporate the ambient water signature.

The rapid spawning hypothesis also appears to be supported by patterns in the strontium and barium profiles of the Hickory Shad otoliths. In other anadromous alosines, the inverse relationship between strontium and barium in freshwater and marine environments is known to be reflected in the regions of otoliths that are deposited during these habitat transitions (Lochet et al. 2008; Walther and Thorrold 2008; Gahagan et al. 2012; Payne Wynne et al. 2015; Turner and Limburg 2014). In Hickory Shad otoliths, this pattern was evident early in ontogeny; in most

cases strontium was high and barium was low near the otolith core, and there was a rapid inversion between these elements (to high Sr and low Ba) at a given distance away from the core indicating the initial transition into euryhaline water. However, after the initial inversion, anadromous migrations became less evident; cyclical patterns were present in the strontium profiles, with periods of decreased strontium likely indicating spawning migrations into freshwater, but barium remained virtually stable after the initial habitat transition. Previous studies have found that barium incorporation into otoliths of other species is almost entirely a function of availability in the ambient environment (Bath et al. 2000; Elsdon and Gillanders 2005b; Miller 2009; Miller 2011; Reis-Santos et al. 2013). Barium typically binds to other compounds in marine waters, but it has a greater bioavailability in freshwater because it occurs there in its free form (Turner et al. 1981; Hüssy et al. 2020). Hickory Shad scales did contain resorption marks (Figure 2-26), which provided further evidence of iteroparity, so the cyclical patterns in strontium were likely a result of spawning events. Under this assumption, periods of decreasing strontium were typically very narrow, and along with the lack of spawning evidence in barium, suggests that Hickory Shad do not remain in freshwater long enough to incorporate detectable freshwater signatures.

Walther and Thorrold (2008) found that otoliths from American Shad (*A. sapidissima*) captured in the St. Johns river had significantly higher strontium ratios compared to otoliths from American Shad captured in the Potomac, Rappahannock, Roanoke, and Altamaha rivers. A similar pattern was found in Blueback Herring otoliths by Turner and Limburg (2014). These patterns are expected because much of Florida's bedrock is made of limestone, which leads to high dissolved strontium levels, particularly in the St. Johns River (Odum 1951; Skougstad and Horr 1963). Numerous studies have observed strong positive relationships between strontium

concentrations in otoliths and ambient water (Bath et al. 2000; Secor and Rooker 2000; Elsdon and Gillanders 2004; Kraus and Secor 2004; Elsdon and Gillanders 2005a; Miller 2011; Gahagan et al. 2012). If the edge of Hickory Shad otoliths represented the ambient water of the capture locations in this study, it would only be logical to expect Hickory Shad that were captured in the St. Johns to have high strontium ratios. Yet this is not what was observed; in fact, Hickory Shad captured in the St. Johns had one of the lowest strontium ratios among all of the capture locations (Figure 3-3, Table 3-4). This suggested that the Hickory Shad captured in the St. Johns river had not been out of the marine environment for very long, and provides further evidence that the otolith edge did not reflect the ambient water of the capture locations, which seems to have been affected by a rapid spawning migration.

Considering the evidence that the edge of Hickory Shad otoliths did not reflect ambient water in the capture locations, it was not surprising that four of the five capture locations that did have unique element ratios were in northern tributaries of Chesapeake Bay. Chesapeake Bay is the largest estuary in North America, covering approximately 300 kilometers from Cape Charles, VA to the mouth of the Susquehanna River, MD. Chesapeake Bay is known to have a diverse range of habitats that show elemental variation on spatial scales (Hall et al. 1988; Dorval et al. 2005a; Dorval et al. 2007; Schaffler et al. 2014), and this spatial variation has been shown to reflect in the otoliths of other species (Atlantic Menhaden: Shaffler et al. 2014; Spotted Seatrout: Dorval et al. 2005b; Weakfish: Thorrold et al. 1998b). Otolith element signatures in resident fish of Chesapeake Bay have been shown to be distinguishable from resident fish in other Atlantic estuaries as well (Weakfish: Thorrold et al. 1998b; Thorrold et al. 2001; Atlantic Croaker: Thorrold et al. 1997; Thorrold and Shuttleworth 2000; Shaffler et al. 2009; Tautog: Mateo et al. 2012). Collectively, the previously mentioned studies found distinct differences in multiple

elements (including Sr, Ba, Mg, Mn, Zn, and Cu), in areas throughout Chesapeake Bay (i.e., upper, and lower areas), as well as its tributaries. It is obvious that if the otolith edge were to reflect the ambient water of the capture locations, Chesapeake Bay and its tributaries would have produced distinct element signatures both interspecifically and intra-specifically (i.e., within Chesapeake Bay and tributaries). Yet, this variation was not observed as one would expect; the fact that four of the five unique capture locations were specifically located in northern tributaries of Chesapeake Bay would suggest that the variance was less a function of the characteristics of Chesapeake Bay, and more likely a function of the fact that in order to reach those capture locations, Hickory Shad must swim a longer distance under the influence of estuarine and fresh water and therefore have a longer period to assimilate the signature of those locations.

It is important to acknowledge that the abundance of bio-available elements in a system are known to vary both spatially and temporally as they are affected by several hydrologic processes (e.g., ion exchange and mixing), microbial activity, and substrate composition (Wilson 1975; Aston 1978; Elsdon and Gillanders 2006; Elsdon et al. 2008). Several of the elements considered here have been shown to vary in watersheds at scales of less than 10 kilometers, across days, and even hours (Elsdon and Gillanders 2006; Elsdon et al. 2008). The Hickory Shad in this study were captured between January and April in 2016, 2017, and 2018. In many cases, the sample size from a given location included Hickory Shad that were captured on different days, months, and even years in a select few cases. This was necessary to obtain a balanced sample size from each location since our samples were donated by state and federal agencies who captured Hickory Shad during their routine sampling efforts, but may not have been specifically targeting Hickory Shad. This could have had an impact on our results, and future studies would benefit from sampling designs that make it practical to control for these covariates.

It is also important to consider that if the edge of Hickory Shad otoliths did reflect the ambient water of each capture location, it most likely would not have been true for each of the seven elements. If otolith element signatures are to serve as accurate biogenic tags and be related to specific locations, there must be a high level of correlation between the elements in otoliths and ambient water. Since our sampling regime did not allow us to quantify the spatial or temporal distribution of elements in each capture location, we were also unable to quantify the relationship between elements in Hickory Shad otoliths and the ambient water. A considerable amount of evidence suggests that incorporation of strontium and barium into otoliths is mostly a function of their availability in the ambient environment because fish do not regulate these elements physiologically (Farrell and Campana 1996; Campana 1999; Bath et al. 2000; Elsdon and Gillanders 2003; Kraus and Secor 2004; Elsdon and Gillanders 2005; McCulloch et al. 2005; Walther and Thorrold 2008). On the other hand, there is much debate about the specific relationship between water chemistry and otolith chemistry for the other elements considered here (Campana 1999; Elsdon and Gillanders 2002; Elsdon et al. 2008; Barnes and Gillanders 2013; Reis-Santos et al. 2013; Sturrock et al. 2015). Magnesium, manganese, zinc, and copper play essential biological roles, and incorporation of these elements into otoliths may be more closely related to metabolic processes, and may be influenced by several exogenous factors such as temperature and salinity (Martin and Thorrold 2005; Ranaldi and Gagnon 2008; Halden and Friedrich 2008; Turner and Limburg 2014; Limburg et al. 2018; Macdonald et al. 2019; Thomas and Swearer 2019). For a detailed review of the factors that influence incorporation of these elements into otoliths, the reader is referred to Hüssy et al. (2020). Ultimately, elemental deposition in otoliths appears to be species specific (Reis-Santos et al. 2008; Walther et al. 2010; Chang and Geffen 2012; Gahagan et al. 2012; Limburg et al. 2015), which is likely a reflection

of species-specific phenotypical traits and physiological responses, and needs to be validated in Hickory Shad before otolith element signatures can be related to specific locations.

Conclusions

Based on our results, along with several pieces of empirical evidence, we conclude that the edge of otoliths from Hickory Shad captured during spawning runs did not reflect the chemistry of the capture locations, and this appears to be related to the swiftness of the spawning migration. This suggests that using the region of the otolith produced during the Hickory Shad spawning migration may not be an accurate way to characterize the spatiotemporal variability of elements in spawning rivers, and therefore may not be useful for identifying Hickory Shad spawning stocks or natal homing rivers. In light of the evidence presented here, there is clearly a need for much more rigorous characterization of the spatial and temporal variation of element concentrations in these systems, as well as Hickory Shad otolith growth and morphology including the mechanisms that influence the rate of element incorporation into Hickory Shad otoliths. Nevertheless, this information will serve as an important inferential baseline in future studies.

Literature cited

Anderson, M. J. 2006. Distance-based tests for homogeneity of multivariate dispersions. Biometrics 62: 245–253.

Anderson, M. J., K. E. Ellingsen, and B. H. McArdle. 2006. Multivariate dispersion as a measure of beta diversity. Ecology Letters 9: 683–693.

Arai, T., and K. Morita. 2005. Evidence of multiple migrations between freshwater and marine habitats of *Salvelinus leucomaenis*. Journal of Fish Biology 66: 888–895.

Aston, S. R. 1978. Estuarine chemistry. Pages 361-440 *In* J.P. Riley & R. Chester, editors. Chemical Oceanography. London Academic Press.

Barnes T. C., and B. M. Gillanders. 2013. Combined effects of extrinsic and intrinsic factors on otolith chemistry: implications for environmental reconstructions. Canadian Journal of Fisheries and Aquatic Sciences 70(8):1159–1166. doi:10.1139/cjfas-2012-0442.

Bath, G., S. Thorrold, C. Jones, S. Campana, J. MaLaren, and J. Lam. 2000. Strontium and barium uptake in aragonitic otoliths of marine fish. Geochimica et Cosmochimica Acta: 64:1705-1714.

Benjamini, Y., and Y. Hochberg. 1995. Controlling the false discovery rate: a practical and powerful approach to multiple testing. Journal of the Royal Statistical Society Series B 57: 289–300. http://www.jstor.org/stable/2346101.

Bergenius, M. A. J., B. D. Mapstone, G. A. Begg, and C. D. Murchie. 2005. The use of otolith chemistry to determine stock structure of three epinepheline serranid coral reef fishes on the Great Barrier Reef, Australia. Fisheries Research 72: 253-270.

Berkeley, S. A., C. Chapman, and S. M. Sogard. 2004. Maternal age as a determinant of larval growth and survival in a marine fish, *Sebastes Melanops*. Ecology 85(5): 1258-1264.

Bloom, D. D., and N. R. Lovejoy. 2014. The evolutionary origins of diadromy inferred from a time-calibrated phylogeny for Clupeiformes (herring and allies). Proceedings of the Royal Society B: Biological Sciences 281:2013-2081.

Bradbury, I. R., S. Hubert, B. Higgins, S. Bowman, I. G. Paterson, P. V. R. Snelgrove, C. J. Morris, R. S. Gregory, D. C. Hardie, T. Borza, and P. Bentzen. 2011. Evaluating SNP ascertainment bias and its impact on population assignment in Atlantic cod, *Gadus morhua*. Molecular Ecology Resources 11: 218–225. doi:10.1111/j.1755-0998.2010. 02949.x.

Brennan, S. R., D. P. Fernandez, C. E. Zimmerman, T. E. Cerling, R. J. Brown, and M. J. Wooller. 2015. Strontium isotopes in otoliths of a non-migratory fish (Slimy sculpin): implications for provenance studies. Geochimica et Cosmochimica Acta: 149: 32-45. doi: https://doi.org/10.1016/j.gca.2014.10.032.

Brown, J. A. 2006. Classification of juvenile flatfishes to estuarine and coastal habitats based on the elemental composition of otoliths. Estuarine Coastal and Shelf Science 66:594–611.

Brown R. J., and K. P. Severin. 2009. Otolith chemistry analyses indicate that water Sr:ca is the primary factor influencing otolith Sr:ca for freshwater and diadromous fish but not for marine fish. Canadian Journal of Fisheries and Aquatic Sciences 66:1790–1808.

Campana, S. E. 1999. Chemistry and composition of fish otoliths: pathways, mechanisms, and applications. Marine Ecology Progress Series 188:263–297.

Campana, S. E., and J. D. Neilson. 1985. Microstructure of fish otoliths. Canadian Journal of Fisheries and Aquatic Science: 42:1014-1032.

Campana, S. E., and S. R. Thorrold. 2001. Otoliths, increments, and elements: keys to a comprehensive understanding of fish populations? Canadian Journal of Fisheries and Aquatic Sciences 58:30–38.

Campana, S. E., G. A. Chouinard, J. M. Hanson, A. Frechet, and J. Brattey. 2000. Otolith elemental fingerprints as biological tracers of fish stocks. Fisheries Research 46:343–357.

Chang, M. Y., and A. J. Geffen. 2012. Taxonomic and geographic influences on fish otolith microchemistry. Fish and Fisheries 14: 458–492. doi: 10.1111/j.1467-2979.2012.00482.x.

Clarke, K. R. 1993. Non-parametric multivariate analyses of changes in community structure. Australian Journal of Ecology 18**:**117-43.

Clarke, L. M., B. D. Walther, S. B. Munch, S. R. Thorrold, and D. O. Conover. 2009. Chemical signatures in the otoliths of a coastal marine fish, *Menidia menidia*, from the northeastern United States: spatial and temporal differences. Marine Ecology Progress Series 384:261–271.

Dorval, E. 2004. Relating water and otolith chemistry in Chesapeake Bay, and their potential to identify essential seagrass habitats for juveniles of an estuarine-dependent fish, spotted seatrout (*Cynoscion nebulosus*). Ph.D. Thesis, Old Dominion University, USA.

Dorval, E., C. M. Jones, and R. Hannigan. 2005a. Chemistry in surface waters: distinguishing fine-scale differences in sea grass habitats of Chesapeake Bay. Limnology and Oceanography 50:1073–1083.

Dorval, E., C. M. Jones, R. Hannigan, and J. van Montfrans. 2005b. Can otolith chemistry be used for identifying essential sea grass habitats for juvenile Spotted Seatrout, *Cynoscion nebulosus*, in Chesapeake Bay? Marine and Freshwater Research 56:645–653.

Dorval, E., C. M. Jones, R. Hannigan, and J. van Montfrans. 2007. Relating otolith chemistry to surface water chemistry in a coastal plain estuary. Canadian Journal of Fisheries and Aquatic Sciences 64: 411–424.

Doubleday Z. A., H. H. Harris, C. Izzo, and B. M. Gillanders. 2014. Strontium randomly substituting for calcium in fish otolith aragonite. Analytical Chemistry 86(1):865–869. doi:10.1021/ ac4034278.

Elfman, M., K. E. Limburg, P. Kristiansson, H. Svedäng, L. Westin, H. Wickström, K. Malmqvist, and J. Pallon. 2000. Complex life histories of fishes revealed through natural information storage

Elsdon, T. S., and B. M. Gillanders. 2002. Interactive effects of temperature and salinity on otolith chemistry: challenges for determining environmental histories of fish. Canadian Journal of Fisheries and Aquatic Sciences 59: 1796-1808.

Elsdon, T. S., and B. M. Gillanders. 2003. Reconstructing migratory patterns of fish based on environmental influences on otolith chemistry. Fish Biology and Fisheries 13: 219-235.

Elsdon, T. S., and B. M. Gillanders. 2004. Fish otolith chemistry influenced by exposure to multiple environmental variables. Journal of Experimental Marine Biology and Ecology 313: 269–284. doi: 10.1016/j.jembe.2004.08.010.

Elsdon T. S., and B. M. Gillanders. 2005a. Alternative life-history patterns of estuarine fish: barium in otoliths elucidates freshwater residency. Canadian Journal of Fisheries and Aquatic Sciences 62(5): 1143–1152. doi:10.1139/f05-029.

Elsdon T. S., and B. M. Gillanders. 2005b. Consistency of patterns between laboratory experiments and field collected fish in otolith chemistry: an example and applications for salinity reconstructions. Marine Freshwater Resources 56(5):609–617. doi:10.1071/MF04146.

Elsdon, T. S. and B. M. Gillanders. 2006. Temporal variability of elemental concentrations in coastal and estuarine waters. Estuarine, Coastal and Shelf Science 66:147–156.

Elsdon, T. S., B. K. Wells, S. E. Campana, B. M. Gillanders, C. M. Jones, K. E. Limburg, D. H. Secor, S. R. Thorrold, and B. D. Walther 2008. Otolith chemistry to describe movements and life-history parameters of fishes: hypotheses, assumptions, limitations and inferences. Oceanography and Marine Biology: An Annual Review 46: 297–330.

Farrell, J., and S. E. Campana. 1996. Regulation of calcium and strontium deposition on the otoliths of juvenile tilapia, *Oreochromis niloticus*. Comparative Biochemistry and Physiology 115A: 103–109.

Friedrich, L. A., and N. M. Halden. 2008. Alkali element uptake in otoliths: a link between the environment and otolith microchemistry. Environmental Science and Technology: 42: 3514-3518.

Friedrich L. A., and N. M. Halden. 2010. Determining exposure history of northern pike and walleye to tailings effluence using trace metal uptake in otoliths. Environmental Science and Technology 44(5):1551–1558. doi:10.1021/es903261q.

Gahagan, B. I., J. C. Vokoun, G. W. Whiteledge, and E. T. Schultz. 2012. Evaluation of otolith microchemistry for identifying natal origin of anadromous River Herring in Connecticut. Marine and Coastal Fisheries: Dynamics, Management, and Ecosystem Science 4:358-372. doi: 10.1080/19425120.2012.675967.

Gillanders, B. M. 2005. Otolith chemistry to determine movements of diadromous and freshwater fish. Aquatic Living Resources 18(3):291–300.

Halden, N. M., J. A. Babaluk, J. L. Campbell, and W. J. Teesdale. 1995. Scanning proton micropobe analysis of strontium in an Arctic charr, *Salvanius alpinus*, otolith: implication for the interpretation of anadromy. Environmental Biology of Fishes: 43:333-339.

Halden, N. M., and L. A. Friedrich. 2008. Trace-element distributions in fish otoliths: natural markers of life histories, environmental conditions and exposure to tailings effluence. Mineral Magazine 72(2):593–605. doi:10.1180/minmag. 2008.072.2.593.

Hall, W. S., S. J. Buchong, W. Lenwood, W. Hall, M. J. Lenkevich, and A. E. Pinkney. 1988. Monitoring dissolved copper concentrations in Chesapeake Bay, U.S.A. Environmental Monitoring and Assessment 11: 33-14.

Hamer, P. A., G. P. Jenkins, and B. M. Gillanders. 2003. Otolith chemistry of juvenile snapper *Pargus auratus* in Victorian waters: natural chemical tags and their temporal variation. Marine Ecology Progress Series 263:261–273.

Harris, J. E., McBride, R. S., and Williams, R. O. 2007. Life history of Hickory Shad in the St. Johns River, Florida. Transactions of the American Fisheries Society 136(6): 1463-1471. Doi:10.1577/T06-187.1.

Hughes, C. S. 2015. Using water chemistry and otolith chemistry to determine strategic habitat areas for Striped Bass (*Morone saxatilis*) in the Albemarle Estuarine system of North Carolina. Dissertation. East Carolina University, Greenville

Hüssy, K., K. E. Limburg, H. De Pontual, O. R. B. Thomas, P. K. Cook, Y. Heimbrand, M. Blass, and A. M. Sturrock. 2020. Trace element patterns in otoliths: the role of biomineralization. Reviews in Fisheries Science and Aquaculture, https://doi.org/10.1080/23308249.2020.1760204.

Hynes, H. B. N. 1975. The stream and its valley. Verhandlungen des Internationalen Verein Limnologie 19:1-15.

Izzo, C., Z. A. Doubleday, and B. M. Gillanders. 2016. Where do elements bind within the otoliths of fish? Marine and Freshwater Research 67(7): 1072-1076. doi: https://doi.org/10.1071/MF15064.

Kafemann, R., S. M. Adlerstein, and R. Neukamm. 2000. Variation in otolith strontium and calcium ratios as an indicator of life histories strategies of freshwater species within a brackish water system. Fisheries Research 46: 313-325.

Kalish, J. M., J. M. Johnston, J. S. Gunn, and N. P. Clear. 1996. Use of the bomb radiocarbon chronometer to determine age of southern bluefin tuna *Thunnus maccoyii*. Marine Ecology Progress Series 143(1/3):1–8.

Kassambara, A. 2017. Machine learning essentials. STHDA. CreateSpace, North Charleston, SC.

Kim, Y. J., and C. Gu. 2004. Smoothing spline Gaussian regression: more scalable computation via efficient approximation. Journal of the Royal Statistical Society B Statistical Methodology 66:337–356. doi: https://doi.org/10.1046/j.1369-7412.2003.05316.x.

Korkmaz, S., D. Goksuluk, and G. Zararsiz. 2014. MVN: An R package for assessing multivariate normality. The R Journal. 6(2):151-162.

Kraus R. T., and D. H. Secor. 2004. Incorporation of strontium into otoliths of an estuarine fish. Journal of Experimental Marine Biology and Ecology 302(1): 85–106. doi:10.1016/j.jembe.2003.10.004

Kursa, M. B., and W. R. Rudnicki. 2010. Feature selection with the Boruta package. Journal of Statistical Software 36(11):1-13. URL: http://www.jstatsoft.org/v36/i11/

Leech, N. L., and A. J. Onwuegbuzie. 2002. A call for greater use of nonparametric statistics. Annual meeting of the Mid-South Educational Research Association, Chattanooga, TN.

Lill, J. O., V. Finnas, Y. Heimbrand, M. Blass, S. Frojdo, Y. Lahaye, J.M.K. Slotte, J. Nyman, E. Jokikokko, M. von Numbers, and H. Hagerstrand. 2019. Information depths of analytical techniques assessing whitefish otolith chemistry. Nuclear Institute and Methods in Physics Research B 477: 104-108. doi: https://doi.org/10.1016/j.nimb.2019.07.033

Limburg K. E., B. D. Walther, Z. Lu, G. Jackman, J. Mohan, Y. Walther, A. Nissling, P. K. Weber, and A. K. Schmitt. 2015. In search of the dead zone: use of otoliths for tracking fish exposure to hypoxia. Journal of Marine Systems 141:167–178. doi:10. 1016/j.jmarsys.2014.02.014.

Limburg, K. E., M. J. Wuenschel, K. Hüssy, Y. Heimbrand, and M. Samson. 2018. Making the otolith magnesium chemical calendar-clock tick: plausible mechanism and empirical evidence. Reviews in Fisheries Science and Aquaculture 26(4):479–493. doi:10.1080/23308249.2018.1458817.

Lochet, A., P. Jatteau, J. Tomas, and E. Rochard. 2008. Retrospective approach to investigating the early life history of a diadromous fish: Allis Shad *Alosa alosa* in the Gironde-Garonne-Dordogne watershed. Journal of Fish Biology 72:946–960.

Macdonald, J. I., R. N. Drysdale, R. Witt., Z. Cságoly, and G. Marteinsdóttir. 2019. Isolating the influence of ontogeny helps predict island wide variability in fish otolith chemistry. Reviews in Fish Biology and Fisheries 30:173-202. doi: https://doi.org/10.1007/s11160-019-09591-x.

Martin, G. B., and S. R. Thorrold. 2005. Temperature and salinity effects on magnesium, manganese, and barium incorporation in otoliths of larval and early juvenile spot *Leiostomus xanthurus*. Marine Ecology Progress Series 293: 223–232.

Mateo, I., E. G. Durbin, D. A. Bengtson, R. Kingsley, P. K. Swart, and D. Durant. 2012. Spatial and temporal variation in otolith chemistry for tautog (*Tautoga onitis*) along the U.S. North East Coast. Northeast Naturalist 19:201–216.

McCulloch, M., M. Cappo, J. Aumend, and W. Muller. 2005. Tracing the life history of individual barramundi using laser ablation MC-ICP-MS Sr-isotopic and Sr/Ba ratios in otoliths. Marine and Freshwater Research: 56:637–644.

Melvin, G. D., M. J. Dadswell., and J. D. Martin. 1986. Fidelity of American Shad, *Alosa sapidissima* (Clupeidae), to its river of previous spawning. Canadian Journal of Fisheries and Aquatic Sciences 43:640-646.

Miller, J. A. 2007. Scales of variation in otolith elemental chemistry of juvenile staghornsculpin (*Leptocottus armatus*) in three Pacific Northwest estuaries. Marine Biology 151(2): 483–494.

Miller, J. A. 2009. The effects of temperature and water concentration on the otolith incorporation of barium and manganese in black rockfish *Sebastes melanops*. Journal of Fisheries Biology 75(1):39–60. doi:10.1111/j.1095-8649.2009.02262.x.

Miller, J. A. 2011. Effects of water temperature and barium concentration on otolith composition along a salinity gradient: implications for migratory reconstructions. Journal of Experimental Marine Biology and Ecology 405:42–52.

Milton, D. A., and S. R. Chenery. 2001. Sources and uptakes of trace metals in otoliths of juvenile barramundi (*Lates calcarifer).* Journal of Experimental Marine Biology and Ecology 264: 47-65.

Mohan, J. A. 2009. Habitat utilization of juvenile Striped Bass *Morone saxatilis* in Albemarle Sound inferred from otolith and water chemistries. Master's Thesis. East Carolina University

Mohan, J. A., R. A. Rulifson, D. R. Corbett, and N. M. Halden. 2012. Validation of oligohaline elemental otolith signatures of striped bass by use of in situ caging experiments and water chemistry. Marine Coastal Fisheries 4(1):57–70. doi:10.1080/ 19425120.2012.656533.

Murdy, E. O., R. S. Birdsong, and J. A. Musick. 1997. Fishes of Chesapeake Bay. Smithsonian Institution Press, Washington, D.C.

Odum, H. T. 1951. Strontium in Florida waters. Florida Water Survey and Research Paper no. 6:20-21.

Oksanen, J., F. G. Blanchet, M. Friendly, R. Kindt, P. Legendre, D. McGlinn, P. R. Minchin, R. B. O'Hara, G. L. Simpson, P. Solymos, M. Henry, H. Stevens, E. Szoecs, and H. Wagner. 2019. vegan: Community ecology package. R package version 2.5-6. https://CRAN.R-project.org/package=vegan.

Palace, V. P., N. M. Halden, P. Yang, R. E. Evans, and G. Sterling. 2007. Determining residence patterns of rainbow trout using laser ablation inductively coupled plasma mass spectrometry (LA-ICP-MS) analysis of selenium in otoliths. Environmental Science and Technology 41:3679-3683.

Pannella, G. 1971. Fish otoliths: daily growth layers and periodical patterns. Science 173:1124-1127.

Payan, P., A. Edeyer, H. de Pontual, G. Borelli, G. Boeuf, and N. Mayer-Gostan. 1999. Chemical composition of saccular endolymph and otolith in fish inner ear: lack of spatial uniformity. American Journal of Physiology 277: 123–131.

Payan, P., H. de Pontual, G. Boeuf, and N. Mayer-Gostan. 2004. Endolymph chemistry and otolith growth in fish. Comptes Rendus PaleVol: General Palaeontology (Palaeobiochemistry) 3(6–7):535–547. doi:10.1016/j.crpv.2004.07.013.

Payne Wynne, M. L., K. A. Wilson, and K. E. Limburg. 2015. Retrospective examination of habitat use by blueback herring (*Alosa aestivalis*) using otolith microchemical methods. Canadian Journal of Fisheries and Aquatic Sciences 72(7):1073–1086. doi:10.1139/cjfas-2014-0206.

Perillo, J. A., and L. H. Butler. 2009. Evaluating the use of Fairmont Dam fish passage facility with application to anadromous fish restoration in the Schuylkill River, Pennsylvania. Journal of the Pennsylvania Academy of Science 83(1): 24-33.

Ranaldi, M. M., and M. M. Gagnon. 2008. Zinc incorporation in the otoliths of juvenile pink snapper (*Pagrus auratus* Forster): the influence of dietary versus waterborne sources. Journal of Experimental Marine Biology and Ecology 360:56-62.

R Development Core Team. 2019. R: A language and environment for statistical computing. Vienna, Austria: R Foundation for Statistical Computing.

Reis-Santos, P., R. P. Vasconcelos, M. Ruano, C. Latkoczy, D. Gnther, M. J. Costa, and H. Cabral. 2008. Interspecific variations of otolith chemistry in estuarine fish nurseries. Journal of Fish Biology 72: 2595–2614. doi: 10.1111/j.1095-8649.2008.01871.x.

Reis-Santos, P., B. M. Gillanders, S. E. Tanner, R. P. Vasconcelos, T. S. Elsdon, and H. N. Cabral. 2012. Temporal variability in estuarine fish otolith elemental fingerprints: implications for connectivity assessments. Estuarine, Coastal and Shelf Science 112: 216–224. doi: 10.1016/j.ecss.2012.07.027.

Reis-Santos, P., S. E. Tanner, R. P. Vasconcelos, T. S. Elsdon, H. N. Cabral, and B. M. Gillanders. 2013. Connectivity between estuarine and coastal fish populations:

contributions of estuaries are not consistent over time. Marine Ecology Progress Series 491: 177-186.

Rooker J. R., D. H. Secor, V.S. Zdanowicz, and T. Itoh. 2001. Discrimination of northern bluefin tuna from nursery areas in the Pacific Ocean using otolith chemistry. Marine Ecology Progress Series 218:275–282.

Rulifson, R. A. 1994.Status of anadromous Alosa along the East Coast of North America. Alosa Symposium, Tidewater Chapter, American Fisheries Society:134–158.

Schaffler, J. J., C. S. Reiss, and C. M. Jones, 2009. Spatial variation in otolith chemistry of Atlantic croaker larvae in the Mid-Atlantic Bight. Marine Ecology Progress Series 382: 185–195.

Schaffler, J. J., T. J. Miller, and C. M. Jones. 2014. Spatial and temporal variation in otolith chemistry of juvenile Atlantic Menhaden in the Chesapeake Bay. Transactions of the American Fisheries Society 243(4): 1061-1071. doi: https://doi.org/10.1080/00028487.2014.889748.

Secor, D. H. 1992. Application of otolith microchemistry analysis to investigate anadromy in Chesapeake Bay striped bass *Morone saxatilis*. Fisheries Bulletin 90:798–806.

Secor, D. H., and J. R. Rooker. 2000. Is otolith strontium a useful scalar of life cycles in estuarine fishes? Fisheries Research. 46(1–3): 359–371. doi:10.1016/S0165-7836(00)00159-4.

Secor, D. H., A. Henderson-Arzapalo, and P. M. Piccoli. 1995. Can otolith microchemistry chart patterns of migration and habitat utilization in anadromous fishes? Journal of

Experimental Marine Biology and Ecology 192(1):15–33. doi:10.1016/0022-0981(95)00054-U.

Secor D. H., J. R. Rooker, E. Zlokovitz, and V. S. Zdanowicz. 2001. Identification of riverine, estuarine, and coastal contingents of Hudson River striped bass based upon otolith elemental fingerprints. Marine Ecology Progress Series 211:245–253.

Skougstad, M. W. and C. A. Horr. 1963. Occurrence and distribution of strontium in natural water. U.S. Geological Survey Water-Supply Paper 1496-0: 55-97.

Soeth, M., H. L. Spach, F. A. Daros, J. P. Castro, and A. T. Correia. 2020. Use of otolith elemental signatures to unravel lifetime movement patterns of Atlantic spadefish, *Chaetodipterus faber*, in the Southwest Atlantic Ocean. Journal of Sea Research 158: 101873. doi: https://doi.org/10.1016/j.seares.2020.101873.

Sturrock, A. M., E. Hunter, J. A. Milton, R. C. Johnson, C. P. Warin, and C. N. Trueman. 2015. Quantifying physiological influences on otolith microchemistry. Methods in Ecology and Evolution 6: 806–816. doi: 10.1111/2041-210X.12381.

Tanner, S. E., R. P. Vasconcelos, H. N. Cabral, and S. R. Thorrold. 2012. Testing an otolith geochemistry approach to determine population structure and movements of European hake in the northeast Atlantic Ocean and Mediterranean Sea. Fisheries Research 12: 198–205. doi: 10.1016/j.fishres.2012.02.013.

Tanner, S. E., P. Reis-Santos, R. P. Vasconcelos, V. F. Fonseca, S. Franca, H. N. Cabral, and S. R. Thorrold. 2013. Does otolith geochemistry record ambient environmental conditions in a temperate tidal estuary? Journal of Experimental Marine Biology and Ecology 441: 7–15. doi: 10.1016/j.jembe.2013.01.009.

Tanner, S. E., P. Reis-Santos, and H. N. Cabral. 2016. Otolith chemistry in stock delineation: A brief overview, current challenges and future prospects. Fisheries Research 173: 206-213.

Thomas, O. R. B., and S. E. Swearer. 2019. Otolith biochemistry—a review. Reviews in Fisheries Science and Aquaculture 27(4):458–489. doi:10.1080/ 23308249.2019.1627285.

Thomas, O. R. B., K. Ganio, B. R. Roberts, and S. E. Swearer. 2017. Trace element–protein interactions in endolymph from the inner ear of fish: implications for environmental reconstructions using fish otolith chemistry. Metallomics 9(3):239–249. doi:10.1039/C6MT00189K.

Thorrold, S. R., C. M. Jones, and S. E. Campana. 1997. Response of otolith microchemistry to environmental variations experienced by larval and juvenile Atlantic Croaker (*Micropogonias undulatus*). Limnology and Oceanography 42:102–111.

Thorrold, S. R., C. M. Jones, S. E. Campana, J. W. McLaren, and J. W. H. Lam. 1998a. Trace element signatures in otoliths record natal river of juvenile American Shad (*Alosa sapidissima*). Limnology and Oceanography 43:1826– 1835.

Thorrold, S. R., C. M. Jones, P. K. Swart, and T. E. Targett. 1998b. Accurate classification of juvenile Weakfish *Cynoscion regalis* to estuarine nursery areas based on chemical signatures in otoliths. Marine Ecology Progress Series 173:253–265.

Thorrold, S. R., and S. Shuttleworth. 2000. In situ analysis of trace elements and isotope ratios in fish otoliths using laser ablation sector field inductively coupled plasma mass spectrometry. Canadian Journal of Fisheries and Aquatic Sciences 57:1232–1242.

Thorrold S. R., C. Latkoczy, P. K. Swart, and C. M. Jones. 2001. Natal homing in a marine fish metapopulation. Science 291:297–299.

Thresher, R. E., and C. H. Procter. 2007. Population structure and life history of orange roughy (*Hoplostethus atlanticus*) in the SW Pacific: inferences from otolith chemistry. Marine Biology 152: 461–473.

Tomczak, M. T., and E. Tomczak. 2014. The need to report effect size estimates revisited. An overview of some recommended measures of effect size. Trends in Sport Sciences 1(21): 19:25. ISSN 2299-9590.

Turner, D., M. Whitfield, and A. Dickson. 1981. The equilibrium speciation of dissolved components in freshwater and sea water at 25C and 1 atm pressure. Geochimica et Cosmochimica Acta 45(6):855–881. doi:10.1016/0016-7037(81)90115-0.

Turner, S. M., and K. E. Limburg. 2014. Determination of River Herring Natal Origin using Otolith Chemical Markers: Accuracy as a Function of Spatial Scale and Choice of Markers. Transactions of the American Fisheries Society 143(6):1530-1543. DOI: 10.1080/00028487.2014.949012

Walther, B. D., and S. R. Thorrold. 2008. Continental-scale variation in otolith geochemistry of juvenile American Shad. Canadian Journal of Fisheries and Aquatic Sciences 65:2623–2635.

Walther, B. D., S. R. Thorrold, and J. E. Olney. 2008. Geochemical signatures in otoliths record natal origins of American Shad. Transactions of the American Fisheries Society 137:57–69.

Walther, B. D., and S. R. Thorrold. 2010. Limited diversity in natal origins of immature anadromous fish during ocean residency. Canadian Journal of Fisheries and Aquatic Sciences 67: 1699–1707.

Walther, B. D., and K. E. Limburg. 2012. The use of otolith chemistry to characterize diadromous migrations. Journal of Fish Biology: 81:796-825.

Wei, T., and V. Simko. 2017. R package "corrplot": Visualization of a Correlation Matrix (Version 0.84). Available from https://github.com/taiyun/corrplot.

Wilson, T. R. S. 1975. Salinity and the major elements of sea water. In Chemical Oceanography, J. P. Riley and G. Skirrow (eds). London: Academic Press, pp. 365–413.

Zapf, D. H. 2012. River herring nursery habitat in Albemarle Sound, North Carolina, inferred from otolith microchemistry. Master's Thesis, East Carolina University, Greenville, NC.

Zimmerman C. E. 2005. Relationship of otolith strontium to calcium ratios and salinity: experimental validation for juvenile salmonids. Canadian Journal of Fisheries and Aquatic Sciences 62(1):88–97. doi:10.1139/f04-182.

Tables and figures

Table 3-1. Results of Mardia's test for multivariate normality where locations that did not meet the assumption of multivariate normality are denoted by stars*.

Parent River	AlphaCode	Skewness	p-val	Kurtosis	p-val
Altamaha	Alt	87.68	0.37	-1.53	0.13
Cape Fear	CF	99.77	0.12	-0.86	0.39
Choptank	Chop	95.67	0.18	-1.36	0.17
Chowan*	Chow	131.44	<0.01	1.53	0.13
James*	James	128.84	<0.01	1.55	0.12
Nanticoke	Nant	87.42	0.38	-1.53	0.13
Neuse*	Neuse	130.65	<0.01	2.00	0.05
Ogeechee	Ogee	82.26	0.53	-1.56	0.12
Pamlico*	Pam	121.79	<0.01	0.87	0.38
Patapsco	Pata	105.39	0.06	-0.66	0.51
Patuxent	Patux	77.68	0.67	-1.80	0.07
Potomac	Poto	93.49	0.22	-1.37	0.17
Rappahannock	Rapp	95.99	0.17	-1.05	0.29
Roanoke	Roan	100.77	0.10	0.07	0.94
South Santee*	SS	-22.03	1.00	-5.90	<0.01
St. Johns	StJo	80.59	0.59	-1.76	0.08
Susquehanna	Susq	87.34	0.38	-1.56	0.12
Waccamaw*	Wacca	74.30	0.77	-2.00	0.05

Table 3-2. Results of Levene's test for homogeneity of variance.

Element	Df	F.Value	Pr(>F)
Sr	17	0.94	0.52
Ba	17	2.30	0.00
Mg	17	1.76	0.03
Mn	17	1.24	0.24
Zn	17	1.46	0.11
Pb	17	1.93	0.02
Cu	17	2.53	0.00

Table 3-3. Descriptive statistics of strontium in the capture watershed as estimated from the otolith edge data. Values have been square root transformed and are grouped by parent river. Included are the skewness and kurtosis measures calculated in Mardia's test for multivariate normality. Parent Rivers are ordered from smallest to largest according to the average strontium ratio

Parent River	Mean	Stdev	Median	Min	Max	25th	75th	Skewness	Kurtosis	SE	CI-L	CI-U
SS	1.04	0.12	1.04	0.89	1.24	1	1.06	0.46	-1	0.05	0.95	1.13
Ogee	1.06	0.11	1.09	0.86	1.22	0.96	1.12	-0.24	-1.17	0.03	1	1.12
Poto	1.07	0.27	1.15	0.3	1.31	1.08	1.18	-2.07	3.3	0.08	0.91	1.23
StJo	1.09	0.1	1.06	0.99	1.29	1.05	1.09	0.86	-0.86	0.03	1.03	1.16
Alt	1.1	0.13	1.09	0.91	1.41	1.04	1.13	0.92	0.55	0.04	1.02	1.18
Wacca	1.11	0.06	1.1	1.01	1.2	1.09	1.16	-0.28	-1.27	0.02	1.07	1.16
Chow	1.14	0.11	1.14	0.85	1.37	1.06	1.21	-0.37	0.13	0.02	1.1	1.19
Susq	1.15	0.14	1.14	0.96	1.38	1.04	1.26	0.13	-1.75	0.05	1.07	1.24
Neuse	1.16	0.11	1.15	0.9	1.45	1.09	1.24	0.28	0.05	0.02	1.13	1.19
Roan	1.16	0.13	1.15	0.93	1.48	1.07	1.24	0.47	-0.03	0.03	1.11	1.21
James	1.17	0.13	1.17	0.78	1.44	1.11	1.24	-0.53	0.99	0.02	1.12	1.22
Pam	1.17	0.1	1.18	0.92	1.39	1.12	1.23	-0.17	0.28	0.02	1.13	1.21
Nant	1.19	0.15	1.16	1.03	1.47	1.07	1.23	0.64	-1.11	0.05	1.1	1.29
Rapp	1.19	0.12	1.16	1	1.4	1.12	1.25	0.37	-0.97	0.02	1.16	1.23
Pata	1.19	0.06	1.18	1.11	1.3	1.16	1.23	0.51	-1.02	0.04	1.12	1.25
CF	1.2	0.13	1.18	1.02	1.44	1.11	1.28	0.22	-1.22	0.03	1.15	1.26
Patux	1.26	0.12	1.28	1.04	1.46	1.22	1.3	-0.24	-0.74	0.04	1.19	1.33
Chop	1.34	0.17	1.39	1.06	1.52	1.19	1.48	-0.34	-1.67	0.05	1.23	1.44

Table 3-4. Descriptive statistics of barium in the capture watershed as estimated from the otolith edge data. Values have been square root transformed and are grouped by parent river. Included are the skewness and kurtosis measures calculated in Mardia's test for multivariate normality, as well as standard errors and confidence intervals calculated from 999 permutations. Capture locations are ordered from smallest to largest according to average barium ratio.

Parent River	Mean	Stdev	Median	Min	Max	25th	75th	Skew	Kurtosis	SE	CI-L	CI-U
Ogee	0.31	0.14	0.32	0	0.53	0.24	0.40	-0.60	-0.06	0.04	0.23	0.39
Neuse	0.38	0.15	0.36	0.10	0.78	0.28	0.47	0.72	0.44	0.02	0.34	0.42
StJo	0.38	0.07	0.36	0.30	0.49	0.32	0.46	0.29	-1.83	0.02	0.33	0.43
Poto	0.40	0.14	0.41	0.10	0.58	0.35	0.5	-0.69	-0.52	0.04	0.32	0.48
Rapp	0.41	0.15	0.35	0.27	0.69	0.28	0.52	0.53	-1.36	0.03	0.35	0.46
Pam	0.41	0.16	0.37	0.10	0.91	0.32	0.47	1.22	2.35	0.03	0.35	0.48
CF	0.41	0.13	0.39	0.22	0.66	0.31	0.47	0.58	-0.84	0.04	0.33	0.50
Pata	0.43	0.33	0.39	0	1.19	0.33	0.50	0.80	0.34	0.10	0.24	0.62
Roan	0.46	0.23	0.41	0	1.22	0.33	0.52	1.13	2.23	0.05	0.37	0.55
Wacca	0.46	0.25	0.46	0.17	0.79	0.24	0.67	0.06	-1.98	0.10	0.28	0.65
Alt	0.47	0.21	0.37	0.32	0.93	0.33	0.54	1.08	-0.34	0.07	0.34	0.60
Patux	0.47	0.13	0.46	0.30	0.71	0.37	0.52	0.46	-1.19	0.04	0.39	0.55
Chop	0.48	0.46	0.37	0	1.30	0.08	0.81	0.49	-1.37	0.15	0.19	0.76
James	0.50	0.21	0.44	0.30	1.29	0.38	0.55	2.10	5.38	0.04	0.42	0.58
Chow	0.52	0.22	0.47	0.22	1.09	0.36	0.66	0.73	-0.24	0.05	0.43	0.61
Susq	0.57	0.24	0.46	0.35	1.17	0.44	0.62	1.47	1.16	0.07	0.42	0.72
Nant	0.59	0.29	0.57	0.28	1.08	0.35	0.72	0.51	-1.30	0.09	0.42	0.77
SS	0.66	0.20	0.69	0.44	0.98	0.50	0.74	0.18	-1.61	0.08	0.50	0.83

Table 3-5. Descriptive statistics of magnesium in the capture watershed as estimated from the otolith edge data. Values have been square root transformed and are grouped by parent river. Included are the skewness and kurtosis measures calculated in Mardia's test for multivariate normality, as well as standard errors and confidence intervals calculated from 999 permutations. Capture locations are ordered from smallest to largest according to average magnesium ratio.

ParentRiver	Mean	Stdev	Median	Min	Max	25th	75th	Skew	Kurtosis	SE	CI-L	CI-U
StJo	0.16	0.02	0.17	0.14	0.17	0.14	0.17	-0.59	-1.81	0.01	0.15	0.17
CF	0.18	0.02	0.17	0.14	0.22	0.17	0.2	0.36	0.13	0	0.17	0.19
Ogee	0.18	0.03	0.17	0.14	0.27	0.17	0.2	1.07	0.92	0.01	0.16	0.2
Neuse	0.19	0.04	0.17	0.1	0.32	0.17	0.2	1.09	2.68	0.01	0.18	0.2
James	0.2	0.05	0.19	0.14	0.35	0.17	0.22	1.04	0.82	0.01	0.18	0.22
Roan	0.2	0.05	0.19	0.14	0.36	0.17	0.2	1.58	2.24	0.01	0.18	0.22
Susq	0.2	0.06	0.19	0.14	0.37	0.17	0.2	1.89	2.52	0.02	0.16	0.24
Alt	0.2	0.03	0.2	0.17	0.25	0.17	0.22	0.38	-1.41	0.01	0.18	0.21
Chow	0.2	0.03	0.2	0.14	0.3	0.17	0.2	1.28	2.37	0.01	0.18	0.21
Pam	0.2	0.04	0.2	0.14	0.28	0.17	0.2	0.59	-0.28	0.01	0.18	0.21
Patux	0.2	0.04	0.2	0.14	0.27	0.18	0.22	-0.03	-1.1	0.01	0.18	0.23
Rapp	0.21	0.11	0.19	0.1	0.53	0.14	0.23	1.84	2.87	0.03	0.15	0.27
Chop	0.21	0.06	0.2	0.14	0.33	0.18	0.22	0.85	-0.62	0.02	0.18	0.25
Pata	0.22	0.08	0.22	0.14	0.42	0.17	0.22	1.43	1.5	0.02	0.17	0.27
Nant	0.26	0.23	0.19	0.14	0.9	0.17	0.22	2.18	3.27	0.07	0.12	0.4
Wacca	0.3	0.18	0.22	0.14	0.69	0.22	0.31	1.27	0.13	0.07	0.17	0.44
SS	0.3	0.16	0.27	0.14	0.57	0.18	0.36	0.55	-1.42	0.07	0.17	0.43
Poto	0.32	0.43	0.17	0.14	1.61	0.17	0.2	2.44	4.44	0.13	0.06	0.57

Table 3-6. Descriptive statistics of manganese in the capture watershed as estimated from the otolith edge data. Values have been square root transformed and are grouped by parent river. Included are the skewness and kurtosis measures calculated in Mardia's test for multivariate normality, as well as standard errors and confidence intervals calculated from 999 permutations. Capture locations are ordered from smallest to largest according to average manganese ratio.

ParentRiver	Mean	Stdev	Median	Min	Max	25th	75th	Skew	Kurtosis	SE	CI-L	CI-U
Susq	0.67	0.22	0.7	0.25	1.01	0.53	0.82	-0.28	-1.01	0.07	0.53	0.81
StJo	0.74	0.29	0.64	0.39	1.35	0.56	0.92	0.84	-0.42	0.1	0.55	0.92
Alt	0.77	0.16	0.78	0.46	0.99	0.73	0.83	-0.36	-0.7	0.05	0.67	0.87
Patux	0.84	0.17	0.83	0.57	1.08	0.76	0.94	-0.12	-1.35	0.06	0.73	0.94
Ogee	0.85	0.28	0.91	0.33	1.16	0.77	1.07	-0.71	-0.98	0.08	0.69	1.01
Wacca	0.86	0.14	0.87	0.66	1.05	0.77	0.94	-0.2	-1.62	0.05	0.75	0.96
Rapp	0.87	0.18	0.87	0.54	1.12	0.73	1.02	-0.32	-1.34	0.05	0.77	0.97
CF	0.88	0.28	0.85	0.45	1.41	0.74	1.08	0.12	-1.08	0.06	0.76	1.01
SS	0.89	0.25	0.93	0.57	1.28	0.73	0.98	0.15	-1.5	0.1	0.69	1.09
Chop	0.94	0.24	1.03	0.53	1.28	0.81	1.09	-0.43	-1.29	0.08	0.79	1.09
Neuse	0.95	0.29	0.96	0.27	1.59	0.76	1.16	-0.06	-0.47	0.04	0.87	1.03
James	0.97	0.27	0.99	0.51	1.49	0.76	1.12	0.16	-1.03	0.05	0.87	1.07
Chow	0.99	0.39	0.95	0.17	2.06	0.77	1.22	0.55	0.65	0.08	0.84	1.15
Nant	1.05	0.27	1.06	0.58	1.63	0.92	1.13	0.36	-0.1	0.09	0.88	1.22
Roan	1.06	0.31	1.05	0.58	1.72	0.84	1.23	0.37	-0.65	0.06	0.94	1.18
Poto	1.14	0.84	1.01	0.53	3.56	0.72	1.15	2.08	3.3	0.25	0.65	1.64
Pam	1.15	0.38	1.24	0	1.7	0.97	1.34	-1.1	1.37	0.08	0.99	1.3
Pata	1.18	0.38	0.99	0.65	1.86	0.95	1.43	0.45	-1.25	0.11	0.96	1.41

Table 3-7. Descriptive statistics of zinc in the capture watershed as estimated from the otolith edge data. Values have been square root transformed and are grouped by parent river. Included are the skewness and kurtosis measures calculated in Mardia's test for multivariate normality, as well as standard errors and confidence intervals calculated from 999 permutations. Capture locations are ordered from smallest to largest according to average zinc ratio.

Parent River	Mean	Stdev	Median	Min	Max	25th	75th	Skew	Kurtosis	SE	CI-L	CI-U
StJo	0.54	0.15	0.49	0.4	0.81	0.44	0.62	0.7	-1.29	0.05	0.44	0.64
Chop	0.62	0.2	0.52	0.39	0.91	0.48	0.82	0.3	-1.89	0.06	0.5	0.74
CF	0.64	0.14	0.6	0.48	1.07	0.53	0.72	1.3	1.6	0.03	0.57	0.7
Alt	0.65	0.36	0.54	0.32	1.51	0.38	0.75	1.2	0.42	0.11	0.42	0.87
Patux	0.69	0.42	0.58	0.25	1.72	0.46	0.74	1.3	0.79	0.13	0.43	0.95
Pam	0.7	0.2	0.72	0.32	1.03	0.57	0.84	-0.19	-0.98	0.04	0.62	0.78
Ogee	0.73	0.27	0.82	0	0.95	0.69	0.89	-1.57	1.65	0.08	0.58	0.88
Neuse	0.74	0.29	0.77	0	1.39	0.5	0.98	-0.04	-0.37	0.04	0.66	0.82
Rapp	0.8	0.41	0.71	0.37	1.89	0.57	0.87	1.41	1.38	0.12	0.57	1.03
Pata	0.84	0.64	0.74	0	2.41	0.55	0.95	1.08	0.66	0.19	0.46	1.22
Roan	0.84	0.29	0.86	0.37	1.5	0.67	0.97	0.28	-0.48	0.06	0.73	0.96
Chow	0.85	0.34	0.89	0	1.43	0.71	1.01	-0.62	0.25	0.07	0.71	0.98
Susq	0.86	0.44	0.75	0.42	1.92	0.57	1.04	1.27	0.67	0.14	0.59	1.13
Wacca	0.87	0.27	0.87	0.5	1.2	0.66	1.09	-0.11	-1.89	0.1	0.66	1.07
James	0.88	0.49	0.71	0.39	2.35	0.6	0.89	1.57	1.46	0.09	0.7	1.06
SS	0.9	0.48	0.84	0.37	1.72	0.58	1.05	0.54	-1.3	0.2	0.51	1.29
Poto	1.08	0.4	1.18	0.62	1.74	0.71	1.31	0.24	-1.59	0.12	0.84	1.32
Nant	1.16	1.13	0.83	0.5	4.25	0.58	0.95	1.96	2.56	0.36	0.46	1.86

Table 3-8. Descriptive statistics of lead in the capture watershed as estimated from the otolith edge data. Values have been square root transformed and are grouped by parent river. Included are the skewness and kurtosis measures calculated in Mardia's test for multivariate normality, as well as standard errors and confidence intervals calculated from 999 permutations. Capture locations are ordered from smallest to largest according to average Pb ratio.

Parent River	Mean	Stdev	Median	Min	Max	25th	75th	Skew	Kurtosis	SE	CI-L	CI-U
Alt	0.03	0.06	0	0	0.14	0	0.08	0.86	-1.2	0.02	0	0.07
SS	0.03	0.05	0	0	0.1	0	0.08	0.54	-1.96	0.02	-0.01	0.07
CF	0.08	0.05	0.1	0	0.14	0.05	0.1	-0.85	-1.06	0.01	0.05	0.1
Chop	0.09	0.04	0.1	0	0.14	0.1	0.1	-1.63	2.25	0.01	0.07	0.12
StJo	0.09	0.05	0.1	0	0.17	0.1	0.1	-0.41	-0.86	0.02	0.05	0.12
Patux	0.1	0.1	0.1	0	0.35	0.03	0.1	1.19	0.84	0.03	0.04	0.16
Wacca	0.1	0.05	0.1	0	0.17	0.1	0.1	-0.49	-0.33	0.02	0.06	0.13
Pam	0.11	0.15	0	0	0.5	0	0.17	1.31	0.61	0.03	0.05	0.17
James	0.11	0.07	0.1	0	0.37	0.1	0.14	1.38	4.4	0.01	0.08	0.14
Neuse	0.11	0.09	0.1	0	0.37	0	0.14	0.48	-0.11	0.01	0.09	0.14
Pata	0.11	0.04	0.1	0	0.17	0.1	0.12	-0.86	0.92	0.01	0.08	0.13
Rapp	0.11	0.06	0.1	0	0.28	0.1	0.11	1.1	2.02	0.02	0.08	0.15
Roan	0.11	0.05	0.1	0	0.2	0.1	0.14	-0.77	0.52	0.01	0.09	0.13
Chow	0.12	0.06	0.14	0	0.22	0.1	0.14	-0.83	0.49	0.01	0.1	0.14
Poto	0.13	0.05	0.1	0.1	0.22	0.1	0.12	1.27	-0.26	0.02	0.1	0.16
Nant	0.14	0.14	0.1	0	0.47	0.1	0.13	1.17	0.22	0.04	0.05	0.23
Ogee	0.19	0.11	0.14	0.1	0.45	0.1	0.22	1.14	-0.04	0.03	0.12	0.25
Susq	0.21	0.23	0.12	0.1	0.85	0.1	0.2	2.06	2.89	0.07	0.07	0.35

Table 3-9. Descriptive statistics of copper in the capture watershed as estimated from the otolith edge data. Values have been square root transformed and are grouped by parent river. Included are the skewness and kurtosis measures calculated in Mardia's test for multivariate normality, as well as standard errors and confidence intervals calculated from 999 permutations. Capture locations are ordered from smallest to largest according to average copper ratio.

ParentRiver	Mean	Stdev	Median	Min	Max	25th	75th	Skew	Kurtosis	SE	CI-L	CI-U
Chop	0.51	0.08	0.49	0.4	0.67	0.46	0.52	0.78	-0.59	0.03	0.46	0.56
Alt	0.52	0.15	0.48	0.33	0.82	0.44	0.6	0.54	-0.94	0.05	0.43	0.62
Patux	0.54	0.21	0.47	0.4	1.09	0.41	0.53	1.67	1.6	0.07	0.41	0.67
StJo	0.55	0.23	0.53	0.3	1.11	0.4	0.57	1.37	0.96	0.08	0.4	0.7
CF	0.57	0.18	0.5	0.35	1.13	0.47	0.59	1.63	2.56	0.04	0.48	0.65
Nant	0.57	0.42	0.51	0	1.47	0.32	0.73	0.67	-0.47	0.13	0.31	0.83
Pata	0.57	0.27	0.6	0	1.07	0.47	0.67	-0.28	0.11	0.08	0.41	0.73
Rapp	0.6	0.11	0.64	0.39	0.72	0.54	0.68	-0.71	-0.99	0.03	0.54	0.66
Roan	0.65	0.22	0.64	0.3	1.11	0.52	0.76	0.36	-0.6	0.04	0.56	0.74
Pam	0.69	0.25	0.61	0.41	1.27	0.49	0.82	0.89	-0.25	0.05	0.59	0.8
Neuse	0.72	0.29	0.65	0.22	1.63	0.52	0.9	0.85	0.44	0.04	0.64	0.8
Ogee	0.72	0.3	0.75	0	1.14	0.64	0.85	-0.86	0.45	0.09	0.55	0.89
Chow	0.73	0.26	0.67	0.4	1.63	0.58	0.76	1.79	3.32	0.05	0.63	0.84
James	0.79	0.37	0.68	0.27	1.66	0.52	1	0.86	-0.2	0.07	0.65	0.92
SS	0.84	0.55	0.61	0.41	1.87	0.48	0.96	0.92	-0.92	0.23	0.39	1.28
Wacca	0.91	0.46	0.84	0.49	1.55	0.5	1.25	0.33	-1.84	0.17	0.57	1.25
Poto	0.95	0.41	0.96	0.42	1.74	0.65	1.11	0.51	-0.99	0.12	0.71	1.19
Susq	1.03	0.79	0.75	0.48	3.12	0.55	1.19	1.72	1.89	0.25	0.54	1.52

Table 3-10. Results of ANOSIM for showing the upper quantiles of the null model, the ANOSIM statistic (R), and the p-value for the parent river grouping variable.

	90%	95%	97.50%	99%	R	P-val
Parent River	0.04	0.05	0.05	0.06	0.10	<0.01

Table 3-11. Results of Kruskal Wallis test on the univariate edge data showing the sample size (n), Kruskal-Wallis test statistic (H), degrees of freedom (df), p-values (p), and effect size (η^2) expressed as η^2, percentage, and magnitude. Element effect size was considered small when the η^2 values were between 0.01-0.06 (1-6%), moderate when η^2 values were between 0.06 - 0.14 (6-14%), and large when η^2 values were greater than 0.14 (>14%).

Element	n	H	df	p	η^2	Effect Size (%)	magnitude
Sr	289	43.021	17	<0.01	0.10	9.6%	moderate
Ba	289	33.558	17	0.01	0.06	6.1%	moderate
Mg	289	25.99	17	0.08	0.03	3.3%	small
Mn	289	41.806	17	<0.01	0.09	9.2%	moderate
Zn	289	31.722	17	0.02	0.05	5.4%	small
Pb	289	40.676	17	<0.01	0.09	9.0%	moderate
Cu	289	40.473	17	<0.01	0.09	9.0%	moderate

Table 3-12. Results of univariate permutation ANOVA conducted on element ratios on the ventral edge of Hickory Shad otoliths.

	Element	Df	SumsOfSqs	MeanSqs	F.Model	R^2	Pr(>F)
Parent River	Sr	17	0.87	0.05	3.11	0.16	<0.01
Residuals	Sr	271	4.44	0.02		0.84	
Total	Sr	288	5.31			1	
Parent River	Ba	17	1.47	0.09	2.01	0.11	0.02
Residuals	Ba	271	11.67	0.04		0.89	
Total	Ba	288	13.14			1	
Parent River	Mg	17	0.34	0.02	1.71	0.1	0.08
Residuals	Mg	271	3.2	0.01		0.9	
Total	Mg	288	3.54			1	
Parent River	Mn	17	4.4	0.26	2.36	0.13	0.01
Residuals	Mn	271	29.75	0.11		0.87	
Total	Mn	288	34.16			1	
Parent River	Zn	17	4.77	0.28	1.75	0.1	0.05
Residuals	Zn	271	43.39	0.16		0.9	
Total	Zn	288	48.16			1	
Parent River	Pb	17	0.31	0.02	2.18	0.12	0.01
Residuals	Pb	271	2.29	0.01		0.88	
Total	Pb	288	2.6			1	
Parent River	Cu	17	4.5	0.26	2.63	0.14	<0.01
Residuals	Cu	271	27.21	0.1		0.86	
Total	Cu	288	31.71			1	

Table 3-13. Results of pairwise ANOSIM tests for each capture location when using parent river as the grouping variable. There is one block for each of the 18 parent rivers. The reference location for each block is shown in bold at the top left corner of each block. Values displayed are the ANOSIM statistic (R) and the p value calculated by comparing the observed R value to the empirical distribution of R under the null model generated through 999 permutations. Capture locations are listed in latitudinal order (North to South) both within and between blocks.

Susq	**R**	**p**	**Pata**	**R**	**p**	**Chop**	**R**	**p**	**Patux**	**R**	**p**	**Poto**	**R**	**p**	**Nant**	**R**	**p**	**Rapp**	**R**	**p**	**James**	**R**	**p**	**Chow**	**R**	**p**
Pata	0.10	0.03	Susq	0.10	0.03	Susq	0.21	0.01	Susq	0.14	0.04	Susq	0.04	0.20	Susq	0.08	0.09	Susq	0.04	0.19	Susq	0.03	0.32	Susq	0.03	0.35
Chop	0.21	0.01	Chop	0.05	0.15	Pata	0.05	0.15	Pata	0.04	0.14	Pata	0.02	0.22	Pata	0	0.43	Pata	0.01	0.32	Pata	0.06	0.27	Pata	0.09	0.15
Patux	0.14	0.03	Patux	0.04	0.15	Patux	0	0.43	Chop	0	0.43	Chop	0.15	0.01	Chop	0.04	0.21	Chop	0.11	0.08	Chop	0.13	0.11	Chop	0.20	0.03
Nant	0.08	0.09	Nant	0	0.43	Nant	0.04	0.21	Nant	0.05	0.14	Patux	0.11	0.04	Patux	0.05	0.16	Patux	0.01	0.38	Patux	0	0.64	Patux	0.08	0.17
Poto	0.04	0.20	Poto	0.02	0.21	Poto	0.15	0.01	Poto	0.11	0.03	Nant	0.08	0.08	Poto	0.08	0.06	Nant	0.12	0.04	Nant	0.14	0.11	Nant	0.16	0.06
Rapp	0.04	0.18	Rapp	0.01	0.31	Rapp	0.11	0.08	Rapp	0.01	0.39	Rapp	0.06	0.08	Rapp	0.12	0.04	Poto	0.06	0.11	Poto	0.02	0.39	Poto	0.03	0.33
James	0.03	0.36	James	0.06	0.27	James	0.13	0.11	James	0	0.64	James	0.02	0.39	James	0.14	0.10	James	0	0.76	Rapp	0	0.79	Rapp	0	0.58
Chow	0.03	0.37	Chowan	0.09	0.15	Chow	0.2	0.03	Chow	0.08	0.17	Chow	0.03	0.33	Chow	0.16	0.06	Chow	0	0.58	Chow	0	0.79	James	0	0.81
Roan	0.06	0.25	Roan	0.06	0.24	Roan	0.14	0.06	Roan	0.04	0.30	Roan	0.07	0.20	Roan	0.17	0.05	Roan	0	0.70	Roan	0	0.67	Roan	0	0.96
Pam	0.18	0.04	Pam	0.05	0.28	Pam	0.17	0.06	Pam	0.05	0.27	Pam	0.14	0.06	Pam	0.16	0.06	Pam	0	0.45	Pam	0.01	0.25	Pam	0.03	0.10
Neuse	0.11	0.15	Neuse	0.16	0.07	Neuse	0.31	<0.01	Neuse	0.07	0.23	Neuse	0.10	0.16	Neuse	0.28	0.01	Neuse	0	0.66	Neuse	0.04	0.17	Neuse	0.04	0.21
CF	0.20	0.01	CF	0.16	0.03	CF	0.23	0.01	CF	0.11	0.10	CF	0.25	0.01	CF	0.25	0.01	CF	0	0.40	CF	0	0.80	CF	0.04	0.21
Wacca	0.01	0.41	Wacca	0.08	0.18	Wacca	0.21	0.02	Wacca	0.16	0.05	Wacca	0	0.57	Wacca	0.01	0.40	Wacca	0.11	0.15	Wacca	0.06	0.30	Wacca	0.10	0.22
SS	0.13	0.13	SS	0.30	0.02	SS	0.41	<0.01	SS	0.29	0.01	SS	0.23	0.05	SS	0.04	0.30	SS	0.38	0.01	SS	0.29	0.05	SS	0.38	0.01
Ogee	0.06	0.15	Ogee	0.17	<0.01	Ogee	0.33	<0.01	Ogee	0.28	<0.01	Ogee	0.08	0.05	Ogee	0.20	<0.01	Ogee	0.14	0.01	Ogee	0.07	0.23	Ogee	0.08	0.17
Alt	0.04	0.22	Alt	0.15	0.01	Alt	0.20	<0.01	Alt	0.04	0.19	Alt	0.22	<0.01	Alt	0.11	0.04	Alt	0.11	0.05	Alt	0	0.48	Alt	0.11	0.13
StJo	0.08	0.11	StJo	0.06	0.12	StJo	0.19	0.01	StJo	0.16	0.02	StJo	0.14	0.03	StJo	0.08	0.08	StJo	0.07	0.14	StJo	0	0.58	StJo	0.08	0.21

Roan	**R**	**p**	**Pam**	**R**	**p**	**Neuse**	**R**	**p**	**CF**	**R**	**p**	**Wacca**	**R**	**p**	**SS**	**R**	**p**	**Ogee**	**R**	**p**	**Alt**	**R**	**p**	**StJo**	**R**	**p**
Susq	0.06	0.27	Susq	0.18	0.04	Susq	0.11	0.15	Susq	0.20	0.01	Susq	0.01	0.41	Susq	0.13	0.13	Susq	0.06	0.15	Susq	0.04	0.21	Susq	0.08	0.09
Pata	0.06	0.22	Pata	0.05	0.27	Pata	0.16	0.05	Pata	0.16	0.03	Pata	0.08	0.20	Pata	0.30	0.02	Pata	0.17	<0.01	Pata	0.15	0.01	Pata	0.06	0.12
Chop	0.14	0.06	Chop	0.17	0.06	Chop	0.31	<0.01	Chop	0.23	0.01	Chop	0.21	0.02	Chop	0.41	<0.01	Chop	0.33	<0.01	Chop	0.20	<0.01	Chop	0.19	0.01
Patux	0.04	0.30	Patux	0.05	0.27	Patux	0.07	0.25	Patux	0.11	0.10	Patux	0.16	0.06	Patux	0.29	0.02	Patux	0.28	<0.01	Patux	0.04	0.19	Patux	0.16	0.02
Nant	0.17	0.05	Nant	0.16	0.05	Nant	0.28	0.01	Nant	0.25	0.01	Nant	0.01	0.41	Nant	0.04	0.33	Nant	0.20	0.01	Nant	0.11	0.04	Nant	0.08	0.08
Poto	0.07	0.21	Poto	0.14	0.06	Poto	0.10	0.15	Poto	0.25	0.01	Poto	0	0.60	Poto	0.23	0.04	Poto	0.08	0.05	Poto	0.22	<0.01	Poto	0.14	0.03
Rapp	0	0.71	Rapp	0	0.47	Rapp	0	0.65	Rapp	0	0.40	Rapp	0.11	0.14	Rapp	0.38	0.01	Rapp	0.14	0.01	Rapp	0.11	0.05	Rapp	0.07	0.13
James	0	0.68	James	0.01	0.24	James	0.04	0.17	James	0	0.79	James	0.06	0.30	James	0.29	0.05	James	0.07	0.23	James	0	0.48	James	0	0.58
Chow	0	0.96	Chow	0.03	0.10	Chow	0.04	0.21	Chow	0.04	0.21	Chow	0.10	0.23	Chow	0.38	0.01	Chow	0.08	0.17	Chow	0.11	0.13	Chow	0.08	0.21
Pam	0.01	0.32	Roan	0.01	0.30	Roan	0.04	0.18	Roan	0.04	0.12	Roan	0.12	0.18	Roan	0.42	<0.01	Roan	0.05	0.24	Roan	0.11	0.12	Roan	0.02	0.44
Neuse	0.04	0.19	Neuse	0.05	0.16	Pam	0.05	0.15	Pam	0.01	0.25	Pam	0.20	0.07	Pam	0.36	0.02	Pam	0.11	0.09	Neuse	0.07	0.26	Pam	0.02	0.40
CF	0.04	0.12	CF	0.01	0.25	CF	0	0.95	Neuse	0	0.95	Neuse	0.14	0.11	Neuse	0.44	<0.01	Neuse	0.02	0.40	Pam	0.07	0.23	Neuse	0	0.82
Wacca	0.12	0.19	Wacca	0.20	0.06	Wacca	0.14	0.12	Wacca	0.26	0.04	CF	0.26	0.04	CF	0.52	<0.01	CF	0.32	<0.01	CF	0.17	0.04	CF	0.09	0.16
SS	0.42	0.01	SS	0.36	0.01	SS	0.44	0.01	SS	0.52	<0.01	SS	0.08	0.21	Wacca	0.08	0.18	Wacca	0.07	0.21	Wacca	0.15	0.06	Wacca	0.15	0.04
Ogee	0.05	0.25	Ogee	0.11	0.08	Ogee	0.02	0.42	Ogee	0.32	<0.01	Ogee	0.07	0.22	Ogee	0.32	0.01	SS	0.32	0.01	SS	0.10	0.19	SS	0.33	0.01
Alt	0.11	0.12	Alt	0.07	0.23	Alt	0.07	0.26	Alt	0.17	0.04	Alt	0.15	0.06	Alt	0.10	0.19	Alt	0.20	<0.01	Ogee	0.20	<0.01	Ogee	0.11	0.08
StJo	0.02	0.38	StJo	0.02	0.43	StJo	0	0.82	StJo	0.09	0.16	StJo	0.15	0.05	StJo	0.33	0.01	StJo	0.11	0.08	StJo	0.12	0.02	Alt	0.12	0.02

Table 3-14. Results of Wald's t-test for unequal variance conducted on barium concentrations using the otolith edge data showing p-values for each pairwise comparison. No significant differences were found.

	Susq	Pata	Chop	Patux	Poto	Nant	Rapp	James	Chow	Roan	Pam	Neuse	CF	Wacca	SS	Ogee	Alt
Pata	0.43																
Chop	0.66	0.81															
Patux	0.64	0.85	0.97														
Poto	0.32	0.90	0.72	0.75													
Nant	0.90	0.32	0.52	0.50	0.25												
Rapp	0.32	0.95	0.75	0.76	0.97	0.28											
James	0.69	0.68	0.90	0.86	0.51	0.53	0.54										
Chow	0.77	0.53	0.77	0.75	0.41	0.68	0.44	0.86									
Roan	0.47	0.86	0.93	0.97	0.72	0.32	0.76	0.75	0.64								
Pam	0.29	0.93	0.72	0.75	0.97	0.18	0.98	0.43	0.32	0.72							
Neuse	0.13	0.75	0.50	0.53	0.9	0.11	0.82	0.17	0.13	0.41	0.77						
CF	0.29	0.90	0.70	0.72	0.98	0.18	0.97	0.43	0.32	0.72	0.97	0.84					
Wacca	0.65	0.89	0.97	0.98	0.76	0.52	0.82	0.86	0.76	0.98	0.77	0.66	0.76				
SS	0.70	0.22	0.32	0.32	0.16	0.76	0.17	0.32	0.43	0.23	0.13	0.09	0.13	0.32			
Ogee	0.11	0.50	0.32	0.32	0.65	0.09	0.54	0.13	0.11	0.28	0.50	0.65	0.53	0.43	0.09		
Alt	0.65	0.82	0.98	0.98	0.72	0.51	0.76	0.89	0.76	0.95	0.72	0.52	0.72	0.97	0.32	0.32	
StJo	0.31	0.82	0.66	0.70	0.94	0.22	0.89	0.44	0.32	0.68	0.89	0.98	0.90	0.72	0.14	0.72	0.68

Table 3-15. Results of Wald's t-test for unequal variance conducted on zinc concentrations using the otolith edge data showing p-values for each pairwise comparison. No significant differences were found.

	Susq	Pata	Chop	Patux	Poto	Nant	Rapp	James	Chow	Roan	Pam	Neuse	CF	Wacca	SS	Ogee	Alt
Pata	0.97																
Chop	0.54	0.54															
Patux	0.64	0.67	0.92														
Poto	0.54	0.53	0.14	0.27													
Nant	0.46	0.41	0.08	0.14	0.88												
Rapp	0.93	0.95	0.61	0.77	0.46	0.30											
James	0.97	0.94	0.46	0.54	0.53	0.35	0.85										
Chow	0.97	0.98	0.51	0.61	0.48	0.30	0.93	0.94									
Roan	0.97	0.98	0.51	0.61	0.47	0.30	0.93	0.93	0.98								
Pam	0.61	0.65	0.85	0.97	0.15	0.08	0.74	0.48	0.54	0.54							
Neuse	0.67	0.74	0.66	0.91	0.15	0.08	0.88	0.53	0.61	0.61	0.89						
CF	0.53	0.54	0.97	0.93	0.08	0.07	0.61	0.34	0.46	0.46	0.88	0.64					
Wacca	0.99	0.97	0.54	0.66	0.61	0.51	0.93	0.98	0.97	0.97	0.65	0.73	0.54				
SS	0.97	0.93	0.54	0.61	0.67	0.54	0.88	0.97	0.94	0.93	0.61	0.66	0.53	0.97			
Ogee	0.71	0.77	0.79	0.95	0.30	0.15	0.88	0.61	0.67	0.68	0.97	0.97	0.8	0.74	0.67		
Alt	0.56	0.61	0.97	0.95	0.15	0.08	0.66	0.48	0.54	0.54	0.93	0.74	0.98	0.61	0.55	0.88	
StJo	0.46	0.46	0.89	0.70	0.08	0.07	0.51	0.28	0.34	0.34	0.61	0.53	0.8	0.48	0.46	0.61	0.83

Table 3-16. Results of SIMPER analysis showing pairwise comparisons with Susquehanna. The average element ratio (μ_{g1}) of each element for the reference capture location (Susq) is shown in the top left corner. The remaining blocks show the average ratio of each element in the capture location being compared (μ_{g2}), the average dissimilarity of each element between Susquehanna and the group being compared (μ_{diss}), the standard deviation of each element's contribution estimate (sd), the average to standard deviation ratio (ϕ), the cumulative (CS) and individual (Ind) contribution of each element to dissimilarity between groups, and the permutation p-value for each elements contribution (p). Comparisons from ANOSIM that had p-values < 0.05 are indicated with a star*.

Susq	Cu	Zn	Mn	Ba	Sr	Pb
	1.03	0.86	0.67	0.57	1.15	0.21

G2	elm	μ_{g2}	μ_{diss}	sd	ϕ	CS	Ind	p
Pata*	Mn	1.18	0.06	0.04	1.40	0.26	0.26	0.04
	Zn	0.84	0.06	0.05	1.26	0.50	0.24	0.10
	Cu	0.57	0.06	0.06	0.98	0.75	0.25	0.02
	Ba	0.43	0.03	0.03	1.22	0.89	0.14	0.13
	Sr	1.19	0.02	0.01	1.75	0.95	0.06	0.71
	Pb	0.10	0.01	0.02	0.67	1	0.05	0.33
Chop*	Cu	0.51	0.05	0.06	0.92	0.24	0.24	0.03
	Ba	0.48	0.05	0.03	1.58	0.46	0.22	<0.01
	Mn	0.94	0.04	0.03	1.42	0.65	0.19	0.52
	Zn	0.62	0.04	0.03	1.28	0.82	0.17	0.71
	Sr	1.34	0.03	0.02	1.42	0.95	0.13	0.01
	Pb	0.09	0.01	0.02	0.65	1	0.05	0.32
Patux*	Cu	0.54	0.06	0.06	0.99	0.30	0.30	0.01
	Zn	0.69	0.05	0.04	1.33	0.55	0.25	0.29
	Mn	0.84	0.03	0.02	1.29	0.71	0.16	0.94
	Ba	0.47	0.02	0.02	1.26	0.82	0.11	0.82
	Sr	1.26	0.02	0.02	1.32	0.92	0.10	0.20
	Pb	0.10	0.02	0.02	0.89	1	0.08	0.07
Poto	Cu	0.95	0.06	0.05	1.18	0.27	0.27	0.01
	Mn	1.14	0.06	0.07	0.80	0.53	0.26	0.08
	Zn	1.08	0.05	0.03	1.46	0.76	0.23	0.25
	Ba	0.40	0.02	0.02	1.24	0.86	0.10	0.83
	Sr	1.07	0.02	0.02	1.04	0.95	0.09	0.18
	Pb	0.13	0.01	0.02	0.65	1	0.05	0.48
Nant	Cu	0.57	0.07	0.06	1.18	0.28	0.28	<0.01
	Zn	1.16	0.06	0.07	0.90	0.54	0.26	0.07
	Mn	1.05	0.05	0.03	1.57	0.73	0.19	0.34
	Ba	0.59	0.03	0.02	1.41	0.86	0.13	0.34
	Sr	1.19	0.02	0.01	1.26	0.94	0.08	0.36
	Pb	0.14	0.01	0.02	0.91	1	0.06	0.08

G2	elm	μ_{g2}	μ_{diss}	sd	ϕ	CS	Ind	p
Rapp	Cu	0.60	0.05	0.06	0.91	0.28	0.28	0.06
	Zn	0.80	0.05	0.04	1.20	0.52	0.24	0.45
	Mn	0.87	0.03	0.02	1.33	0.70	0.18	0.92
	Ba	0.41	0.02	0.02	1.43	0.84	0.14	0.61
	Sr	1.19	0.02	0.01	1.44	0.94	0.10	0.38
	Pb	0.11	0.01	0.02	0.70	1	0.06	0.28
James	Cu	0.79	0.06	0.05	1.07	0.29	0.29	0.01
	Zn	0.88	0.05	0.04	1.15	0.52	0.23	0.37
	Mn	0.97	0.04	0.03	1.40	0.73	0.21	0.53
	Ba	0.50	0.02	0.02	1.13	0.85	0.12	0.82
	Sr	1.17	0.02	0.01	1.45	0.94	0.09	0.45
	Pb	0.11	0.01	0.02	0.74	1	0.06	0.20
Chow	Cu	0.73	0.05	0.05	0.97	0.25	0.25	0.05
	Mn	0.99	0.05	0.04	1.20	0.50	0.25	0.21
	Zn	0.85	0.04	0.03	1.39	0.73	0.23	0.49
	Ba	0.52	0.03	0.02	1.34	0.86	0.13	0.54
	Sr	1.14	0.02	0.01	1.44	0.94	0.08	0.60
	Pb	0.12	0.01	0.02	0.75	1	0.06	0.24
Roan	Cu	0.65	0.05	0.05	1.00	0.26	0.26	0.03
	Mn	1.06	0.05	0.04	1.39	0.51	0.25	0.13
	Zn	0.84	0.04	0.03	1.40	0.72	0.21	0.62
	Ba	0.46	0.03	0.02	1.23	0.85	0.13	0.47
	Sr	1.16	0.02	0.01	1.37	0.94	0.09	0.45
	Pb	0.11	0.01	0.02	0.71	1	0.06	0.25
Neuse	Cu	0.72	0.06	0.05	1.02	0.28	0.28	0.01
	Mn	0.95	0.04	0.03	1.39	0.49	0.21	0.41
	Zn	0.74	0.04	0.03	1.34	0.71	0.22	0.59
	Ba	0.38	0.03	0.02	1.36	0.84	0.13	0.51
	Sr	1.16	0.02	0.01	1.44	0.93	0.09	0.55
	Pb	0.11	0.01	0.02	0.91	1	0.07	0.04
Pam*	Mn	1.15	0.06	0.04	1.76	0.30	0.30	0.02
	Cu	0.69	0.05	0.05	0.99	0.55	0.25	0.03
	Zn	0.70	0.04	0.03	1.28	0.72	0.17	0.86
	Ba	0.41	0.02	0.02	1.27	0.83	0.11	0.71
	Pb	0.11	0.02	0.02	1.21	0.92	0.09	<0.01
	Sr	1.17	0.02	0.01	1.50	1	0.08	0.60

G2	elm	μ_{g2}	μ_{diss}	sd	ϕ	CS	Ind	p
CF*	Cu	0.57	0.06	0.06	0.95	0.30	0.30	0.01
	Mn	0.88	0.04	0.03	1.32	0.51	0.21	0.66
	Zn	0.64	0.04	0.03	1.18	0.70	0.19	0.87
	Ba	0.41	0.02	0.02	1.35	0.83	0.13	0.70
	Sr	1.20	0.02	0.01	1.37	0.93	0.10	0.28
	Pb	0.08	0.01	0.02	0.76	1	0.07	0.10
Wacca	Cu	0.91	0.06	0.05	1.18	0.33	0.33	0.01
	Zn	0.87	0.04	0.03	1.38	0.54	0.21	0.62
	Ba	0.46	0.03	0.02	1.60	0.70	0.16	0.28
	Mn	0.86	0.03	0.02	1.28	0.86	0.16	0.97
	Sr	1.11	0.02	0.01	1.72	0.94	0.08	0.75
	Pb	0.10	0.01	0.02	0.70	1	0.06	0.27
SS	Cu	0.84	0.06	0.06	1.13	0.30	0.30	0.03
	Zn	0.90	0.05	0.04	1.39	0.54	0.24	0.32
	Mn	0.89	0.04	0.03	1.33	0.70	0.16	0.77
	Ba	0.66	0.03	0.02	1.43	0.83	0.13	0.52
	Sr	1.04	0.02	0.01	1.33	0.91	0.08	0.43
	Pb	0.03	0.02	0.02	1.06	1	0.09	0.03
Ogee	Cu	0.72	0.06	0.06	1.03	0.28	0.28	0.01
	Zn	0.73	0.04	0.04	1.20	0.49	0.21	0.55
	Mn	0.85	0.04	0.03	1.48	0.68	0.19	0.64
	Ba	0.31	0.03	0.02	1.29	0.83	0.15	0.22
	Sr	1.06	0.02	0.01	1.47	0.92	0.09	0.36
	Pb	0.19	0.02	0.02	0.86	1	0.08	0.04
Alt	Cu	0.52	0.06	0.06	0.98	0.29	0.29	0.01
	Zn	0.65	0.05	0.04	1.35	0.54	0.25	0.27
	Mn	0.77	0.03	0.02	1.29	0.68	0.14	0.98
	Ba	0.47	0.03	0.02	1.38	0.81	0.13	0.46
	Pb	0.03	0.02	0.02	1.12	0.90	0.09	<0.01
	Sr	1.10	0.02	0.01	1.49	1	0.10	0.30
StJo	Cu	0.55	0.06	0.06	1.01	0.32	0.32	0.01
	Zn	0.54	0.04	0.03	1.26	0.54	0.22	0.52
	Mn	0.74	0.04	0.03	1.28	0.72	0.18	0.81
	Ba	0.38	0.02	0.02	1.23	0.84	0.12	0.71
	Sr	1.09	0.02	0.01	1.35	0.93	0.09	0.53
	Pb	0.09	0.01	0.02	0.76	1	0.07	0.13

Table 3-17. Results of SIMPER analysis showing pairwise comparisons with Potomac. The average element ratio (μ_{g1}) of each element for the reference capture location (Poto) is shown in the top left corner. The remaining blocks show the average ratio of each element in the capture location being compared (μ_{g2}), the average dissimilarity of each element between Potomac and the group being compared (μ_{diss}), the standard deviation of each element's contribution estimate (sd), the average to standard deviation ratio (ϕ), the cumulative (CS) and individual (Ind) contribution of each element to dissimilarity between groups, and the permutation p-value for each elements contribution (p). Comparisons from ANOSIM that had p-values < 0.05 are indicated with a star*.

Poto	Zn	Cu	Mn	Sr	Ba	Pb
	1.08	0.95	1.14	1.07	0.40	0.13

G2	elm	μ_{g2}	μ_{diss}	sd	φ	CS	Ind	p
Susq	Cu	0.86	0.06	0.05	1.18	0.27	0.27	0.01
	Mn	0.67	0.06	0.07	0.80	0.53	0.26	0.08
	Zn	0.86	0.05	0.03	1.46	0.76	0.23	0.25
	Ba	0.57	0.02	0.02	1.24	0.86	0.10	0.83
	Sr	1.15	0.02	0.02	1.04	0.95	0.09	0.18
	Pb	0.21	0.01	0.02	0.65	1	0.05	0.48
Pata	Zn	0.84	0.06	0.05	1.42	0.28	0.28	0.03
	Mn	1.18	0.06	0.06	1.00	0.56	0.28	0.03
	Cu	0.57	0.05	0.04	1.24	0.79	0.23	0.06
	Ba	0.43	0.03	0.02	1.14	0.91	0.12	0.41
	Sr	1.19	0.02	0.02	0.71	0.98	0.07	0.70
	Pb	0.10	0.00	0.01	0.81	1	0.02	0.99
Chop*	Zn	0.62	0.06	0.04	1.56	0.23	0.23	0.15
	Mn	0.94	0.05	0.07	0.79	0.45	0.22	0.14
	Cu	0.51	0.05	0.04	1.33	0.66	0.21	0.07
	Ba	0.48	0.04	0.03	1.40	0.85	0.19	0.01
	Sr	1.34	0.03	0.03	1.20	0.98	0.13	<0.01
	Pb	0.09	0.00	0.01	0.70	1	0.02	1.00
Patux*	Zn	0.69	0.06	0.04	1.54	0.29	0.29	0.05
	Cu	0.54	0.05	0.04	1.36	0.53	0.24	0.03
	Mn	0.84	0.05	0.07	0.73	0.77	0.24	0.16
	Sr	1.26	0.02	0.02	1.00	0.88	0.11	0.05
	Ba	0.47	0.02	0.01	1.29	0.96	0.08	0.95
	Pb	0.10	0.01	0.01	1.02	1	0.04	0.70
Nant	Zn	1.16	0.07	0.06	1.09	0.28	0.28	0.03
	Cu	0.57	0.06	0.04	1.40	0.54	0.26	0.01
	Mn	1.05	0.05	0.06	0.83	0.75	0.21	0.20
	Ba	0.59	0.03	0.02	1.33	0.87	0.12	0.41
	Sr	1.19	0.02	0.02	0.92	0.96	0.09	0.20
	Pb	0.14	0.01	0.01	1.01	1	0.04	0.63
Rapp	Zn	0.80	0.05	0.04	1.43	0.28	0.28	0.18
	Mn	0.87	0.05	0.07	0.74	0.54	0.26	0.20
	Cu	0.60	0.04	0.04	1.27	0.77	0.23	0.17
	Sr	1.19	0.02	0.02	0.86	0.88	0.11	0.26
	Ba	0.41	0.02	0.01	1.45	0.97	0.09	0.94
	Pb	0.11	0.01	0.01	0.80	1	0.03	0.99
James	Zn	0.88	0.05	0.04	1.08	0.27	0.27	0.14
	Mn	0.97	0.05	0.06	1.14	0.54	0.27	0.10
	Cu	0.79	0.05	0.04	0.95	0.77	0.23	0.07
	Ba	0.50	0.02	0.02	0.40	0.87	0.10	0.96
	Sr	1.17	0.02	0.02	1.07	0.97	0.10	0.28
	Pb	0.11	0.01	0.01	0.13	1	0.03	0.99
Chow	Mn	0.91	0.06	0.07	0.89	0.30	0.30	0.04
	Zn	0.85	0.05	0.04	1.37	0.54	0.24	0.31
	Cu	0.73	0.04	0.03	1.27	0.76	0.22	0.23
	Ba	0.52	0.02	0.02	1.26	0.88	0.12	0.71
	Sr	1.14	0.02	0.02	0.85	0.97	0.09	0.43
	Pb	0.12	0.01	0.01	1.17	1	0.03	0.99
Roan	Mn	1.06	0.06	0.06	0.89	0.29	0.29	0.05
	Zn	0.84	0.05	0.03	1.46	0.53	0.24	0.39
	Cu	0.65	0.05	0.03	1.29	0.76	0.23	0.12
	Ba	0.46	0.02	0.02	1.12	0.87	0.11	0.83
	Sr	1.16	0.02	0.02	0.89	0.97	0.10	0.25
	Pb	0.11	0.01	0.01	0.94	1	0.03	1.00
Neuse	Mn	0.95	0.06	0.07	0.83	0.28	0.28	0.05
	Zn	0.74	0.05	0.04	1.39	0.54	0.26	0.14
	Cu	0.72	0.05	0.04	1.30	0.77	0.23	0.06
	Sr	1.16	0.02	0.02	0.86	0.86	0.09	0.30
	Ba	0.46	0.02	0.01	1.32	0.96	0.10	0.98
	Pb	0.11	0.01	0.01	1.20	1	0.04	0.80
Pam	Mn	1.15	0.06	0.06	1.04	0.31	0.31	0.01
	Zn	0.69	0.05	0.03	1.42	0.54	0.23	0.32
	Cu	0.70	0.04	0.03	1.31	0.76	0.22	0.14
	Sr	1.17	0.02	0.02	0.82	0.85	0.09	0.46
	Ba	0.41	0.02	0.01	1.18	0.93	0.08	0.98
	Pb	0.11	0.01	0.01	1.42	1	0.07	0.08
CF*	Mn	0.64	0.06	0.07	0.82	0.28	0.28	0.07
	Zn	0.88	0.05	0.04	1.40	0.53	0.25	0.20
	Cu	0.41	0.05	0.04	1.33	0.78	0.25	0.04
	Sr	1.20	0.02	0.02	0.94	0.88	0.10	0.10
	Ba	0.57	0.02	0.01	1.45	0.97	0.09	0.97
	Pb	0.08	0.01	0.01	0.85	1	0.03	0.98
Wacca	Cu	0.86	0.05	0.04	1.37	0.27	0.27	0.09
	Mn	0.91	0.05	0.07	0.71	0.52	0.25	0.29
	Zn	0.87	0.04	0.03	1.40	0.75	0.23	0.46
	Ba	0.46	0.03	0.02	1.72	0.89	0.14	0.54
	Sr	1.11	0.02	0.02	0.77	0.97	0.08	0.72
	Pb	0.10	0.01	0.01	0.78	1	0.03	0.98
SS	Zn	0.84	0.05	0.04	1.47	0.25	0.25	0.18
	Cu	0.89	0.05	0.04	1.37	0.49	0.24	0.07
	Mn	0.90	0.05	0.07	0.77	0.72	0.23	0.17
	Ba	0.66	0.03	0.02	1.65	0.86	0.14	0.32
	Sr	1.04	0.02	0.02	1.17	0.95	0.09	0.19
	Pb	0.03	0.01	0.01	1.41	1	0.05	0.38
Ogee	Mn	0.85	0.06	0.07	0.81	0.27	0.27	0.08
	Zn	0.73	0.05	0.04	1.25	0.52	0.25	0.21
	Cu	0.72	0.05	0.04	1.18	0.75	0.23	0.08
	Sr	0.31	0.02	0.02	1.02	0.85	0.10	0.23
	Ba	1.06	0.02	0.02	1.16	0.95	0.10	0.86
	Pb	0.19	0.01	0.01	0.80	1	0.05	0.36
Alt*	Zn	0.52	0.06	0.04	1.58	0.28	0.28	0.04
	Cu	0.77	0.05	0.04	1.34	0.52	0.24	0.03
	Mn	0.65	0.05	0.07	0.73	0.76	0.24	0.12
	Ba	0.47	0.02	0.02	1.23	0.86	0.10	0.76
	Sr	0.03	0.02	0.02	0.97	0.95	0.09	0.18
	Pb	1.10	0.01	0.01	1.63	1	0.05	0.26
StJo*	Zn	0.54	0.06	0.04	1.59	0.29	0.29	0.04
	Mn	0.74	0.06	0.08	0.84	0.57	0.28	0.04
	Cu	0.55	0.06	0.04	1.38	0.81	0.24	0.02
	Sr	1.09	0.02	0.02	0.99	0.90	0.09	0.24
	Ba	0.38	0.02	0.01	1.40	0.97	0.07	0.98
	Pb	0.09	0.01	0.01	0.87	1	0.03	0.95

Table 3-18. Results of SIMPER analysis showing pairwise comparisons with Choptank. The average element ratio (μ_{g1}) of each element for the reference capture location (Chop) is shown in the top left corner. The remaining blocks show the average ratio of each element in the capture location being compared (μ_{g2}), the average dissimilarity of each element between Choptank and the group being compared (μ_{diss}), the standard deviation of each element's contribution estimate (sd), the average to standard deviation ratio (ϕ), the cumulative (CS) and individual (Ind) contribution of each element to dissimilarity between groups, and the permutation p-value for each elements contribution (p). Comparisons from ANOSIM that had p-values < 0.05 are indicated with a star*.

Chop	Ba	Mn	Sr	Zn	Cu	Pb
	0.48	0.94	1.34	0.62	0.51	0.09

G2	**elm**	**μ_{g2}**	**μ_{diss}**	**sd**	**φ**	**CS**	**Ind**	**p**
Susq*	Cu	1.03	0.05	0.06	0.92	0.24	0.24	0.03
	Ba	0.57	0.05	0.03	1.58	0.46	0.22	<0.01
	Mn	0.67	0.04	0.03	1.42	0.65	0.19	0.52
	Zn	0.86	0.04	0.03	1.28	0.82	0.17	0.71
	Sr	1.15	0.03	0.02	1.42	0.95	0.13	0.01
	Pb	0.21	0.01	0.02	0.65	1	0.05	0.32
Pata	Zn	0.84	0.05	0.05	1.17	0.27	0.27	0.16
	Ba	0.43	0.05	0.04	1.27	0.52	0.25	<0.01
	Mn	1.18	0.05	0.03	1.32	0.74	0.22	0.32
	Cu	0.57	0.02	0.02	1.13	0.86	0.12	0.97
	Sr	1.19	0.02	0.02	1.53	0.98	0.12	0.06
	Pb	0.10	0.00	0.01	0.74	1	0.02	1.00
Patux	Ba	0.54	0.05	0.03	1.47	0.29	0.29	<0.01
	Zn	0.47	0.04	0.03	1.16	0.52	0.23	0.74
	Mn	0.84	0.03	0.02	1.36	0.71	0.19	0.91
	Sr	1.26	0.02	0.02	1.47	0.85	0.14	0.08
	Cu	0.69	0.02	0.02	0.97	0.95	0.10	1.00
	Pb	0.10	0.01	0.01	0.90	1	0.05	0.8
Poto*	Zn	1.08	0.06	0.04	1.56	0.23	0.23	0.15
	Mn	1.14	0.05	0.07	0.79	0.45	0.22	0.14
	Cu	0.95	0.05	0.04	1.33	0.66	0.21	0.07
	Ba	0.40	0.04	0.03	1.40	0.85	0.19	0.01
	Sr	1.07	0.03	0.03	1.20	0.98	0.13	<0.01
	Pb	0.10	0.00	0.01	0.70	1	0.02	1.00
Nant	Zn	1.16	0.06	0.07	0.79	0.28	0.28	0.09
	Ba	0.59	0.05	0.03	1.48	0.52	0.24	<0.01
	Cu	0.57	0.04	0.02	1.66	0.69	0.17	0.61
	Mn	1.05	0.03	0.02	1.30	0.83	0.14	0.95
	Sr	1.19	0.03	0.02	1.37	0.96	0.13	0.01
	Pb	0.14	0.01	0.01	0.91	1	0.04	0.63

G2	**elm**	**μ_{g2}**	**μ_{diss}**	**sd**	**φ**	**CS**	**Ind**	**p**
Rapp	Ba	0.41	0.05	0.03	1.40	0.29	0.29	<0.01
	Zn	0.80	0.04	0.04	1.09	0.53	0.24	0.70
	Mn	0.87	0.03	0.02	1.38	0.71	0.18	0.96
	Sr	1.19	0.03	0.02	1.51	0.87	0.16	0.02
	Cu	0.60	0.02	0.01	1.62	0.97	0.10	1.00
	Pb	0.11	0.00	0.01	0.71	1	0.03	0.99
James	Ba	0.50	0.05	0.03	1.43	0.25	0.25	<0.01
	Zn	0.88	0.04	0.04	1.04	0.47	0.22	0.61
	Cu	0.79	0.04	0.03	1.15	0.66	0.19	0.58
	Mn	0.97	0.03	0.02	1.38	0.84	0.18	0.92
	Sr	1.17	0.03	0.02	1.45	0.97	0.13	0.01
	Pb	0.11	0.01	0.01	0.80	1	0.03	1.00
Chow*	Ba	0.52	0.05	0.03	1.49	0.25	0.25	<0.01
	Zn	0.82	0.04	0.03	1.51	0.47	0.22	0.54
	Mn	0.99	0.04	0.03	1.22	0.69	0.22	0.46
	Cu	0.73	0.03	0.03	1.09	0.83	0.14	0.94
	Sr	1.14	0.03	0.02	1.49	0.97	0.14	<0.01
	Pb	0.12	0.01	0.01	1.11	1	0.03	0.98
Roan	Ba	0.46	0.05	0.04	1.37	0.26	0.26	<0.01
	Zn	0.84	0.04	0.03	1.37	0.47	0.21	0.79
	Mn	1.06	0.04	0.03	1.33	0.68	0.21	0.74
	Sr	1.16	0.03	0.02	1.51	0.83	0.15	<0.01
	Cu	0.65	0.03	0.02	1.36	0.97	0.14	0.98
	Pb	0.11	0.01	0.01	0.87	1	0.03	1.00
Neuse*	Ba	0.38	0.05	0.04	1.32	0.25	0.25	<0.01
	Mn	0.95	0.04	0.03	1.36	0.45	0.20	0.82
	Zn	0.74	0.04	0.03	1.41	0.64	0.19	0.90
	Cu	0.72	0.03	0.03	1.17	0.81	0.17	0.88
	Sr	1.16	0.03	0.02	1.47	0.95	0.14	<0.01
	Pb	0.11	0.01	0.01	1.15	1	0.05	0.73
Pam	Mn	1.15	0.05	0.03	1.40	0.25	0.25	0.23
	Ba	0.41	0.05	0.03	1.33	0.50	0.25	<0.01
	Zn	0.69	0.03	0.02	1.46	0.65	0.15	0.99
	Cu	0.70	0.03	0.02	1.12	0.79	0.14	0.97
	Sr	1.17	0.03	0.02	1.49	0.93	0.14	0.01
	Pb	0.11	0.01	0.01	1.22	1	0.07	0.10

G2	**elm**	**μ_{g2}**	**μ_{diss}**	**sd**	**φ**	**CS**	**Ind**	**p**
CF*	Ba	0.57	0.05	0.03	1.38	0.30	0.30	<0.01
	Mn	0.64	0.04	0.03	1.41	0.54	0.24	0.75
	Sr	1.20	0.03	0.02	1.46	0.70	0.16	0.01
	Zn	0.88	0.02	0.02	1.43	0.86	0.16	1.00
	Cu	0.41	0.02	0.02	0.95	0.97	0.11	1.00
	Pb	0.08	0.00	0.01	0.77	1	0.03	1.00
Wacca*	Ba	0.46	0.05	0.03	1.46	0.25	0.25	<0.01
	Cu	0.86	0.05	0.04	1.13	0.49	0.24	0.15
	Zn	0.87	0.04	0.02	1.56	0.68	0.19	0.70
	Sr	1.11	0.03	0.02	1.48	0.83	0.15	<0.01
	Mn	0.91	0.03	0.02	1.48	0.98	0.15	0.96
	Pb	0.10	0.00	0.01	0.73	1	0.02	1.00
SS*	Ba	0.66	0.05	0.03	1.74	0.24	0.24	<0.01
	Zn	0.84	0.05	0.03	1.38	0.45	0.21	0.38
	Cu	0.89	0.04	0.04	0.92	0.64	0.19	0.36
	Sr	1.03	0.04	0.02	1.68	0.81	0.17	<0.01
	Mn	0.90	0.03	0.02	1.37	0.96	0.15	0.80
	Pb	0.03	0.01	0.01	1.31	1	0.04	0.63
Ogee*	Ba	1.03	0.05	0.04	1.20	0.23	0.23	<0.01
	Cu	0.72	0.04	0.03	1.56	0.41	0.18	0.39
	Sr	0.31	0.04	0.02	1.59	0.59	0.18	<0.01
	Mn	0.85	0.04	0.03	1.23	0.77	0.18	0.74
	Zn	0.73	0.04	0.03	1.29	0.94	0.17	0.82
	Pb	0.19	0.01	0.02	0.79	1	0.06	0.15
Alt*	Ba	0.47	0.05	0.04	1.39	0.28	0.28	<0.01
	Zn	0.95	0.04	0.03	1.18	0.48	0.20	0.75
	Mn	0.65	0.04	0.02	1.54	0.67	0.19	0.80
	Sr	0.54	0.04	0.02	1.57	0.86	0.19	<0.01
	Cu	0.77	0.02	0.01	1.27	0.95	0.09	1.00
	Pb	1.10	0.01	0.01	1.54	1	0.05	0.49
StJo*	Ba	0.38	0.05	0.04	1.29	0.26	0.26	<0.01
	Mn	0.74	0.05	0.03	1.59	0.52	0.26	0.27
	Sr	1.09	0.04	0.02	1.64	0.71	0.19	<0.01
	Zn	0.54	0.03	0.02	1.23	0.85	0.14	0.99
	Cu	0.55	0.02	0.02	0.95	0.97	0.12	0.99
	Pb	0.09	0.01	0.01	0.80	1	0.03	0.99

Table 3-19. Results of SIMPER analysis showing pairwise comparisons with Patuxent. The average element ratio (μ_{g1}) of each element for the reference capture location (Patux) is shown in the top left corner. The remaining blocks show the average ratio of each element in the capture location being compared (μ_{g2}), the average dissimilarity of each element between Patuxent and the group being compared (μ_{diss}), the standard deviation of each element's contribution estimate (sd), the average to standard deviation ratio (ϕ), the cumulative (CS) and individual (Ind) contribution of each element to dissimilarity between groups, and the permutation p-value for each elements contribution (p). Comparisons from ANOSIM that had p-values < 0.05 are indicated with a star*.

Patux	Ba	Zn	Mn	Sr	Cu	Pb
	0.47	0.69	0.84	1.26	0.54	0.10

G2	elm	μ_{g2}	μ_{diss}	sd	φ	CS	Ind	p
Susq*	Cu	1.03	0.06	0.06	0.99	0.30	0.30	0.01
	Zn	0.86	0.05	0.04	1.33	0.55	0.25	0.29
	Mn	0.67	0.03	0.02	1.29	0.71	0.16	0.94
	Ba	0.57	0.02	0.02	1.26	0.82	0.11	0.82
	Sr	1.15	0.02	0.02	1.32	0.92	0.10	0.20
	Pb	0.21	0.02	0.02	0.89	1	0.08	0.07
Pata	Zn	1.18	0.06	0.05	1.22	0.32	0.32	0.05
	Mn	0.84	0.05	0.04	1.24	0.57	0.25	0.21
	Ba	0.57	0.03	0.03	1.14	0.73	0.16	0.22
	Cu	0.43	0.03	0.02	1.24	0.88	0.15	0.82
	Sr	1.19	0.01	0.01	1.49	0.96	0.08	0.82
	Pb	0.10	0.01	0.01	0.99	1	0.04	0.72
Chop	Ba	0.48	0.05	0.03	1.47	0.29	0.29	<0.01
	Zn	0.62	0.04	0.03	1.16	0.52	0.23	0.74
	Mn	0.94	0.03	0.02	1.36	0.71	0.19	0.91
	Sr	1.34	0.02	0.02	1.47	0.85	0.14	0.08
	Cu	0.51	0.02	0.02	0.97	0.95	0.10	1.00
	Pb	0.09	0.01	0.01	0.90	1	0.05	0.80
Poto*	Zn	0.95	0.06	0.04	1.54	0.29	0.29	0.05
	Cu	1.14	0.05	0.04	1.36	0.53	0.24	0.03
	Mn	1.09	0.05	0.07	0.73	0.77	0.24	0.16
	Sr	0.40	0.02	0.02	1.00	0.88	0.11	0.05
	Ba	1.07	0.02	0.01	1.29	0.96	0.08	0.95
	Pb	0.13	0.01	0.01	1.02	1	0.04	0.70
Nant	Zn	1.16	0.07	0.07	0.93	0.34	0.34	0.02
	Cu	0.57	0.04	0.02	1.57	0.53	0.19	0.43
	Mn	1.05	0.03	0.02	1.42	0.70	0.17	0.89
	Ba	0.59	0.03	0.02	1.30	0.84	0.14	0.34
	Sr	1.19	0.02	0.01	1.45	0.94	0.10	0.27
	Pb	0.14	0.01	0.01	1.07	1	0.06	0.24

G2	elm	μ_{g2}	μ_{diss}	sd	φ	CS	Ind	p
Rapp	Zn	0.80	0.05	0.04	1.17	0.34	0.34	0.25
	Mn	0.87	0.03	0.02	1.37	0.51	0.17	1.00
	Cu	0.60	0.02	0.02	1.58	0.67	0.16	0.97
	Ba	0.59	0.02	0.02	1.33	0.81	0.14	0.83
	Sr	1.19	0.02	0.01	1.51	0.94	0.13	0.36
	Pb	0.11	0.01	0.01	0.99	1	0.06	0.56
James	Zn	0.88	0.05	0.05	1.13	0.30	0.30	0.18
	Cu	0.79	0.04	0.03	1.25	0.53	0.23	0.30
	Mn	0.97	0.03	0.02	1.38	0.72	0.19	0.95
	Ba	0.50	0.02	0.02	1.06	0.84	0.12	0.91
	Sr	1.17	0.02	0.01	1.38	0.95	0.11	0.37
	Pb	0.11	0.01	0.01	1.02	1	0.05	0.64
Chow	Zn	0.85	0.05	0.03	1.55	0.29	0.29	0.14
	Mn	0.99	0.04	0.04	1.11	0.52	0.23	0.55
	Cu	0.73	0.03	0.03	1.27	0.71	0.19	0.73
	Ba	0.52	0.02	0.02	1.25	0.84	0.13	0.65
	Sr	1.14	0.02	0.01	1.38	0.94	0.10	0.30
	Pb	0.12	0.01	0.01	1.22	1	0.06	0.51
Roan	Zn	0.84	0.05	0.03	1.42	0.28	0.28	0.28
	Mn	1.03	0.04	0.03	1.29	0.52	0.24	0.62
	Cu	0.65	0.03	0.02	1.40	0.69	0.17	0.87
	Ba	0.46	0.02	0.02	1.11	0.83	0.14	0.66
	Sr	1.16	0.02	0.01	1.46	0.95	0.12	0.21
	Pb	0.11	0.01	0.01	1.07	1	0.05	0.65
Neuse	Zn	0.74	0.05	0.04	1.35	0.27	0.27	0.33
	Cu	0.65	0.04	0.03	1.27	0.48	0.21	0.56
	Mn	0.95	0.04	0.03	1.34	0.69	0.21	0.91
	Ba	0.38	0.02	0.02	1.22	0.82	0.13	0.84
	Sr	1.16	0.02	0.01	1.40	0.93	0.11	0.27
	Pb	0.11	0.01	0.01	1.18	1	0.07	0.19
Pam	Mn	1.15	0.05	0.03	1.57	0.30	0.30	0.08
	Zn	0.69	0.04	0.03	1.29	0.53	0.23	0.72
	Cu	0.70	0.03	0.03	1.21	0.71	0.18	0.82
	Ba	0.41	0.02	0.02	1.15	0.82	0.11	0.90
	Sr	1.16	0.02	0.01	1.38	0.92	0.10	0.56
	Pb	0.11	0.01	0.01	1.11	1	0.08	0.04

G2	elm	μ_{g2}	μ_{diss}	sd	φ	CS	Ind	p
CF	Zn	0.88	0.04	0.03	1.15	0.26	0.26	0.82
	Mn	0.64	0.03	0.02	1.38	0.50	0.24	0.91
	Cu	0.41	0.02	0.02	1.03	0.67	0.17	0.99
	Ba	0.57	0.02	0.02	1.28	0.81	0.14	0.91
	Sr	1.20	0.02	0.01	1.40	0.94	0.13	0.32
	Pb	0.08	0.01	0.01	0.93	1	0.06	0.71
Wacca*	Cu	0.86	0.05	0.04	1.20	0.29	0.29	0.08
	Zn	0.87	0.05	0.03	1.54	0.56	0.27	0.27
	Ba	0.46	0.03	0.02	1.57	0.72	0.16	0.38
	Mn	0.91	0.02	0.02	1.33	0.84	0.12	1.00
	Sr	1.11	0.02	0.01	1.54	0.95	0.11	0.24
	Pb	0.10	0.01	0.01	0.95	1	0.05	0.70
SS*	Zn	0.84	0.06	0.04	1.35	0.28	0.28	0.16
	Cu	0.89	0.04	0.05	0.99	0.51	0.23	0.23
	Mn	0.90	0.03	0.02	1.34	0.66	0.15	0.94
	Sr	1.04	0.03	0.02	1.71	0.81	0.15	0.02
	Ba	0.66	0.03	0.02	1.54	0.95	0.14	0.40
	Pb	0.03	0.01	0.01	1.01	1	0.05	0.48
Ogee*	Zn	0.73	0.05	0.04	1.35	0.25	0.25	0.29
	Cu	0.72	0.04	0.03	1.63	0.47	0.22	0.20
	Mn	0.85	0.03	0.03	1.34	0.64	0.17	0.89
	Sr	0.31	0.03	0.02	1.58	0.78	0.14	0.01
	Ba	1.06	0.03	0.02	1.12	0.91	0.13	0.54
	Pb	0.19	0.02	0.02	0.97	1	0.09	0.01
Alt*	Zn	0.52	0.05	0.04	1.15	0.31	0.31	0.32
	Sr	0.03	0.03	0.02	1.74	0.47	0.16	0.03
	Mn	0.65	0.03	0.02	1.38	0.63	0.16	1.00
	Ba	0.47	0.02	0.02	1.21	0.79	0.16	0.63
	Cu	0.77	0.02	0.02	1.17	0.93	0.14	0.98
	Pb	1.10	0.01	0.01	1.09	1	0.07	0.33
StJo*	Zn	0.54	0.04	0.04	1.05	0.25	0.25	0.72
	Mn	0.74	0.04	0.03	1.48	0.49	0.24	0.70
	Cu	0.55	0.03	0.03	0.98	0.66	0.17	0.92
	Sr	1.09	0.03	0.02	1.64	0.82	0.16	0.03
	Ba	0.38	0.02	0.02	1.15	0.94	0.12	0.92
	Pb	0.09	0.01	0.01	0.98	1	0.06	0.55

Table 3-20. Results of SIMPER analysis showing pairwise comparisons with Ogeechee. The average element ratio (μ_{g1}) of each element for the reference capture location (Ogee) is shown in the top left corner. The remaining blocks show the average element ratio in the capture location being compared (μ_{g2}), the average dissimilarity of each element between Ogeechee and the group being compared (μ_{diss}), the standard deviation of each element's contribution estimate (sd), the average to standard deviation ratio (ϕ), the cumulative (CS) and individual (Ind) contribution of each element to dissimilarity between groups, and the permutation p-value for each elements contribution (p). Comparisons from ANOSIM that had p-values < 0.05 are indicated with a star*.

Ogee	Mn	Zn	Cu	Sr	Ba	Pb
	0.85	0.73	0.72	1.06	0.31	0.19

G2	elm	μ_{g2}	μ_{diss}	sd	φ	CS	Ind	p
Susq*	Cu	0.72	0.06	0.06	1.03	0.28	0.28	0.01
	Zn	0.73	0.04	0.04	1.20	0.49	0.21	0.55
	Mn	0.85	0.04	0.03	1.48	0.68	0.19	0.64
	Ba	0.31	0.03	0.02	1.29	0.83	0.15	0.22
	Sr	1.06	0.02	0.01	1.47	0.92	0.09	0.36
	Pb	0.19	0.02	0.02	0.86	1	0.08	0.04
Pata*	Zn	0.84	0.06	0.05	1.08	0.27	0.27	0.12
	Mn	1.18	0.05	0.04	1.21	0.51	0.24	0.13
	Cu	0.57	0.04	0.03	1.20	0.71	0.20	0.31
	Ba	0.43	0.03	0.03	1.11	0.86	0.15	0.18
	Sr	1.19	0.02	0.01	1.37	0.94	0.08	0.44
	Pb	0.10	0.01	0.02	0.79	1	0.06	0.19
Chop*	Ba	0.48	0.05	0.04	1.20	0.23	0.23	<0.01
	Cu	0.51	0.04	0.03	1.56	0.41	0.18	0.39
	Sr	1.34	0.04	0.02	1.59	0.59	0.18	<0.01
	Mn	0.94	0.04	0.03	1.23	0.77	0.18	0.74
	Zn	0.62	0.04	0.03	1.29	0.94	0.17	0.82
	Pb	0.09	0.01	0.02	0.79	1	0.06	0.15
Patux*	Zn	0.69	0.05	0.04	1.35	0.25	0.25	0.29
	Cu	0.54	0.04	0.03	1.63	0.47	0.22	0.20
	Mn	0.84	0.03	0.03	1.34	0.64	0.17	0.89
	Sr	1.26	0.03	0.02	1.58	0.78	0.14	0.01
	Ba	0.47	0.03	0.02	1.12	0.91	0.13	0.54
	Pb	0.10	0.02	0.02	0.97	1	0.09	0.01
Poto	Mn	1.14	0.06	0.07	0.81	0.27	0.27	0.08
	Zn	1.08	0.05	0.04	1.25	0.52	0.25	0.21
	Cu	0.95	0.05	0.04	1.18	0.75	0.23	0.08
	Sr	1.07	0.02	0.02	1.02	0.85	0.10	0.23
	Ba	0.40	0.02	0.02	1.16	0.95	0.10	0.86
	Pb	0.13	0.01	0.01	0.80	1	0.05	0.36

G2	elm	μ_{g2}	μ_{diss}	sd	φ	CS	Ind	p
Nant*	Zn	0.80	0.06	0.08	0.82	0.28	0.28	0.06
	Cu	0.57	0.05	0.03	1.48	0.50	0.22	0.08
	Mn	1.05	0.04	0.03	1.20	0.67	0.17	0.79
	Ba	0.59	0.04	0.03	1.23	0.84	0.17	0.04
	Sr	1.19	0.02	0.02	1.15	0.93	0.09	0.18
	Pb	0.14	0.02	0.02	1	1	0.07	0.04
Rapp*	Zn	0.80	0.04	0.04	1.07	0.26	0.26	0.48
	Cu	0.60	0.03	0.03	1.21	0.47	0.21	0.68
	Mn	0.87	0.03	0.03	1.31	0.66	0.19	0.90
	Ba	0.41	0.02	0.02	1.11	0.80	0.14	0.74
	Sr	1.19	0.02	0.02	1.25	0.92	0.12	0.15
	Pb	0.11	0.01	0.02	0.83	1	0.08	0.12
James	Zn	0.88	0.05	0.04	0.73	0.24	0.24	0.40
	Cu	0.79	0.04	0.03	0.72	0.48	0.24	0.16
	Mn	0.97	0.04	0.03	0.85	0.68	0.20	0.74
	Ba	0.50	0.03	0.03	0.31	0.83	0.15	0.45
	Sr	1.17	0.02	0.02	1.06	0.93	0.10	0.22
	Pb	0.11	0.01	0.02	0.19	1	0.07	0.08
Chow	Mn	0.99	0.05	0.04	1.17	0.25	0.25	0.29
	Zn	0.85	0.04	0.04	1.05	0.48	0.23	0.66
	Cu	0.73	0.04	0.03	1.12	0.67	0.19	0.60
	Ba	0.52	0.03	0.03	1.14	0.84	0.17	0.13
	Sr	1.14	0.02	0.01	1.24	0.93	0.09	0.54
	Pb	0.12	0.01	0.01	0.83	1	0.07	0.18
Roan	Mn	1.06	0.04	0.04	1.25	0.25	0.25	0.37
	Zn	0.84	0.04	0.04	1.07	0.46	0.21	0.79
	Cu	0.65	0.04	0.03	1.24	0.67	0.21	0.50
	Ba	0.46	0.03	0.03	1.05	0.82	0.15	0.37
	Sr	1.16	0.02	0.02	1.19	0.93	0.11	0.33
	Pb	0.11	0.01	0.02	0.82	1	0.07	0.15
Neuse	Mn	0.95	0.04	0.03	1.31	0.23	0.23	0.56
	Cu	0.72	0.04	0.03	1.24	0.46	0.23	0.24
	Zn	0.74	0.04	0.04	1.15	0.69	0.23	0.78
	Ba	0.38	0.02	0.02	1.08	0.81	0.12	0.92
	Sr	1.16	0.02	0.01	1.26	0.91	0.10	0.39
	Pb	0.11	0.02	0.02	0.98	1	0.09	0.01

G2	elm	μ_{g2}	μ_{diss}	sd	φ	CS	Ind	p
Pam	Mn	1.15	0.06	0.04	1.41	0.30	0.30	0.06
	Cu	0.70	0.04	0.03	1.25	0.50	0.20	0.47
	Zn	0.69	0.03	0.03	1.07	0.68	0.18	0.97
	Ba	0.41	0.02	0.02	1.00	0.79	0.11	0.83
	Pb	0.11	0.02	0.02	1.25	0.90	0.11	<0.01
	Sr	1.17	0.02	0.01	1.31	1	0.10	0.39
CF*	Mn	0.64	0.04	0.03	1.37	0.23	0.23	0.61
	Cu	0.41	0.04	0.03	1.42	0.46	0.23	0.30
	Zn	0.88	0.03	0.03	1.26	0.66	0.20	0.91
	Sr	1.20	0.02	0.02	1.37	0.79	0.13	0.05
	Ba	0.57	0.02	0.02	1.11	0.91	0.12	0.85
	Pb	0.08	0.02	0.02	0.88	1	0.09	0.01
Wacca	Cu	0.86	0.05	0.04	1.34	0.30	0.30	0.05
	Zn	0.87	0.04	0.03	1.17	0.51	0.21	0.67
	Ba	0.46	0.03	0.02	1.46	0.68	0.17	0.25
	Mn	0.91	0.03	0.02	1.30	0.85	0.17	0.96
	Pb	0.10	0.01	0.02	0.81	0.93	0.08	0.15
	Sr	1.11	0.01	0.01	1.29	1	0.07	0.91
SS*	Cu	0.89	0.05	0.04	1.28	0.24	0.24	0.08
	Zn	0.84	0.05	0.04	1.32	0.47	0.23	0.26
	Ba	0.66	0.04	0.03	1.65	0.67	0.20	0.02
	Mn	0.90	0.04	0.03	1.34	0.84	0.17	0.74
	Pb	0.03	0.02	0.02	1.14	0.93	0.09	0.01
	Sr	1.04	0.02	0.01	1.49	1	0.07	0.76
Alt*	Zn	0.52	0.05	0.04	1.42	0.25	0.25	0.26
	Cu	0.77	0.04	0.03	1.48	0.47	0.22	0.23
	Mn	0.65	0.04	0.02	1.58	0.65	0.18	0.82
	Ba	0.47	0.03	0.03	1.03	0.80	0.15	0.30
	Pb	1.10	0.02	0.02	1.17	0.91	0.11	<0.01
	Sr	0.03	0.02	0.01	1.15	1	0.09	0.55
StJo	Cu	0.55	0.05	0.03	1.55	0.25	0.25	0.11
	Mn	0.74	0.05	0.03	1.66	0.50	0.25	0.31
	Zn	0.54	0.04	0.03	1.60	0.73	0.23	0.55
	Ba	0.38	0.02	0.02	1.08	0.83	0.10	0.90
	Sr	1.09	0.02	0.01	1.32	0.92	0.09	0.71
	Pb	0.09	0.02	0.02	0.86	1	0.08	0.03

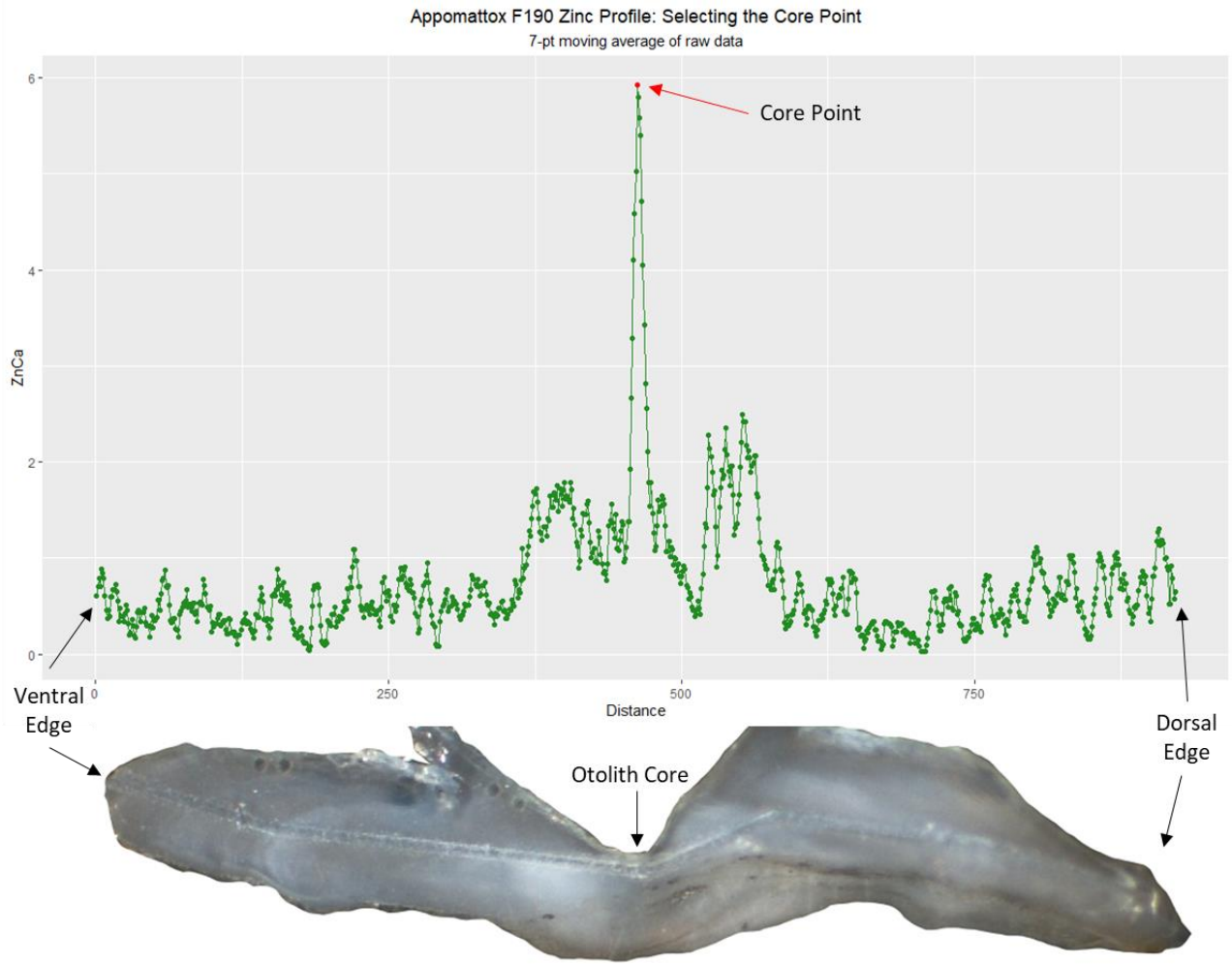

Figure 3-1. Sectioned otolith and zinc profile from a Hickory Shad captured in the Appomattox River showing the highest value of zinc near the central node of the otolith core (red dot) that was selected as the core point to represent birth. Distance (x-axis) represents data points, where each consecutive data point is approximately 2.5 micrometers away from the previous data point.

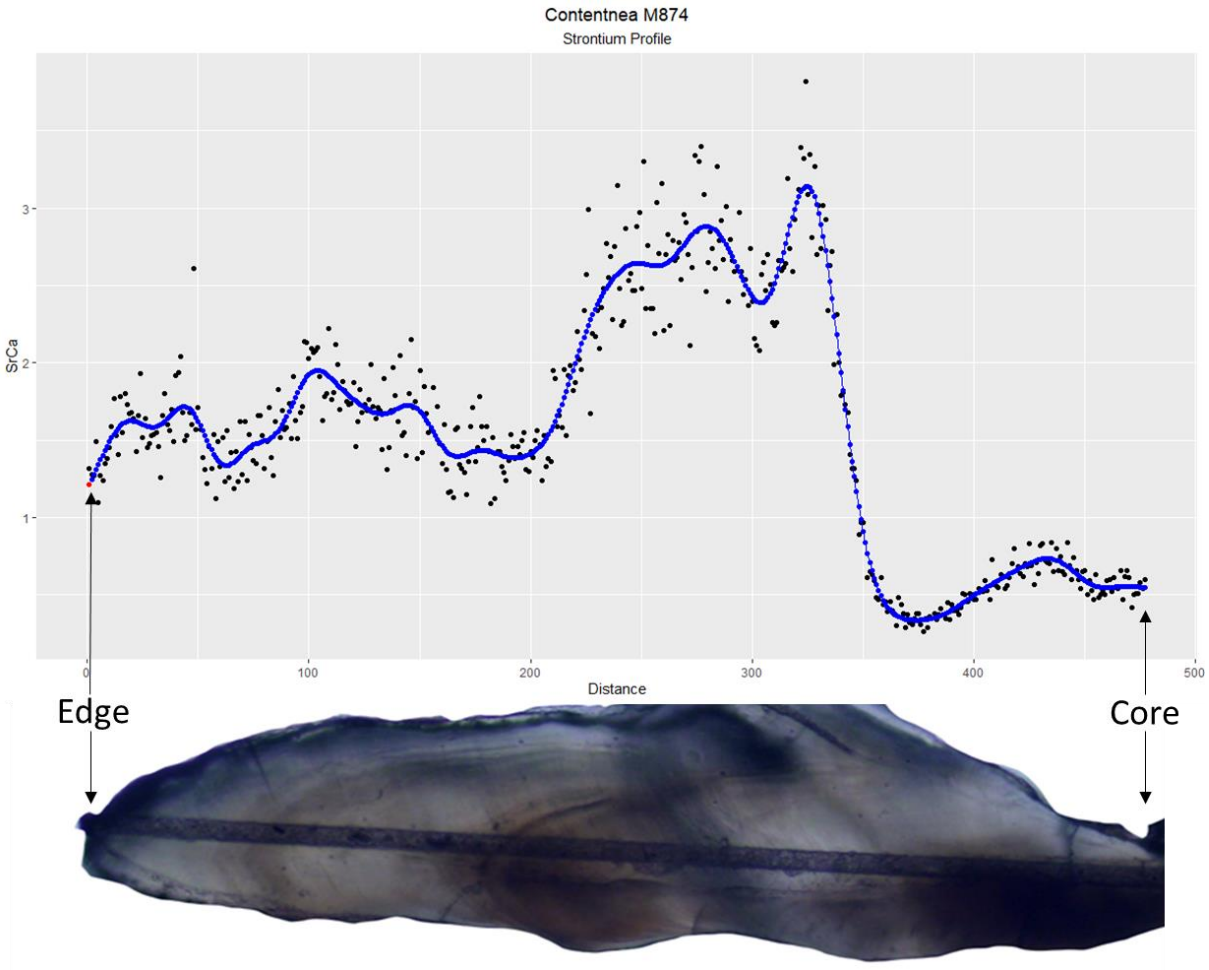

Figure 3-2. Example of GAM profile (blue dots connected by blue lines) that was fit to the raw strontium profile (black dots) of a Hickory Shad that was captured in the Contentnea Creek, NC, between the otolith core (data point 477) and otolith edge (point 0), where the red dot shows the last data point of the GAM profile that was used to represent the capture location. Distance (x-axis) represents data points, where each consecutive data point is approximately 2.5 micrometers away from the previous data point.

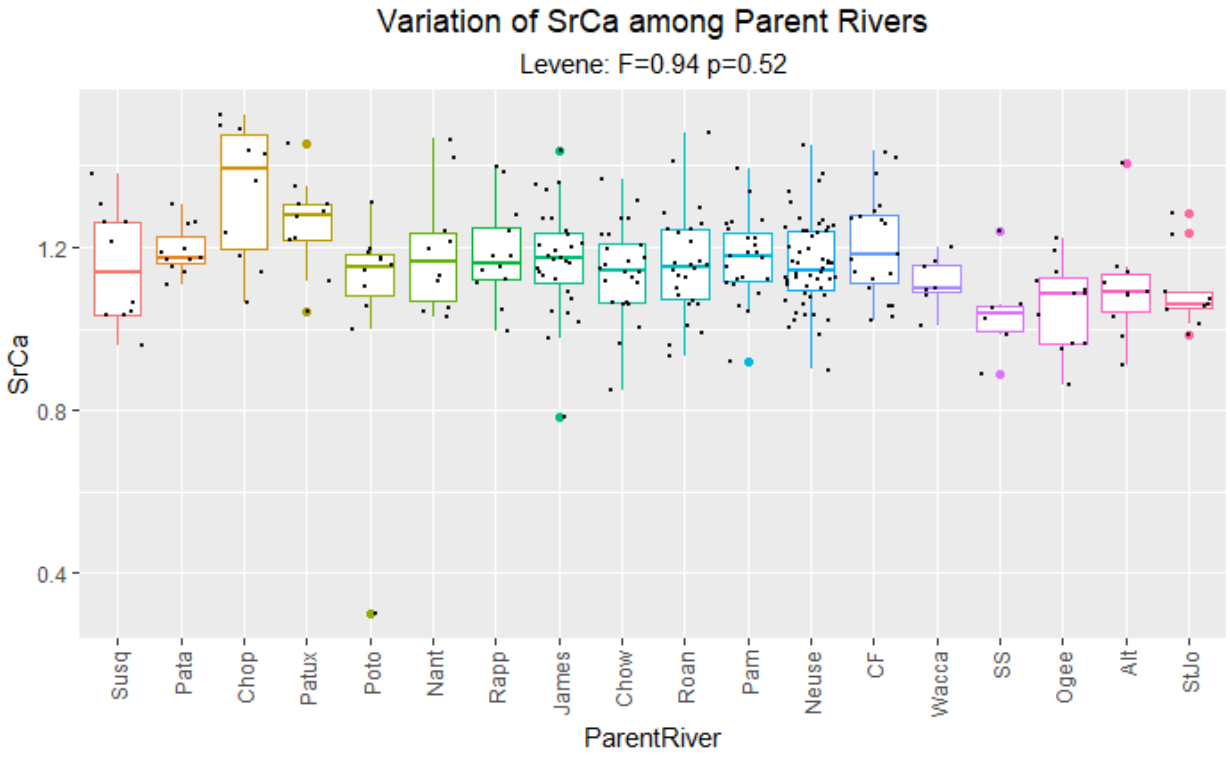

Figure 3-3. Boxplots illustrating the variation in strontium ratios among capture locations when using the parent river grouping variable on the otolith edge data. Values for Levene's test are included in the subtitle. Black dots represent real values. The center line of the boxplots indicate the median for the respective group. The lower and upper hinges of each box represent the 25th and 75th percentiles. Whiskers extend from the hinges to the smallest and largest value within the bounds of 1.5 times the interquartile range. Values beyond these boundaries are indicated as individual colored dots

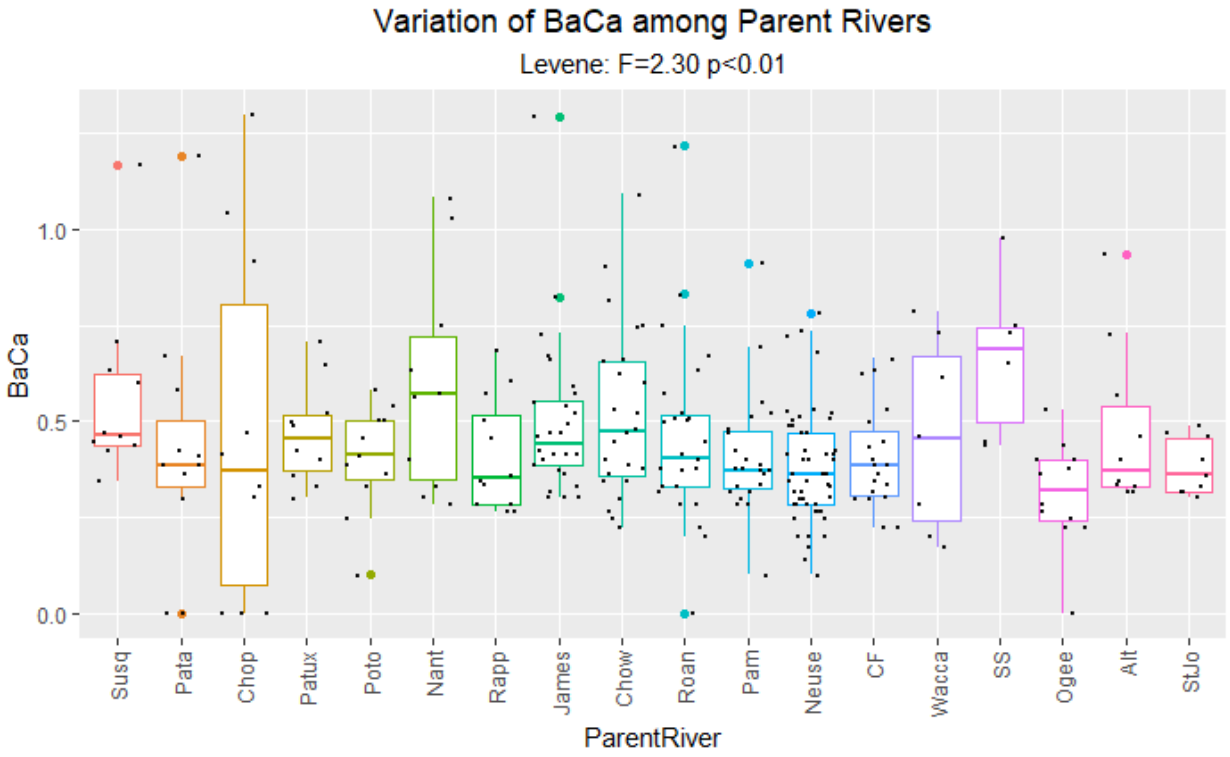

Figure 3-4. Boxplots illustrating the variation in barium ratios among capture locations when using the parent river grouping variable on the otolith edge data. Values for Levene's test are included in the subtitle. Black dots represent real values. The center line of the boxplots indicate the median for the respective group. The lower and upper hinges of each box represent the 25th and 75th percentiles. Whiskers extend from the hinges to the smallest and largest value within the bounds of 1.5 times the interquartile range. Values beyond these boundaries are indicated as individual colored dots.

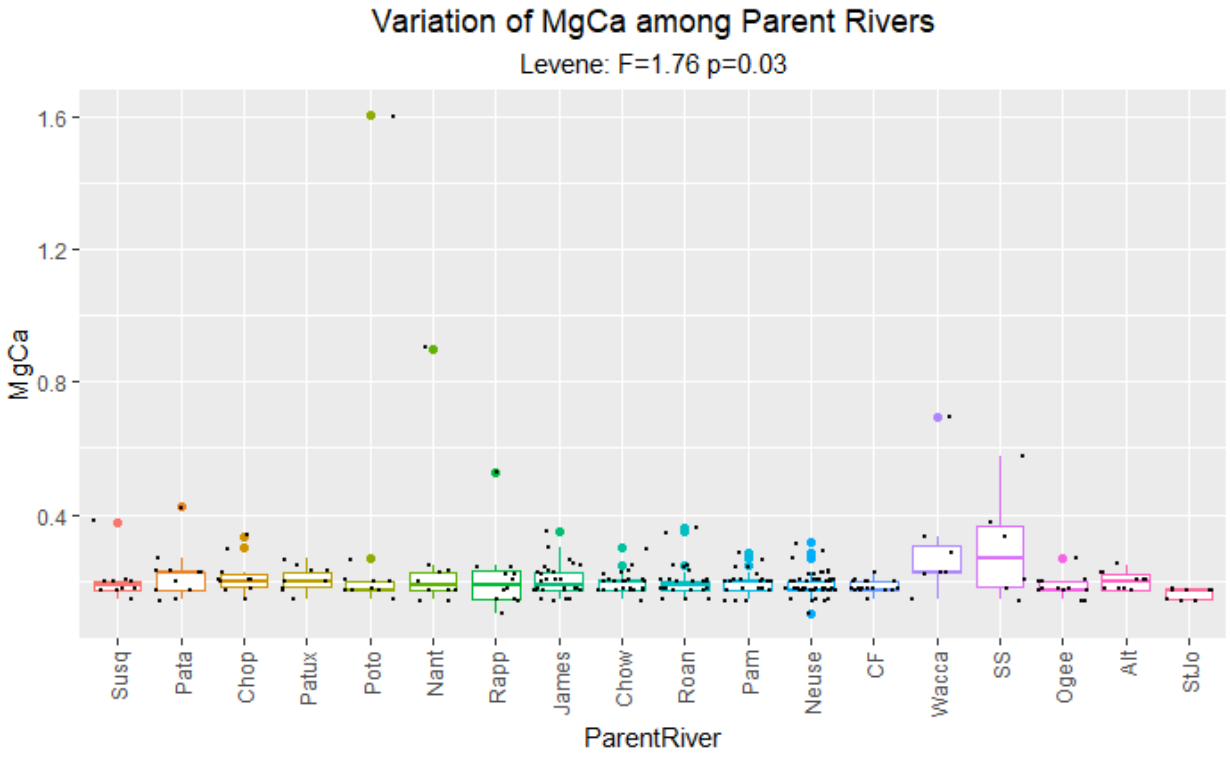

Figure 3-5. Boxplots illustrating the variation in magnesium ratios among capture locations when using the parent river grouping variable on the otolith edge data. Values for Levene's test are included in the subtitle. Black dots represent real values. The center line of the boxplots indicate the median for the respective group. The lower and upper hinges of each box represent the 25th and 75th percentiles. Whiskers extend from the hinges to the smallest and largest value within the bounds of 1.5 times the interquartile range. Values beyond these boundaries are indicated as individual colored dots.

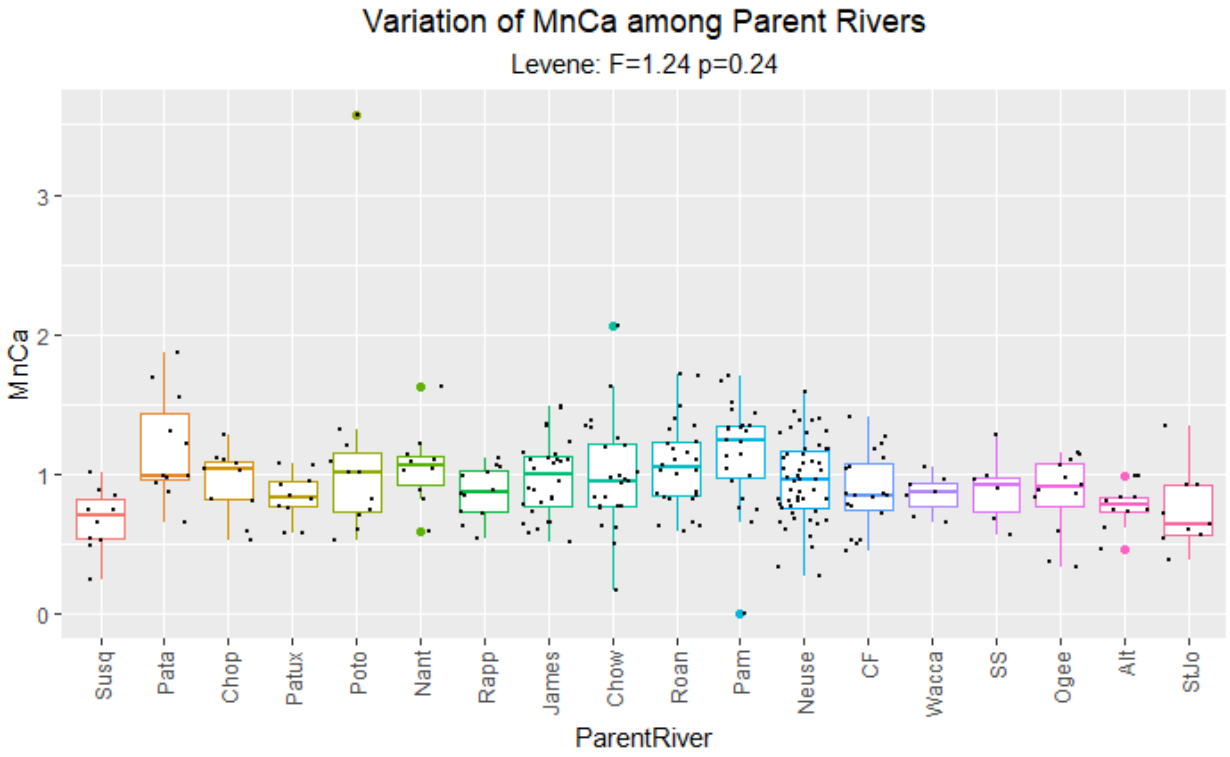

Figure 3-6. Boxplots illustrating the variation in manganese ratios among capture locations when using the parent river grouping variable on the otolith edge data. Values for Levene's test are included in the subtitle. Black dots represent real values. The center line of the boxplots indicate the median for the respective group. The lower and upper hinges of each box represent the 25th and 75th percentiles. Whiskers extend from the hinges to the smallest and largest value within the bounds of 1.5 times the interquartile range. Values beyond these boundaries are indicated as individual colored dots.

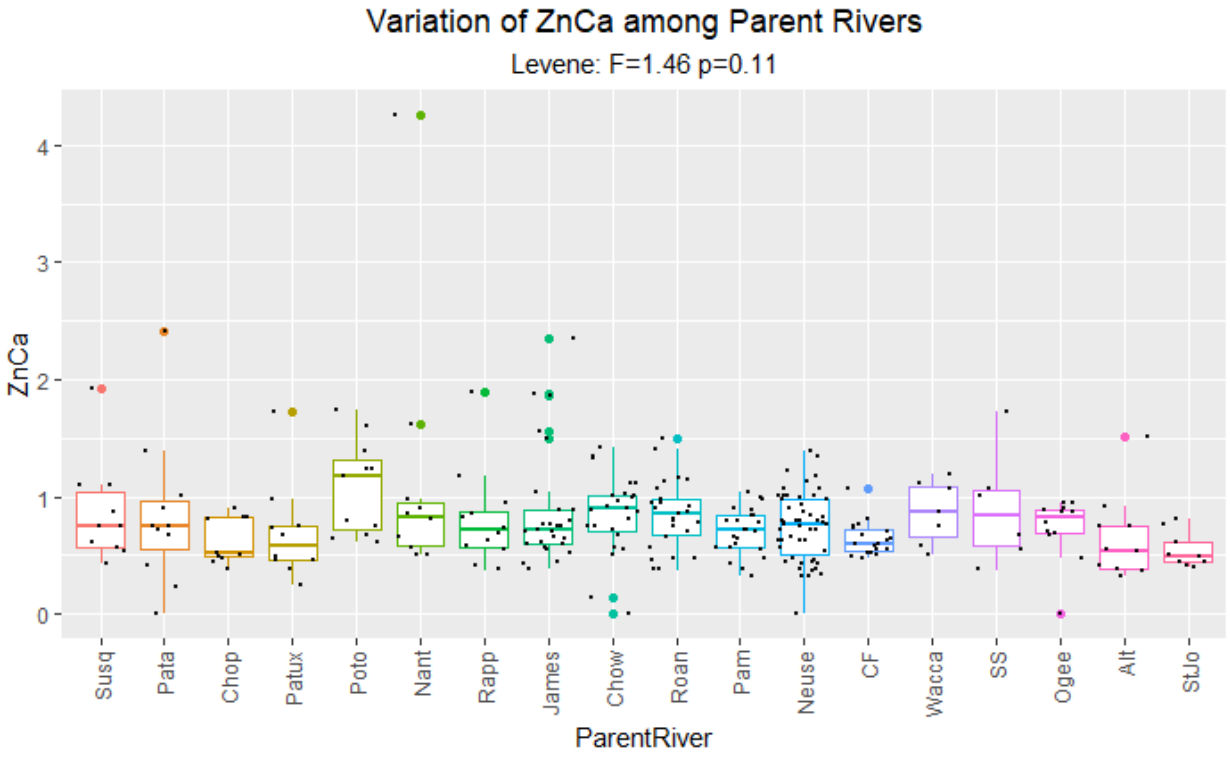

Figure 3-7. Boxplots illustrating the variation in zinc ratios among capture locations when using the parent river grouping variable on the otolith edge data. Values for Levene's test are included in the subtitle. Black dots represent real values. The center line of the boxplots indicate the median for the respective group. The lower and upper hinges of each box represent the 25th and 75th percentiles. Whiskers extend from the hinges to the smallest and largest value within the bounds of 1.5 times the interquartile range. Values beyond these boundaries are indicated as individual colored dots.

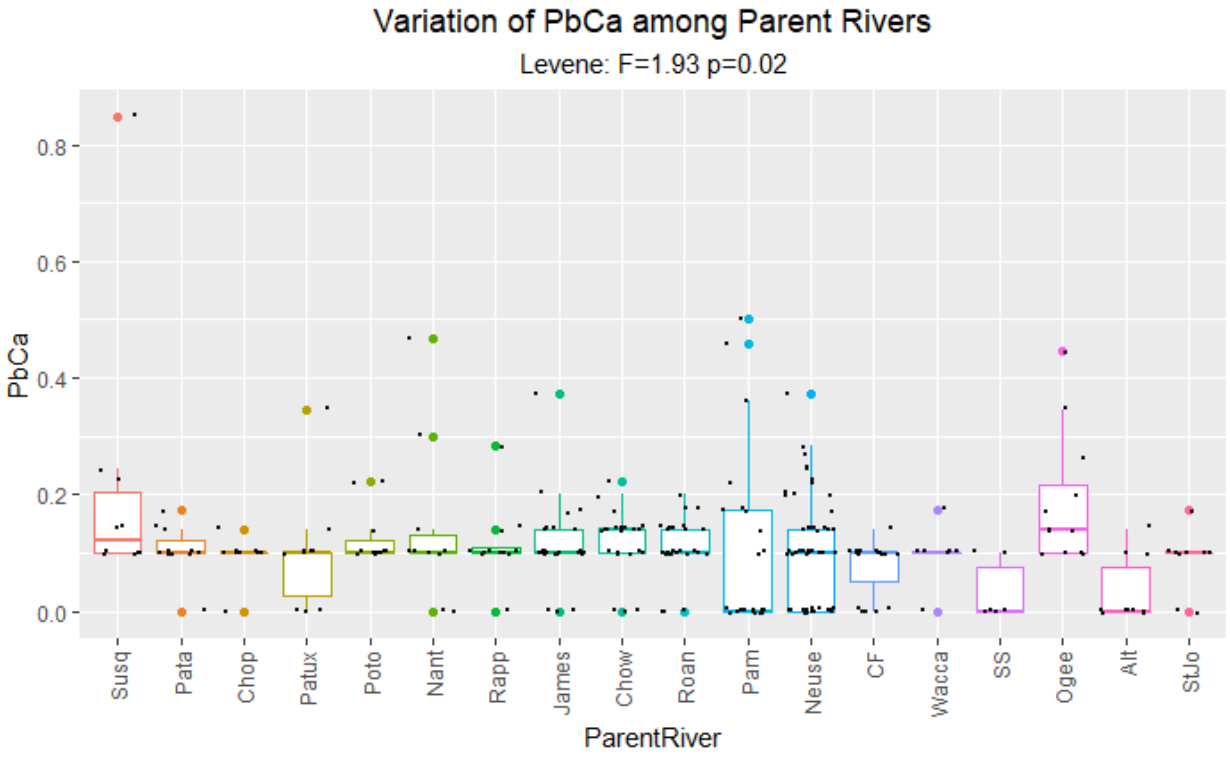

Figure 3-8. Boxplots illustrating the variation in lead ratios among capture locations when using the parent river grouping variable on the otolith edge data. Values for Levene's test are included in the subtitle. Black dots represent real values. The center line of the boxplots indicate the median for the respective group. The lower and upper hinges of each box represent the 25th and 75th percentiles. Whiskers extend from the hinges to the smallest and largest value within the bounds of 1.5 times the interquartile range. Values beyond these boundaries are indicated as individual colored dots.

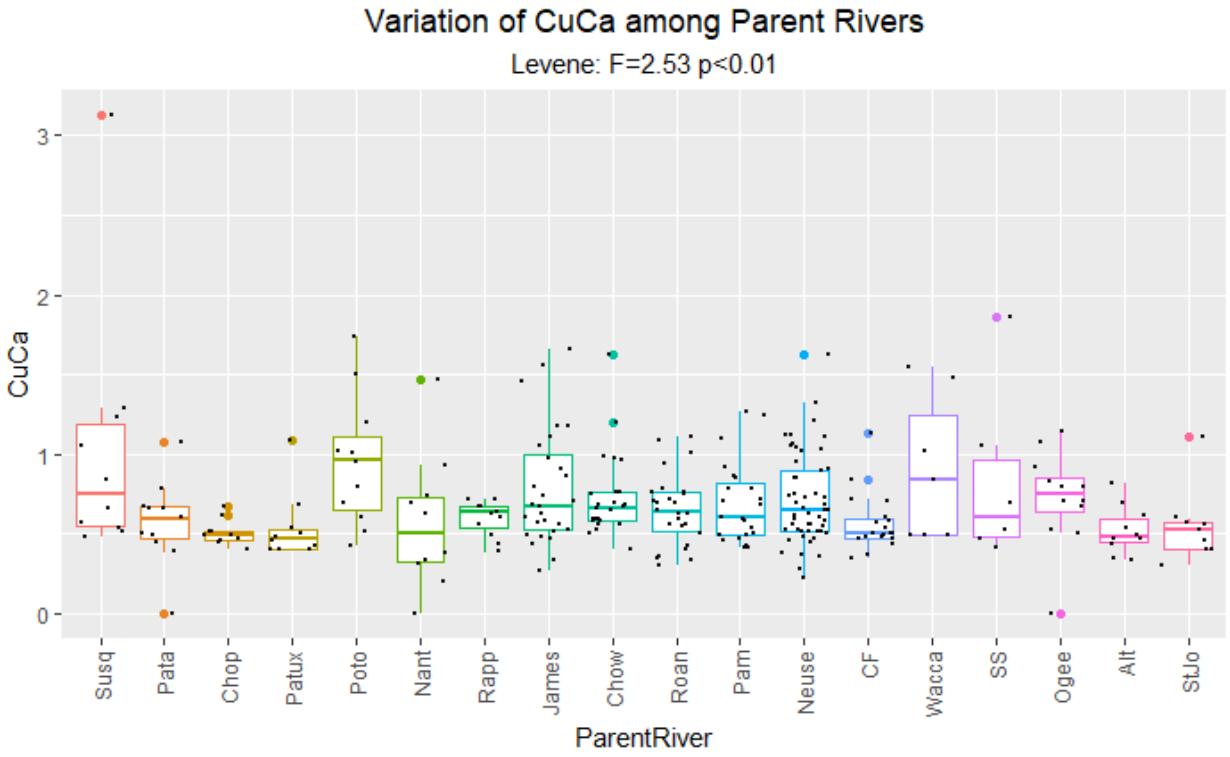

Figure 3-9. Boxplots illustrating the variation in Cu ratios among capture locations when using the parent river grouping variable on the otolith edge data. Values for Levene's test are included in the subtitle. Black dots represent real values. The center line of the boxplots indicate the median for the respective group. The lower and upper hinges of each box represent the 25th and 75th percentiles. Whiskers extend from the hinges to the smallest and largest value within the bounds of 1.5 times the interquartile range. Values beyond these boundaries are indicated as individual colored dots.

	Mg	Mn	Sr	Ba	Pb	Zn	Cu
Mg	1						
Mn	0.44*	1					
Sr	-0.27*	-0.16*	1				
Ba	0.11	-0.16*	-0.01	1			
Pb	0.15*	0.10	-0.03	0.14*	1		
Zn	0.46*	0.19*	-0.13*	0.23*	0.48*	1	
Cu	0.25*	0.02	-0.06	0.3*	0.56*	0.56*	1

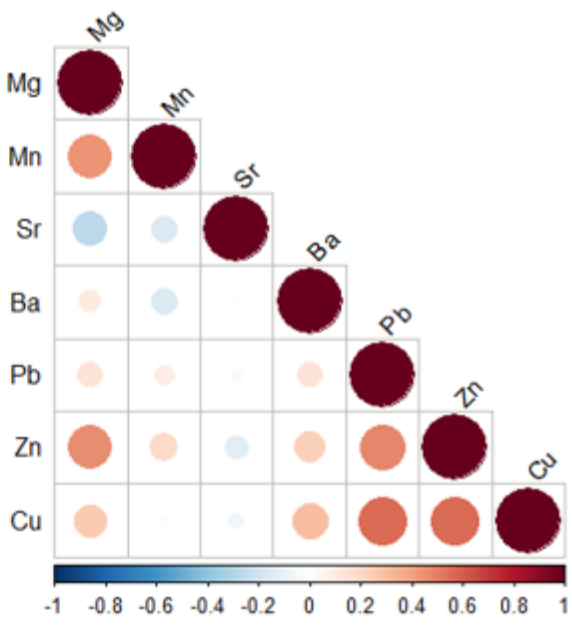

Figure 3-10. Results of correlation tests on the otolith edge data showing Pearson's correlation coefficient (r) between each element, with significant r values ($p < 0.05$) denoted by stars* (table), high r values represented by large and dark red circles (factor plot), and low r values represented by large blue circles (factor plot).

	Eigenvalue	Variance(%)	Cumulative Variance (%)
PC1	2.48	35.42	35.42
PC2	1.45	20.76	56.19
PC3	0.96	13.70	69.89
PC4	0.81	11.50	81.40
PC5	0.54	7.74	89.14
PC6	0.39	5.58	94.71
PC7	0.37	5.29	100

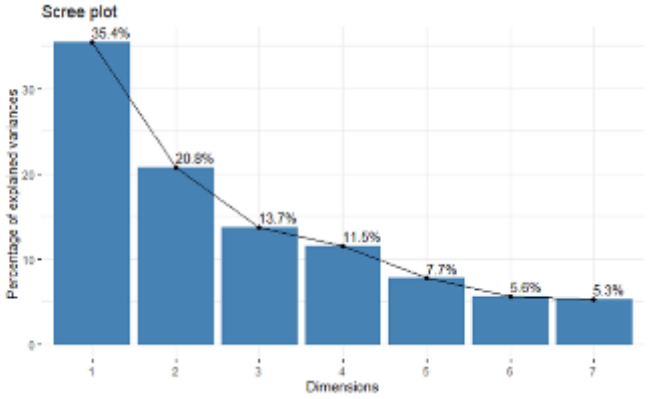

Figure 3-11. Results of principle component analysis on the otolith edge data showing eigenvalues, cumulative variance (table), and individual variance (table and scree plot) explained by each principle component.

	PC1	PC2	PC3	PC4	PC5	PC6	PC7
Sr	2.89	14.79	36.70	43.70	1.35	0.00	0.57
Ba	5.37	15.18	37.77	22.59	18.10	0.81	0.18
Mg	16.03	18.31	2.24	12.40	15.16	0.40	35.46
Mn	4.51	36.53	8.62	7.28	32.60	3.13	7.33
Zn	28.09	0.15	0.51	0.22	17.04	12.29	41.71
Pb	19.22	5.99	13.30	11.70	15.20	19.94	14.65
Cu	23.88	9.05	0.86	2.11	0.54	63.44	0.11

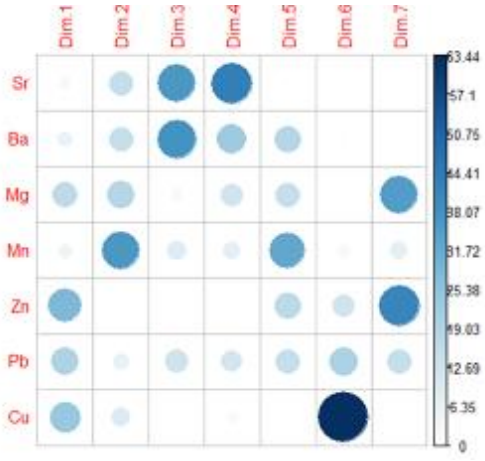

Figure 3-12. Results of principle components analysis on the edge data showing the loading scores of elements on each principle component axis displayed numerically (table), and graphically (factor plot), where increasing loading scores are represented by larger and darker circles.

	Dim.1	Dim.2	Dim.3	Dim.4	Dim.5	Dim.6	Dim.7
Sr	0.07	0.21	0.35	0.35	0.01	0	0
Ba	0.13	0.22	0.36	0.18	0.1	0	0
Mg	0.4	0.27	0.02	0.1	0.08	0	0.13
Mn	0.11	0.53	0.08	0.06	0.18	0.01	0.03
Zn	0.7	0	0	0	0.09	0.05	0.15
Pb	0.48	0.09	0.13	0.09	0.08	0.08	0.05
Cu	0.59	0.13	0.01	0.02	0	0.25	0

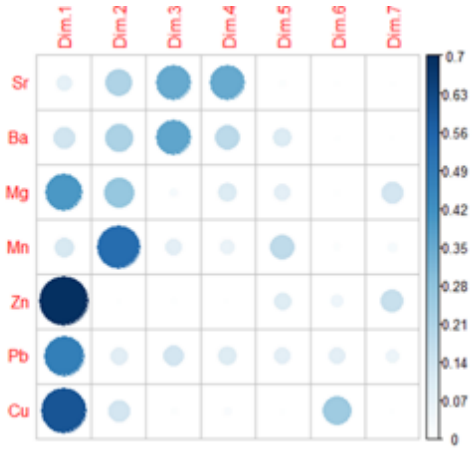

Figure 3-13. Results of principle components analysis on the edge data showing the loading scores of elements on each principle component axis displayed numerically (table), and graphically (factor plot), where increasing loading scores are represented by larger and darker circles.

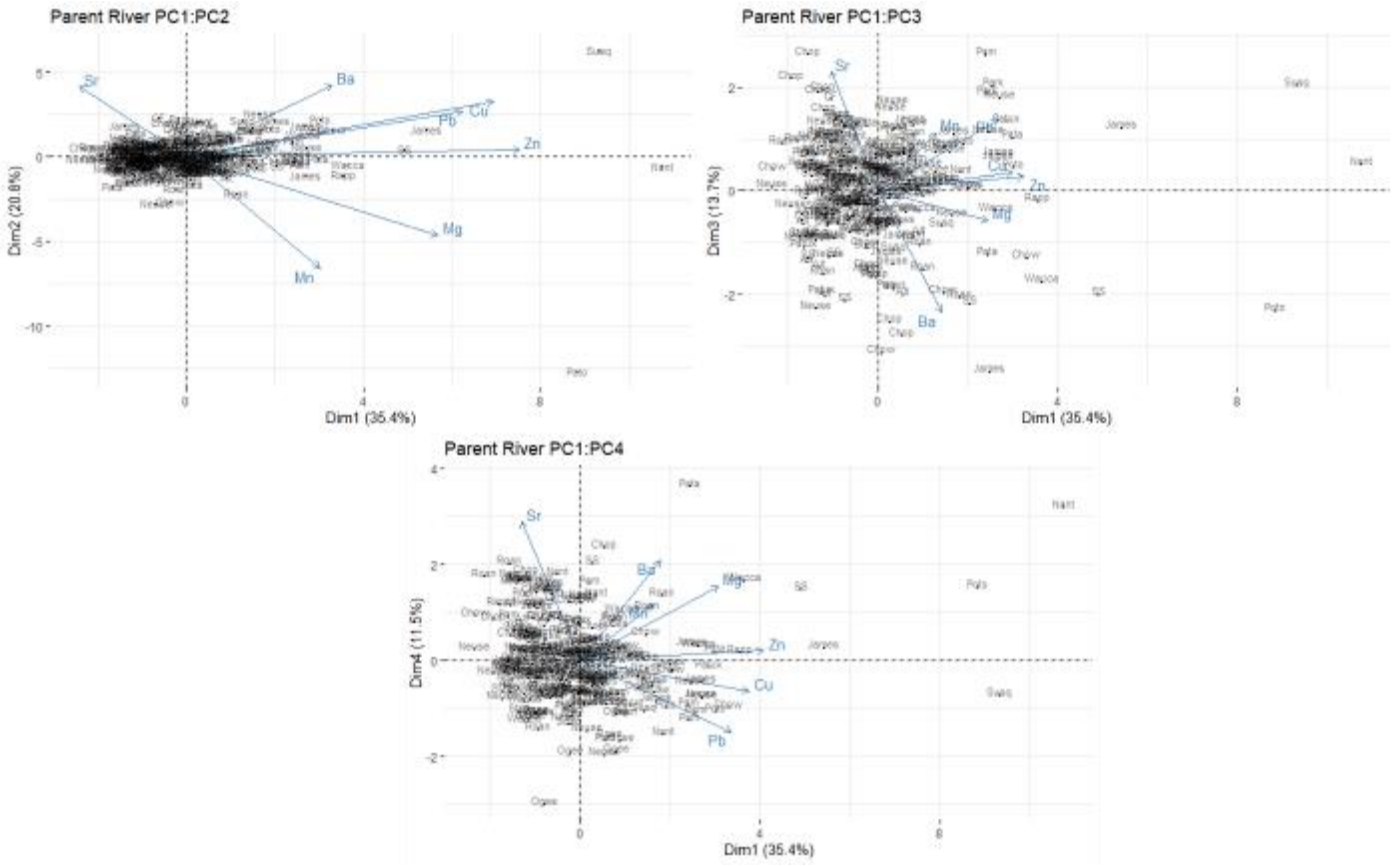

Figure 3-14. Biplots produced during principle components analysis on the otolith edge data comparing PC1 with PC2 through PC4, with individual points labeled by parent river.

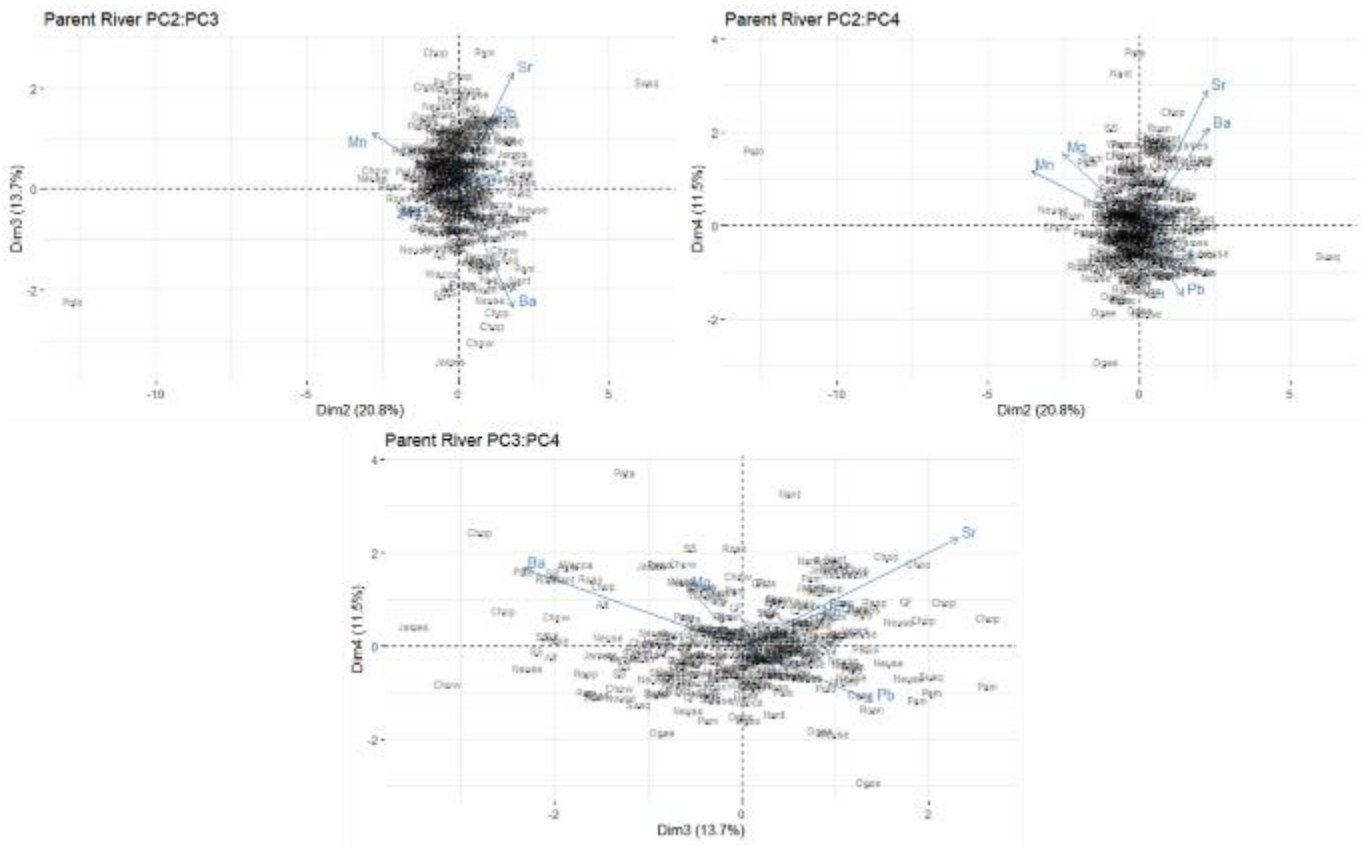

Figure 3-15. Biplots produced during principle components analysis on the otolith edge data comparing PC2 vs PC3 and PC4, and PC3 vs PC4, with individual points labeled by parent river.

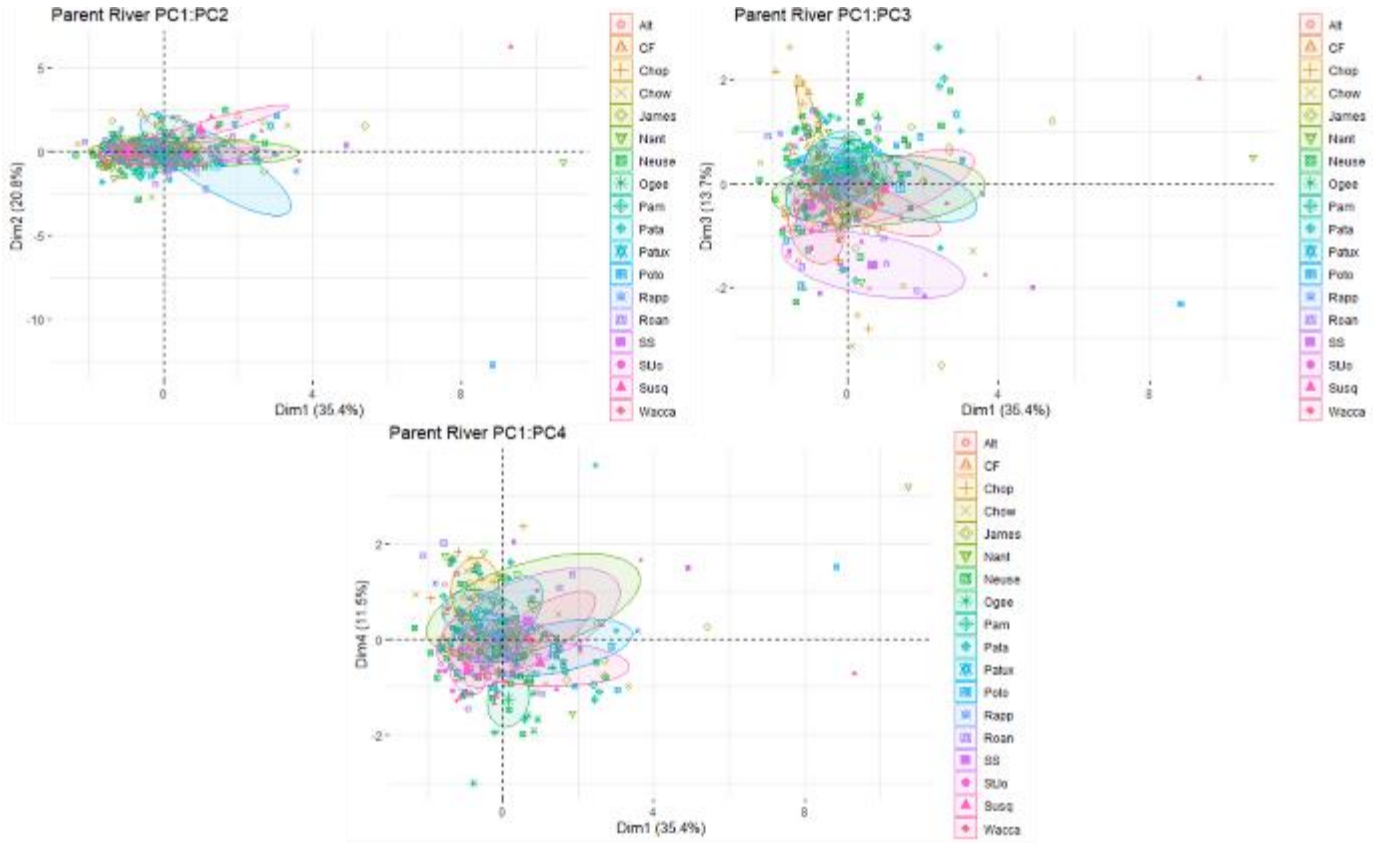

Figure 3-16. Biplots produced during principle components analysis on the otolith edge data comparing PC1 with PC2 through PC4, 95% confidence ellipses and individual points labeled by parent river.

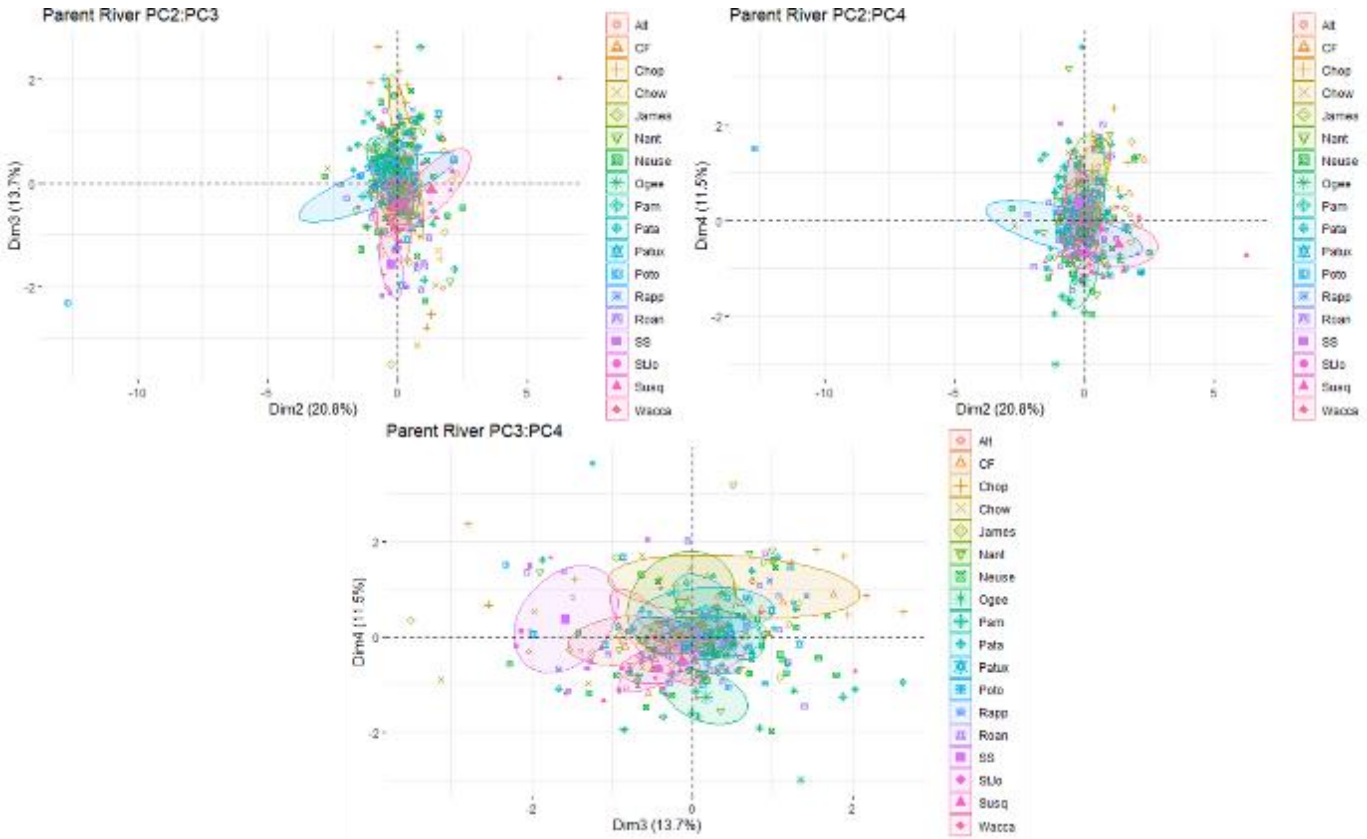

Figure 3-17. Biplots produced during principle components analysis on the otolith edge data comparing PC2 vs PC3, and PC4, and PC3 vs PC4, with 95% confidence ellipses and individual points labeled by parent river.

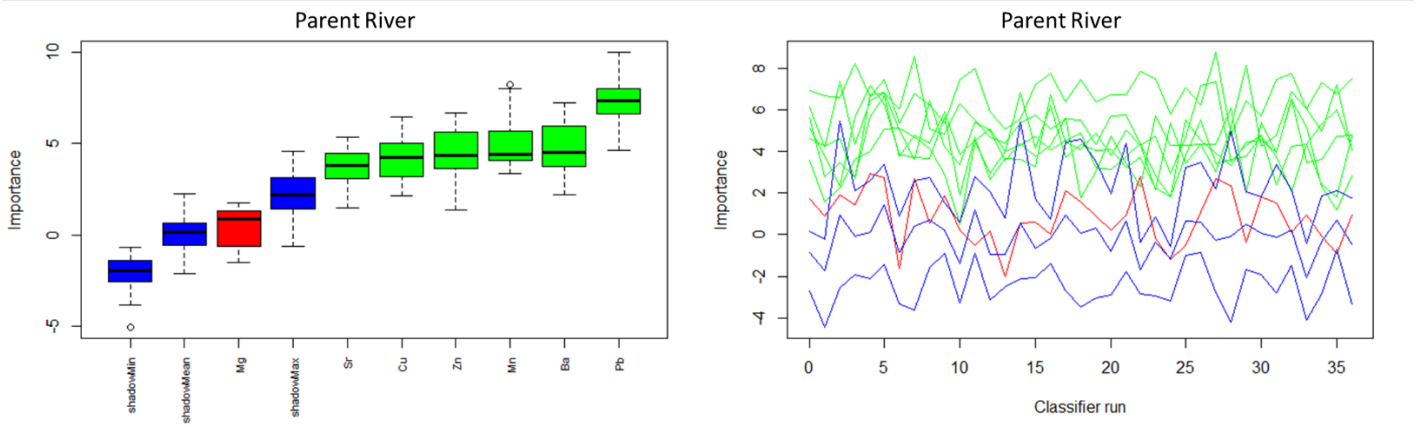

Element	meanImp	medianImp	minImp	maxImp	normHits	decision
Sr	3.74	3.78	1.45	5.33	0.85	Confirmed
Ba	4.77	4.50	2.18	7.24	0.9	Confirmed
Mg	0.44	0.88	-1.51	1.72	0.1	Rejected
Mn	5.00	4.38	3.34	8.19	0.9	Confirmed
Zn	4.46	4.33	1.36	6.64	0.95	Confirmed
Pb	7.34	7.35	4.64	10.00	1	Confirmed
Cu	4.16	4.23	2.16	6.44	0.95	Confirmed

Figure 3-18. Results of Boruta algorithm on the otolith edge data showing the mean, median, minimum, and maximum importance scores, the number of hits normalized to the number of importance source runs, and the algorithms final decision (table), the average importance score of each element and shadow feature (boxplot), and variation in importance scores through each iteration (line plot).

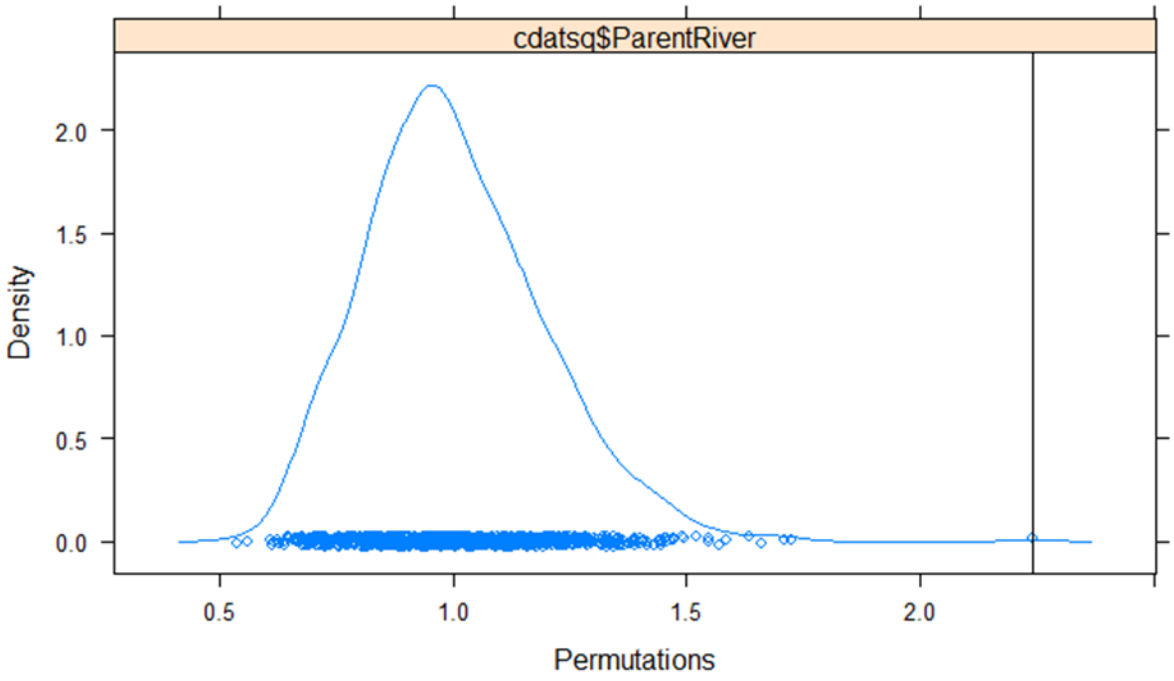

	Df	SumsOfSqs	MeanSqs	F.Model	R2	Pr(>F)
ParentRiver	17	248.35	14.609	2.240	0.123	0.001
Residuals	271	1767.65	6.523		0.877	
Total	288	2016			1	

Figure 3-19. Results of PERMANOVA conducted on the otolith edge data (table), with a density plot illustrating Kernel density estimates obtained from 999 permutations.

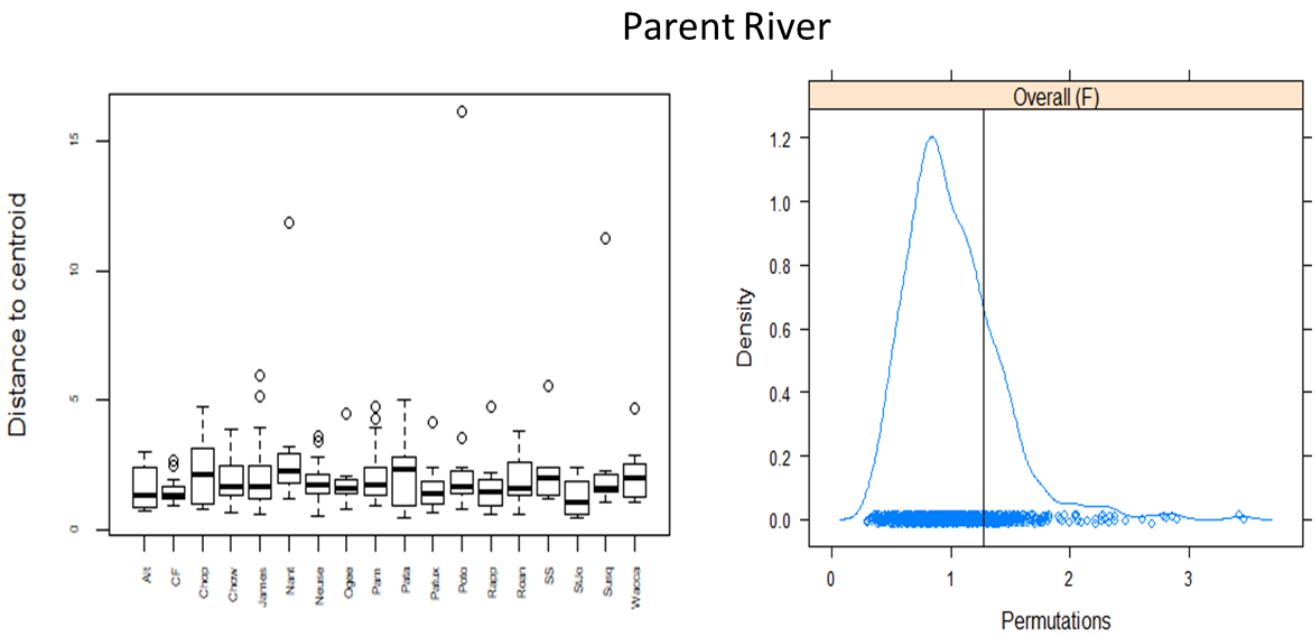

	Df	SumSq	MeanSq	F-val	Pr(>F)	n-perm	Pr(>F)
Groups	17	48.85	2.87	1.28	0.21	999	0.22
Residuals	271	608.71	2.25				

Figure 3-20. Results of multivariate dispersion tests following significant PERMANOVA results showing results of ANOVA and permutation tests (table), centroid dispersions for each capture location (boxplot), and Kernel density estimates obtained through 999 permutations where the observed value is denoted by a vertical black line (density plot). The p-value left of the vertical line is from the ANOVA, and the p-value right of the vertical line is from the permutation test (table).

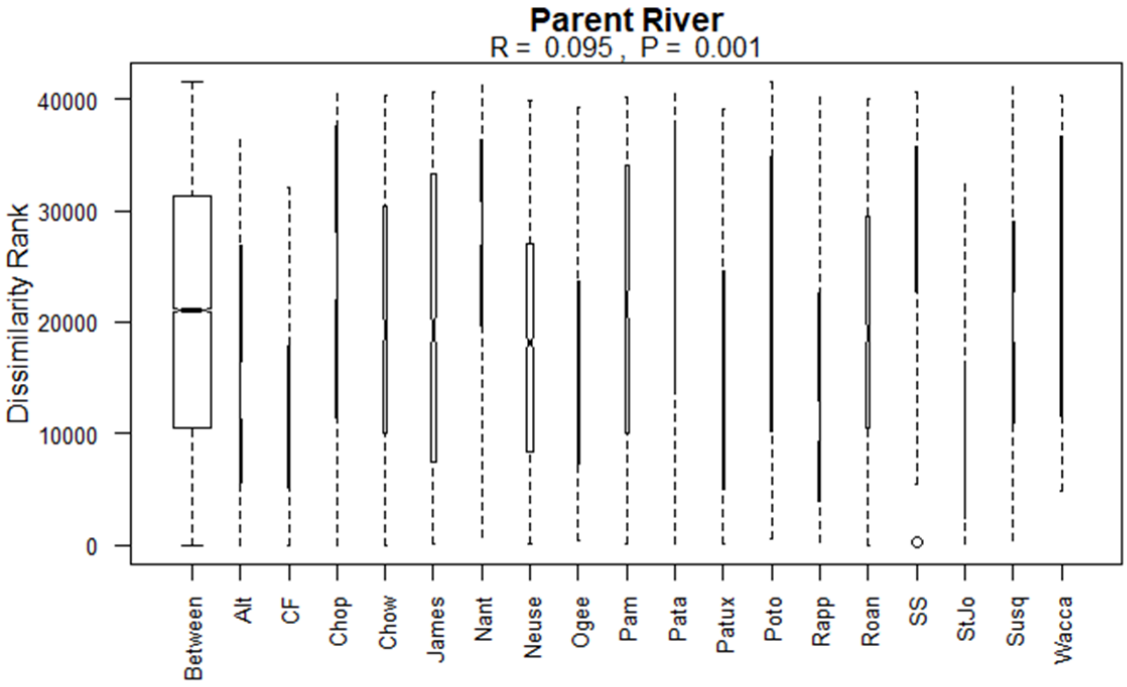

	0%	25%	50%	75%	100%	N
CF	3	5160	9715	17893.5	32092	171
StJo	62	2461.5	10013	15662.5	32387	36
Alt	13	5702	13824	26865	36318	45
Patux	40	5027	13603	24615	39148	45
Ogee	400	7309	18663	23653.75	39245	66
Neuse	52	8438.5	18157	26982.5	39955	1275
Roan	9	10548	18979	29469	39971	325
Rapp	220	4043.5	11120.5	22385.5	40139	66
Pam	164	10113	21597	34117	40228	253
Chow	24	10049	19346.5	30410.75	40343	276
Wacca	4875	11526	26354	36673	40399	21
Pata	154	13998	28338	37719.5	40445	55
Chop	19	11388	25033	37671	40467	45
SS	320	22708	29031	35837.5	40601	15
James	94	7506.25	19262.5	33227.75	40703	378
Susq	473	10831	20360	29017	41138	45
Nant	749	19706	28904	36436	41260	45
Poto	490	10277	22857	34885.5	41564	55
Between	1	10576.5	21032	31382.5	41616	38399

Figure 3-21. Results of ANOSIM for the parent river grouping variable showing the dissimilarity ranks between and within capture locations.

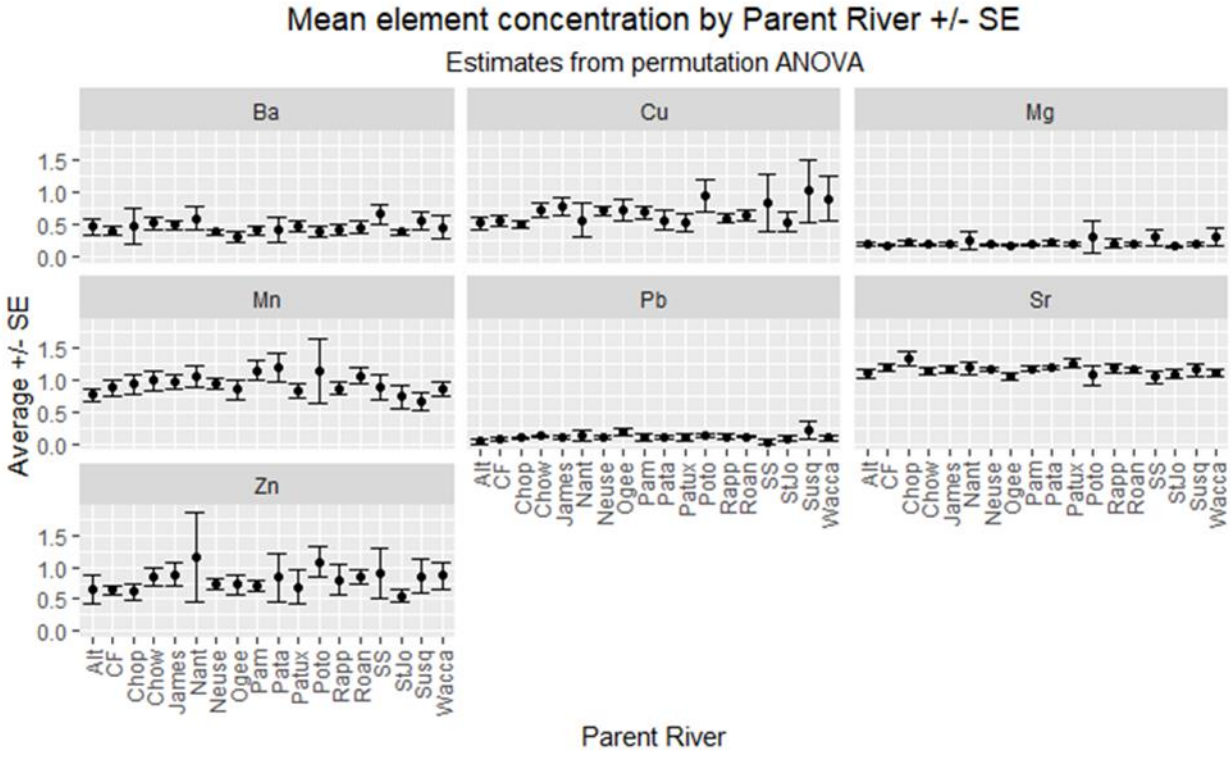

Figure 3-22. Illustration of mean element ratio of the edge data +/- the standard error estimated by permutation ANOVA.

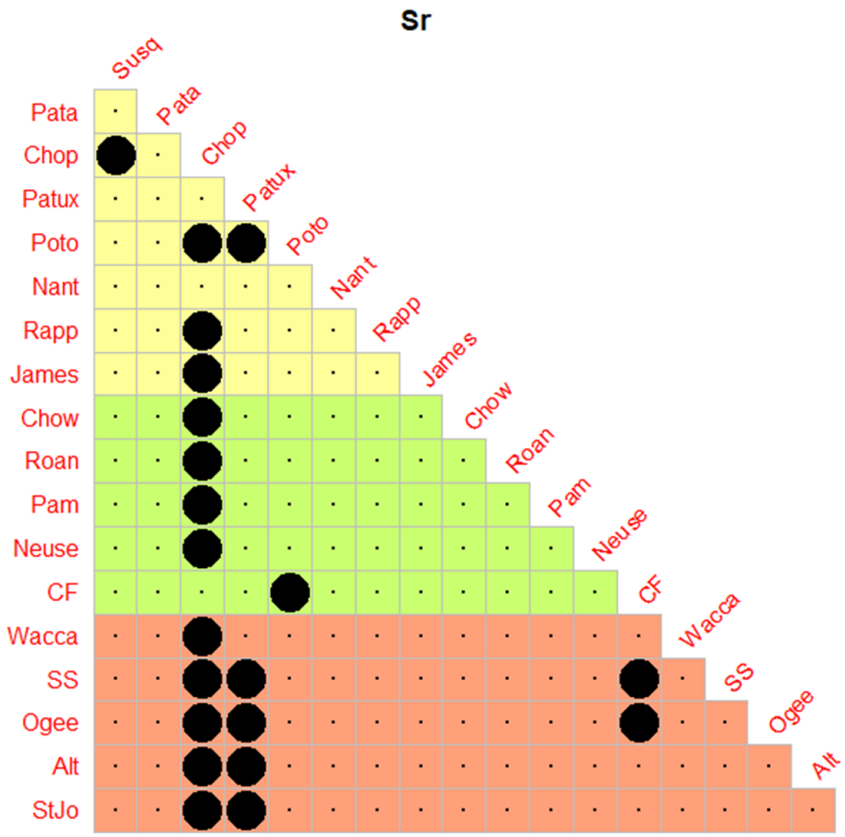

	Susq	Pata	Chop	Patux	Poto	Nant	Rapp	James	Chow	Roan	Pam	Neuse	CF	Wacca	SS	Ogee	Alt
Pata	0.67																
Chop	0.02	0.08															
Patux	0.21	0.45	0.36														
Poto	0.30	0.11	<0.01	0.01													
Nant	0.70	0.97	0.08	0.45	0.12												
Rapp	0.74	0.93	0.05	0.38	0.12	0.94											
James	0.85	0.75	0.01	0.18	0.12	0.78	0.81										
Chow	0.86	0.50	<0.01	0.09	0.29	0.52	0.55	0.66									
Roan	0.96	0.64	<0.01	0.12	0.19	0.67	0.70	0.85	0.80								
Pam	0.81	0.8	0.01	0.22	0.12	0.82	0.86	0.93	0.62	0.80							
Neuse	0.94	0.63	<0.01	0.11	0.13	0.67	0.70	0.85	0.75	0.96	0.80						
CF	0.52	0.86	0.07	0.51	0.05	0.85	0.80	0.54	0.27	0.42	0.63	0.38					
Wacca	0.70	0.39	0.01	0.11	0.68	0.42	0.45	0.52	0.76	0.63	0.50	0.57	0.27				
SS	0.23	0.10	<0.01	0.01	0.78	0.11	0.11	0.11	0.22	0.14	0.11	0.12	0.05	0.52			
Ogee	0.22	0.08	<0.01	0.01	0.86	0.09	0.09	0.08	0.19	0.11	0.08	0.08	0.02	0.57	0.85		
Alt	0.54	0.24	<0.01	0.05	0.78	0.27	0.27	0.31	0.57	0.42	0.29	0.36	0.12	0.86	0.57	0.66	
StJo	0.51	0.22	<0.01	0.05	0.82	0.24	0.26	0.29	0.53	0.38	0.27	0.32	0.12	0.85	0.64	0.71	0.94

Figure 3-23. Results of Welch's t-test for unequal variance conducted on strontium ratios using the otolith edge data showing p-values for each comparison (table) and the location of significant values ($p \leq 0.05$) indicated by large black dots (factor map). Capture location comparisons in the factor map are colored by region: yellow denotes tributaries of Chesapeake Bay, green denotes North Carolina locations, and orange denotes locations south of North Carolina.

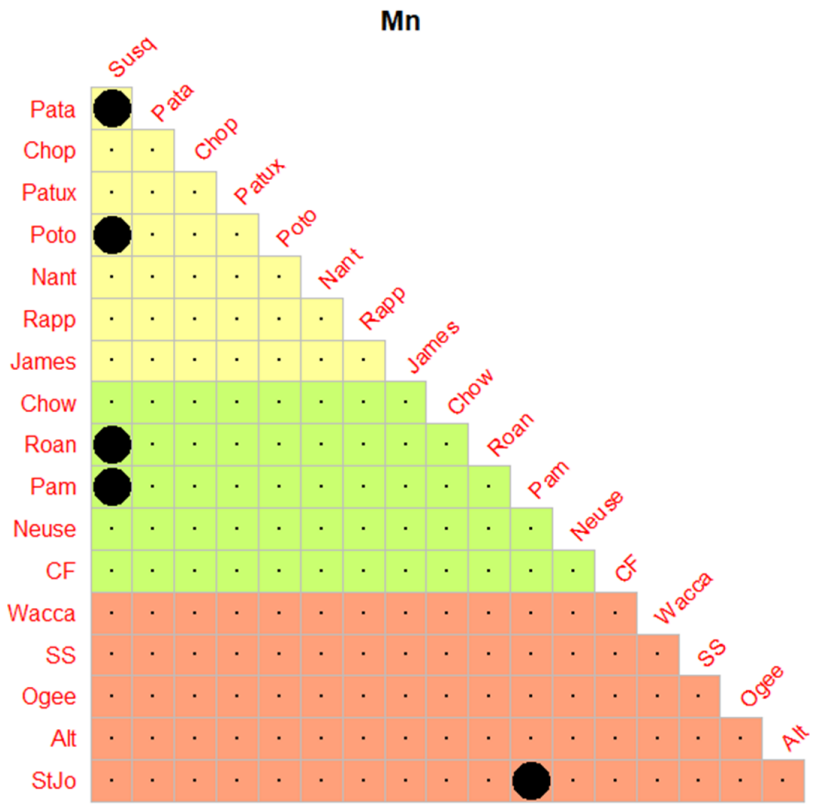

	Susq	Pata	Chop	Patux	Poto	Nant	Rapp	James	Chow	Roan	Pam	Neuse	CF	Wacca	SS	Ogee	Alt
Pata	0.03																
Chop	0.26	0.28															
Patux	0.52	0.12	0.67														
Poto	0.05	0.89	0.38	0.19													
Nant	0.12	0.61	0.66	0.37	0.70												
Rapp	0.38	0.15	0.79	0.89	0.22	0.44											
James	0.12	0.26	0.89	0.53	0.36	0.67	0.62										
Chow	0.12	0.33	0.8	0.45	0.46	0.80	0.54	0.89									
Roan	0.05	0.56	0.57	0.26	0.67	0.96	0.29	0.56	0.67								
Pam	0.02	0.89	0.29	0.12	0.97	0.66	0.12	0.23	0.32	0.60							
Neuse	0.12	0.19	0.95	0.57	0.27	0.62	0.66	0.91	0.78	0.41	0.12						
CF	0.29	0.12	0.81	0.85	0.20	0.44	0.95	0.62	0.53	0.26	0.12	0.66					
Wacca	0.52	0.20	0.78	0.95	0.26	0.48	0.95	0.66	0.58	0.37	0.20	0.67	0.92				
SS	0.44	0.27	0.89	0.88	0.36	0.60	0.95	0.78	0.67	0.52	0.28	0.81	0.97	0.91			
Ogee	0.44	0.12	0.72	0.95	0.19	0.38	0.95	0.56	0.47	0.26	0.12	0.60	0.89	0.98	0.89		
Alt	0.67	0.09	0.53	0.81	0.12	0.26	0.67	0.32	0.26	0.13	0.07	0.33	0.63	0.78	0.67	0.76	
StJo	0.80	0.07	0.44	0.69	0.11	0.20	0.61	0.26	0.22	0.12	0.05	0.26	0.53	0.67	0.62	0.66	0.89

Figure 3-24. Results of Welch's t-test for unequal variance conducted on manganese ratios using the otolith edge data showing p-values for each comparison (table) and the location of significant values ($p \leq 0.05$) indicated by large black dots (factor map). Capture location comparisons in the factor map are colored by region: yellow denotes tributaries of Chesapeake Bay, green denotes North Carolina locations, and orange denotes locations south of North Carolina.

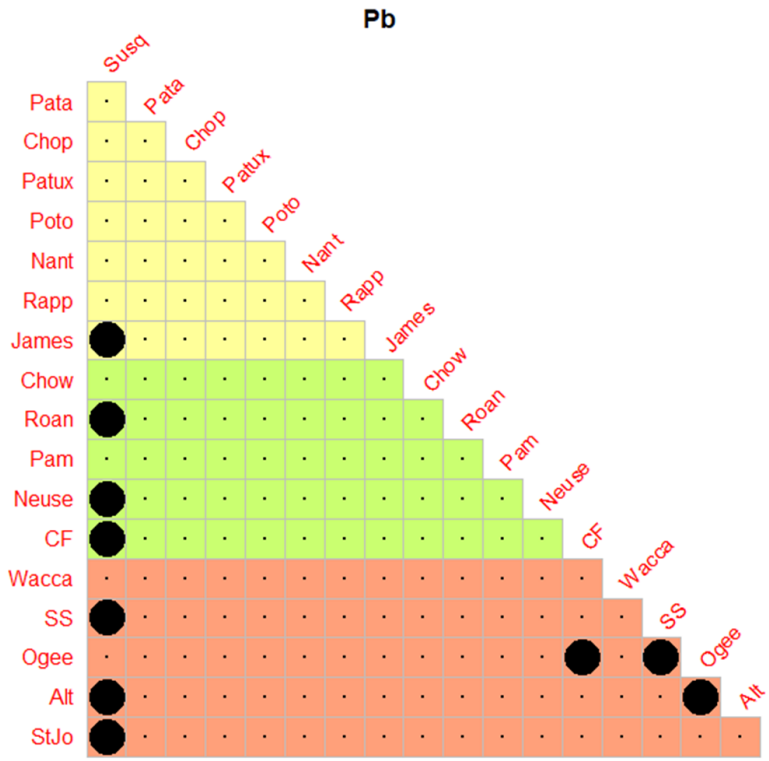

	Susq	Pata	Chop	Patux	Poto	Nant	Rapp	James	Chow	Roan	Pam	Neuse	CF	Wacca	SS	Ogee	Alt
Pata	0.09																
Chop	0.07	0.94															
Patux	0.08	0.96	0.96														
Poto	0.16	0.92	0.80	0.87													
Nant	0.30	0.72	0.58	0.67	0.92												
Rapp	0.10	0.96	0.92	0.92	0.93	0.87											
James	0.05	0.96	0.92	0.93	0.92	0.71	0.96										
Chow	0.09	0.92	0.83	0.88	0.96	0.90	0.96	0.92									
Roan	0.05	0.96	0.92	0.94	0.92	0.71	0.96	0.98	0.92								
Pam	0.06	0.96	0.92	0.94	0.92	0.71	0.96	0.98	0.92	1.00							
Neuse	0.05	0.96	0.92	0.92	0.92	0.71	0.98	0.98	0.92	0.96	0.96						
CF	0.01	0.77	0.92	0.88	0.41	0.25	0.59	0.54	0.35	0.56	0.58	0.41					
Wacca	0.10	0.96	0.98	0.98	0.87	0.69	0.92	0.92	0.89	0.93	0.93	0.92	0.92				
SS	0.01	0.37	0.52	0.46	0.18	0.13	0.26	0.23	0.16	0.25	0.25	0.18	0.69	0.55			
Ogee	0.92	0.15	0.11	0.13	0.34	0.56	0.18	0.10	0.16	0.10	0.10	0.09	0.03	0.16	0.03		
Alt	<0.01	0.26	0.41	0.35	0.13	0.09	0.18	0.13	0.10	0.15	0.15	0.10	0.58	0.46	0.99	0.01	
StJo	0.05	0.92	0.96	0.94	0.69	0.51	0.87	0.87	0.70	0.88	0.88	0.81	0.94	0.96	0.62	0.10	0.55

Figure 3-25. Results of Welch's t-test for unequal variance conducted on lead ratios using the otolith edge data showing p-values for each comparison (table) and the location of significant values ($p \leq 0.05$) indicated by large black dots (factor map). Capture location comparisons in the factor map are colored by region: yellow denotes tributaries of Chesapeake Bay, green denotes North Carolina locations, and orange denotes locations south of North Carolina.

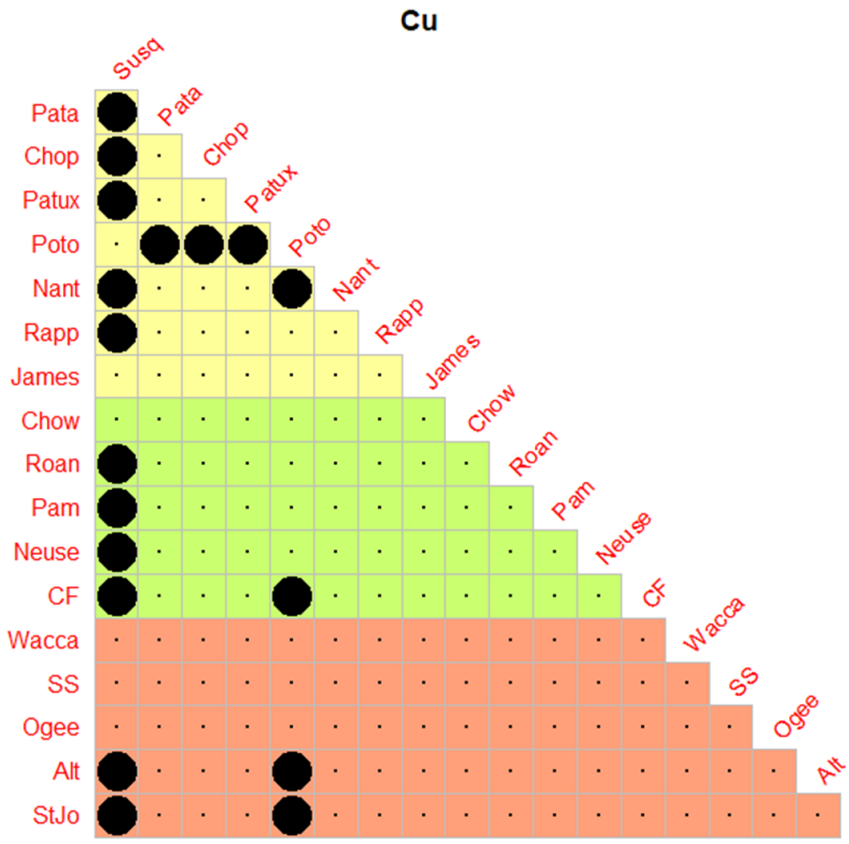

	Susq	Pata	Chop	Patux	Poto	Nant	Rapp	James	Chow	Roan	Pam	Neuse	CF	Wacca	SS	Ogee	Alt
Pata	0.02																
Chop	0.02	0.82															
Patux	0.02	0.90	0.90														
Poto	0.75	0.05	0.02	0.04													
Nant	0.02	0.98	0.83	0.90	0.05												
Rapp	0.02	0.90	0.68	0.82	0.07	0.90											
James	0.15	0.20	0.10	0.15	0.31	0.22	0.26										
Chow	0.09	0.35	0.20	0.27	0.20	0.36	0.43	0.75									
Roan	0.02	0.69	0.42	0.55	0.07	0.69	0.83	0.29	0.55								
Pam	0.05	0.51	0.30	0.38	0.13	0.51	0.63	0.49	0.83	0.82							
Neuse	0.05	0.36	0.20	0.27	0.13	0.36	0.45	0.55	0.90	0.57	0.88						
CF	0.02	0.97	0.82	0.90	0.02	0.98	0.88	0.11	0.24	0.57	0.38	0.24					
Wacca	0.64	0.13	0.08	0.10	0.90	0.14	0.17	0.55	0.38	0.20	0.28	0.31	0.09				
SS	0.43	0.27	0.18	0.22	0.67	0.27	0.31	0.87	0.67	0.38	0.52	0.57	0.22	0.84			
Ogee	0.13	0.45	0.28	0.36	0.24	0.45	0.55	0.75	0.96	0.70	0.90	0.97	0.36	0.40	0.67		
Alt	0.02	0.87	0.95	0.95	0.03	0.88	0.75	0.13	0.24	0.48	0.35	0.24	0.87	0.09	0.20	0.31	
StJo	0.02	0.92	0.90	0.97	0.05	0.93	0.85	0.20	0.31	0.60	0.44	0.31	0.94	0.13	0.24	0.40	0.93

Figure 3-26. Results of Welch's t-test for unequal variance conducted on copper ratios using the otolith edge data showing p-values for each comparison (table) and the location of significant values ($p \leq 0.05$) indicated by large black dots (factor map). Capture location comparisons in the factor map are colored by region: yellow denotes tributaries of Chesapeake Bay, green denotes North Carolina locations, and orange denotes locations south of North Carolina.

CHAPTER 4: CONCLUSIONS

Abstract

The goal of this thesis was to determine if otolith microchemistry could be used to discriminate spawning stocks of Hickory Shad. Hickory Shad were captured during spawning runs at 26 locations within 18 major rivers along their known spawning range, and LA-ICP-MS was used to quantify seven elements (Mg^{2+}, Mn^{2+}, Cu^{2+}, Zn^{2+}, Sr^{2+}, Ba^{2+}, and Pb^{2+}), along a continuous transect that ran from the ventral to dorsal edge, and through the otolith core, resulting in a time resolved model of the environmental exposure history of each fish. Otolith element signatures incorporated during the first year of life were informative, and were able to provide evidence that Hickory Shad exhibit natal homing. On the other hand, the edge of Hickory Shad otoliths did not appear to reflect the ambient water in which the fish were captured, which suggested that the Hickory Shad spawning run may be so rapid that it influences the ability to detect the freshwater signatures. Overall, these results suggest that otolith chemistry has the potential to identify spawning stocks and provide life history information that is important to consider in stock discrimination, but otolith element signatures obtained early in life may be more useful than element signatures produced later in life.

Conclusions

The goal of this thesis was to determine if otolith microchemistry could be used to discriminate spawning stocks of Hickory Shad. The first objective was to determine if the method could provide evidence that Hickory Shad exhibit natal homing. Most of the Hickory

Shad captured at the same location had strikingly similar element profiles in the otolith core that were distinguishable from other capture locations, which was highly suggestive of natal homing. Testing the premise of natal homing deductively required developing a quantitative approach. Hickory Shad from the same capture location had very similar element signatures within the otolith core, which is the natal region of the otolith. In the majority of cases, between 50% and 100% of Hickory Shad captured in the same location were assigned to the same cluster. A Chi-Square test confirmed that there was a significant relationship between capture location and cluster assignment. Collectively, these results provide the first real evidence that Hickory Shad do exhibit natal homing, and that otolith microchemistry can be used to detect natal homing in Hickory Shad.

In order for otolith microchemistry to be an effective tool for discriminating Hickory Shad spawning stocks, Hickory Shad otoliths must serve as accurate biogenic tags and incorporate elemental variation between different environmental signatures at detectable magnitudes. The second objective of this study was to use the otolith edge as a proxy for the element signature of each capture location to determine if different capture locations would produce distinct element signatures. Spatial variation is known to occur in most of these systems, but the edge of Hickory Shad otoliths showed very little variation in elements. Our results suggested that the edge of Hickory Shad otoliths did not reflect the ambient water of each capture location, which may be related to a rapid spawning migration. Therefore, we concluded that otolith microchemistry may not be able to provide accurate information about life history events that occur beyond the first year of life.

Overall, the results of this study suggest that otolith microchemistry is a potentially valuable tool that can be used to identify Hickory Shad spawning stocks and learn about their life

history characteristics, but the amount of information it can provide is constrained by a number of physiological, ecological, and life history traits that need further refinement, and its accuracy may be limited to specific regions of the otolith such as those produced in early life. Our results support the hypothesis that Hickory Shad exhibit natal homing, but we were not able to quantify the rate or spatial extent of natal homing and straying. Knowledge gaps included the spatiotemporal distribution of elements in spawning rivers as well as Hickory Shad otolith growth, microstructure development, metabolic regulation of elements during different life stages, spawning duration, and spawning ground locations. A better understanding of these factors and how they influence element incorporation into Hickory Shad otoliths would have greatly benefited this study, and we will be able to more accurately evaluate the true viability of using otolith chemistry to identify Hickory Shad spawning stocks once these factors are explored in detail.

From results of this study it was apparent that Hickory Shad exhibit natal homing at a high rate, which suggests that river-specific spawning populations likely exist and will require independent harvest regulations. However, the rate of natal homing and straying did not appear to be consistent across watersheds. For instance, based on the distinct element profiles and natal signatures, a high rate of natal homing was fairly obvious in the St. Johns, Altmaha, and Ogeechee rivers, as well as in several tributaries of Chesapeake Bay. Hickory Shad captured in North Carolina watersheds had more variable element profiles and natal signatures, which suggests that the degree of straying is not constant across watersheds. We recommend that future research prioritize developing a better understanding of how the rate and spatial extent of natal homing and straying vary throughout the Hickory Shad spawning range so that we can determine how to define individual spawning stocks sustainably.

Hickory Shad are currently managed under Amendment 3 of the Atlantic States Marine Fisheries Commission (ASMFC) Interstate Fishery Management Plan (FMP) for Shad and River Herring. Amendment 3 does not directly address Hickory Shad, but it gives management authority to the Atlantic coastal states and requires them to develop habitat plans for Shad and River Herring, which includes both Hickory Shad and American Shad, and Alewife and Blueback Herring marketed together as river herring (ASMFC 2010). States are required to conduct fishery-dependent monitoring programs for Hickory Shad under Amendment 1 of the FMP (ASMFC 1999). States are required to develop sustainable fishery plans (SFPs) in all systems open to commercial or recreational harvest for River Herring under Amendment 2 (ASMFC 2009), and for American Shad under Amendment 3 (ASMFC 2010), but they are not required to develop (SFPs) for Hickory Shad. The ASMFC defines a sustainable fishery as "a commercial and/or recreational fishery that will not diminish the potential future stock reproduction and recruitment" (ASMFC 2010). We recommend that states maintain the authority to allocate harvest regulations for Hickory Shad, and we recommend that the ASMFC require states to develop sustainable fishery plans for Hickory Shad within their jurisdictions.

The North Carolina Sustainable Fishery Plan for American Shad was approved by the ASMFC Shad and River Herring Management Board in 2012 for the years 2013 through 2017 (NCDMF and NCWRC 2012). This SFP developed methods to conduct recreational creel surveys and defined sustainability parameters to monitor American Shad and Hickory Shad in the Roanoke, Tar, Neuse, and Cape Fear rivers (NCDMF and NCWRC 2012). The sustainability parameters for this SFP were updated in 2017 (NCDMF and NCWRC 2017), and revised in 2020 (NCDMF and NCWRC 2020). Since the results of this study suggest that Hickory Shad return to their natal rivers to spawn, we recommend that North Carolina fishery management agencies

continue to monitor Hickory Shad on a river by river basis and maintain aggregated harvest regulations with American Shad. We also recommend that the state collect consistent biological data for Hickory Shad as a part of their fishery-independent monitoring programs, and prioritize identifying Hickory Shad spawning and nursery grounds.

Literature Cited

ASMFC (Atlantic States Marine Fisheries Commission). 1985. Fishery management plan for the anadromous alosid stocks of the eastern United States: American Shad, Hickory Shad, Alewife, and Blueback Herring: Phase II in interstate management planning for migratory alosids of the Atlantic Coast. Washington, D.C. Report 25.

ASMFC (Atlantic States Marine Fisheries Commission). 2002. Addendum I to amendment 1 and technical addendum #1 to the interstate fishery management plan for shad and river herring. Washington, D.C. Report 35b.

ASMFC (Atlantic States Marine Fisheries Commission). 2009. Amendment 2 to the interstate fishery management plan for shad and river herring. Washington, D.C.

ASMFC (Atlantic States Marine Fisheries Commission). 2010. Amendment 3 to the interstate fishery management plan for shad and river herring. Washington, D.C.

ASMFC, 1999. Amendment 1 to the Interstate Fishery Management Plan for Shad & River Herring. April, 1999. Washington, D.C. 76 pp.

NCDMF (North Carolina Division of Marine Fisheries) and NCWRC (North Carolina Wildlife Resources Commission). 2017. North Carolina American Shad Sustainable Fishery Plan. NCDMF. Morehead City, NC. 54P.

NCDMF (North Carolina Division of Marine Fisheries) and NCWRC (North Carolina Wildlife Resources Commission). 2017. North Carolina American Shad Sustainable Fishery Plan. NCDMF. Morehead City, NC. 54P.

NCDMF (North Carolina Division of Marine Fisheries) and NCWRC (North Carolina Wildlife Resources Commission). 2020. North Carolina American Shad Sustainable Fishery Plan: 2020 Update to Resolve Regulatory Inconsistencies. NCDMF. Morehead City, NC. 56P.

APPENDIX A: COMPARING OTOLITH EDGE SIGNATURES FROM SIMILAR GEOGRAPHIC LOCATIONS

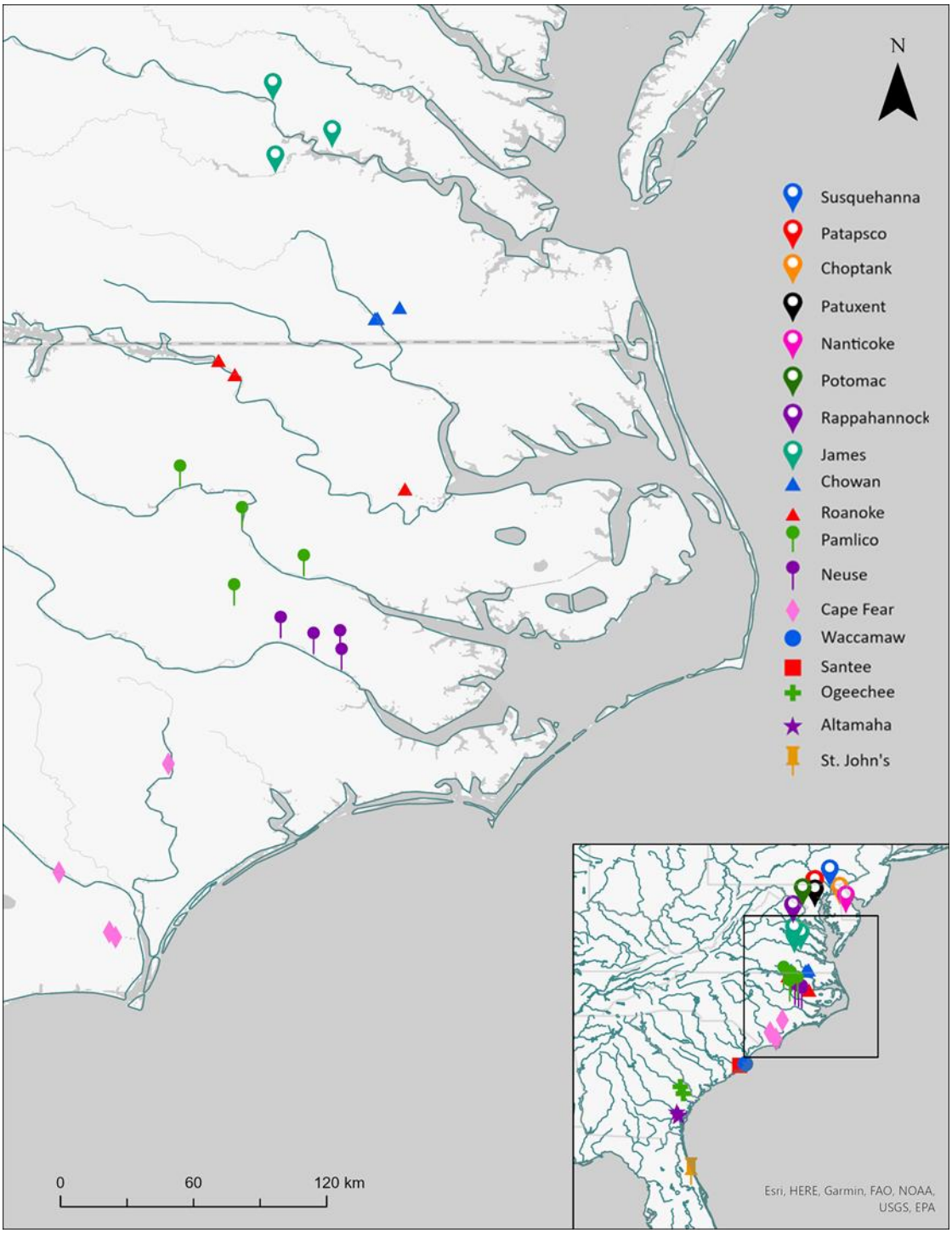

A-1. Map showing capture location pairs that were close in geographic proximity, and part of the same parent rivers which were compared to validate statistical treatment

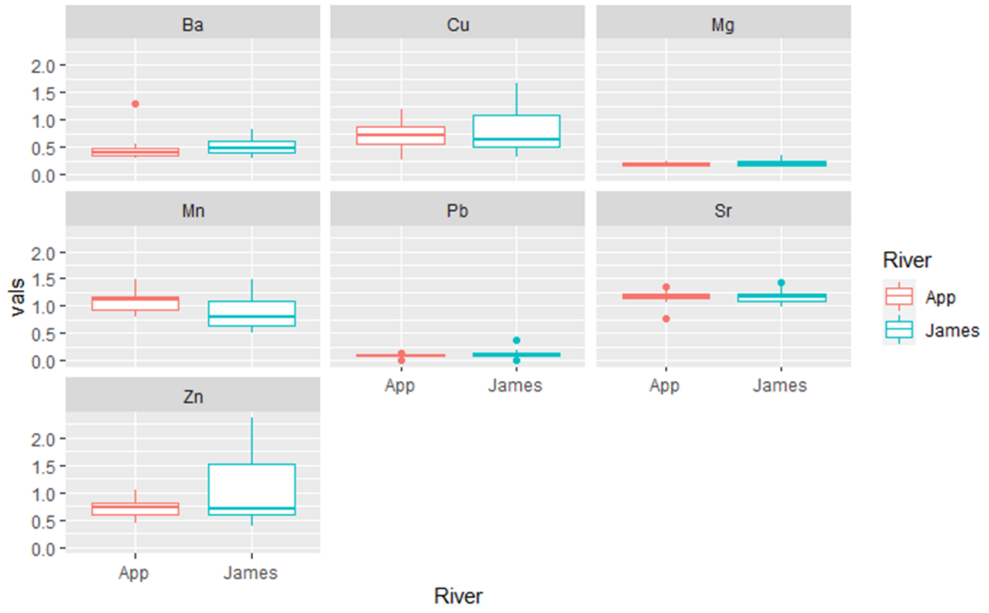

G1	G2	Element	F.Stat	p	CI-L	CI-U	$\widehat{\sigma^2}(r)$	T.Stat	df	p	$\hat{\mu}_{g1}$	$\hat{\mu}_{g2}$	SE	CI-L	CI-U	Boot1	Boot2
App	James	Sr	1.46	0.49	0.48	4.85	1.46	-0.13	26	0.90	1.16	1.17	0.05	-0.11	0.10	0.92	-
		Ba	3.17	0.04	1.05	10.57	3.17	-0.47	26	0.65	0.48	0.51	0.08	-0.20	0.13	-	0.68
		Mn	0.50	0.25	0.17	1.66	0.50	2.15	26	0.04	1.09	0.88	0.10	0.01	0.41	0.53	-
		Zn	0.08	<0.01	0.03	0.25	0.08	-1.50	26	0.15	0.72	1.00	0.18	-0.65	0.10	-	0.10
		Pb	0.17	<0.01	0.06	0.55	0.17	-0.52	26	0.61	0.10	0.12	0.03	-0.07	0.04	-	0.56
		Cu	0.37	0.10	0.12	1.22	0.37	-0.70	26	0.49	0.73	0.83	0.14	-0.39	0.19	0.58	-

A-2. Results of F-tests (left of vertical line) and appropriate bootstrap procedure (right of vertical line) that were used to compare element ratios (boxplots) on the ventral edge of otoliths from Hickory Shad captured in the Appomattox and James Rivers. Values for the F-tests include the F-statistic, p-value, upper and lower confidence intervals, and estimated ratio of variance $\widehat{\sigma^2}(r)$, which were used to determine the appropriate bootstrap procedure. Values for the bootstrap procedure include the t-statistic, degrees of freedom, observed p-value, mean estimates for each capture location ($\hat{\mu}_{gx}$), standard errors, confidence intervals, and bootstrap p-values. In the boxplots, the center line indicates the median. The lower and upper hinges of each box represent the 25th and 75th percentiles, respectively. Whiskers extend from the hinges to the smallest and largest value within the bounds of 1.5 times the interquartile range. Values beyond these boundaries are indicated as individual dots.

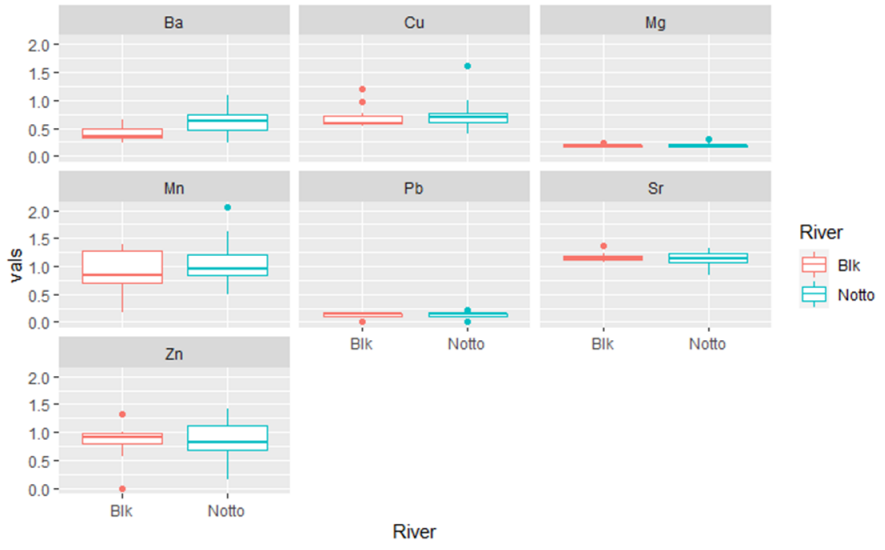

G1	G2	Element	F.Stat	p	CI-L	CI-U	$\widehat{\sigma^2}(r)$	T.Stat	df	p	$\hat{\mu}_{g1}$	$\hat{\mu}_{g2}$	SE	CI-L	CI-U	Boot1
Blk	Notto	Sr	0.40	0.15	0.12	1.44	0.40	0.64	22	0.53	1.16	1.13	0.05	-0.07	0.13	0.61
		Ba	0.32	0.08	0.10	1.17	0.32	-2.63	22	0.02	0.41	0.62	0.08	-0.38	-0.05	0.58
		Mn	0.88	0.86	0.26	3.20	0.88	-0.93	22	0.36	0.91	1.06	0.16	-0.48	0.18	0.55
		Zn	0.88	0.86	0.26	3.20	0.88	-0.21	22	0.84	0.83	0.86	0.14	-0.32	0.26	0.84
		Pb	0.43	0.19	0.13	1.55	0.43	-0.27	22	0.79	0.12	0.12	0.02	-0.05	0.04	0.79
		Cu	0.47	0.24	0.14	1.71	0.47	-0.56	22	0.58	0.70	0.76	0.11	-0.29	0.16	0.65

A-3. Results of F-tests (left of vertical line) and appropriate bootstrap procedure (right of vertical line) that were used to compare element ratios (boxplots) on the ventral edge of otoliths from Hickory Shad captured in the Blackwater and Nottoway Rivers. Values for the F-tests include the F-statistic, p-value, upper and lower confidence intervals, and estimated ratio of variance $\widehat{\sigma^2}(r)$, which were used to determine the appropriate bootstrap procedure. Values for the bootstrap procedure include the t-statistic, degrees of freedom, observed p-value, mean estimates for each capture location ($\hat{\mu}_{gx}$), standard errors, confidence intervals, and bootstrap p-values. In the boxplots, the center line indicates the median. The lower and upper hinges of each box represent the 25th and 75th percentiles, respectively. Whiskers extend from the hinges to the smallest and largest value within the bounds of 1.5 times the interquartile range. Values beyond these boundaries are indicated as individual dots.

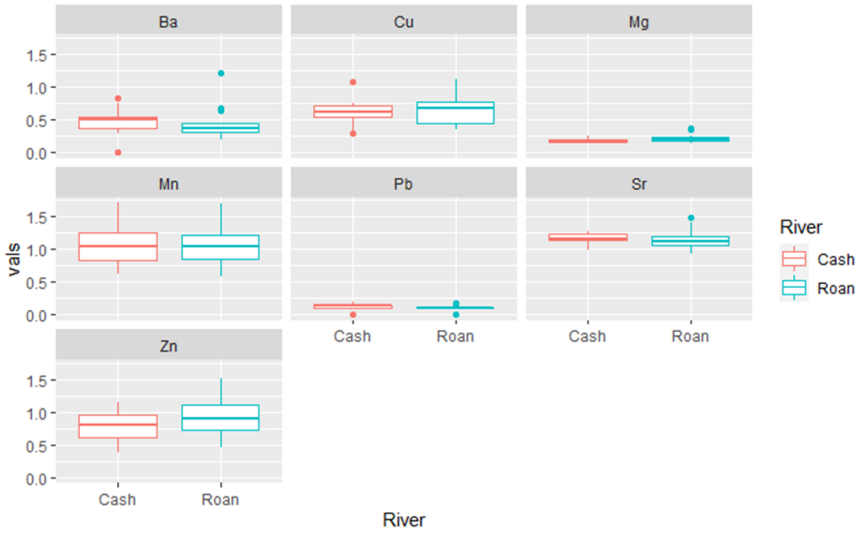

G1	G2	Element	F.Stat	p	CI-L	CI-U	$\widehat{\sigma^2}(r)$	T.Stat	df	p	$\hat{\mu}_{g1}$	$\hat{\mu}_{g2}$	SE	CI-L	CI-L	Boot1
Roan	Cash	Sr	3.27	0.06	0.96	10.46	3.27	-0.41	24	0.69	1.15	1.17	0.05	-0.13	0.09	0.68
		Ba	1.43	0.56	0.42	4.59	1.43	-0.28	24	0.78	0.45	0.47	0.09	-0.22	0.17	0.78
		Mn	0.92	0.87	0.27	2.93	0.92	-0.01	24	0.99	1.06	1.06	0.12	-0.26	0.26	0.99
		Zn	1.59	0.45	0.47	5.09	1.59	1.27	24	0.22	0.91	0.77	0.11	-0.09	0.38	0.55
		Pb	0.88	0.82	0.26	2.83	0.88	-1.39	24	0.18	0.10	0.12	0.02	-0.07	0.01	0.51
		Cu	1.40	0.58	0.41	4.49	1.40	0.47	24	0.64	0.67	0.63	0.09	-0.14	0.23	0.69

A-4. Results of F-tests (left of vertical line) and appropriate bootstrap procedure (right of vertical line) that were used to compare element ratios (boxplots) on the ventral edge of otoliths from Hickory Shad captured in the Roanoke and Cashie Rivers. Values for the F-tests include the F-statistic, p-value, upper and lower confidence intervals, and estimated ratio of variance $\widehat{\sigma^2}(r)$, which were used to determine the appropriate bootstrap procedure. Values for the bootstrap procedure include the t-statistic, degrees of freedom, observed p-value, mean estimates for each capture location ($\hat{\mu}_{gx}$), standard errors, confidence intervals, and bootstrap p-values. In the boxplots, the center line indicates the median. The lower and upper hinges of each box represent the 25th and 75th percentiles, respectively. Whiskers extend from the hinges to the smallest and largest value within the bounds of 1.5 times the interquartile range. Values beyond these boundaries are indicated as individual dots.

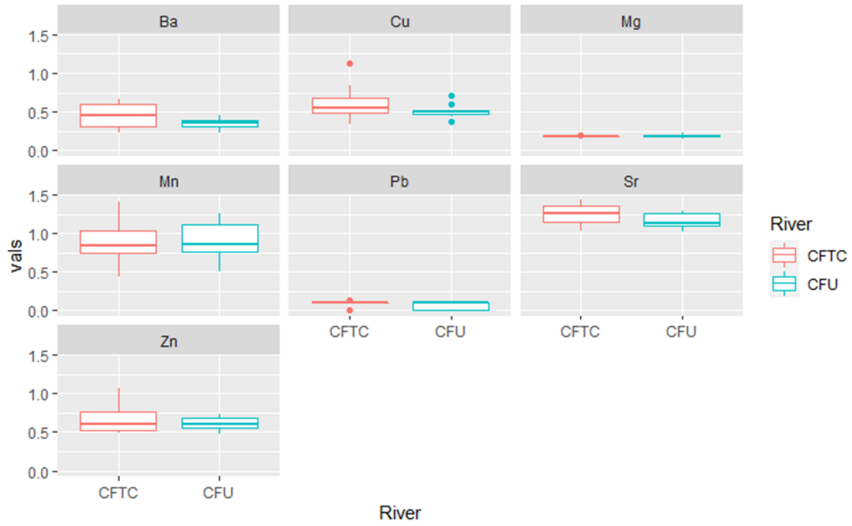

G1	G2	Element	F.Stat	p	CI-L	CI-U	$\widehat{\sigma^2}(r)$	T.Stat	df	p	$\hat{\mu}_{g1}$	$\hat{\mu}_{g2}$	SE	CI-L	CI-U	Boot1	Boot2
CFTC	CFU	Sr	2.06	0.32	0.47	8.46	2.06	1.48	17	0.16	1.24	1.16	0.06	-0.04	0.21	-	0.16
		Ba	5.13	0.03	1.18	21.03	5.13	1.69	17	0.11	0.45	0.35	0.06	-0.02	0.22	0.51	-
		Mn	1.18	0.83	0.27	4.84	1.18	0.16	17	0.87	0.89	0.87	0.13	-0.25	0.30	-	0.89
		Zn	4.49	0.05	1.03	18.43	4.49	0.89	17	0.39	0.67	0.61	0.07	-0.08	0.20	-	0.37
		Pb	0.85	0.81	0.20	3.49	0.85	0.79	17	0.44	0.08	0.07	0.02	-0.03	0.06	-	0.44
		Cu	5.33	0.03	1.22	21.86	5.33	1.31	17	0.21	0.62	0.51	0.08	-0.07	0.28	0.54	-

A-5. Results of F-tests (left of vertical line) and appropriate bootstrap procedure (right of vertical line) that were used to compare element ratios (boxplots) on the ventral edge of otoliths from Hickory Shad captured Cape Fear Town Creek and Cape Fear Upper. Values for the F-tests include the F-statistic, p-value, upper and lower confidence intervals, and estimated ratio of variance $\widehat{\sigma^2}(r)$, which were used to determine the appropriate bootstrap procedure. Values for the bootstrap procedure include the t-statistic, degrees of freedom, observed p-value, mean estimates for each capture location ($\hat{\mu}_{gx}$), standard errors, confidence intervals, and bootstrap p-values. In the boxplots, the center line indicates the median. The lower and upper hinges of each box represent the 25th and 75th percentiles, respectively. Whiskers extend from the hinges to the smallest and largest value within the bounds of 1.5 times the interquartile range. Values beyond these boundaries are indicated as individual dots.

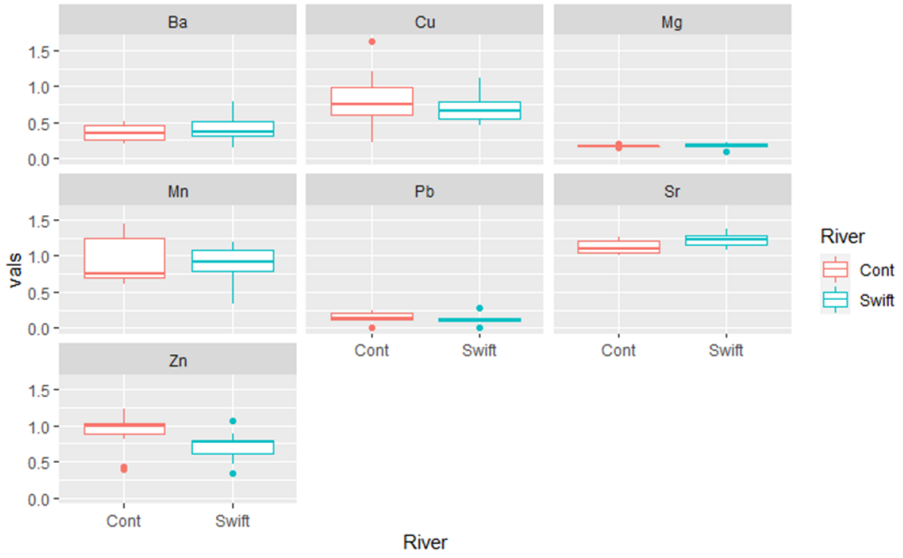

G1	G2	Element	F.Stat	p	CI-L	CI-U	$\widehat{\sigma^2}(r)$	T.Stat	df	p	$\hat{\mu}_{g1}$	$\hat{\mu}_{g2}$	SE	CI-L	CI-U	Boot1
Cont	Swift	Sr	0.99	0.99	0.28	3.62	0.99	-2.39	21	0.03	1.13	1.22	0.04	-0.18	-0.01	0.53
		Ba	0.37	0.13	0.11	1.36	0.37	-1.1	21	0.28	0.36	0.43	0.06	-0.21	0.06	0.53
		Mn	1.46	0.54	0.41	5.35	1.46	0.69	21	0.50	0.97	0.88	0.12	-0.17	0.34	0.60
		Zn	1.90	0.31	0.54	6.97	1.90	2.05	21	0.05	0.90	0.71	0.10	0	0.40	0.53
		Pb	1.55	0.48	0.44	5.69	1.55	0.65	21	0.52	0.14	0.12	0.03	-0.04	0.08	0.60
		Cu	3.63	0.05	1.03	13.31	3.63	0.74	21	0.47	0.81	0.71	0.13	-0.17	0.37	0.56

A-6. Results of F-tests (left of vertical line) and appropriate bootstrap procedure (right of vertical line) that were used to compare element ratios (boxplots) on the ventral edge of otoliths from Hickory Shad captured in the Contentnea Creek and Swift Creek of the Neuse River. Values for the F-tests include the F-statistic, p-value, upper and lower confidence intervals, and estimated ratio of variance $\widehat{\sigma^2}(r)$, which were used to determine the appropriate bootstrap procedure. Values for the bootstrap procedure include the t-statistic, degrees of freedom, observed p-value, mean estimates for each capture location ($\hat{\mu}_{gx}$), standard errors, confidence intervals, and bootstrap p-values. In the boxplots, the center line indicates the median. The lower and upper hinges of each box represent the 25th and 75th percentiles, respectively. Whiskers extend from the hinges to the smallest and largest value within the bounds of 1.5 times the interquartile range. Values beyond these boundaries are indicated as individual dots.

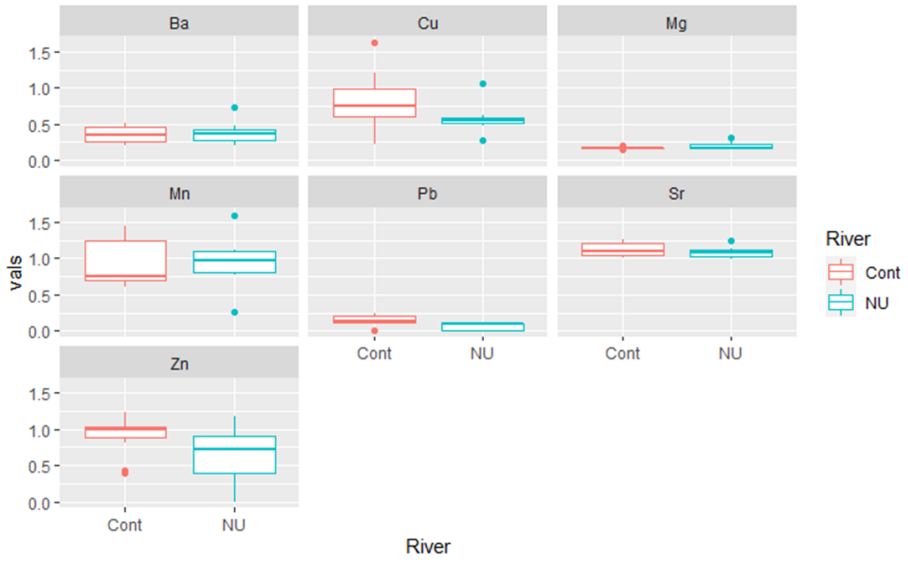

G1	G2	Element	F.Stat	p	CI-L	CI-U	$\widehat{\sigma^2}(r)$	T.Stat	df	p	$\hat{\mu}_{g1}$	$\hat{\mu}_{g2}$	SE	CI-L	CI-U	Boot1	Boot2
Cont	NU	Sr	1.61	0.51	0.37	6.21	1.61	0.97	18	0.34	1.13	1.09	0.04	-0.05	0.12	0.51	0.32
		Ba	0.52	0.33	0.12	2	0.52	-0.36	18	0.72	0.36	0.38	0.06	-0.15	0.11	0.74	0.72
		Mn	0.84	0.78	0.2	3.24	0.84	0.08	18	0.93	0.97	0.95	0.15	-0.31	0.33	0.93	0.93
		Zn	0.52	0.33	0.12	2	0.52	1.81	18	0.09	0.9	0.65	0.14	-0.04	0.56	0.53	0.12
		Pb	2.29	0.25	0.53	8.84	2.29	2.72	18	0.01	0.14	0.06	0.03	0.02	0.15	0.56	0.02
		Cu	3.65	0.08	0.85	14.08	3.65	1.59	18	0.13	0.81	0.58	0.15	-0.07	0.54	0.53	0.11

A-7. Results of F-tests (left of vertical line) and appropriate bootstrap procedure (right of vertical line) that were used to compare element ratios (boxplots) on the ventral edge of otoliths from Hickory Shad captured in the Contentnea Creek and Neuse Upper. Values for the F-tests include the F-statistic, p-value, upper and lower confidence intervals, and estimated ratio of variance $\widehat{\sigma^2}(r)$, which were used to determine the appropriate bootstrap procedure. Values for the bootstrap procedure include the t-statistic, degrees of freedom, observed p-value, mean estimates for each capture location ($\hat{\mu}_{gx}$), standard errors, confidence intervals, and bootstrap p-values. In the boxplots, the center line indicates the median. The lower and upper hinges of each box represent the 25th and 75th percentiles, respectively. Whiskers extend from the hinges to the smallest and largest value within the bounds of 1.5 times the interquartile range. Values beyond these boundaries are indicated as individual dots.

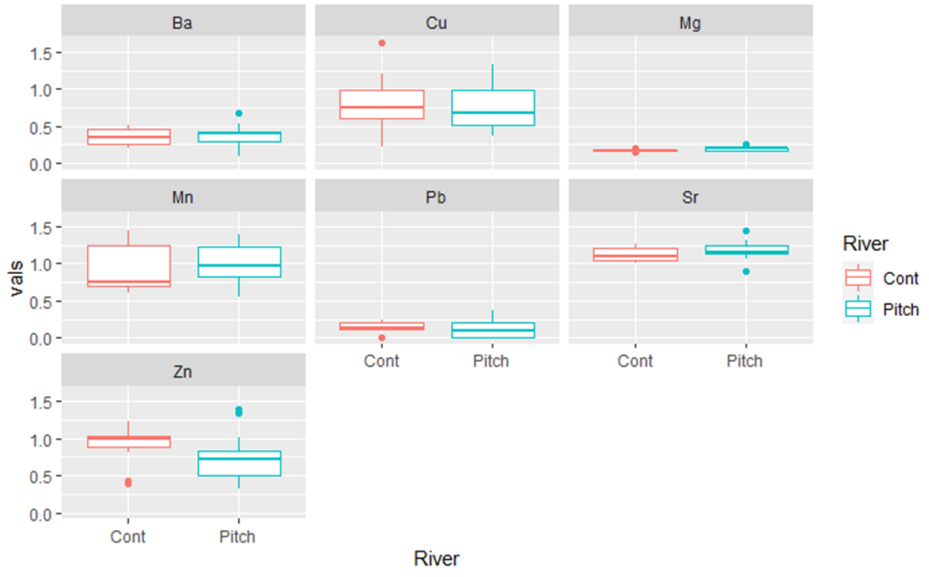

G1	G2	Element	F.Stat	p	CI-L	CI-U	$\widehat{\sigma^2}(r)$	T.Stat	df	p	$\hat{\mu}_{g1}$	$\hat{\mu}_{g2}$	SE	CI-U	CI-L	Boot1	Boot2
Cont	Pitch	Sr	0.79	0.73	0.28	2.74	0.79	-1.13	28	0.27	1.13	1.17	0.04	-0.13	0.04	0.56	0.26
		Ba	0.68	0.55	0.24	2.36	0.68	-0.22	28	0.83	0.36	0.37	0.05	-0.11	0.09	0.84	0.82
		Mn	1.45	0.48	0.50	5.00	1.45	-0.21	28	0.83	0.97	0.99	0.11	-0.25	0.20	0.85	0.88
		Zn	0.79	0.71	0.27	2.71	0.79	1.68	28	0.10	0.90	0.72	0.11	-0.04	0.41	0.55	0.10
		Pb	0.49	0.26	0.17	1.71	0.49	0.60	28	0.55	0.14	0.12	0.04	-0.06	0.10	0.60	0.50
		Cu	1.96	0.21	0.68	6.76	1.96	0.62	28	0.54	0.81	0.73	0.12	-0.18	0.33	0.65	0.57

A-8. Results of F-tests (left of vertical line) and appropriate bootstrap procedure (right of vertical line) that were used to compare element ratios (boxplots) on the ventral edge of otoliths from Hickory Shad captured in the Contentnea Creek and Pitchkettle Creek of the Neuse River. Values for the F-tests include the F-statistic, p-value, upper and lower confidence intervals, and estimated ratio of variance $\widehat{\sigma^2}(r)$, which were used to determine the appropriate bootstrap procedure. Values for the bootstrap procedure include the t-statistic, degrees of freedom, observed p-value, mean estimates for each capture location ($\hat{\mu}_{gx}$), standard errors, confidence intervals, and bootstrap p-values. In the boxplots, the center line indicates the median. The lower and upper hinges of each box represent the 25th and 75th percentiles, respectively. Whiskers extend from the hinges to the smallest and largest value within the bounds of 1.5 times the interquartile range. Values beyond these boundaries are indicated as individual dots.

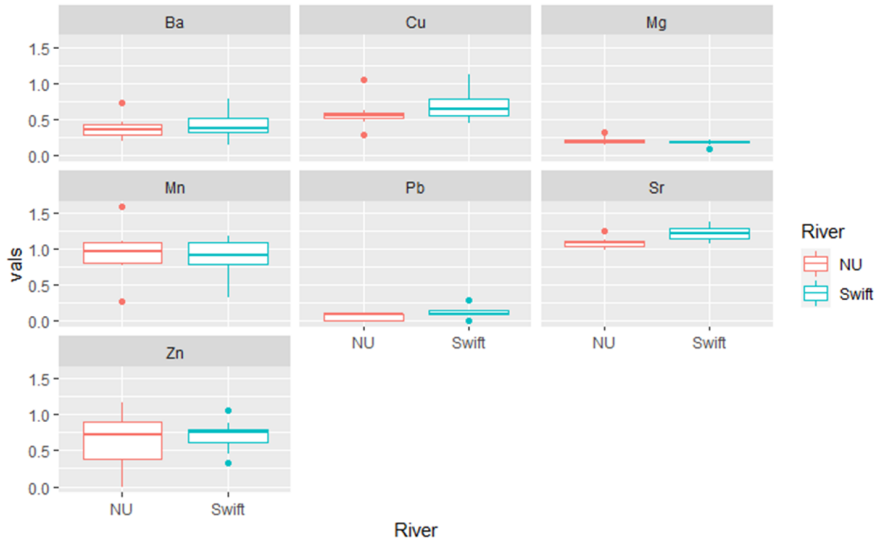

Group1	Group2	Element	F.Stat	p	CI-L	CI-U	$\widehat{\sigma^2}(r)$	T.Stat	df	p	$\hat{\mu}_{g1}$	$\hat{\mu}_{g2}$	SE	CI-L	CI-U	Boot1
Swift	NU	Sr	1.63	0.50	0.38	5.97	1.63	3.44	19	<0.01	1.22	1.09	0.04	0.05	0.22	0.56
		Ba	1.39	0.65	0.33	5.11	1.39	0.65	19	0.53	0.43	0.38	0.08	-0.11	0.21	0.61
		Mn	0.58	0.39	0.14	2.11	0.58	-0.54	19	0.6	0.88	0.95	0.14	-0.36	0.21	0.66
		Zn	0.27	0.05	0.06	1.00	0.27	0.48	19	0.63	0.71	0.65	0.12	-0.2	0.32	0.69
		Pb	1.48	0.59	0.35	5.41	1.48	2.48	19	0.02	0.12	0.06	0.03	0.01	0.12	0.57
		Cu	1.01	0.98	0.24	3.68	1.01	1.50	19	0.15	0.71	0.58	0.09	-0.05	0.33	0.54

A-9. Results of F-tests (left of vertical line) and appropriate bootstrap procedure (right of vertical line) that were used to compare element ratios (boxplots) on the ventral edge of otoliths from Hickory Shad captured in the Neuse Upper and Swift Creek. Values for the F-tests include the F-statistic, p-value, upper and lower confidence intervals, and estimated ratio of variance $\widehat{\sigma^2}(r)$, which were used to determine the appropriate bootstrap procedure. Values for the bootstrap procedure include the t-statistic, degrees of freedom, observed p-value, mean estimates for each capture location ($\hat{\mu}_{gx}$), standard errors, confidence intervals, and bootstrap p-values. In the boxplots, the center line indicates the median. The lower and upper hinges of each box represent the 25th and 75th percentiles, respectively. Whiskers extend from the hinges to the smallest and largest value within the bounds of 1.5 times the interquartile range. Values beyond these boundaries are indicated as individual dots.

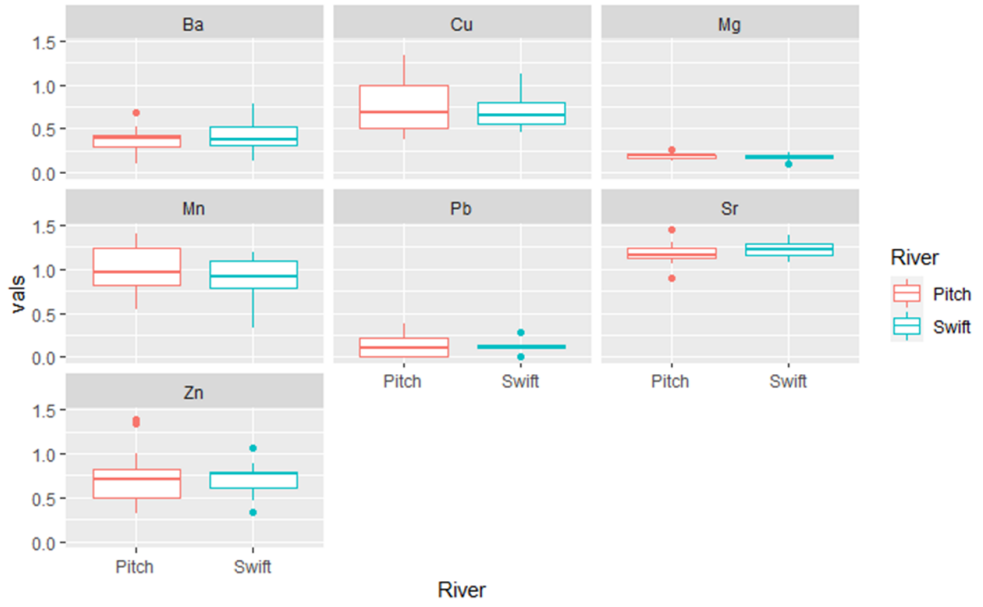

G1	G2	Element	F.Stat	p	CI-L	CI-U	$\widehat{\sigma^2}(r)$	T.Stat	df	p	CI-L	CI-U	$\hat{\mu}_{g1}$	$\hat{\mu}_{g2}$	SE	Boot1
Swift	Pitch	Sr	0.8	0.73	0.29	2.62	0.8	1.35	29	0.19	-0.03	0.13	1.22	1.17	0.04	0.53
		Ba	1.84	0.24	0.65	6.01	1.84	1.05	29	0.3	-0.06	0.18	0.43	0.37	0.06	0.56
		Mn	0.99	0.98	0.35	3.23	0.99	-1.1	29	0.28	-0.31	0.09	0.88	0.99	0.1	0.54
		Zn	0.41	0.14	0.15	1.35	0.41	-0.15	29	0.88	-0.21	0.19	0.71	0.72	0.1	0.88
		Pb	0.32	0.06	0.11	1.04	0.32	0.11	29	0.91	-0.07	0.08	0.12	0.12	0.04	0.88
		Cu	0.54	0.3	0.19	1.76	0.54	-0.2	29	0.85	-0.21	0.18	0.71	0.73	0.09	0.83

A-10. Results of F-tests (left of vertical line) and appropriate bootstrap procedure (right of vertical line) that were used to compare element ratios (boxplots) on the ventral edge of otoliths from Hickory Shad captured in the Swift Creek and Pitchkettle Creek of the Neuse River. Values for the F-tests include the F-statistic, p-value, upper and lower confidence intervals, and estimated ratio of variance $\widehat{\sigma^2}(r)$, which were used to determine the appropriate bootstrap procedure. Values for the bootstrap procedure include the t-statistic, degrees of freedom, observed p-value, mean estimates for each capture location ($\hat{\mu}_{gx}$), standard errors, confidence intervals, and bootstrap p-values. In the boxplots, the center line indicates the median. The lower and upper hinges of each box represent the 25th and 75th percentiles, respectively. Whiskers extend from the hinges to the smallest and largest value within the bounds of 1.5 times the interquartile range. Values beyond these boundaries are indicated as individual dots.

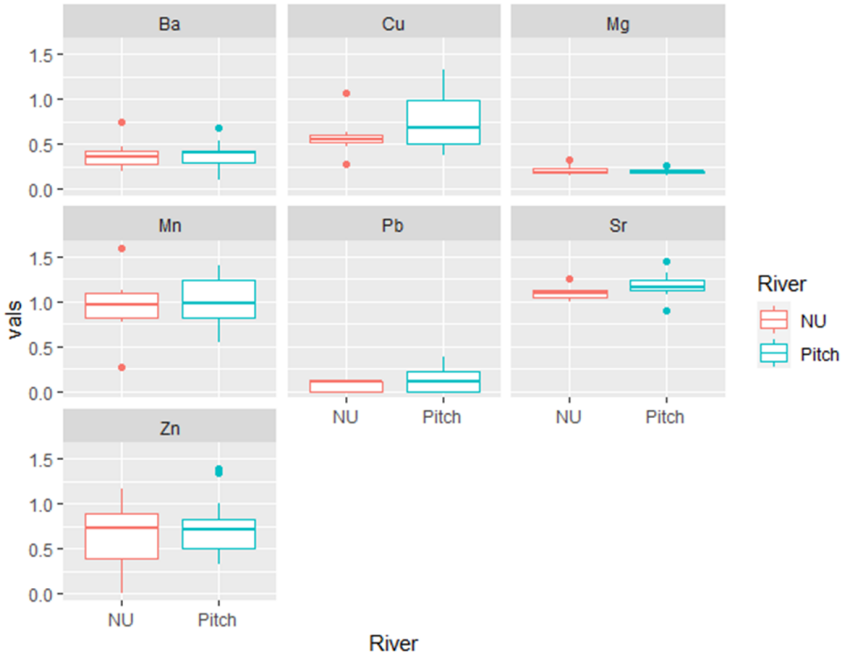

G1	G2	Element	F.Stat	p	CI-L	CI-U	$\widehat{\sigma^2}(r)$	T.Stat	df	p	CI-L	CI-U	$\hat{\mu}_{g1}$	$\hat{\mu}_{g2}$	SE	Boot1
NU	Pitch	Sr	0.49	0.31	0.16	1.99	0.49	-2.06	26	0.05	-0.17	0.00	1.09	1.17	0.04	0.58
		Ba	1.32	0.59	0.44	5.33	1.32	0.19	26	0.85	-0.11	0.13	0.38	0.37	0.06	0.87
		Mn	1.72	0.32	0.57	6.94	1.72	-0.3	26	0.76	-0.28	0.21	0.95	0.99	0.12	0.80
		Zn	1.51	0.44	0.50	6.09	1.31	-0.57	26	0.58	-0.34	0.2	0.65	0.72	0.13	0.64
		Pb	0.22	0.03	0.07	0.87	0.22	-1.52	26	0.14	-0.14	0.02	0.06	0.12	0.04	0.54
		Cu	0.54	0.37	0.18	2.16	0.54	-1.47	26	0.15	-0.37	0.06	0.58	0.73	0.11	0.53

A-11. Results of F-tests (left of vertical line) and appropriate bootstrap procedure (right of vertical line) that were used to compare element ratios (boxplots) on the ventral edge of otoliths from Hickory Shad captured in the Pitchkettle Creek and Neuse Upper. Values for the F-tests include the F-statistic, p-value, upper and lower confidence intervals, and estimated ratio of variance $\widehat{\sigma^2}(r)$, which were used to determine the appropriate bootstrap procedure. Values for the bootstrap procedure include the t-statistic, degrees of freedom, observed p-value, mean estimates for each capture location ($\hat{\mu}_{gx}$), standard errors, confidence intervals, and bootstrap p-values. In the boxplots, the center line indicates the median. The lower and upper hinges of each box represent the 25th and 75th percentiles, respectively. Whiskers extend from the hinges to the smallest and largest value within the bounds of 1.5 times the interquartile range. Values beyond these boundaries are indicated as individual dots.